ENHANCED RECEIVER ARCHITECTURES FOR PROCESSING MULTI GNSS SIGNALS IN A SINGLE CHAIN

BASED ON PARTIAL DIFFERENTIAL EQUATIONS MATHEMATICAL MODEL

BY

MAHER AL-ABOODI

Applied Computing Department

School of Science and Postgraduate Medicine

The University of Buckingham

The United Kingdom

A Thesis

Submitted for the Degree of Doctor of Philosophy in

Computer Science at the University of Buckingham

April 2016

Abstract

The focus of our research is on designing a new architecture (RF front-end and digital) for processing multi GNSS signals in a single receiver chain. The motivation is to save in overhead cost (size, processing time and power consumption) of implementing multiple signal receivers side-by-side on-board Smartphones.

This thesis documents the new multi-signal receiver architecture that we have designed. Based on this architecture, we have achieved/published eight novel contributions. Six of these implementations focus on multi GNSS signal receivers, and the last two are for multiplexing Bluetooth and GPS received signals in a single processing chain. We believe our work in terms of the new innovative and novel techniques achieved is a major contribution to the commercial world especially that of Smartphones. Savings in both silicon size and processing time will be highly beneficial to reduction of costs but more importantly for conserving the energy of the battery. We are proud that we have made this significant contribution to both industry and the scientific research and development arena.

The first part of the work focus on the Two GNSS signal detection front-end approaches that were designed to explore the availability of the L1 band of GPS, Galileo and GLONASS at an early stage. This is so that the receiver devotes appropriate resources to acquire them. The first approach was based on folding the carrier frequency of all the three GNSS signals with their harmonics to the First Nyquist Zone (FNZ), as depicted by the BandPass Sampling Receiver technique (BPSR). Consequently, there is a unique power distribution of these folded signals based on the actual present signals that can be detected to alert the digital processing parts to acquire it. Volterra Series model is used to estimate the existing power in the FNZ by extracting the kernels of these folded GNSS signals, if available. The second approach filters out the right-side lobe of the GLONASS signal and the left-side lobe of the Galileo signal, prior to the folding process in our BPSR implementation. This filtering is important to enable none overlapped folding of these two signals with the GPS signal in the FNZ. The simulation results show that adopting these two

approaches can save much valuable acquisition processing time.

Our Orthogonal BandPass Sampling Receiver and Orthogonal Complex BandPass Sampling Receiver are two methods designed to capture any two wireless signals simultaneously and use a single channel in the digital domain to process them, including tracking and decoding, concurrently. The novelty of the two receivers is centred on the Orthogonal Integrated Function (OIF) that continuously harmonies the two received signals to form a single orthogonal signal allowing the "tracking and decoding" to be carried out by a single digital channel. These receivers employ a Hilbert Transform for shifting one of the input signals by 90-degrees. Then, the BPSR technique is used to fold back the two received signals to the same reference frequency in the FNZ. Results show that these designed methods also reduce the sampling frequency to a rate proportional to the maximum bandwidth, instead of the summation of bandwidths, of the input signals.

Two combined GPS L1CA and L2C signal acquisition channels are designed based on applying the idea of the OIF to enhance the power consumption and the implementation complexity in the existing combination methods and also to enhance the acquisition sensitivity. This is achieved by removing the Doppler frequency of the two signals; our methods add the in-phase component of the L2C signal together with the in-phase component of the L1CA signal, which is then shifted by 90-degree before adding it to the remaining components of these two signals, resulting in an orthogonal form of the combined signals. This orthogonal signal is then fed to our developed version of the parallel-code-phase-search engine. Our simulation results illustrate that the acquisition sensitivity of these signals is improved successfully by 5.0 dB, which is necessary for acquiring weak signals in harsh environments.

The last part of this work focuses on the tracking stage when specifically multiplexing Bluetooth and L1CA GPS signals in a single channel based on using the concept of the OIF, where the tracking channel can be shared between the two signals without losing the lock or degrading its performance. Two approaches are designed for integrating the two signals based on the mathematical analysis of the main function of the tracking channel, which the Phase-Locked Loop (PLL). A mathematical model of a set of differential equations has been developed to evaluate

the PLL when it used to track and demodulated two signals simultaneously. The simulation results proved that the implementation of our approaches has reduced by almost half the size and processing time.

Acknowledgements

I offer my most humble bow to Almighty Allah, the Most Gracious and Merciful for blessing me with inspiration and the drive to fulfil my aspiration of achieving this milestone. I am further grateful to Allah for blessing me with my family, teachers, friends, and colleagues who offered their support and insights along the way.

Give the duration and depth of such a journey, one cannot appropriately express one's gratitude or acknowledge the contributions of so many people, so my concern is of somehow omitting or not duly appreciating the generosity and help offered along the way. I humbly admit that I could not have done it on my own; my work is the outcome of every little gesture of support and encouragement that was so openly offered, it was all the succour I'd say any wounded soul required.

To My Parents, I would like to dedicate my entire future that this endeavour will lead me to, especially to my mother whose prayers and blessings were the driving force behind my efforts, to my father whose saintly patience taught me the need for determination and effort to accomplish this worthy task that I undertook.

To My Family, for all their patience and empathy, I can never truly express my gratitude and appreciation for my wife and amazing children. You have all been there when I needed you the most, just being in your presence sometimes was all the help and inspiration I needed, and I thank you especially for the trying times when I tested your patience with what I often became given the pressures of finishing the thesis. My wife's support, encouragement and quiet patience were undeniably the foundation upon which our family blossomed together. She helped me get through this demanding and stressful period in the most positive way. Stepping onto this side of the shore and looking back did I truly come to appreciate how much depth and support she has offered. She has stood by me through all my trials, my absences, my shifting moods and often untimely and abrupt departures from home. My children too have been great sources of love and relief from my academic aspirations.

Also, in no lesser vein goes my gratitude to my extended family; my brothers and

sisters and to my friends for your encouragement and support and advice. I must specifically mention my friends who were with me during hard times, cheered me on, and celebrated even the smallest of my accomplishments.

To My Supervisor, Dr. Ihsan Lami with my gratitude for teaching me what it truly means to be a researcher. His patience, advice in numerous aspects of the study, impassioned discussions, and most pertinently for his amazing friendship, which taught me about being both a learner in life and about drinking from the wealth of wisdom. I wish him all the best for the future. I owe him a most profound debt of gratitude, which no words can appropriately convey.

To My sponsors, I would like to express my eternal gratitude to the Ministry of Higher Education and Scientific Research in Iraq for sponsoring my PhD programme of study. I would like to especially thank the European Cooperation Science and Technology (COST) group who have been truly gracious and empathetic in offering all their help, monetary and otherwise, without the hype of the red tape usually associated with similar organisations.

I would especially like to mention Dr. Hamid AL-Aasadi (The University of Basrah, Basrah, Iraq) who is most responsible for putting me on this path, his guidance, his advice and his encouragement have offered me inspiration to not only to pursue a Masters but to also aspire to a PhD. His vision, scholarly depth and motivation inspired me deeply. He inspired me to become an independent researcher and helped develop in me the importance of scientific thought. His assistance and guidance in paving the path for my graduate career cannot be adequately expressed. Also, I would acknowledge the efforts of my M.Sc. supervisors, Late Dr. Fouad Hamid and Dr. Ra'ad Salah (The University of Basrah, Basrah, Iraq) were both instrumental in my postgraduate studies. Their genuine passion for a ward's growth and intellectual development and their mathematical genius lit in me the spark of wanting to probe the logical and structural nature of mathematics.

My long lasting appreciation goes to the Department of Applied Computing, the University of Buckingham. The colleagues, the friends I made and the staff who were there always, to guide and direct. Your company, encouragement and time spent with you will always be the stepping-stone any aspirant would need in life.

Abbreviations

ACPR	Adjacent Channel Power Ratio
ADC	Analogue-to-Digital Converter
AMM-PLL	Adaptive Multi-Mode PLL
AR	Amplitude Ratio
AWGN	Additive White Gaussian Noise
BER	Bit Error Rate
BOC	Binary Offset Carrier
BPF	Band Pass Filter
BPSK	Binary Phase Shift Keying
BPSR	BandPass Sampling Receiver
BT	Bluetooth
CA	Coarse Acquisition Code
CCS	Complex Correlated Signal
CDMA	Code Division Multiple Access
CL	Long Code
CM	Moderate Code
C/No	Carrier to Noise density ratio
CQPLL	Complex Quadrature-PLL
DAC	Digital-to-Analogue Converter
DFT	Discreet Fourier Transform
DSP	Digital signal processing
DSSS	Direct Sequence Spread Spectrum
EVM	Error Vector Magnitude
FD	Frequency Difference between two signals frequencies
FE	Frequency Estimator
FFT	Fast Fourier Transform
FHSS	Frequency Hopping Spread Spectrum

FNZ	First Nyquist Zone
Galileo	European Union navigation system
GLONASS	Russian navigation system
GNSS	Global Navigation Satellite System
GPS	American navigation system
HT	Hilbert Transform
IF	Intermediate-Frequency
IFFT	Inverse Fast Fourier Transform
IIR	Infinite Impulse Response
ISI	Inter Symbol Interference
LF	Loop Filter
LNA	Low Noise Amplifier
LO	Local Oscillator
LPF	Low Pass Filter
NC	Non-Coherent
NCO	Numerically Controlled Oscillator
NFC	Near Field Communication
NMSE	Normalized Mean Squared Error
OBPSR	Orthogonal BandPass Sampling Receiver
OCBPSR	Orthogonal Complex BandPass Sampling Receiver
OFDM	Orthogonal Frequency-Division Multiplexing
OIF	Orthogonal Integrated Function
OPC	Orthogonal Parallel acquisition Channel
OS	Open Service
OSC	Orthogonal Single acquisition Channel
P_D	Probability of Detection
PDE	Partial Differential Equations
P_{fa}	Probability of false alarm
PLL	Phase-Locked Loop
PRN	Pseudo Random Noise
QPSK	Quadrature Phase Shift Keying
RF	Radio Frequency

RMS	Root Mean Square
ROC	Receiver Operating Characteristics Curve
SNR	Signal to Noise Ratio
SSB	Single Sideband
STD	Standard Deviation
SV	Satellite Vehicle
TF	Transfer Function
VCO	Voltage-Controlled Oscillator
WCDMA	Wideband Code Division Multiple Access
α	The ratio of (L2/L1) GPS signals frequencies
β	Acquisition threshold
γ	The ratio between the first and second maximum correlation peaks
ΔF	The residual carrier frequency
ω	The frequency difference between the generated VCO and the desired signal frequencies

Contents

List of Figures

List of Tables

Declaration

*I hereby declare that all the work in my thesis entitled "**Enhanced Receiver Architectures for Processing Multi-GNSS Signals in a Single Chain Based on Partial Differential Equations Mathematical Model**" is the result of my own work except where due reference is made within the text of the thesis.*

I also declare that, to the best of my knowledge, none of the material has been submitted for a degree in this or any other university.

Chapter 1 **Introduction**

Global Navigation Satellite System (GNSS) receivers targeted for use in Smartphones to provide localisation for many Location-Based-Services have reached 4.5 billion in 2015, and it is expected to grow to 9 billion in 2022 [1]. Since, a typical Smartphone includes, in addition to the GNSS, other wireless technologies such as Bluetooth (BT), NFC, and Wi-Fi; therefore, sharing parts of the receive chain functions between GNSS and these technologies will help reduce solutions overall silicon and physical size and cost, as well as reducing processing time and power consumption.

Our research focus is on integrating multi-signals in a single processing chain based on using the BPSR technique. Parts of this work rely on solving Partial Differential Equations (PDE's) that model the multiplexing of the various receiver functionalities, as details in Chapter 5.

The first part of our research was to investigate mathematically the availability of integrating/combining wireless signals in a single receive chain functions; We have subsequently found that this kind of integration can be implemented at the analogue front end stage as well as at the acquisition and tracking stage. We have come up with eight hypotheses, 4 in the RF front-end, 2 in the acquisition, and 2 in the tracking stages to achieve such integration. All these 8 hypotheses were duly evaluated, including literature survey, and proved using MATLAB/Simulink simulations as shall be discussed in the following chapters. The following is a brief on each of these hypothesis and our conclusions on it:

- The current receiver designs employ multi acquisition channels to find the availability of GNSS signals that share the same transmitted frequency and that can thrash all the receiver resources to find signals that might not be available. Therefore, we designed two approaches that rapidly detect the availability of these GNSS signals at an early stage in the receiver to

keep it from enabling acquisition channels for acquiring signals that are not present.

- When the BPSR technique is used to capture multi-signal states on each received signal, they should be folded to a unique frequency band in the FNZ. This can complicate the task of combining more than one signal in a single channel. Therefore, two receivers are designed to fold any two received signals to the same folding-frequency (or the frequency band) in FNZ, based on orthogonalising the two received signals to become a single orthogonal signal. This will also reduce the sampling frequency rate, which is proportional to maximum information bandwidth of the two received signals.
- GNSS signals, such as L1CA and L2C GPS signals, are transmitted from the same Satellite Vehicle (SV); ergo, most of their errors are related. Combining these signals in acquisition channel is possible and will assure better signal acquisition and improved reliability at wider operating areas. However, the current combined L1CA and L2C GPS signal implementations are side-by-side solutions (parallel processing scenario), which will be costly (processing, power, size, etc.). Therefore, two novel acquisition channels are designed to combine these signals into a single processing channel based on applying one of our orthogonal receiver designs.
- BT transceiver, in the most demanding profile run, is active intermittently with large inactive 2150 μsec window-slots. Consequently, we will use this inactive time to track GPS-L1 signal for eliminating the use of a complete tracking channel. This requires designing a new tracking channel, so it changes its tracking mode based on the available signals "BT or GPS" without losing the lock of the signal phase. After mathematically analysing the behavioural response of the Costas PLL when fed two signals, two approaches are proposed based on integrating a frequency estimator inside the PLL loop. Note that one of the main applications of Fokker-Planck Equation (FPE) [2] is the PLL. Where, FPE is a parabolic PDE that describes the probability density function of the

particle's position undergoing Brownian motion. Mathematically, the state of the FPE, $(x(t))$ of the probability density function is described as follows:

$$\frac{\partial f(x,t)}{\partial t} = \frac{\partial}{\partial t}\big(\zeta(x,t)\, f(x,t)\big) + \frac{N_o}{4}\frac{\partial^2 f(x,t)}{\partial x^2}$$

where - $\zeta(x,t)$ *and* $\frac{N_o}{2}$ *are the moments of the FPE, and* N_o *is power spectral density of the Gaussian white noise*. This type of Nonlinear PDE is very difficult to solve it analytically; therefore, we derived a mathematical model (system of ordinary differential equations) to analyse and describe the behaviour of our new PLL design.

1.1 Research Motivation

With having both of my BSc and MSc in mathematics, I wanted to research into an applied Mathematics area that has an association with modelling and implementing communication systems, with a focus on the role of Partial differential equations in the applied solution. I have come to learn; after some investigation, that most of today's wireless signals and associated receiver algorithms has a big PDE component in it. When I met Dr Ihsan Lami in the Applied Computing at the University of Buckingham) and discussed my topic "*Combine Multi-GNSS signal in a single chain*" with him, he explained that I had to appreciate truly the physical problem before attempting to solve it. In addition, he further explained that my potential subject needed to be state-of-art to be of any value, given that communication and wireless-signal technology evolve at a rapid pace. Although I realised I would be facing quite a few challenges and that it would not be plain sailing, I was truly inspired, and I knew that this would enliven the study and research ahead of me, it fired my enthusiasm, and I rose to the task. Some of the more severe initial challenges I had to face were:

1. The biggest challenge that I had to overcome was to build on my abstract mathematical background for real-time application.
2. Building a background about the communication systems; transmitters, wireless channels, noise, and receivers and how signals are processed amongst

them.

3. Setting proper criteria for each solution since not all the mathematical assumptions are applicable to be real-time solutions.
4. Answering the questions of "when, where and how" we can combine the signals without affecting the system performance.
5. To design efficient solutions for combining/integrating more than one signal in a single chain with the minimum overhead cost possible.

Looking back at this experience, I am very happy that I have had the chance to expand on my prior knowledge, and successfully apply my previous knowledge in a thriving area of technology that is part of our everyday life.

1.2 Research Methodology and Progress

My methodology was to cover the two following aspects of combining and integrating signals in a single receiver chain:

1. Understand the mathematical representation of each and every functional component at any stage in the transmit and receive chain for the GNSS and BT signals.
2. Each of these functions is then broken down to its basic mathematical model to help me develop an enhanced model, especially for the algorithms of the ADC and PLL.

I started my research with collecting fundamental information on GNSS and BT signals (mainly the characteristics of these two signals in terms of frequency range, modulation type, spread spectrum type, and transmitted/received power). Then, I focussed on understanding the receiver stage and its components by doing simulation implementations of the most common receiver architecture functions on MATLAB. Comprehensive literary investigations done on algorithms and techniques have been used to detect, acquire, and track GNSS and BT signals. This investigation has led to my hypotheses and subsequently proposed solutions on designing multi-signal receivers. My findings on multi-GNSS, with BT, acquisition and tracking solutions can be easily adopted to other types of signals.

In the process of researching receiver architecture, I found that BandPass Sampling was the most fascinating architecture. Therefore, I considered the BPSR architecture closely, which has resulted in designing a new receiver architectures based on orthogonalising multiple received signals. We called this “the Orthogonal BandPass Sampling Receiver (OBPSR)” which formed the flagship for our subsequent novelties. OBPSR architecture folds the received signals in the digital domain at the same frequency, which will for example, facilitate in combining them in the acquisition or in tracking stage. The concept of OBPSR is used first for the acquisition of L1 and L2 combined GPS signals in a single channel. Subsequently, I have succeeded in combining GPS and BT signals in a single PLL tracking channel. Figure 1-1 shows a time line, highlighting the progress of my achievements and publications.

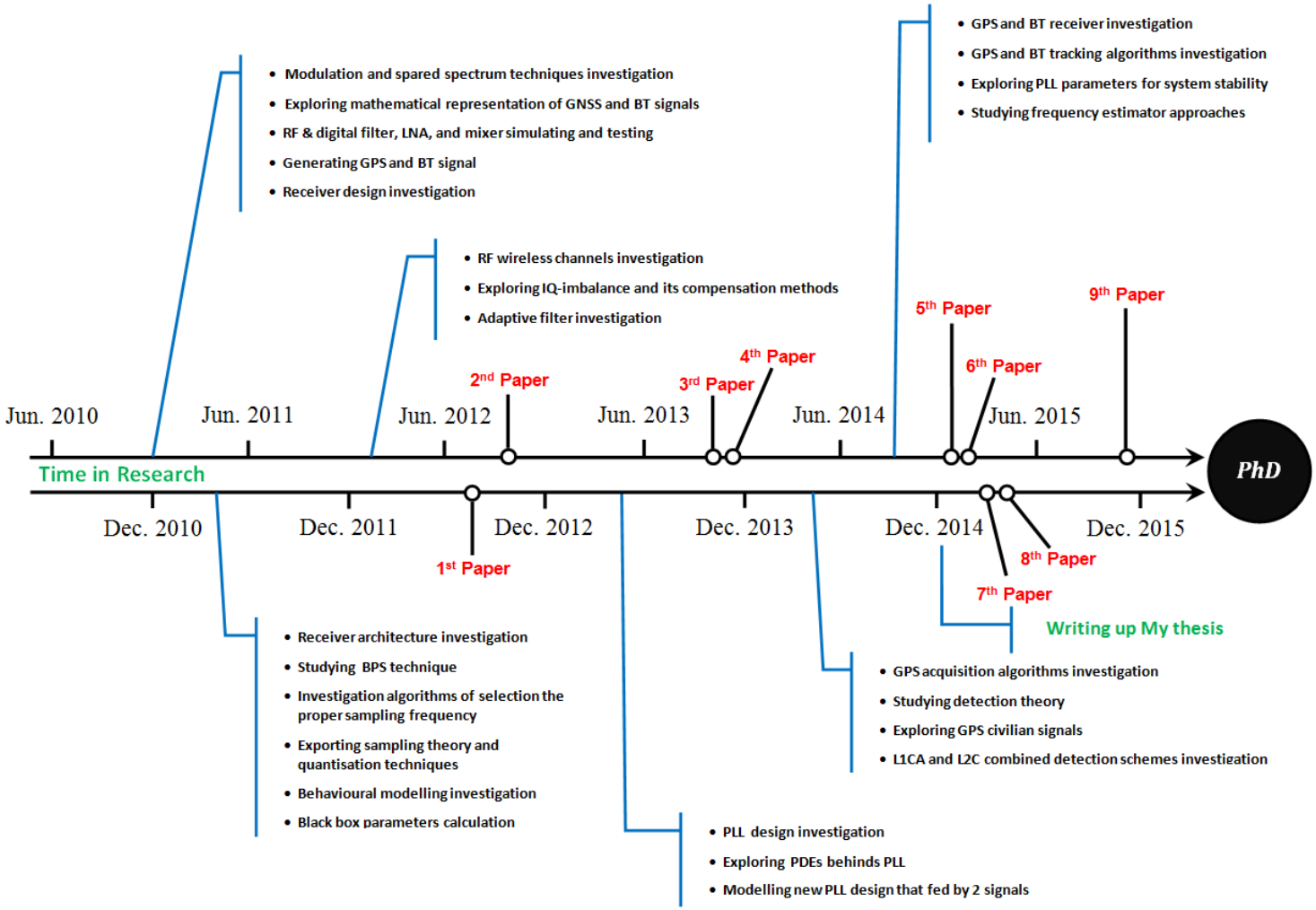

Figure 1-1 PhD research progress and achievements

1.3 Thesis Organisation

Figure 1-2 illustrates the structure of this thesis in terms of the receiver chain relevance. The thesis consists of six chapters. The structure of the thesis chapters is described below.

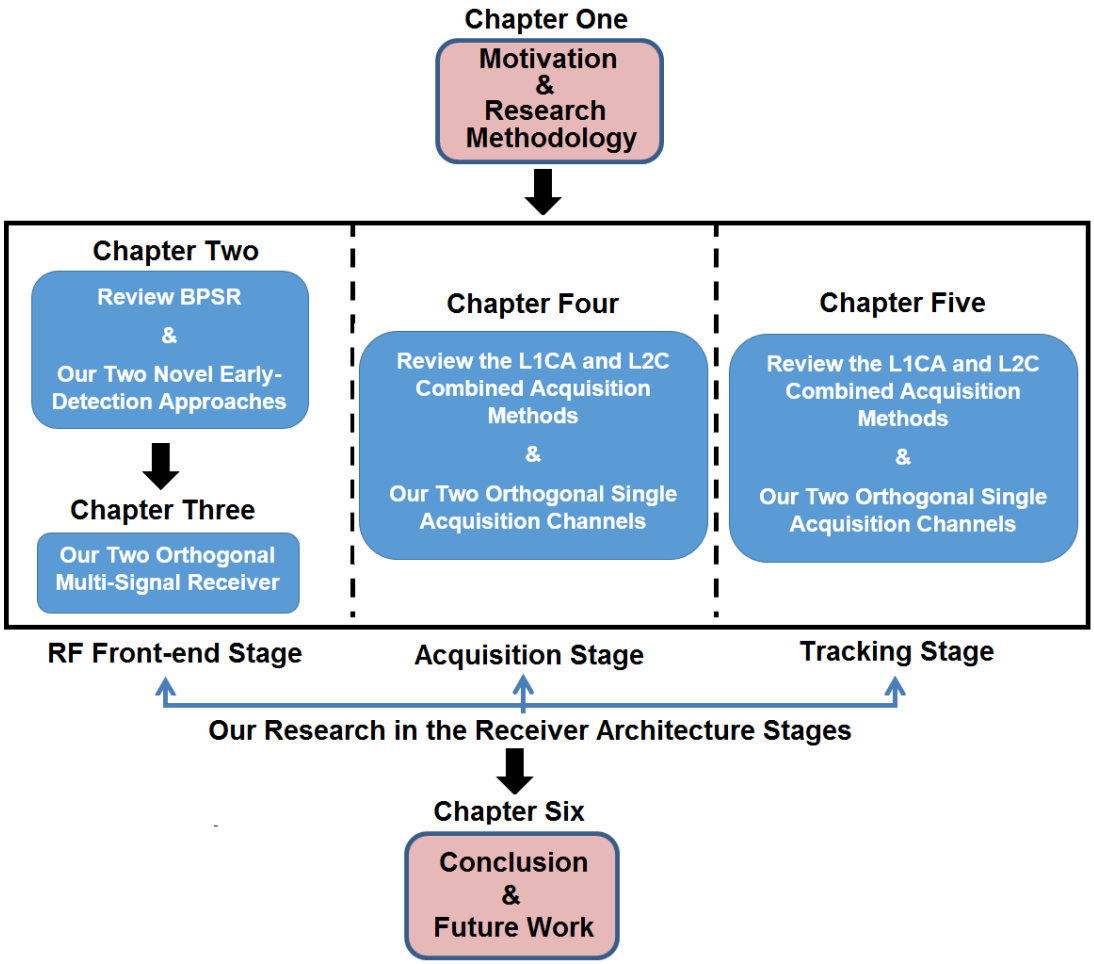

Figure 1-2 Thesis organisation

Chapter 1 introduces the research topics of this thesis, as well as offering an insight into the motivation, the objectives and the methodology of this research.

Chapter 2 reviews the current receiver architectures and explains the concept of the BPSR. It also presents the two quick-early (L1-GNSS signals) detection approaches whose MATLAB simulation and results are analysed.

Chapter 3 describes our two multi-signal receivers "OBPSR & OCBPSR" in detail with their mathematical representations. In this chapter, *Orthogonal Integrated*

Function will be explained and how it combines the signals without overlapping each other. MATLAB simulation results of the two receivers will be evaluated by sets of criteria such as BER and EVM.

Chapter 4 starts with an overview of the structure and the properties of two GPS (L1CA and L2C) signals. Further, literature survey will be provided to cover the traditional and the state-of-art L1CA and L2C combination acquisition methods. This chapter also presents our two novel orthogonal combined L1CA and L2C acquisition channels with a comprehensive evaluation of their performance, with a further discussion of their simulation results.

Chapter 5 exhibits a literature review and analysis of PLL system when it inputs two signals. This chapter will provide our developed mathematical model of the PLL based on measuring the effect phase-change on the system stability also. A Novel PLL design "AMM-PLL" for tracking dual signals "GPS and Bluetooth" concurrently is also discussed in this chapter.

Chapter 6 draws conclusions, discussions and recommendations for future work.

1.4 List of My Published Papers

During the PhD program, the following papers were published with fellow researchers within the Department of Applied Computing at The University of Buckingham as well as with colleagues at the Ghent University, Belgium as part of the COST project and at Saint-Petersburg State University, Russia.

1. **Maher Al-Aboodi**, Ali. Albu-Rghaif and Ihsan Lami, "GPS, Galileo and GLONASS L1 signal detection algorithms based on bandpass sampling techniques" in Ultra-Modern Telecommunications and Control Systems and Workshops (ICUMT), 4th International Congress, pp. 255-261, IEEE, **2012**.

2. Ihsan Lami and **Maher Al-Aboodi**, "OBPSR: A multi-signal receiver based on the orthogonal and bandpass sampling techniques" In Computer Applications Technology (ICCAT), International Conference on, IEEE, **2013**.

3. **Maher AL-Aboodi** and Ihsan Lami, "OCBPSR: Orthogonal Complex

BandPass Sampling Receiver" Computer Applications and Information Systems (WCCAIS), 2014 World Congress on, pp. 1-6. IEEE, **2014**

4. Ihsan Lami, Ali Albu-Rghaif and **Maher Al-Aboodi**, "GCSR: A GPS Acquisition Technique using Compressive Sensing enhanced implementation" International Journal of Engineering and Innovative Technology (IJEIT), vol. 3, no.5, pp. 250-255, **2013**.

5. **Maher AL-Aboodi,** N. V. Kuznetsov, G. A. Leonov, M. V. Yuldashev, and R. V. Yuldashev, "Response of Costas PLL in the Presence of In-band Interference" IFAC-PapersOnLine 48, pp.714-719, **2015**.

6. Albu-Rghaif, Ali, Ihsan A. Lami, **Maher Al-Aboodi**, Patrick Van Torre, and Hendrik Rogier, "Galileo Signals Acquisition Using Enhanced Subcarrier Elimination Conversion and Faster Processing" third International Conference on Advances in Computing, Communication and Information Technology- CCIT, 10 - 14 pages, UK, **2015**.

7. Albu-Rghaif, Ali, Ihsan A. Lami, and **Maher Al-Aboodi**, "OGSR: A Low Complexity Galileo Software Receiver using Orthogonal Data and Pilot Channels" third International Conference on Advances in Computing, Communication and Information Technology- CCIT, UK, **2015**.

8. **Maher Al-Aboodi,** Ihsan A. Lami, Albu-Rghaif, Ali, Van Torre, Patrick, Rogier, Hendrik, "A Single Acquisition Channel Receiver for GPS L1CA and L2C Signals Based on Orthogonal Signal Processing" Proceedings of the 28th International Technical Meeting of The Satellite Division of the Institute of Navigation (ION GNSS+2015), Tampa, Florida, September **2015**.

9. **Maher AL-Aboodi** and Ihsan Lami, "Two New Approaches for Extended "Lock-in Range" Multi-Mode PLL Used to Track and Demodulate GPS+Bluetooth Signals in a Single Receive Chain" Proceedings of IEEE/ION PLANS, Savannah, Georgia, April **2016**. (Accepted)

Chapter 2 **The Choice of BPSR for Our Multi-Signal Receivers**

To save in overhead costs, we believe that multi-GNSS-signal (for example using GPS, Galileo, and, GLONASS) and multi-wireless-signal solutions (for example GNSS and BT) will roll out in most Smartphones shortly. No doubt, lots of research and development are ongoing to integrate these signals in a single-chain integrated-processing receiver since GNSS solutions are receivers only. For this research, this has necessitated the study/review of not only the signals' characteristics of GNSS and other Smartphone wireless technologies that can be candidate for such integration, but also the study/review of the various relevant architectures of wireless signals.

This chapter, therefore, starts with a review of four of the most used/common or relevant receiver architectures (super-Heterodyne, Homodyne, Low-IF and BPSR) that can be implemented to achieve our integration, in terms of studying their capability of handling multi-signals efficiently, and understanding/comparing their advantages and drawbacks. It has become clear to us that the BPSR is the best candidate for integrating the front-end of multi-signals integration into a single receiver chain that we are targeting. The main advantage of BPSR (detailed later in Section 2.1.4) is acquiring the signals at the same time instance and processing them directly to the digital domain (the only architecture to do this for multi-signals). Our review of the latest published literature that uses the BPSR architecture to combine multi signals is detailed in Section 2.2.

Finally, this chapter will detail the two BPSR implementations that we have published to detect multi-GNSS signals at an early stage, in the analogue front-end. These two implementations will eliminate having the GNSS-receiver thrashing all of its available resources to find/acquire a signal that does not exist at the vicinity. i.e.

In harsh environments such as urban canyons and indoors, the GNSS signals will most likely be blocked (or no physical existence of any signal at receiver's antenna at the reception time). These two implementations are important because current GNSS receivers employ hundreds of correlators [3] that will deplete the receiver's battery resources when trying to acquire signals in harsh environments [4]. This means that, when a solution using our implementation, the digital processing back-end (correlators acquisition and after) will only be invoked if the signal(s) actually exists, and thus achieving further overhead saving to having the integrated multi-GNSS receiver in a single chain rather than in a side-by-side implementation.

Note that, the line amplifiers (LNA) and filters are nowadays combined with ADCs to produce so-called *mixed-signal system*, which consists of an analogue input part on one side, and a digital output part on the other side. This *mixed-signal system* development is to make an integrated *all-digital receiver* [5] for high flexibility and power efficiency. For this thesis, it was decided to not model this LNA-ADC integration for our simulations, in favour of using an off-the-shelf model of the ADC.

2.1 Review of Multi-Signal Receiver Architectures

For designing or developing a multi-signal receiver, specifically for Smartphones' signals, firstly we need to determine what type of the receiver architecture front-end that will be employed based on power consumption, cost, size, requirements of performance, and implementation complexity. Therefore, the aim of this section is to provide an overview of the most commonly used receiver architectures and their ability to process more than one signal at the same time. This section will clarify the pros and cons of those architectures, and our architecture choice for this research aims.

2.1.1 Super-Heterodyne Receiver

The design of the super-Heterodyne is based on two down-conversion stages, as shown in Figure 2-1. The first stage is converting the RF signal to low/Intermediate-Frequency (IF) signal by using a Local Oscillator (LO) and mixer. While in the second stage, the low-frequency signal is converted to the baseband signal (in-phase and quadrature signals) by utilising quadrature mixers. Finally, the two separate

components in-phase and quadrature-phase signals are converted to the digital domain by two ADCs.

The receiver front-end is probably the most used in current wireless receivers due to (1) its ability to separate the narrow-band-high-frequency signals from the surrounding interfering frequencies, and (2) its excellent capability to cope with the minimum signal levels at acceptable signal-to-noise ratio.

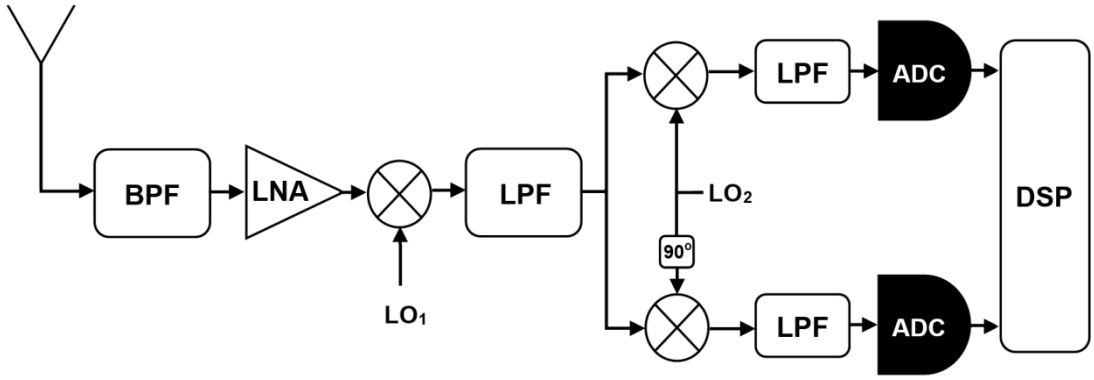

Figure 2-1 Super-Heterodyne receiver architecture

The main drawback of this receiver is that the harmonics and intermodulation components fall in the in-band of the desired signal as a result of the down-conversion stages. Consequently, several filters are required to reject the unwanted harmonics and intermodulation components, which make the receiver costly. For a multi-signal scenario, the first "LO_1" will need to be changed by a synthesiser to switch quickly between the received signals standards. Because of the bandwidth of the received signals is different, so that require banks of filters after each down-conversion stage to remove the unwanted signals. Therefore, that will limit the flexibility of this receiver and so is not a feasible/suitable solution for multi-signal scenario.

2.1.2 Homodyne Receiver

The design of Homodyne receivers is based on one down-conversion stage of, as depicted in Figure 2-2; in this stage, the RF signal is converted directly to baseband signal without using an intermediate stage. Obviously, this architecture is a

simplified version of the super-Heterodyne architecture, i.e., it is excluding the intermediate stage.

The RF signal once captured by the antenna is passed through BPF, centred on a frequency equal to the transmitted signal frequency, to eliminate all frequencies outside the signal band. The filtered signal is then amplified by a LNA. The amplified signal is then converted directly to baseband signals (in-phase and quadrature signals) by utilizing two mixers with a delay of 90-degree between them. A locally generated signal is used to mix with the amplified signal, which has a centre frequency identical to the frequency of the received RF signal. This architecture is also called the direct-conversion or Zero-IF architecture.

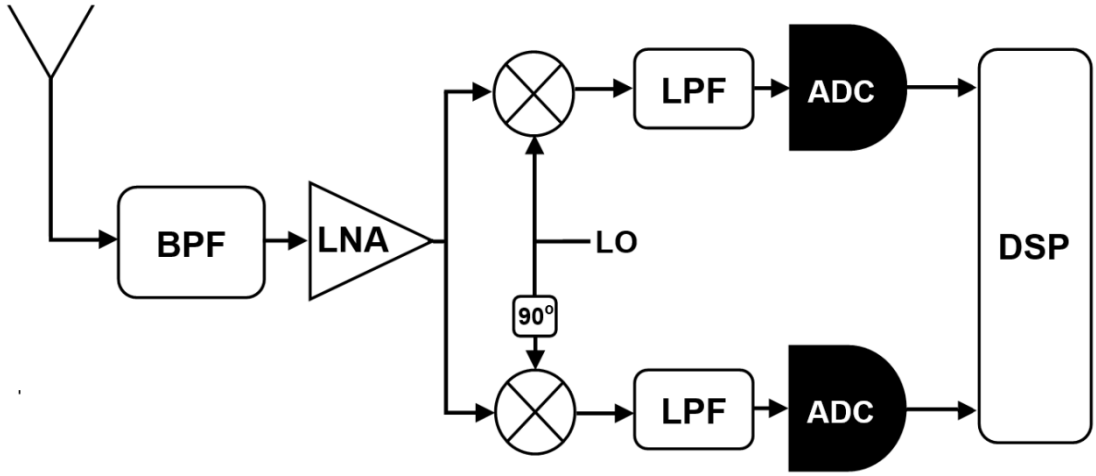

Figure 2-2 Homodyne receiver architecture

This receiver has two advantages compared to the previous super-heterodyne receiver; (1) it has less implementation complexity since no intermediate stage is required; (2) it avoids the in-band noise that comes from the harmonics and intermodulation components, snice IF is set to be 0 Hz. The homodyne receiver is more flexible to allow a higher level of integration than the super-Heterodyne receiver as the number of analogue components are reduced.

However, this receiver suffers from two limitations: (1) IQ imbalance [6] and (2) DC-offset [7]. The IQ imbalances issue occurs due to the mismatch between the in-phase and quadrature of the digitised signal. This is because in the analogue domain, the delay branch in the LO is never exactly 90-degree, and also the gain is never to

be the same for both signals (in-phase and quadrature). While the DC-offset issue is the result of the LO leak to the input signal port or to the mixer or LNA due to imperfect isolation. The leaked signal will be mixed with the input signal and after down-conversion it shows as a DC component in the digital domain.

2.1.3 Low-IF Receiver

The Low-IF receiver architecture is similar to the architecture of the Homodyne receiver but the main difference between them is as shown in the Figure 2-3, that the Low-IF architecture converts the signal to low-IF frequency (1st down-conversion) and then in the digital domain converts (2nd down-conversion) the signal to the baseband signal "0 Hz". While in the Homodyne receiver, the received signal is directly converted to the 0 Hz frequency.

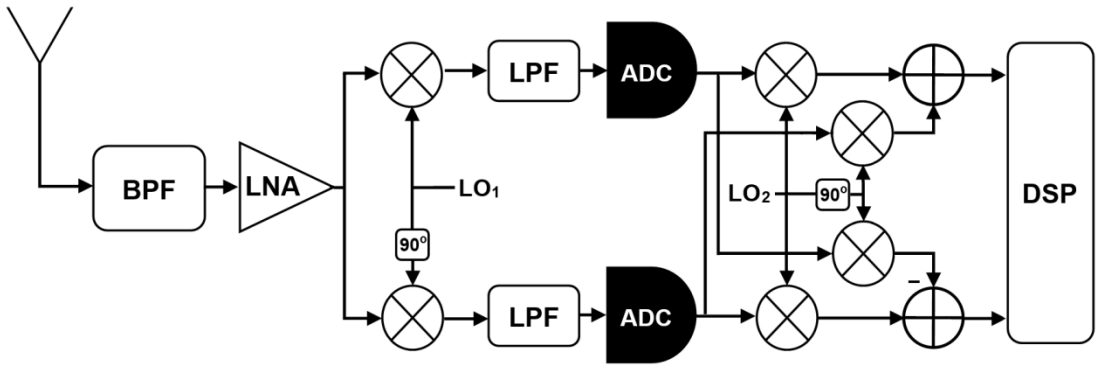

Figure 2-3 Low-IF receiver architecture

The Low-IF receiver combines the advantages of both super-heterodyne and homodyne architectures, such that (1) the architecture of the Low-IF receiver is simple like homodyne receiver and that will increase the level of integration. (2) the Low-IF receiver has no DC-offset issue likes super-heterodyne, since the signal after the 1st down-conversion is not around DC. However, the issue of the harmonics and intermodulation components that fall in the in-band of the desired signal in the super-heterodyne receiver will come up again in this receiver. Therefore, for multi-signal scenario, several filters are required to eliminate the unwanted harmonics and intermodulation components in this receiver, which will make it unfavourable.

2.1.4 Bandpass Sampling Receiver

Bandpass sampling receiver refers to an established front-end architecture where analogue bandpass signal is down-converted (or folded) directly to baseband/near to the baseband [8]. That has been done based on placing the ADC as near to the antenna as possible, as shown in Figure 2-4; without utilising an analogue mixer, local oscillator and image filters as they are existing in the previous mentioned receiver's architectures. This BPSR depends on using under-sampling technique or Nyquist second-order sampling theorem [9] that states on sampling the signal based on its bandwidth rather than the maximum frequency. This means the minimum sampling frequency has to be double the bandwidth of the received signal, which will be folding back the "information band" of the received signal to low-frequency at First Nyquist Zone (FNZ). In fact, BPSR architecture can be utilised to receive a Single Signal (BPSR-SS) or Multi-Signal (BPSR-MS) simultaneously, as shown in Figure 2-4 and Figure 2-5 respectively.

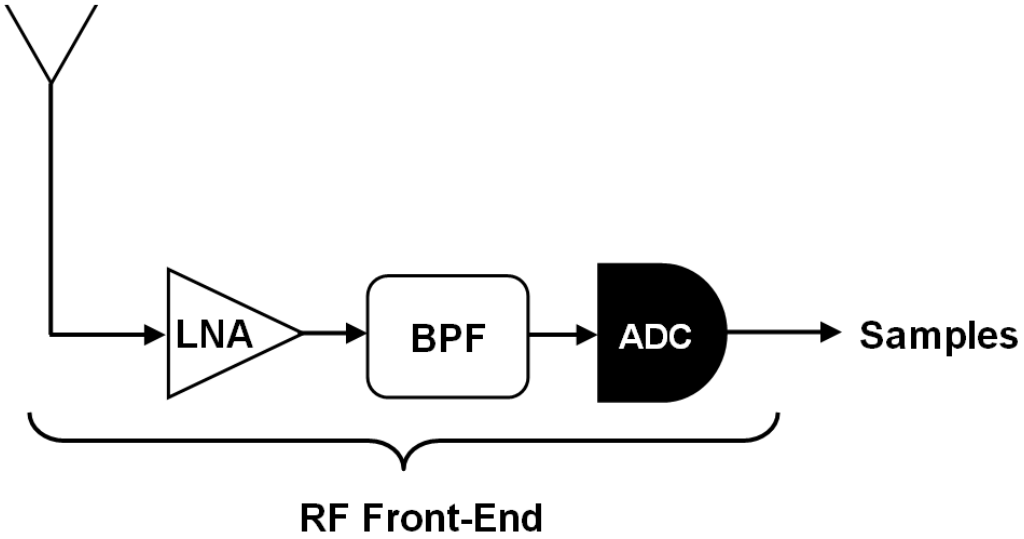

Figure 2-4 BPSR-SS: Bandpass sampling architecture for a single signal

In multi-signal scenario, the received signals are amplified, then are filtered out undesired signals and then are directly converted to the digital domain with a single ADC, as shown in Figure 2-5. The following algorithm is used to calculate the proper sampling frequency and the folding-frequencies in the FNZ of the received multi-signal. Further, it shows that there are two constrictions to guarantee no

overlapping among the folded information bandwidth in FNZ.

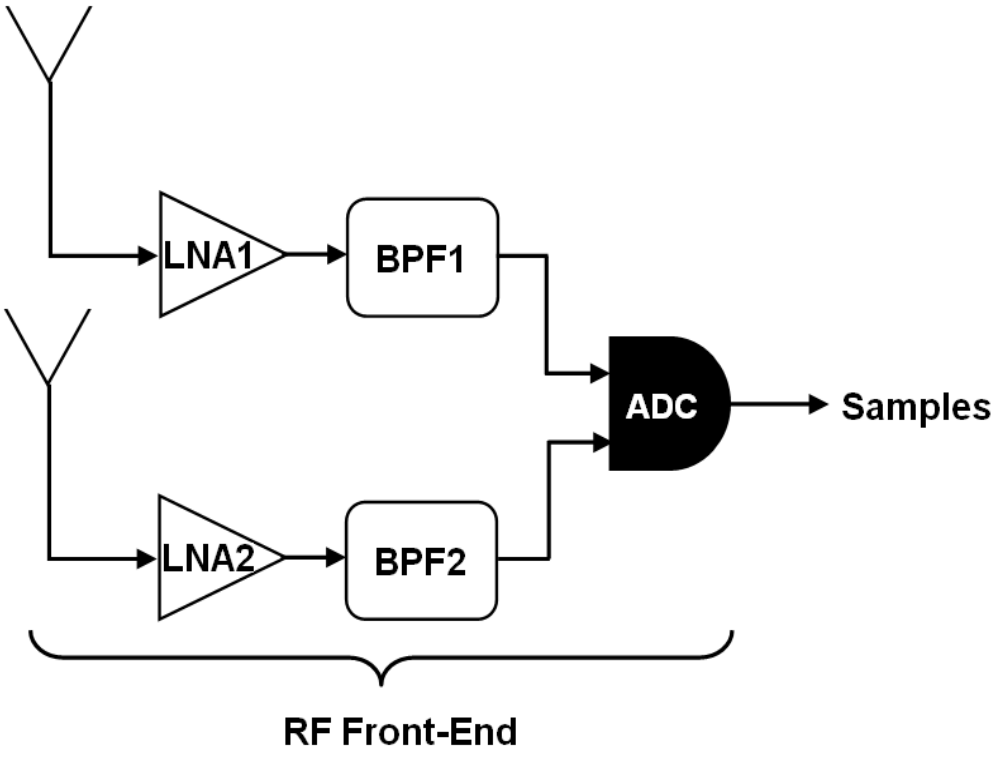

Figure 2-5 BPSR-MS: Bandpass sampling architecture for multi-signals

---

Algorithm: Selecting the sampling frequency of a multi signals

---

Begin

1- *Choose sampling frequency* ($f_s > 2BW$)
y = fix $[f_c/(0.5*f_s)]$

if (*y is even*)
$f_{fold} = rem[f_c, f_s]$
else
$f_{fold} = f_s - rem[f_c, f_s]$
end

if ($f_{fold} - 0.5*BW < 0$) / ($f_{fold} + 0.5*BW > 0.5*f_s$) *Restriction One*

Choose another sampling frequency (go to step 1)

elseif ($|f_{fold\_b} - f_{fold\_a}| < (BW_b+BW_a)/2$), *Restriction Two*

Choose another sampling frequency (go to step 1)
else
Return (f_{fold} *and* f_s)
end

End

---

where a = 2,…,n, b =1,…, (a-1); n=total # of desired signals

To view the sampling theory mathematically, it is actually a convolution between the DFT of this received signal and the summation of the shifted direct-delta function [10]. Let us assume the $x(t)$ is the time domain representation of a received RF signal and $X(f)$ is the frequency domain representation of the same RF signal. The sampled signal "$x_s(t)$" that comes from multiplication of $x(t)$ with Dirac delta function (δ function) is given by:

$$x_s(t) = x(t) \sum_{n=-\infty}^{\infty} \delta(t - n.T_s) \quad (2\text{-}1)$$

where, T_s is the sampling time and $f_s = 1/T_s$; f_s is the sampling frequency.

In the frequency domain, the multiplication operation in (2-1) will be converted to convolution operation "$*$" as it is expressed in (2-2)

$$X_s(f) = X(f) \frac{1}{T_s} * \sum_{n=-\infty}^{\infty} \delta(f - n.f_s). \quad (2\text{-}2)$$

Convolving the Direct delta function with $X(f)$ and substituting f_s in the (2-2), the new equation becomes as followed:

$$X_s(f) = f_s \ [X(f)\ \delta(f) + \ X(f)\ \delta\big(f \mp f_f\big) + X(f)\ \delta\big(f \mp 2f_f\big) + \cdots]$$

$$X_s(f) = f_s \ [X(f) \ + \ \ X\big(f \mp f_f\big) + X\big(f \mp 2f_f\big) + \cdots]$$

After simplified the above equation, the spectral representation of $x_s(t)$ is shown by:

$$X_s(f) = f_s \ \sum_{n=-\infty}^{\infty} X(f - N\ f_s). \quad (2\text{-}3)$$

Obviously, from (2-3) the spectrum of $x(t)$ will be replicated on $N\ f_s$ and N=1, 2, 3, etc. The value of f_s needs to be selected at least doubles then the value of f to avoid spectrum overlapping ($f_s - f > f$). The proper sampling frequencies that sample the signal without overlapping can be expressed as a function of both the bandwidth and the centre frequency of the RF signal [11]. The sampling frequency intervals can be expressed as:

$$\frac{2.f_c + BW}{K+1} \ \leq \ f_s \ \leq \ \frac{2.f_c - BW}{K}$$

where, K is an integer number bounded between 0 and normalize carrier frequency "fix(fc/BW - 0.5)", where fix is a function that rounds its input values to toward zero, and BW is the bandwidth of the signal.

In the BPSR technique, (2-4) shows the mathematical relationship that defines the folding-frequency value in the FNZ; obviously, it is a function of carrier frequency of the received signal and the chosen sampling frequency.

$$f_{fold} = \begin{cases} rem(f_c, f_s) & if \quad fix\left(\frac{f_c}{0.5*f_s}\right) \quad is\ even \\ f_s - rem(f_c, f_s) & if \quad fix\left(\frac{f_c}{0.5*f_s}\right) \quad is\ \ odd \end{cases} \tag{2-4}$$

where f_c and f_{fold} are the carrier frequency and the folding-frequency respectively.

Figure 2-4 and Figure 2-5 show the structures of the first-order implementations of the BPSR. The limitation in this implementation is that it is unable to translate the bandwidth information of input signal directly to the reference frequency at 0 Hz [12], due to the signal will overlap with itself. Also, it requires a sampling frequency that needs to be double the summation of the information-bands of the received signals.

The limitations in the first-order implementation can be relaxed by using a complex/second-order implementation of BPSR, where this implementation allows to sample the received signals below the Nyquist frequency, because it combines the real and the imaginary part (the real part shifted by 90-degree) of the same received signal. That will reject all the negative frequencies part of the received signals. In addition, the second-order implementation allows to the received signal to be translated directly to the baseband "0 Hz frequency", since the signal become an "analytical signal". The "analytic signal" means that only a single-side band of any double-band signals is actually processed by this second-order sampling receiver. As shown in Figure 2-6, this is achieved by splitting the received signals into two paths. The Q-component path passes through an HT filter (90-degree phase shifting) before an ADC, while the I-component path of the signal is passed to an ADC directly and then both paths are recombined. This allows the ADC's to sample the signals at sampling frequency proportional to the summation of the input signals' bandwidths

rather than double of the bandwidth summation of the received signals in first-order implementation. The second-order implementation of BPSR suffers from IQ-imbalance issue that comes from the analogue implementation of HT; this implementation is complex to achieve equal amplitude and 90-degree phase balances [13]. Therefore, this issue needs to be compensated in the digital domain model for accurate simulation [14].

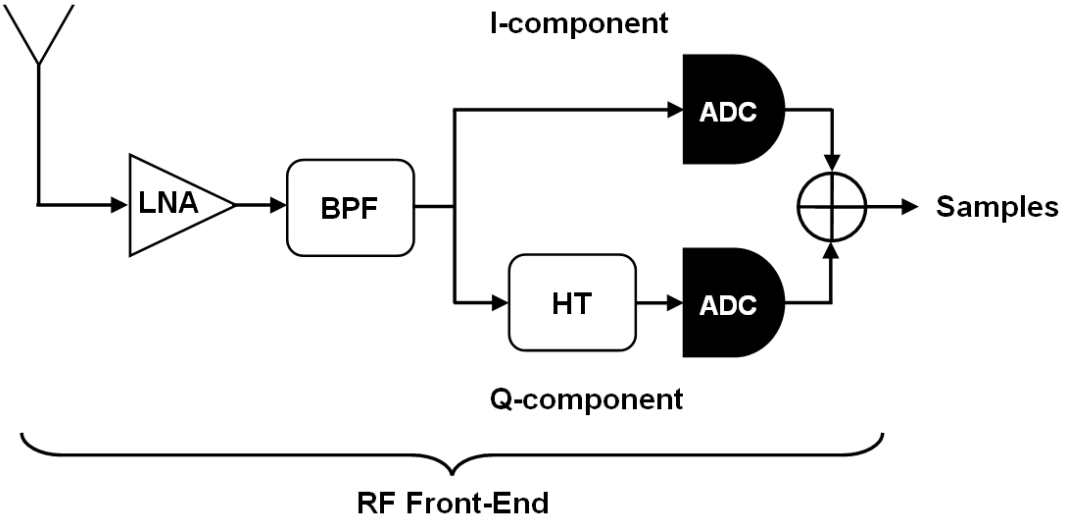

Figure 2-6 Architecture of second-order BPSR implementation

The main drawbacks in the BPSR architecture (both implementations) are:

- Require a wideband ADC frequency range that should be covering the highest received inputs signal RF frequency.
- Degradation in the Signal-to-Noise Ratio (SNR) [15] that comes from: (1) folding the entire noise that are not filtered out by the band selected filter to the desired signals bands only; (2) the clock jitter in the ADC.
- Require a high quality (expensive) analogue BPF's after the antennae to remove all noise from the received signals so to avoid the noise being folded back with the signal.

However, the BPSR architecture has desirable properties for handling multi-signal, which are:

- Multi standard signals can be down-converted directly, *at the same time*,

to the digital domain without tuning/changing the receiver components.

- The channels in the digital part of BPSR can be easily selected the desired signal/signals by utilising a LPF/BPF in the digital domain.
- Completely flexibility/reconfigurable and can be employ different software for different signal standard in the digital domain.
- Sampling frequency is proportional to the summation information-bands of the received signals, rather than the highest frequency value.
- Its implementation is simple and smaller size, since it does not require analogue components such as VCO and mixer.

Therefore, in all of our multi-signal receiver designs, the BPSR architecture is chosen to be our selected front-end.

2.2 Literature Review of Recent Multi-Signal BPSR Implementations

One of the first approaches that combined L1 and L2 GPS signals in a single front-end/receiver using BPSR technique was designed by choosing a high sampling frequency "800 MHz" [16]. The sampling frequency was adopted high for digitising the two signals due to the wider bandwidth between the two signals bands, where the L1 and L2 bands centre on 1575.42 MHz and 1227.60 MHz respectively. The sampling frequency has chosen high based on the double of the bandwidth "400 MHz", which is not the sum of the bandwidth of the two signals; but is the width of the lower band of the L1 signal and the higher band of the L2 signal. The front-end of this approach comprised two main stages; sampler and pre-correlation. In the sampler stage, the two singles are firstly amplified by two LNA's and then their out-band noise is filtered out by two BPF's. A single ADC then digitised the filtered RF signals. The digitised signal is then passed to pre-correlation stage, which includes two FIR filters that are utilised to separate the signals and also to decimate the signal samples to 25 MS/s. However, manipulating samples at that rate of "800 MHz" is a complex discrete processing that is computationally expensive.

An alternative efficient method of using BPSR technique is to fold information band of the desired signals only, which will significantly reduce the sampling rate.

This means the BPSR front-end allows folding the information bands of different signals only (which have wide separation frequencies in the RF spectrum) near to each other in the FNZ. The challenging issue in this new method is to select sampling frequency that can find the position of the signals in FNZ without overlapping between their information bands with the signal itself.

Mathematical formulae have been offered to find appropriate sampling frequency that directly allows folding/digitising multiple signals, which have non-adjacent frequency bands in RF, to non-overlapping area in the FNZ. In addition, the same formulae are used to calculate the folding/IF-frequency of each signal in the FNZ [8]. This solution is considered the keystone for all recent front-end designs that rely on BPSR approach to handle multi-signals. The same authors have moved on to design a front-end that has ability to handle two signals at the same time with low sampling frequency. The receive two distinct RF signals are GPS-CDMA (1575.42 MHz) and GLONASS-OFDM (1605.656 MHz), and the sampling frequency that use in this front-end is only equal to 24.205 MHz, so both information bands of the GPS and GLONASS signals will fold back to the FNZ at 2.095 MHz and 8.1260 MHz respectively [17].

Similarly, the same authors have designed a multiple frequency to improve the GNSS positioning performance by doing ionospheric corrections. The front-end of this receiver has been designed to handle three GPS signals, which are L1 (1575.42 MHz), L2 (1227.6 MHz) and L5 (1176.45 MHz). Based the BPSR formulas for selecting the folding frequencies possible for any multi signals (see Section 2.1.4 for details), the sampling frequency calculated for folding the signals information bandwidth to the FNZ without overlapping is 221 MHz. The receiver's front-end includes 3 BPF's with 24 MHz bandwidth for each filter and single ADC [18].

In the same vein, a multiple frequency GNSS receiver has been designed to capture three GNSS signals, which are L1/E1, L2 and L5/E5. The aim of this work is to analyse the noise, gain and linearity of the RF components to minimise the sampling frequency [19]. The three signals are processed through three independent channels, where each channel includes LNA and BPF to amplify the signals and then remove the out-of-band noise. The filtered signals are then combined and sampled by

single ADC that operates at sampling frequency equal to 227 MHz.

Undoubtedly, the aliasing-noise and the jitter noise are directly proportional to the selected sampling rate; that means choosing a low sample rate will increase the noise. Quadrature BandPass Sampling Receiver (GQBPSR) has been designed for reducing the aliasing-noise [20] and the jitter noise [21] to promote the effective sampling rate. The GQBPSR includes two branches (I- and Q-branch), and in each, one of them there is a sampler. Therefore, the received signal goes through two samplers that use the same sampling rate, but one of the samplers is delayed by certain time (in special implementation the delay time is sometimes chosen as 1/4*fc, where fc is the carrier frequency of the received signal). The sampled signals are then combined by a moving average FIR filter [22], and that will effectively double the number of samples (doubling sampling rate) and halving/reducing the aliasing-noise.

Despite the GQBPSR receiver efficiently reducing the aliasing-noise, but it becomes limited to addressing the noise problem in nonlinear scenario. The nonlinearity will affect the FIR filter performance and also the harmonic and intermodulation of the sampled signals will fold back to the different NZ, which could be located in the in-band of the desired signal spectrum.

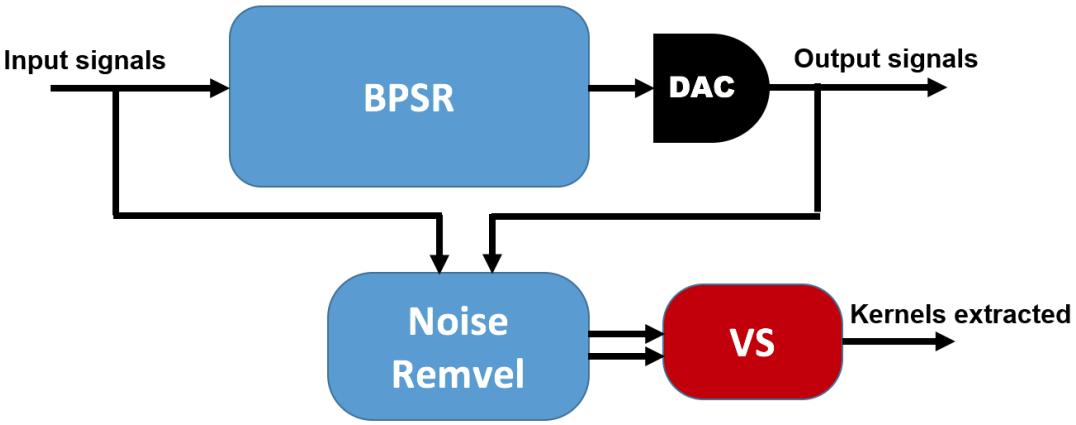

Figure 2-7 Block diagram of model BPSR based on VS

Therefore, the simpler and easier way to analysis and simulate the nonlinear BPSR is to use a behavioural model. The behavioural model plays an important role in studying and designing a linearization technique that can be used to overcome the

effects of nonlinear distortion. The first behavioural model that mathematically describes the nonlinear behaviour of wideband BPSR was based on using Volterra-Series (VS) [23]. This model helps to understand and characterise the BPSR in terms of nonlinear distortion and extra noise that comes from quantization error in ADC. Figure 2-7 shows the experimental setup that use to evaluate the accuracy of VS model that describing the BPSR under nonlinear scenario.

VS is defined as an approximation model to describe any nonlinear system, as shown in below mathematical equation, where *x(t)* and *y(t)* are the input and output respectively, and h(t) are the Volterra kernels.

$$y(t) = \sum_{n=0}^{\infty} \int_{-\infty}^{\infty} \dots \int_{-\infty}^{\infty} h_n(\tau_1, \dots, \tau_n)\, x_{in}(t-\tau_1) \dots\, x_{in}(t-\tau_n)\, d\tau_1 \dots\, d\tau_n$$

To obtain valid characteristics to the nonlinear behaviour of the BPSR, VS kernels need to be extracted and the way of extract it as followed:

The analogue signals are firstly fed to the BPSR. The output digital signals of the BPSR are converted back to the analogue in order to compare with input signals, which is an analogue. Ideal Digital-to-Analogue Converter (DAC) is used to convert the BPSR's output. Since the output signal is strongly effect by noise, which will make the VS kernels are impractical to extract. Therefore, a noise removal approach is used in the frequency domain to clean the signal as followed:

- Both signals (BPSR's input and output) are fed to the FFT separately.
- Select only the interest frequency bins of both signals in the frequency domain.
- Use IFFT to convert back the signal to the time domain, most of the undesired frequency are eliminated by this approach, which will facilitate to calculated VS kernels.
- VS is applied to these new input and output signals and then the desired VS kernels are calculated by least square method.

In this model, VS has been truncated at the third-order nonlinearity and the memory taps that used to describe the nonlinearity in the first, second and third

harmonics of the signal was the same amount of memory. That has led to achieve identical matching between the simulated data of the mathematical behavioural mode based-VS and the measurement data of the BPSR at higher frequency, but that matching is a slightly less at lower frequencies.

The same authors have been proposed a new approach to overcome this problem by applying the same mathematical model "VS", with a modification of extracting kernels procedure by applying a cluster to the signal based on its harmonics order [24]. Four clusters are used in the new approach; which are the baseband, the fundamental, the 2^{nd} harmonic, and the 3^{rd} harmonic. For each cluster there are different amount of memory tap, i.e., different number of VS kernels will be extracted. This new approach has estimated the kernels well such that the data of the mathematical behavioural model “VS model” and the measurement data of the BPSR model are identically in all frequency bands, at the higher or lower frequencies. Furthermore, the new approach "model based-VS" is flexible and can be generalised to cover higher NZs and also can be used to model a multi-carrier wideband BPSR [25]. Despite of that succeed, increase the memory length will exponential increase in the number of unknown parameters (kernels), which will make the model complicated.

We have found that this model is very helpful model to understand the behaviour of the BPSR as a single quantity/black-box. Therefore, we can go further with this mathematical model to do a track and decode the transmitted data with a single function in the digital domain such as using Kalman model [26], which means using a single front-end and back-end to process multi-signals. This project needs more study and analysis; therefore, it has been scheduled as a future work.

In this work, we have applied VS as an approval mathematical model to evaluate our GNSS early-detection approaches.

2.3 Our Two Approaches for GNSS Signals Early-Detection

As detailed in Section 2.2, all the aforementioned multi-GNSS receiver

implementations were designed to handle signals that transmit at different frequency bands. While, our work is concentrated on the GNSS signals that share the same frequency band, which are GNSS L1-signals (1- GPS CA-BPSK, 2- Galileo-OS-BOC (1, 1), 3- GLONASS-OS-BOC (2, 2); *where CA, BPSK, OS, and BOC stand for Coarse Acquisition Code, Binary Phase Shift Keying, Open Service, and Binary Offset Carrier).* More specifically, this work centres on detecting the multi-GNSS signals at an early stage to turn off the unrequired acquisition channels. Note that, the existing receivers can only distinguish between those type of GNSS signals (GNSS L1- signals) based on their spreading code. i.e., correlating their codes with locally generate code, but that exploiting a lot of the receiver resource for looking for signal could be not present. Therefore, our multi-GNSS receiver approaches will avoid chasing any signals that do not available. These approaches are jointly developed with my co-research colleague Mr. Ali Albu-Rghaif [27].

1- The first approach: the information bandwidth of the three GNSS L1- signals will be folded to the FNZ with guard band to isolate between the fundamental frequency of the signals and their 2^{nd} and 3^{rd} harmonics based on choosing sampling rate equals “92.07 MHz”, as shown in Figure 2-8.
2- The second approach: Because all three GNSS signals are transmitted with the same carrier frequency, this approach filters out the right-side-lobe of the GLONASS signal and the left-side-lobe of the Galileo signal. This will enable none overlapped folding of these two signals with the 3^{rd} GPS harmonic in the FNZ based on BPSR technique, as depicted in Figure 2-16. The sampling frequency of this approach is 34.782 MHz.

The MATLAB simulation of these signals (GPS+Galileo+GLONASS) is based on the mathematical representation that details in [28]. Table 2-1 shows seven scenarios are used to test each of the two approaches. These scenarios are based on satellite transmissions from GPS (CA-BPSK), Galileo (OS-BOC (1,1)) and GLONASS (BOC (2,2)) using code division multiple access (CDMA) with a centre frequency of 1575.42 MHz.

2.3.1 BPSR Non-Linear (BPSR-NL) Approach

Figure 2-8 shows the block diagram of the BPSR-NL approach setup, as it

implemented in MATLAB platform. Simulated GNSS signals, for each of the seven scenarios (see Table 2-1) are fed to additive White Gaussian Noise Channels (AWGN). These signals are then processed by a BPSR implementation that includes a BPF, LNA and an ADC. The BPF is cantered at L1-frequency of 1575.42 MHz, with a 10 MHz band, to filter out undesired signals. A 10 MHz band is chosen so to include all three GNSS bands (2 MHz-GPS band, 4 MHz-Galileo band and 8 MHz-GLONASS band). All passed signals are then amplified by the LNA (+10 dBm compression point, 35 dB gain and 3 dB noise figure). A 10-bit ADC, with 92.07 MHz as a sampling frequency, is then used to digitize these signals. This initial sampling frequency is chosen to prevent overlapping between the fundamental frequencies of these signals and their harmonics in the FNZ.

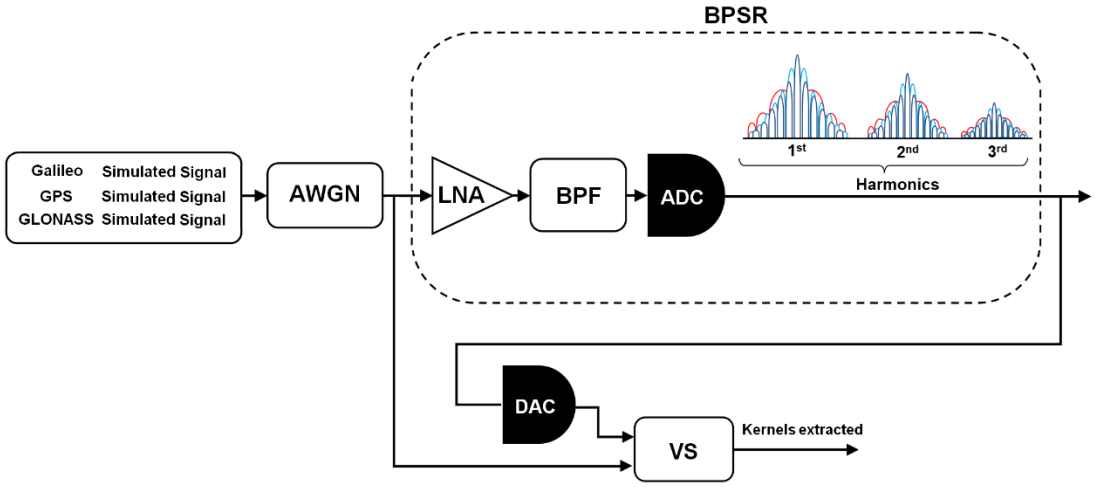

Figure 2-8 Block diagram of the multi-signal BPSR-NL

Furthermore, since the received GNSS signals are sharing the same carrier frequency, the intermodulation distortion/signals will not produce as a result of the non-linearity in BPSR, but the non-linearity will only create fundamental frequencies and their harmonics frequency in the FNZ. These harmonics are generated from the non-linear behaviour of the LNA and based on our design, the fundamental, the second harmonies, and the third harmonics frequencies of the received GNSS signals will be folded and located at 10.23 MHz, 20.46 MHz and 30.69 MHz respectively. As we mentioned in the literature review Section 2.2, VS is the accurate mathematical model that can express the non-linearity of the BPSR. Therefore, we will follow the same VS setup in [24] in order to evaluate the obtained signal power of our approach with simulated results of VS model.

The non-linearity in LNA is modelled in this approach by third-order polynomial, as follows:

$$v(t)_o = v(t)_o + v(t)_{in}^2 + v(t)_{in}^3,$$

where $v(t)_o$ is the output signal form LNA and $v(t)_{in}$ is the input signal.

Table 2-1 Seven test scenarios for evaluating early-detection approaches

Scenar	GNSS Signals Present	Single Available	NMSE (dB)
1	**GPS + Galileo + GLONASS**	**3**	**-38.19**
2	**GPS + GLONASS**	**2**	**-39.72**
3	**Galileo + GLONASS**	**2**	**-35.26**
4	**GPS + Galileo**	**2**	**-42.20**
5	**GLONASS**	**1**	**-39.30**
6	**Galileo**	**1**	**-43.05**
7	**GPS**	**1**	**-46.11**

The BPSR-NL approach finally detects the status of the available GNSS signals based on the extracted values of the kernels. i.e. the changing power distribution in the input and output signals of the BPSR "fundamentals and their harmonics" will result in different combinations of VS kernels unique to the input GNSS signals present. Therefore, for each of our 7 GNSS-signal scenarios, unique power distributions with different kernel values have been obtained, as documented in the following results discussion.

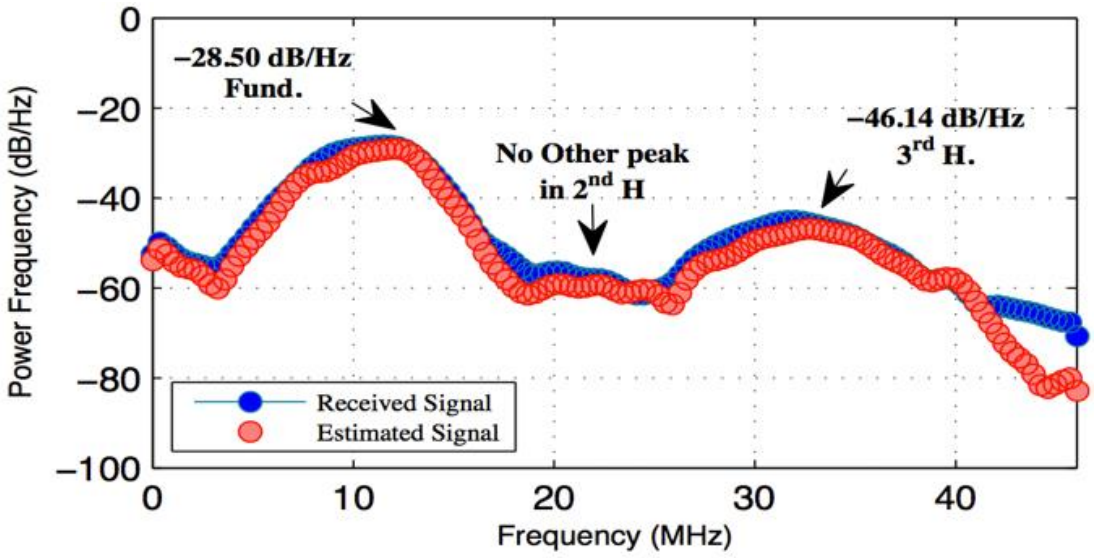

Figure 2-9 VS Estimation of GPS, Galileo and GLONASS Signals

GPS + Galileo + GLONASS Signals: Figure 2-9 shows the frequency domain simulated result of the first test scenario. The estimated behavioural model of VS is close enough to the BPSR behaviour based on the extracted kernels parameters in each test scenario, and the Normalized Mean Squared Error (NMSE) of the seven scenarios is around -40 dB (see Table 2-1). The NMSE is used as a parameter to evaluate the performance of the estimation between the original BPSR model and the VS model [29]. The distribution power of this test scenario in frequency domain includes two peaks only; one at the fundamental band and the other peak at the 3rd harmonic band.

GPS + GLONASS Signals: based on BPSR-NL approach design, if the GLONASS signal is one of the input signals, the output signals will have peaks in the fundamentals and the 3rd harmonic band only. i.e., the peaks in the 2nd harmonic band will fade out under the noise level. Note that, the simulation result of the first and the second test scenarios is almost identical, as shown Figure 2-9 and Figure 2-10; however, there is a different in the 3rd harmonic power by 4 dB. Therefore, in the DPS domain will shut down the Galileo channel and prepare two channels, one for the GPS and the other one for GLONASS.

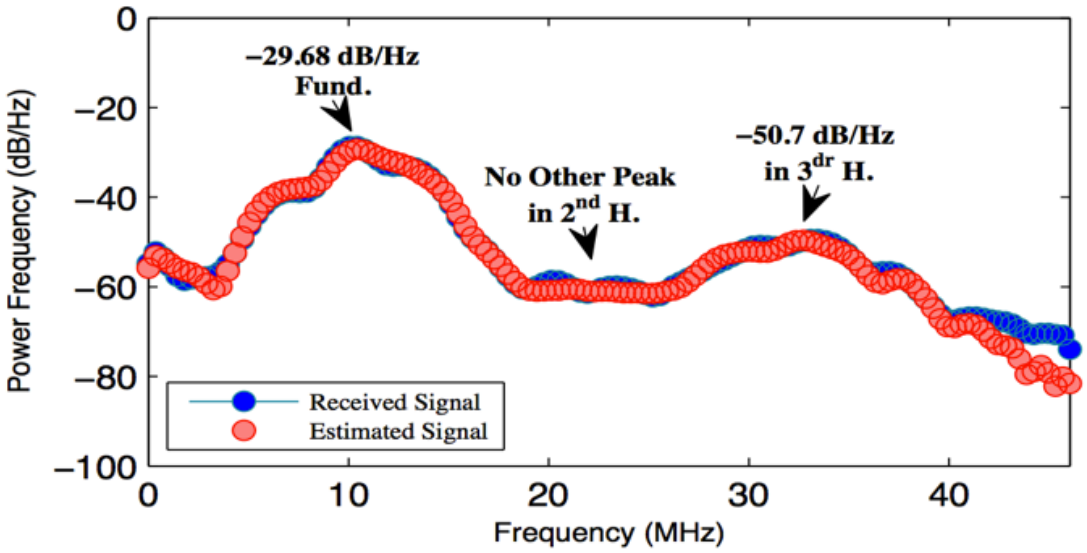

Figure 2-10 Received and VS Estimation for GPS and GLONASS Signals

Galileo + GLONASS Signals: Galileo and GLONASS signals use BOC modulation with different subcarrier frequency and the GPS signal uses BPSK modulation. Therefore, if the combination does not include a GPS signal then two peaks power will be present in the fundamental band and one peak in the 3rd harmonic band, as shown in Figure 2-11.

GPS + Galileo Signals: in contrast to the previous test scenario, any combination of two signals that include GPS will have only one peak power in the fundamental band, and one peak in the 2nd and the 3rd harmonics, as illustrated in Figure 2-12.

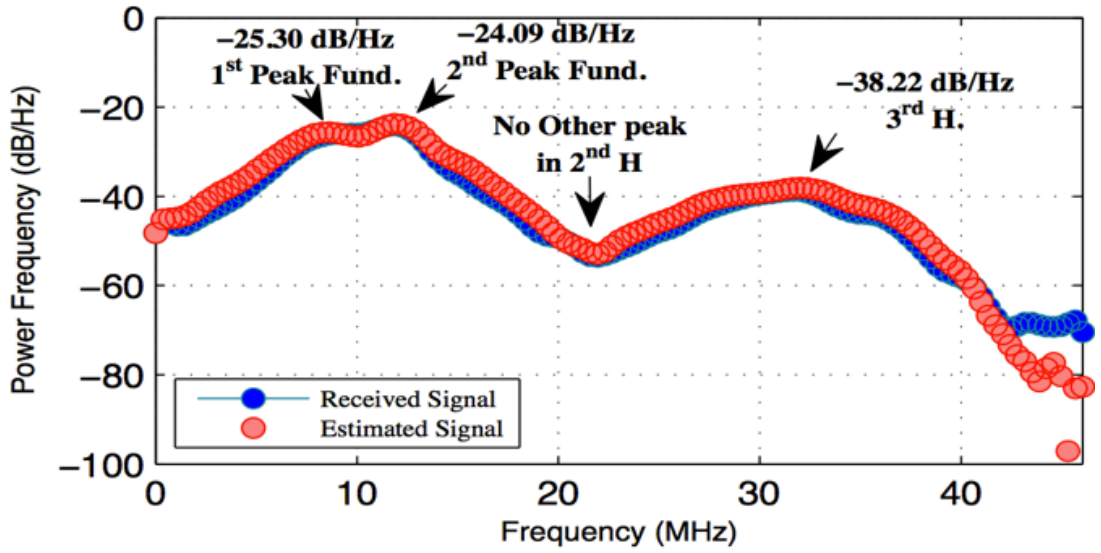

Figure 2-11 Received and VS Estimation for Galileo and GLONASS Signals

GLONASS Signal: Figure 2-13 shows that the power peaks of received GLONASS signal in the fundamental band is located away from the centre frequency by ±2.046 MHz, and there are no power peaks in the 2nd harmonic band. While, there are two power peaks in the 3rd harmonic, and their location are also away from the centre frequency of third harmonic by ±2.046 MHz.

Galileo Signal: Figure 2-14 illustrates that there are two power peaks of the received Galileo signal in the fundamental band and their location are away from the centre frequency by ±1.023 MHz. In contrast to the GLONASS's test scenario, there is a power peak in the 2nd harmonic place of the received Galileo signal. Further, the power in the 3rd harmonic location either two peaks or one peak, it depends on the noise level and both cases the location of this power peak is far away from the centre frequency of the 3rd harmonics by ±1.023 MHz.

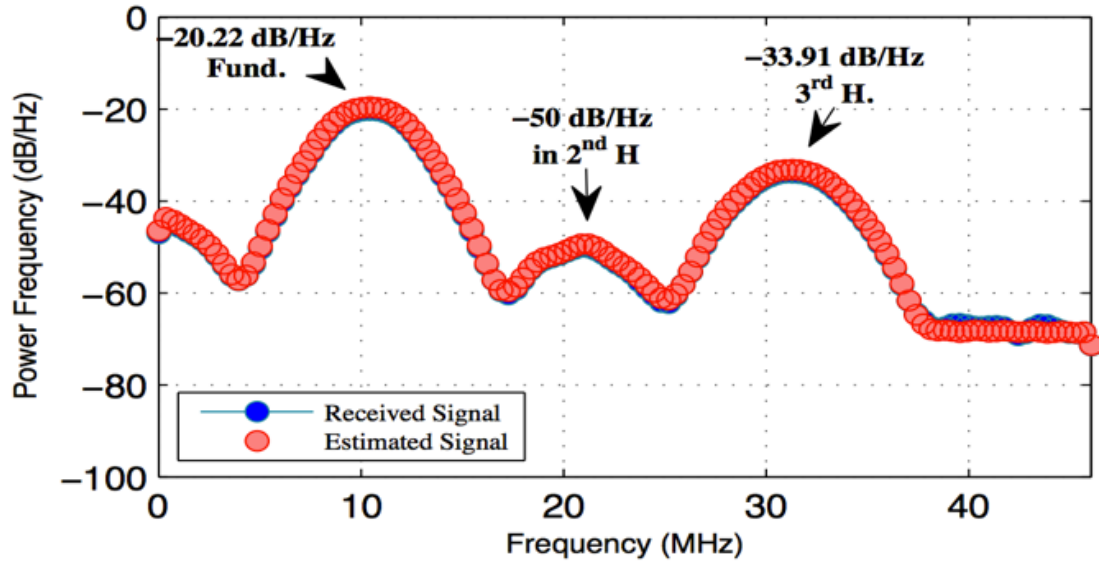

Figure 2-12 Received and VS Estimation for GPS and Galileo Signals

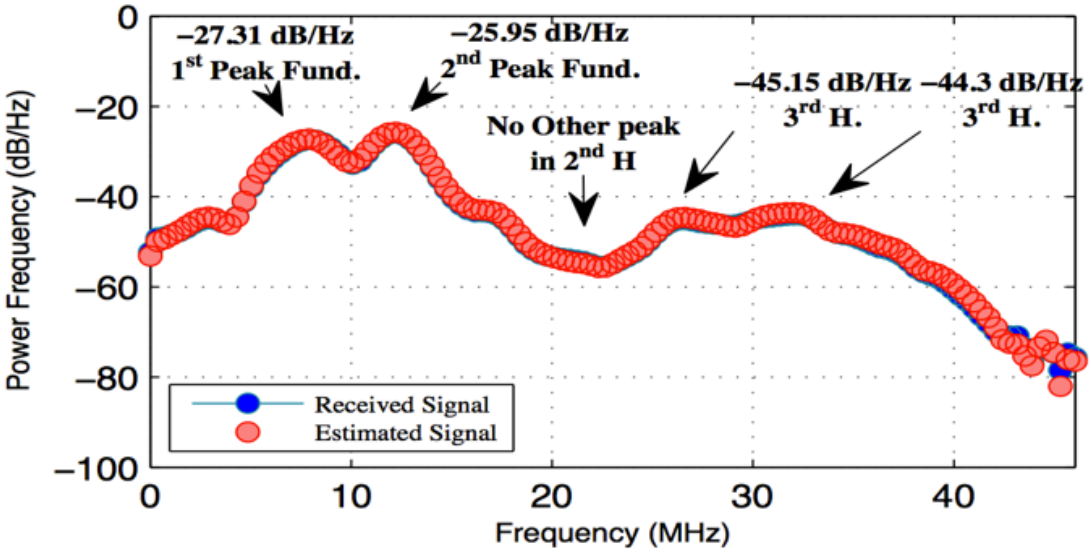

Figure 2-13 Received and VS Estimation for GLONASS Signal

GPS Signal: Figure 2-15 displays the power spectrum of the received GPS signal in FNZ. There are three power peaks and each one of them is locate at the centre frequency of the fundamental, 2nd harmonic and 3rd harmonics band, which will make it easy to distinguish between the pervious test scenarios.

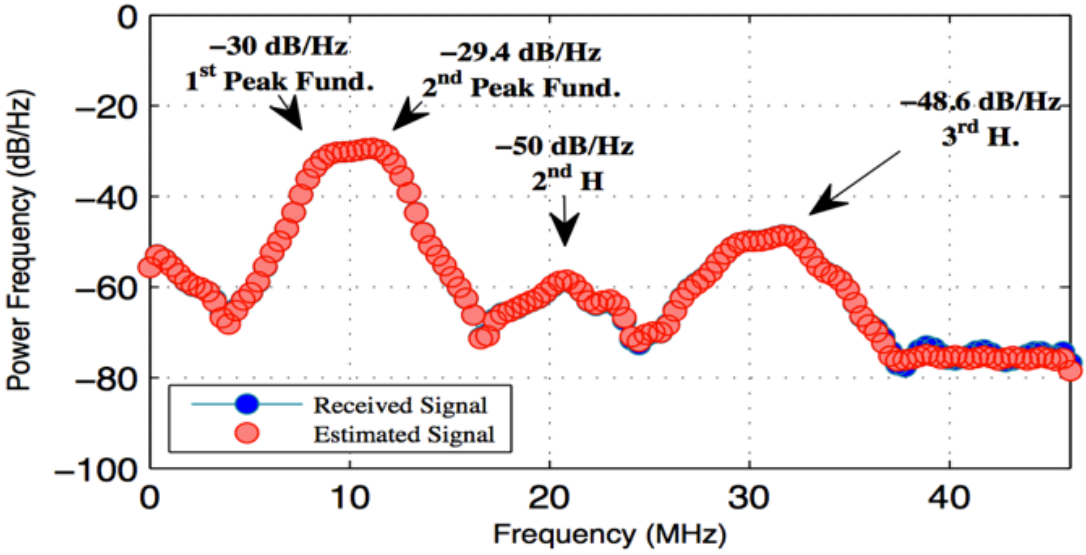

Figure 2-14 Received and VS Estimation for Galileo Signal

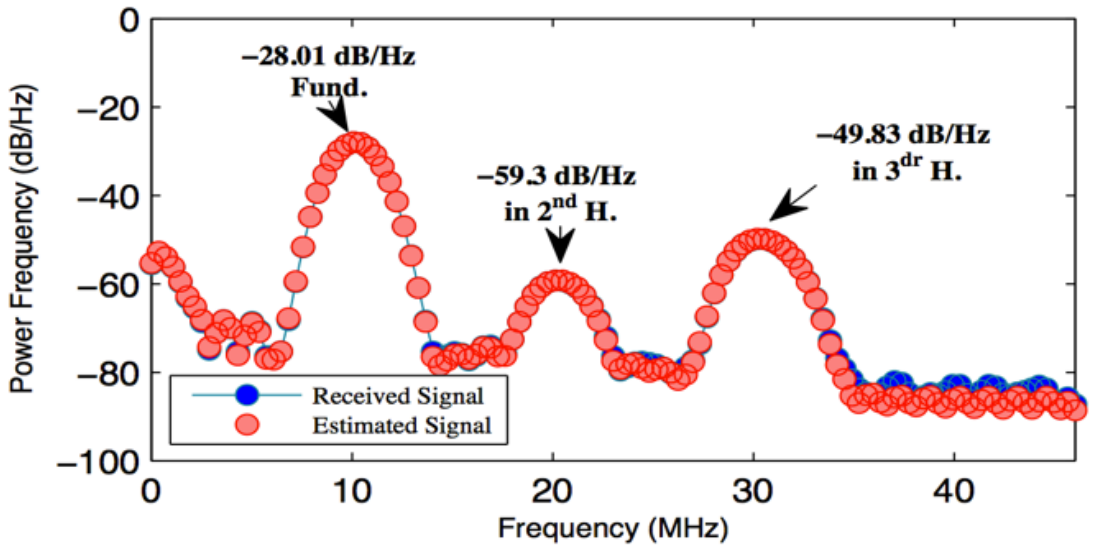

Figure 2-15 Received and VS Estimation for GPS Signal

2.3.2 BPSR-Side Lobe Filtering (BPSR-SLF) Approach

The aim of this approach is the same as the first approach in detecting the availability of the GNSS signals based on their power peaks that present in the FNZ; but the mechanism has developed by placing pre-processing stage. The main aim of the pre-processing stage is to remove the overlapping between all the folded GNSS signals in the FNZ by filtering one of the symmetric signals lobes, so that will facilitate the detection. This stage contains three BPFs that used to pass the right

single-sideband (SSB) of the Galileo, the left SSB of GLONASS and the third harmonics of the GPS signals. The SSB is produced by modulation the subcarrier frequency in the BOC modulation that will split the power spectrum of the BOC signal into two symmetrical components around the centre, therefore by removing one of them will not effect on the signal's data or code. This approach filters out the left-SB of the Galileo signal and right-SB of the GLONASS signals. The reverse is also possible with different sampling frequency that guarantee non-overlapping between the three filtered GNSS signals. The rate of the sampling frequency will be reducing to be less based on the result of the detecting GNSS signals.

Figure 2-16 shows the block diagram of the BPSR-SLF approach setup, as it implemented in MATLAB platform. The simulated signals are passed through a nonlinear channel. The first three BPFs, in the pre-processing stage, are used to get the right-SB of the Galileo signal, left-SB of the GLONASS signal and the 3rd harmonic of the GPS signal. The LNA (38 dB, 3 dB noise figure and IIP3 24 dBm) is to amplify the filtered GNSS signals in a similar way to the LNA model mentioned in 2.3.1. Then, the amplified signals are converted by a 10-bit ADC converts with sampling frequency of 34.782 MHz.

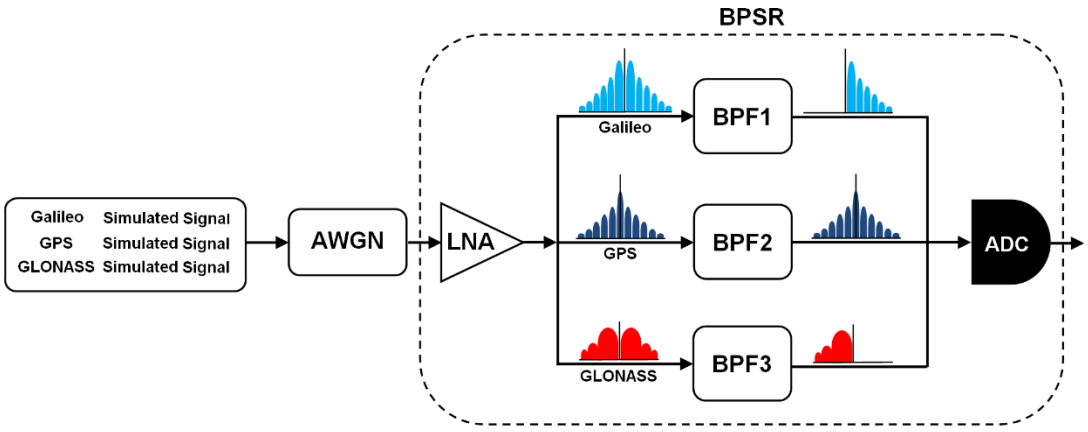

Figure 2-16 Block diagram of multi-signal BPSR-SLF

The seven test scenarios shown in Table 2-1 are used to assess the BPSR-SLF approach. As we mentioned earlier, the BPSR will treat the input signals as three distinct GNSS signals. This means each signal has a separate folding-frequency (or distinct power peaks) in the FNZ. The 1st power peak is cantered at 4.092 MHz (GPS

signal) with bandwidth of 2 MHz, the 2nd power peak is at 8.184 MHz (GLONASS signal) with a bandwidth of 4 MHz, and the 3rd power peak is at 11.253 MHz (Galileo signal) with a bandwidth of 2 MHz. There is no overlapping between these power peaks.

Three signals scenario: based on the first test scenario in Table 2-1, the three signals are presented. Figure 2-17 proves that the BPSR-SLF approach detected three signals power peaks in the FNZ. Obviously, there are three distinct peaks are located at specific 3 folding-frequencies in the FNZ, which are representing the three available signals.

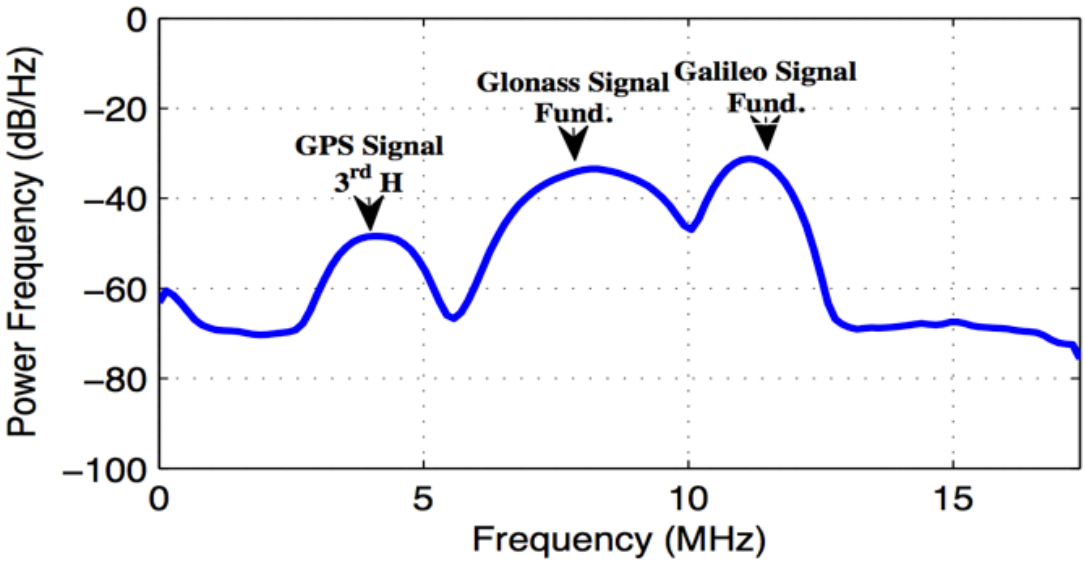

Figure 2-17 Power spectrums of GPS, Galileo and GLONASS signals

Two signals scenario: the results of the test scenarios (2, 3 and 4) are illustrated in (Figure 2-18, Figure 2-19, and Figure 2-20) respectively. The simulation results prove that there are two distinct power peaks for any the two received signals. So, based on the location of the folding-frequency, the unrequired channel will be turned off in the receiver.

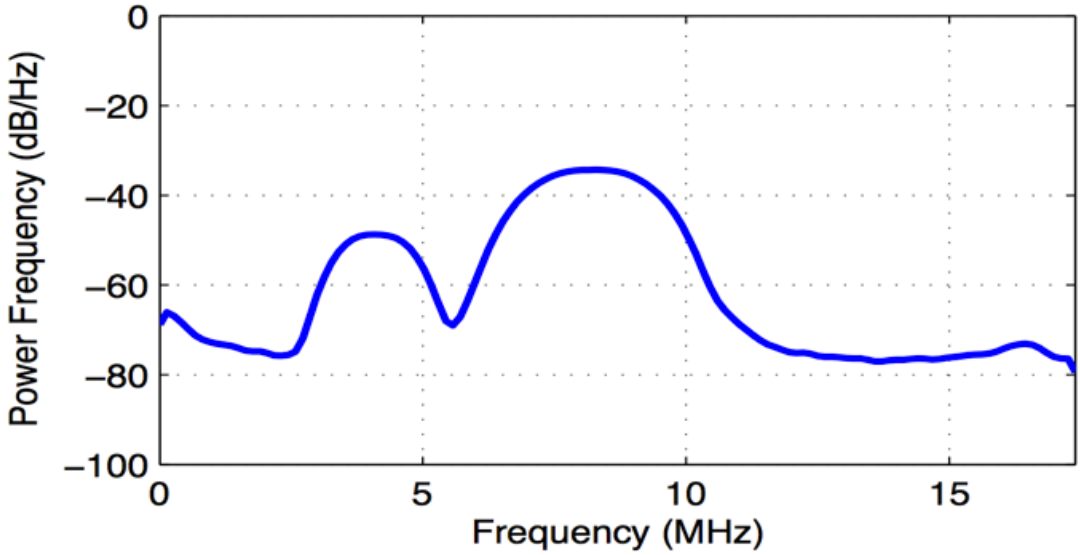

Figure 2-18 Power spectrum of GPS and GLONASS signals

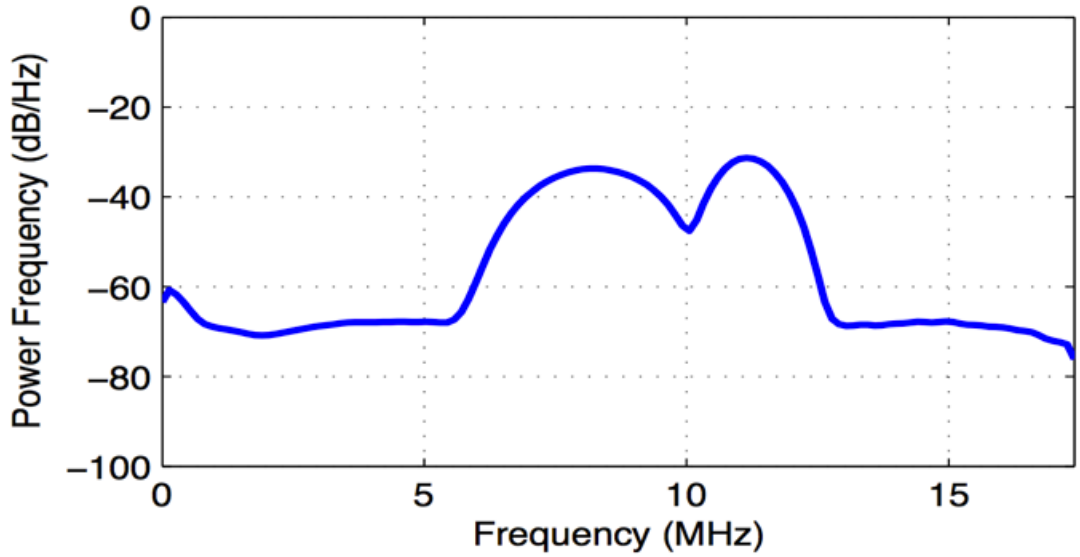

Figure 2-19 Power spectrum of Galileo and GLONASS signals

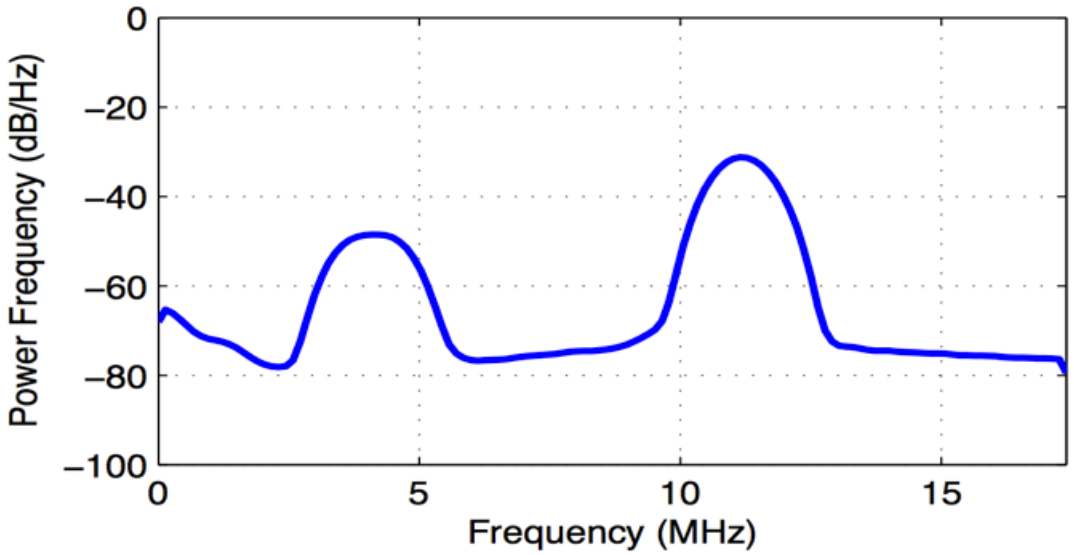

Figure 2-20 Power spectrum of GPS and Galileo signals

One signal scenario: the simulation results of the remaining test scenarios (5, 6 and 7) are presented in (Figure 2-21, Figure 2-22 and Figure 2-23) respectively. These figures prove that there is a single power peak that present in the FNZ for each received signal. The location band of the power peak will be indicated the type of the received GNSS signals.

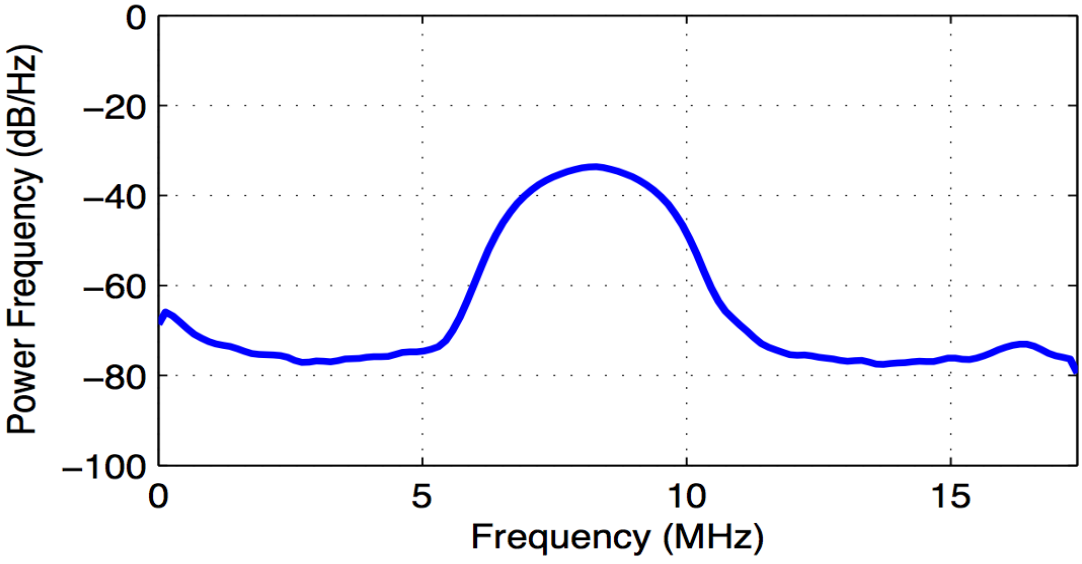

Figure 2-21 Power Spectrum of GLONASS Signal

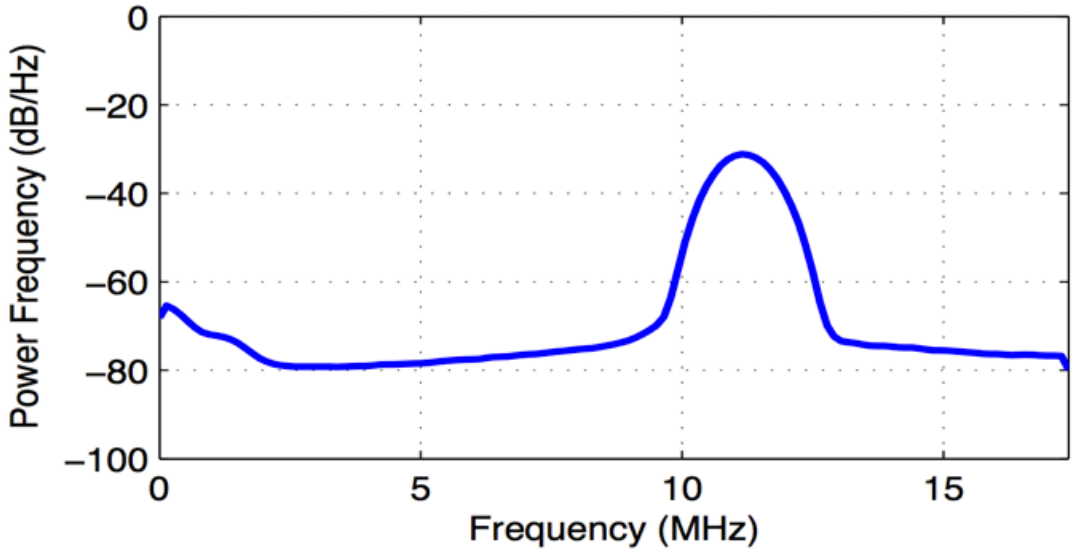

Figure 2-22 Power Spectrum of Galileo Signal

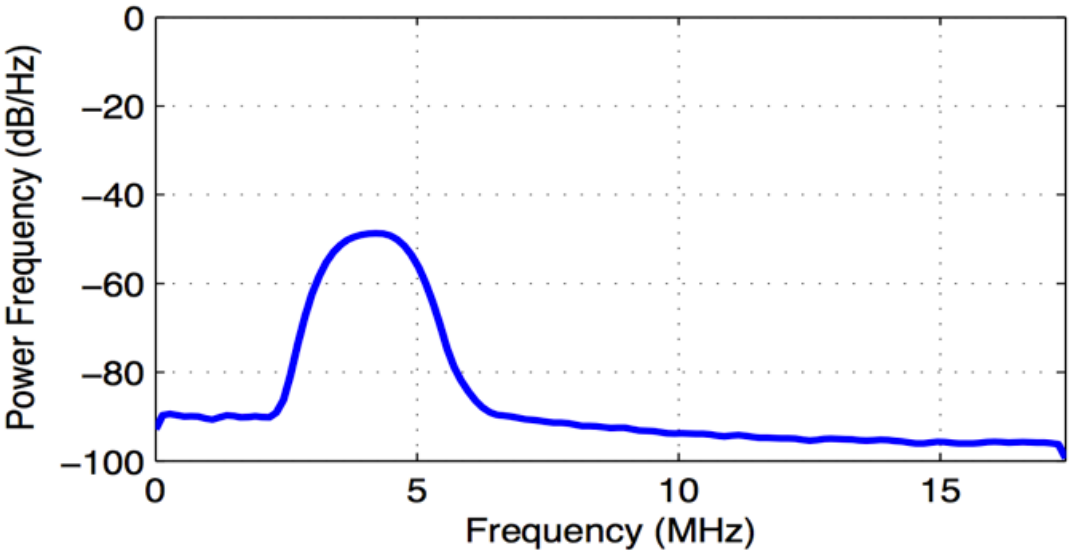

Figure 2-23 Power Spectrum of GPS Signal

2.4 Concluding Remarks on Multi-Signal Receiver

In this chapter, after reviewing the most common receiver architectures, BPSR has been chosen as a best candidate for handling multi-signal. Further, two approaches were designed, as in a rapid-early signals detection, to find the present signal of three L1 GNSS signals (GSP, Galileo, and GLONASS), thus eliminating the need to process signals that are not actual present at the time, that has saved valuable resources.

The first detection approach was using a BPSR to fold the three signals with their harmonics to FNZ without overlapping with each other and that is based on choosing sampling frequency equals to 92.07 MHz as calculated by the BPSR formulas (see Section 2.1.4); i.e. the power of the signals at fundamental frequency has not overlap with power at second and the third harmonics. This made the signal detecting easy based on the available power on the location of the fundamental and harmonics of the folded GNSS signals.

The second detection approach was based on using filtering to remove the left-sideband and the right-sideband from the Galileo signal and the GLONASS signal respectively. This has prevented the overlapping between these two folded signals with the 3rd harmonic of the GPS signal in the FNZ with choosing a sampling frequency equals to 34.782 MHz as dictated by the rules for BPSR technique of non-overlapping folded signals. That made the power distribution of the folded signals unique, so it easily detects the available signals.

Chapter 3 Two New Orthogonal Multi-Signal Receivers

The literature survey (see Chapter 2, Section 2.2) has concluded that the BPSR provides a fixable front-end architecture that can digitises multi-signal at once and folds them back to the baseband zone without overlapping with each other. Therefore, the focus of this chapter is on designing a new multi-signal receiver, based on BPSR, that have the ability of capturing two or multi signals and then tracking them in a single channel simultaneously (our implemented scenario is for 2-signals receiver). The novelty of this work is centred on the Orthogonal Integrated Function (OIF) that continuously harmonies the two received signals to form a single orthogonal signal allowing the "tracking and decoding" to be carried out by a single Complex Quadrature PLL (CQPLL) [30] in the digital domain. Our new receivers are designed based on the first- and second-order of the BPSR technique, which are named Orthogonal BandPass Sampling Receiver (OBPSR) and Orthogonal Complex BandPass Sampling Receiver (OCBPSR) respectively. The OBPSR samples the signals based on the double of the maximum input signals bandwidth, while the OCBPSR samples the signals based on the maximum bandwidth of the input signals.

Note that BPSR requires choosing a sampling frequency at least double of the summation of their information bandwidth. Hence, the sampling frequency becomes large with increase in the number of required digitised signals and that will consume more processing time and power in the receiver resources, either to decimate or manipulate the digitised signals [8]. Furthermore, in order to satisfy the other BPSR restriction that state that the folded signals should not overlap with each other or with themselves; the sampling frequency will become larger.

For example, the appropriate sampling frequency, in the BPSR technique, to sample three of civilian Galileo signals, which are E1 (1575.42 MHz), E5 (1191.795

MHz) and E6 (1278.75 MHz), and their information bandwidths are 32 MHz, 40 MHz and 50 MHz respectively without overlapping is "434.775 MHz" [18]. In fact, there is a direct relationship between the power consumed and the sample rate [31], which is given by:

$$P \propto V^2 f_s$$

where P is the power consumption, V is the supply voltage and f_s is the sampling/clock frequency.

Furthermore, reducing the sample rate leads to reduced supply voltage [32] and that will enable more energy saving, where the energy is the time integral of power [33]. Therefore, our new orthogonal receivers design will be less costly (processing, power, area, etc.) than BPSR.

3.1 Orthogonal BandPass Sampling Receiver

Our OBPSR is designed to capture two signals simultaneously and process them using a single channel in the digital domain, such as tracking and decoding concurrently. In addition, the minimum sampling frequency is chosen based on the "double maximum bandwidth of the input signals" rather than the "double summation the bandwidths of the input signals"; thus reducing the number of samples and saving processing time and power.

3.1.1 Mathematical Representation of Our OBPSR

As shown in Figure 3-1, our 2-signals OBPSR architecture consists of two LNAs, two BPFs, a 90-degree phase-shifter and an ADC. The phase-shifter (such as Hilbert Transform (HT)) with the ADC make up the OIF that is used for harmonizing the orthogonality of the filtered received signals. As shown in Figure 3-2, the HT is used as the first stage for shifting the phase of the second received signal by 90-degree to prevent the signals overlapping prior to using the BPS technique. By choosing an appropriate sampling frequency, the second stage uses a BPSR technique to fold both received signals (now orthogonal) to the same fold-frequency in the FNZ. Thus producing an orthogonal baseband signal that is fed into a single CQPLL to track and decode the orthogonal signal. This makes both signals' information available at the

same time and effectively reducing the tracking channels in the digital domain to a half.

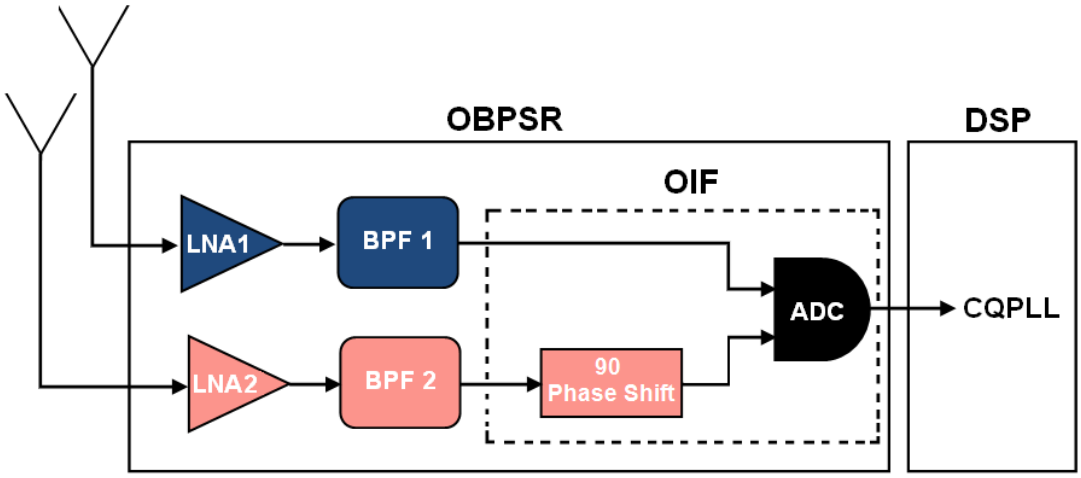

Figure 3-1 Structure of our OBPSR

In addition, the OBPSR can be used cluster the spectrum of the received signals based on choosing the sampling frequency that folds each two signals to one specific band in the NZ's. For instance, the proper sampling frequency based on our receiver design for three civilian Galileo signals E1, E5, and E6 is only 247.0545 MHz instead of 434.775 MHz, as we are mentioned in entry of this chapter, which almost the half. This is achieved by orthogonalising and folding the E5 and E6 signals at folding-frequency equal to 43.4775 MHz and the E1 folds alone at frequency equals 93.039 MHz. Note that, capturing three signals or more based on our OBPSR requires more testing and evaluating, therefore it scheduled as future works.

Equations (3-1) and (3-2) represent 2 BPSK bandpass signals S_1 and S_2 that are received through Additive White Gaussian Noise channel (AWGN).

$$S_1 = A_1 \cos(2\pi f_{c1} t + \overline{m_1}) + n_1 \quad (3\text{-}1)$$

$$S_2 = A_2 \cos(2\pi f_{c2} t + \overline{m_2}) + n_2 \quad (3\text{-}2)$$

where, $(A_1, f_{c1}, \overline{m_1}, n_1)$ and $(A_2, f_{c2}, \overline{m_2}, n_2)$ represent the amplitude, the carrier frequency, phase, and the Gaussian noise of the first and second signals respectively. And, m_1 and m_2 represent the information message of the first and the second signals respectively, and can be expressed as:

$m_1 = \pi(1 - b_1), where\ b_1 = 0{,}1\ bits$

$m_2 = \pi(1 - b_2), where\ b_2 = 0{,}1\ bits$

As described earlier, by applying HT to (3-2), and then added it with (3-1) that will generate a new signal that will be folded to the FNZ, which expressed in (3-4).

$$S_{dig} = \pm m_1\, cos(2\pi f_{fold} t) \pm m_2\, sin(2\pi f_{fold} t) + N \qquad (3\text{-}4)$$

where, S_{dig} is the orthogonal digital signal at the folding-frequency (f_{fold}) and it carries two different information massages m_1 and m_2. N represents the combined noise $n_1 + n_2$.

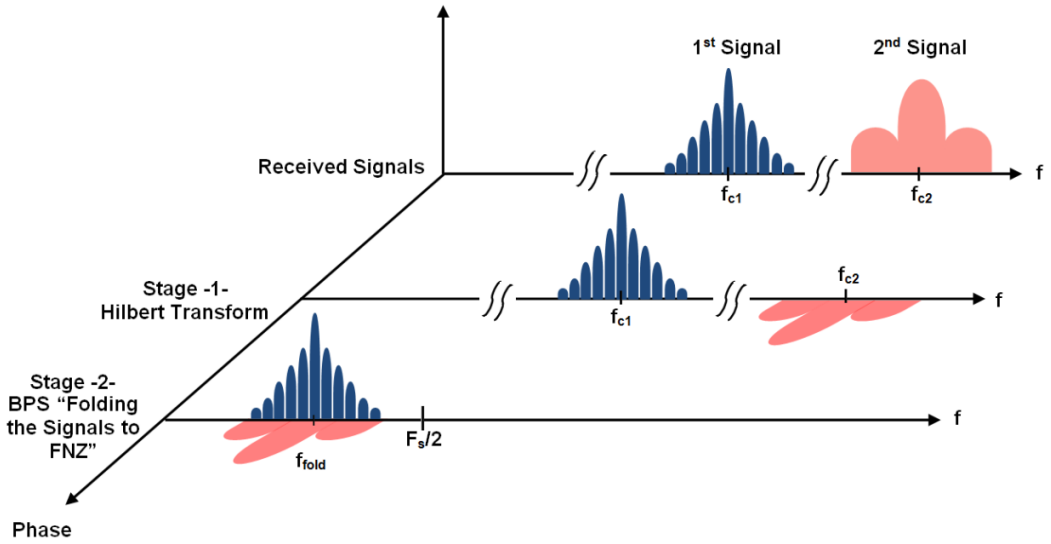

Figure 3-2 Frequency and phase representation of the OBPSR integrated function

3.1.2 Experimental Setup and Results

MATLAB is used to simulate our OBPSR. To represent the transmitted signals, two BPSK modulated signals with 4 MHz bandwidth are passed through a "root raised cosine filter" with a roll-off factor of 0.2. Two different carrier frequencies of 1575 MHz and 2400 MHz are used for the first signal and the second signal respectively. AWGN is then used to simulate transmission channel noise. Simulation is run for 1 *msec*, which represents 2000 bits of data. These two simulated signals once captured by their respective antennae, are passed through two LNAs and two narrow BPF's centred on carrier frequencies of 1575 MHz and 2400 MHz to

eliminate all frequencies outside the signals bandwidth. The resulted in-band signals are then fed to the OIF. Note that the phase of the signal with 2400 MHz frequency is shifted by 90-degree and combined with the other signal in order to digitize them, at the same time, by a 10-bit ADC, with 12 MHz sampling frequency. The sampling frequency is chosen so the ADC can fold the combined signal and its images to the desired zone; in our case, we selected FNZ (folding-frequency = 3 MHz), as shown in Figure 3-3. The output orthogonal digital signal is then processed through a CQPLL for tracking and extracting the information data/messages. Note that the CQPLL function is implemented in MATLAB too.

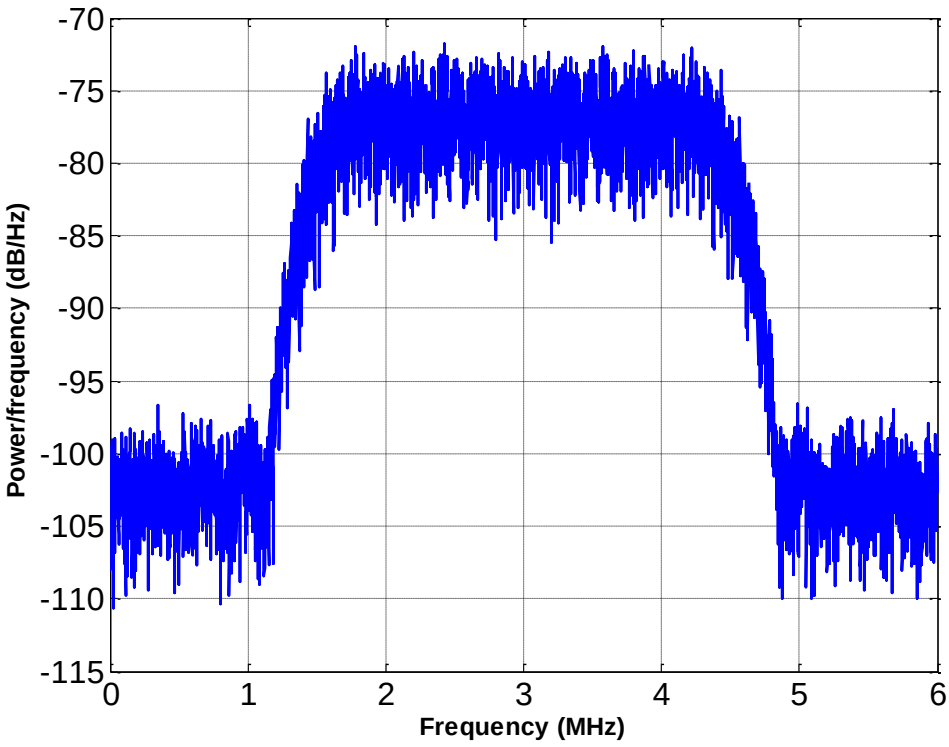

Figure 3-3 Power spectral density of the orthogonal signal in the FNZ band with 4 MHz

Figure 3-4 shows the CQPLL structure that consists of Phase Detector (PD), Loop Gain (LG), Loop Filter (LF), and Numerical Control Oscillator (NCO). PD includes 4 Multipliers, 2 LPFs, 2 Hard-limiter functions and 1 Adder. The received signal is processed through two branches; the output signal of the in-phase branch is multiplied with the output of the hard-limiter function of the quadrature component. The resultant signal is then subtracted from the multiplication of the quadrature

component of the baseband signal with output of the hard-limiter function of the in-phase component. This subtraction produces an error signal. This error signal is amplified and filtered by a LG and LF respectively, and then it is used to adjust the phase of the reference signal NCO with respect to the previously processed received signal. The output is then fed back to the PD block by the quadrature reference signal (I-arm & Q-arm) to close the loop.

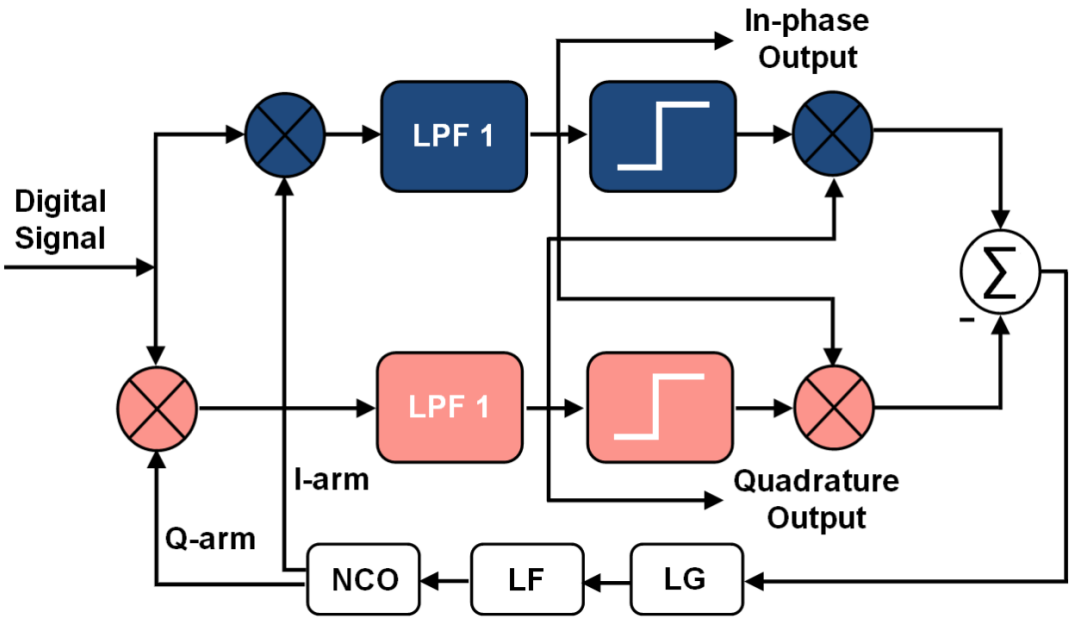

Figure 3-4 Costas Quadrature Phase Locked Loop (CQPLL)

Adjacent Channel Power Ratio (ACPR) [34], Bit Error Rate (BER) and Error Vector Magnitude (EVM) [35] are used to: (a) Analyse the effect of the OIF on the in-band/out-of-band of the desired signal spectrum in terms of the re-growth in bandwidth, the total power and the adjacent channels effect. (b) Check the behaviour of the CQPLL during tracking the orthogonal signals, and (c) Evaluate the overall performance of the OBPSR.

The following discussion documents our findings:

Readings of high and low ACPR measurements of the signals after and before the OIF are shown in Table 3-1. The results show a slight increase only in the main channel power around 3 dB, which proves that the spectrum of the OIF output signal (the orthogonal signal) has no re-growth outside its determined channel. Note that,

the ACPR values are slightly high but these are acceptable for our simulation example because ACPR values are depended on the type of the evaluated signal [36]. For example, the acceptable value for WCDMA signals is -45 dBc for high and low ACPR at 5 MHz offset, while acceptable value is –33 dBc for QPSK subcarrier modulation signal.

Note that, the value of the main channel power has increased by 3 dB after applying the OIF that means that the noise has also been increased by the same value. This extra noise has an insignificant effect on the OBPSR performance, as discussed in this section.

Table 3-1 simulated power measurement for the input and the output signals of our proposed architecture

	Power of the main channel	ACPR Low	ACPR High
1st signal before the OIF	**5.24 dBm**	**-34.61 dB**	**-34.59 dB**
2nd signal before the OIF	**5.20 dBm**	**-34.64 dB**	**-34.61 dB**
S_{dig} signal after the OIF	**8.26 dBm**	**-34.56 dB**	**-34.57 dB**

As shown in Figure 3-5, the CQPLL has a steady-state value during tracking the two received signals. This proves a successful process in the OIF to achieve the orthogonality between these signals. Otherwise, we will notice a significant fluctuation in the phase difference (unsteady-state) of the CQPLL due to the presence of offset frequency between the folding-frequencies of these signals in the FNZ. However, this stability in CQPLL does not mean that the estimated in-phase and quadrature-phase are identical to the actual value of the in-phase and quadrature-phase of the received signals. Therefore, the next point will discuss the results based on the BER.

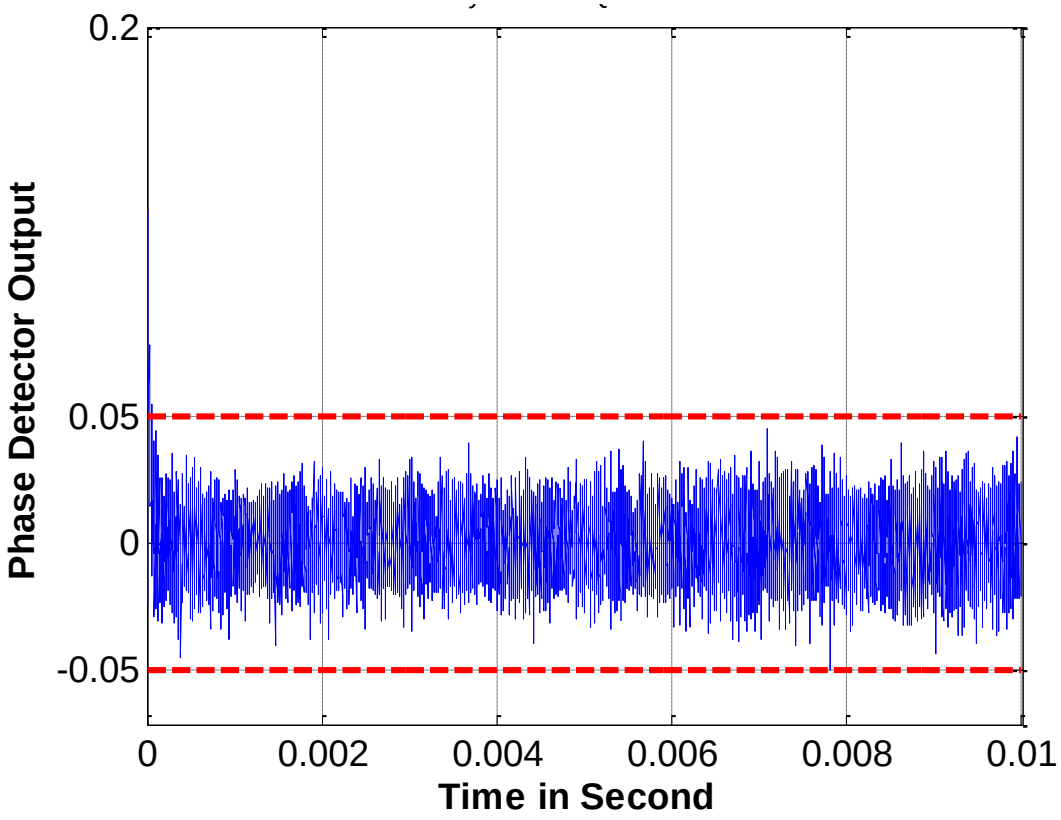

Figure 3-5 Discriminator stability of the CQPLL

The 3 dB extra noise (power growth in the main channel) gathered with our orthogonal signal is due to the OIF. The BER values versus the energy per bit to noise power spectral density ratio (Eb/No) is therefore measured, as shown in Figure 3-6, which illustrates a small increase in the value of the BER of the OBPSR in comparison with the theoretical value. Besides, the curve of the BER of the OBPSR is approximately identical to the curve of the BPSR. Note that the BPSR setup is same as the OBPSR (one input signal (BPSK)). Consequently, the extra noise has insignificant effect in the performance of our receiver.

The EVM is used to help us define the difference between the estimated complex voltage of the demodulated symbol and the value of the actual received symbol. The new phase of the orthogonal signal has been shifted up and down from its original position. The EVM can precisely examine the shifting operation of our OIF, as well as help to evaluate the effect of the ISI. In order to measure the EVM correctly, we have generated a reference signal based on (3-4), but without the noise, and this will be compared with the estimated signal using the BPSR setup. Table 3-2 shows the

values of the EVM_{RMS} and the maximum EVM peak of the OBPSR.

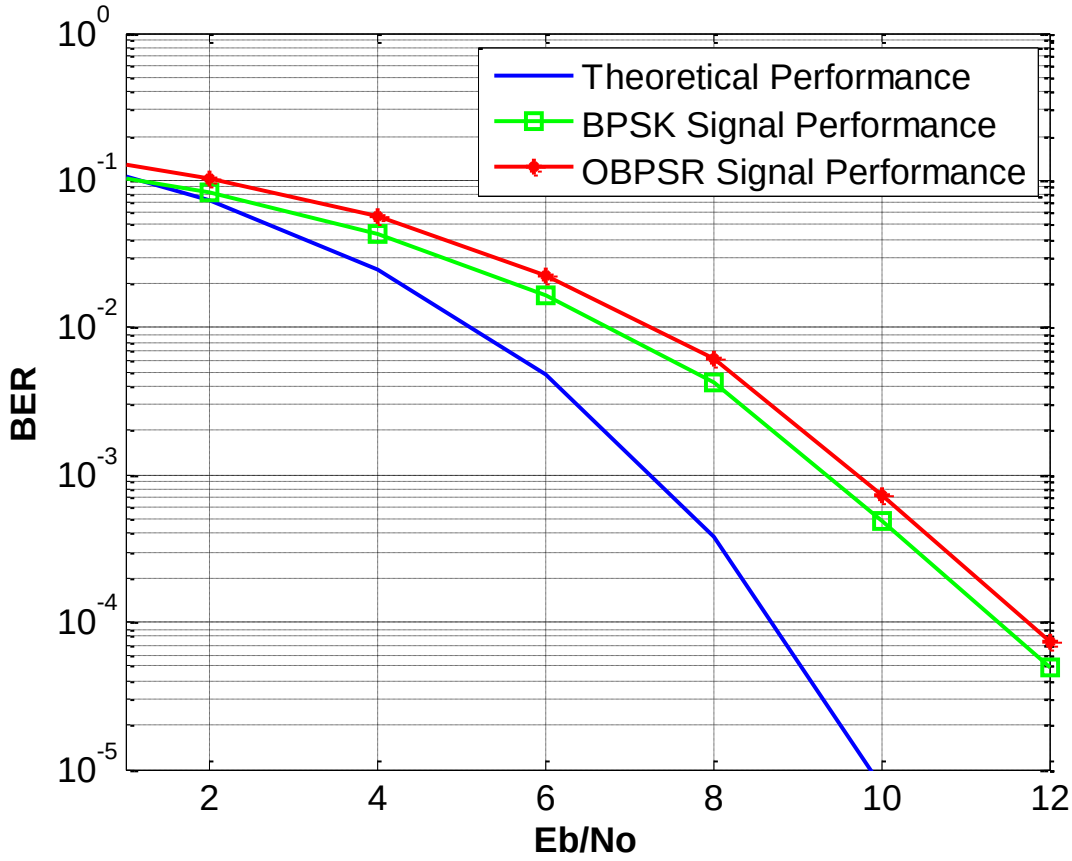

Figure 3-6 BER curves for theoretical, BPSK, and orthogonal signal, AWGN channel.

Table 3-2 EVM Values BPSK and Orthogonal Signal

	EVM_{RMS}	EVM max peak at symbol
OBPSR	**6.02 %**	**16.53 %**
BPSR	**5.85 %**	**16.66 %**

The estimated phase and amplitude of the orthogonal signal are approximately matching to the value of the reference signal. In addition, the performance of the OBPSR is almost identical to that of the BPSR, indicating that there are no ISI in our receiver, as shown in Figure 3-7. This further proves that the shifting operation during the OIF has been carried out accurately.

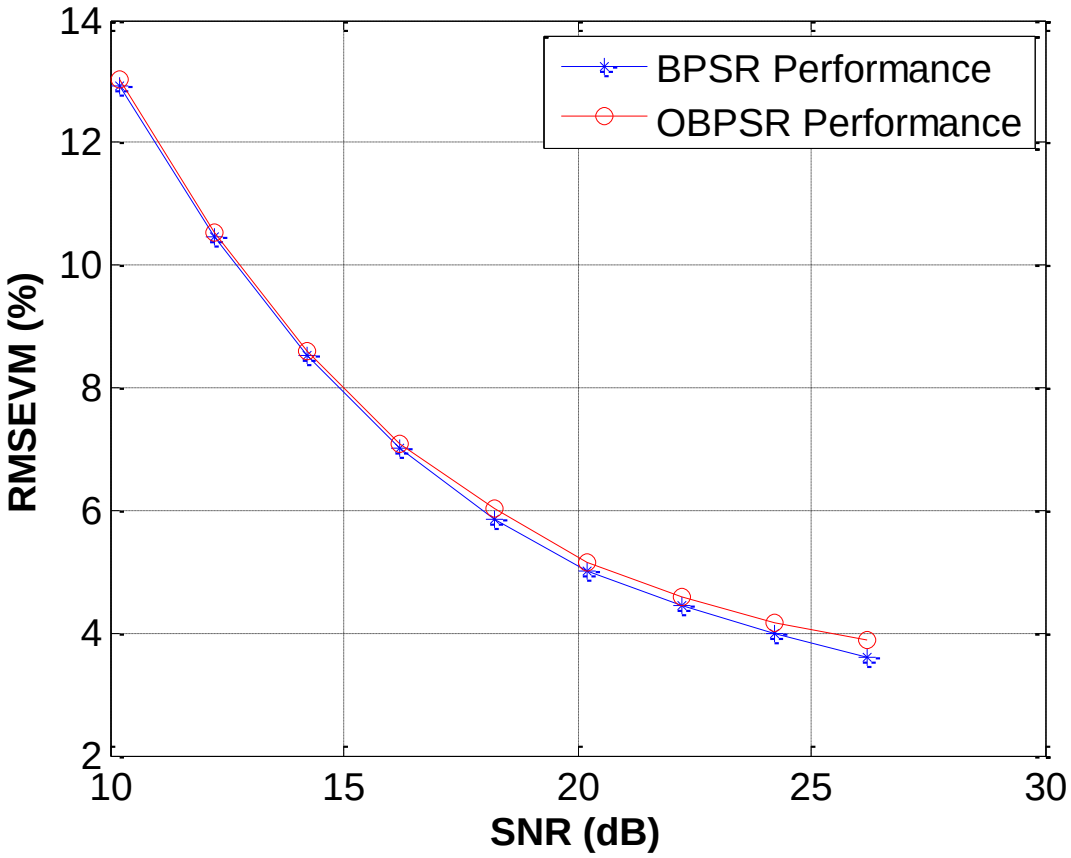

Figure 3-7 Error vector magnitude curve (RMS) for BPSK and the orthogonal signals

In this experiment, our OBPSR used a sample rate at 12 MHz (based on double of the maximum bandwidth of the two signals) instead of at least sample rate 16 MHz (based on double of the summation of the bandwidths of all of the two signals). Thus, a significant number "4 million" of samples has reduced and that will reflect on economising the receiver power.

3.1.3 Two Challenges and Solutions When Orthogonally Folding Multi-Signals

1. The first of these two challenges is calculating the sampling frequency that can fold and orthogonalise any two received signals. We can use a pre-processing RF-stage that down-converts the signals to their intermediate frequencies such that it is easy to find a sampling frequency that can fold and orthogonalise the received signals at the FNZ. This method is not new and it

applies to overcoming the limitation of ADC bandwidth when used to directly digitise the signals that have frequencies in GHz [37].

2. The orthogonality concept in 2-signal OBPSR states that both digitised signals should share the same folding-frequency in the FNZ, which is achievable when applied in a AWGN channel. The second challenge is that this concept is not valid when these two signals (or one of them) have Doppler-frequency-shifts, i.e., the signals should be simulated with a fading channel. Indeed, the BPSR technique will fold any of these two signals based on its actual received frequency. So, if the signals have a Doppler-frequency-shifts, then the folding-frequency will be "theoretically folded" based on the actual transmitted frequency plus the amount of the Doppler-frequency-shifts. This issue will break the orthogonality relationship stated in (3-4). To clarify, for the example, if the transmitted frequencies of L1CA signal is 1575.42 MHz and L2C GPS signal is 1227.60 MHz, then, theoretically the folding-frequency of these two signals will be 7.161 MHz, based on choosing a sampling frequency equal to 17.391 MHz. However, practically, these received GPS signals are received with a Doppler-frequency-shifts (we assume in this example the Doppler-frequency-shifts of the L1CA and L2C GPS signals are 8 KHz and 6.232 KHz respectively). Consequently, the folding-frequency of both of these signals will be different (with the folding-frequency is 7.153 MHz for the L1CA signal and 7.1548 MHz for L1CA signal), which will break the orthogonality. The solution we chose to overcome the Doppler and fading channel issues is to utilise an adaptive equalizer filter after the ADC to re-orthogonalise the signals continuously, which we have used in our OCBPSR design.

3.2 Orthogonal Complex BandPass Sampling Receiver

A new multi-signal receiver is designed to capture and track two signals at the same time based on second-order BPSR implementation. Our receiver will reduce the sampling frequency to a rate proportional to the maximum bandwidth information (not double of the maximum bandwidth information as in the OBPSR) of the input signals, and therefore requiring less processing time and more saving

power.

3.2.1 Mathematical Representation of Our OCBPSR

As shown in Figure 3-8, our dual OCBPSR architecture consists of two LNAs, two BPFs, one 90-degree phase-shifter, and two ADC's; each one of them is specified for a particular received signal. The phase shifters (HT) and the ADC's make up the OIF used for reforming the orthogonality of the filtered received signals. The HT is used as the first stage of OIF for shifting the phase of the second received signal by 90-degree to prevent the signals overlapping prior to using the BPSR technique. By choosing an appropriate sampling frequency, the second stage of OIF uses a BPS technique to fold both received signals directly to the same folding-frequency in the FNZ, thus producing a complex orthogonal signal (analytic signal) that comprises the two input signals. The mathematical representation of the signal is shown in (3-8). It is clear that the signals are orthogonalised at the folding-frequency. In spite of the signals have different modulation, the negative lobe of the two signals will be eliminated and that will allow sampling the signal at rate proportional to their bandwidth (not double).

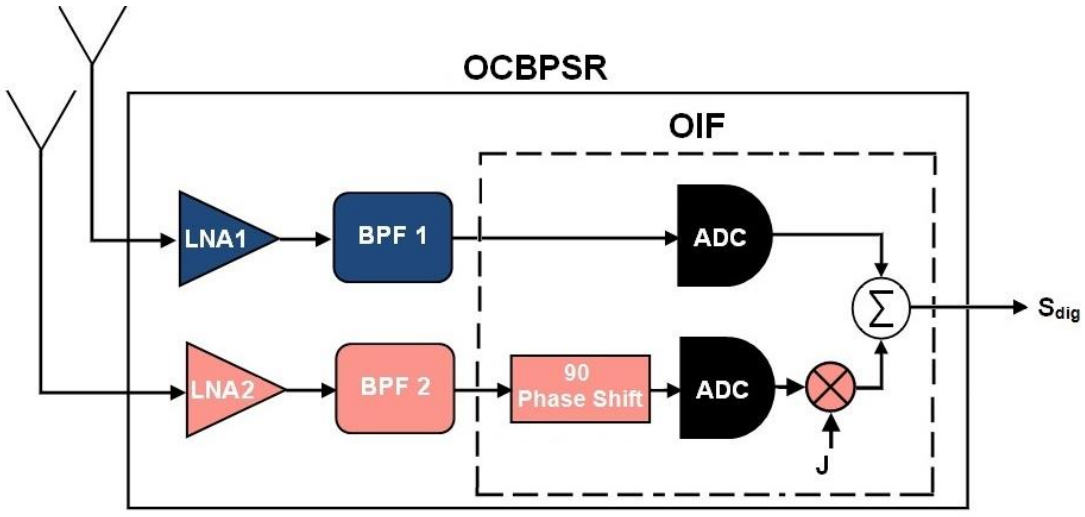

Figure 3-8 Orthogonal Complex BandPass Sampling Receiver (OCBPSR)

Two different approaches are utilized for processing and tracking the orthogonal signal.

The first approach feeds the real and the imaginary parts of the complex signal

(S_{dig}, see (3-8)) independently into two separate PLLs, as shown in Figure 3-9. Where, the real part represents the first received\digitised signal and the imaginary-part represents the second received\digitised signal. The gain in this approach is the reduction that happened in the number of samples, while there is no saving in the digital tracking channel, i.e. in the digital domain, two channels are used to track and demodulate the two signals.

The second approach feeds the complex signal (S_{dig}) into a single baseband CQPLL (after removing the carrier frequency as shown in Figure 3-9) to track and decode the signal because both the signals' information is available at the same time. However, this approach needs to solve the mathematical system in (3-10) when the received signals passed through a fading channel. RLS or LSM adaptive algorithms (Equalizer) are chosen "individually" to solve the re-orthogonalised system in (3-10), i.e., one of the two mentioned algorithms need to integrate inside the CQPLL. In this approach, the achievement is that eliminating one of the tracking channels, beside the reduction in the number of the signals samples. Note that, the PLL, the CQPLL and the equalizer algorithms are implemented in MATLAB.

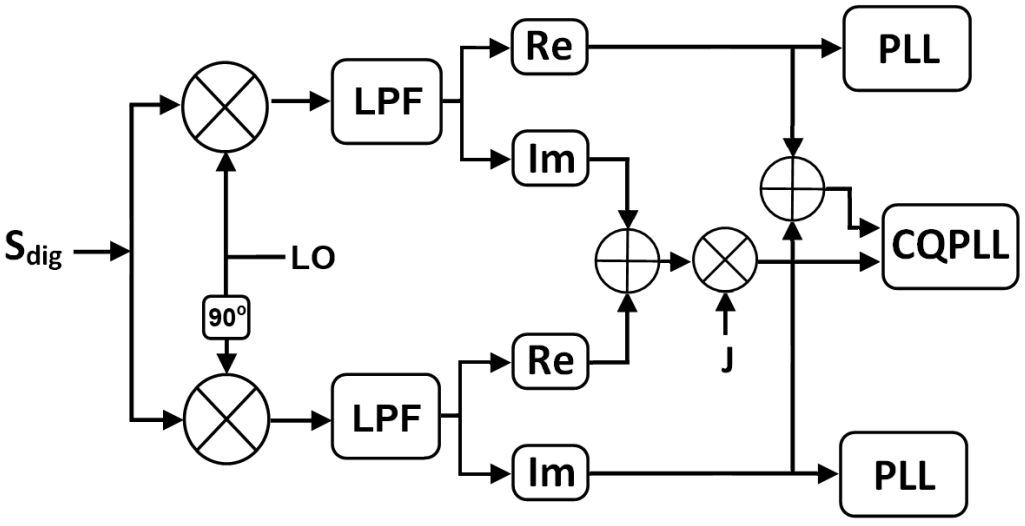

Figure 3-9 Block diagram of the two digital approaches

Equations (3-5) and (3-6) represent 2 BPSK's S_1 and S_2, which are received through fading channel.

$$S_1 = A_1 \cos(2\pi(f_1 + f_{d1})t + \varphi_1) + n_1 \quad (3\text{-}5)$$

$$S_2 = A_2\, cos(2\pi(f_2 + f_{d2})t + \varphi_2) + n_2 \quad (3\text{-}6)$$

where, (A_1, f_1, f_{d1}, n_1) and (A_2, f_2, f_{d2}, n_2) represent the amplitude, the carrier frequency, the Doppler frequency and the Gaussian noise of the first and second signals respectively. φ_1 and φ_2 represent the information message/the instantaneous phase of the first and second signals respectively, and can be expressed as:

$$\varphi_1 = \pi(1 - b_1), where\ b_1 = 0{,}1\ bits$$

$$\varphi_2 = \pi(1 - b_2), where\ b_2 = 0{,}1\ bits.$$

As described earlier, by applying HT to (3-6), then summing with (3-5) will generate the analytic signal that will be folded to the FNZ as shown in (3-7). Let us assume that there are two the impairments in the HT implementation, which are σ in the phase and η in amplitude. For simplifying the system derivation, let assume that the signals have the same relative power, and amplitudes of the two signals and equal to one.

$$S_{dig} = m_1\, cos\big(2\pi nT f_{fold} + \beta_1\big) + j\ \eta\ (m_2\, sin\big(2\pi nT f_{fold} + \sigma\ \beta_2\big)) + N \quad (3\text{-}7)$$

where, S_{dig} is the orthogonal complex digital signal at the folding-frequency (f_{fold}) and it carries two different information massages $m_1 = \pm 1$ and $m_2 = \pm 1$ and $\beta_1 = 2\pi nT f_{d1}$ and $\beta_2 = 2\pi nT f_{d2}$, where N represents the combined noise.

By rewriting (3-7), we can see the complex signal is orthogonalised at f_{fold} frequency:

$$\begin{aligned} S_{dig} = {} & [m_1\, cos(\beta_1) + j\ \eta\ m_2\, sin(\sigma\ \beta_2)]\ \ cos\big(2\pi nT f_{fold}\big) \\ & + [-m_1\, sin(\beta_1) + j\ \eta\ m_2\, cos(\sigma\ \beta_1)]\ sin\big(2\pi nT f_{fold}\big) \end{aligned} \quad (3\text{-}8)$$

After removing the carrier and recombining the real and imaginary parts of the signals as depicted in Figure 3-9, the resulting signal is given by:

$$S_{comb} = (m_1 e^{j\beta_1} + j\ \eta\ m_2 e^{j\ \sigma\beta_2}) \quad (3\text{-}9)$$

Further processing is requiring for tracking the S_{comb} signal in the second

approach. That will require solving the Doppler frequency difference in the two signals. Equation (3-10) expresses the mathematical system that can solve the difference.

$$\begin{bmatrix} m1 \\ m2 \end{bmatrix} = \begin{bmatrix} 1 & \alpha\ sin(\varepsilon) \\ 0 & \alpha\ cos(\varepsilon) \end{bmatrix} \begin{bmatrix} I \\ Q \end{bmatrix} \quad (3\text{-}10)$$

where, ε is the difference between β_1 and β_2. I and Q represent the in-phase and quadrature-phase components of the CQPLL.

3.2.2 Choice of Fading Channels for Our OBPSR

A typical transmitted signal over a wireless channel will suffer from various "fading" phenomena [38] such as Doppler effects, multipath, path loss, shadowing, etc. For signal analysis, there are two models of fading channel representations. These are: 1) The *Large-scale* fading channel is characterized mostly by the degradation of the signal power due to shadowing by large objects such as buildings and hills as well as path loss of signal over a large distance between the transmitter and receiver, e.g. GNSS signals. However, this type of fading has a slow fluctuation effect on the signal strength because fluctuations occur when the receiver moves over many wavelengths of the signal carrier. 2) The *Small-scale* fading channel refers to rapid fluctuations of the amplitude and phase of the received signals due to constructive and destructive interference among signals that arrive at the receiver at different times. In the Small-scale fading channel, there are two types; A) "*Fast-fading*" has a high Doppler spread and channel coherence time (*commonly defined as the time in which the channel can be considered constant*) less than the symbol period. i.e. channel variations are faster than baseband signal variations. B) "*Slow-fading*" has a low Doppler spread and the channel coherence time is greater than the symbol period. i.e. the channel variations are slower than the baseband signal variations.

For our simulation, one type of Small-scale Slow-fading channels is used, which is a *frequency-selective* fading channel. This type of channel is chosen because it is considered to be the most challenging type for wireless signals that can be received by a wireless device in a harsh environment such near-indoors. Note that, there are

two types of the Small-scale Slow-fading channel; a frequency-flat fading channel and a frequency-selective fading channel. Typically, in time-domain, a channel characterises as a flat fading when a multipath delay spread (*defined as the difference in propagation time between the longest and shortest path of the received signal*) is less than the symbol period. Correspondingly, in frequency-domain, the bandwidth of the received signal is less than a coherence bandwidth of the channel, which is inversely related to the value of delay spread. A channel becomes frequency-selective when the delay spread is larger than the symbol duration, i.e. the bandwidth of the received signal is larger than a coherence bandwidth.

3.2.3 Experimental Setup and Results

MATLAB is used for simulating the OCBPSR implementation. To represent the transmitted signals, two BPSK are modulated signals with 1 MHz and 0.5 MHz bandwidths representing the first and the second signal respectively. These signals are passed through a "root raised cosine filter" with a roll-off factor of 0.25. Two different carrier frequencies of 900 MHz and 850 MHz are used for the first signal and the second signal respectively. A Rician fading (frequency-selective fading) is then used to simulate transmission channel. The frequency-selective channel characteristic parameters are shown in Table 3-3.

Table 3-3 Parameter for Frequency-Selective Fading Channel

	Symbol	**Values of 1st Signal**	**Values of 2nd Signal**
Carrier frequency	**fc**	**900 MHz**	**850 MHz**
Communication bandwidth	**W**	**1 MHZ**	**0.5 MHz**
Velocity of mobile	**V**	**70 Km/h**	**70 Km/h**
Doppler shifts for a path	**D**	**60 Hz**	**55 Hz**
Coherence time	**Tc=1/(2D)**	**8.3 *msec***	**9.1 *msec***
Delay spread	**Td**	**2.2 *μsec***	**4 *μsec***
Coherence bandwidth	**Wc**	**500 KHz**	**250 KHz**

These two simulated signals once captured by their respective antennae, are

passed through two LNA's and two narrow BPF's centred on carrier frequencies of 900 MHz and 850 MHz to eliminate all frequencies outside the signals bandwidth. The resulting in-band signals are then fed to the OIF. Note that the phase of the second signal is shifted by 90-degree and digitised with the first signal by two of the ADCs that run in the same sampling frequency at 7 MHz. This sampling frequency is chosen so the ADCs fold the two signals directly to the analytic signal at 3 MHz folding-frequency. The output complex orthogonal digital signal can be then tracked and demodulated through two digital approaches, as we explained earlier.

1. Results of the first approach: Two PLL's

Figure 3-10 illustrates that the BER curves of the demodulated signals are approximately similar to the theoretical curve. This proves that tracking and decoding the signals in the separate PLLs are carried out properly. Note that, the BER values of the theoretical curve are for the BPSK in Gaussian Environment.

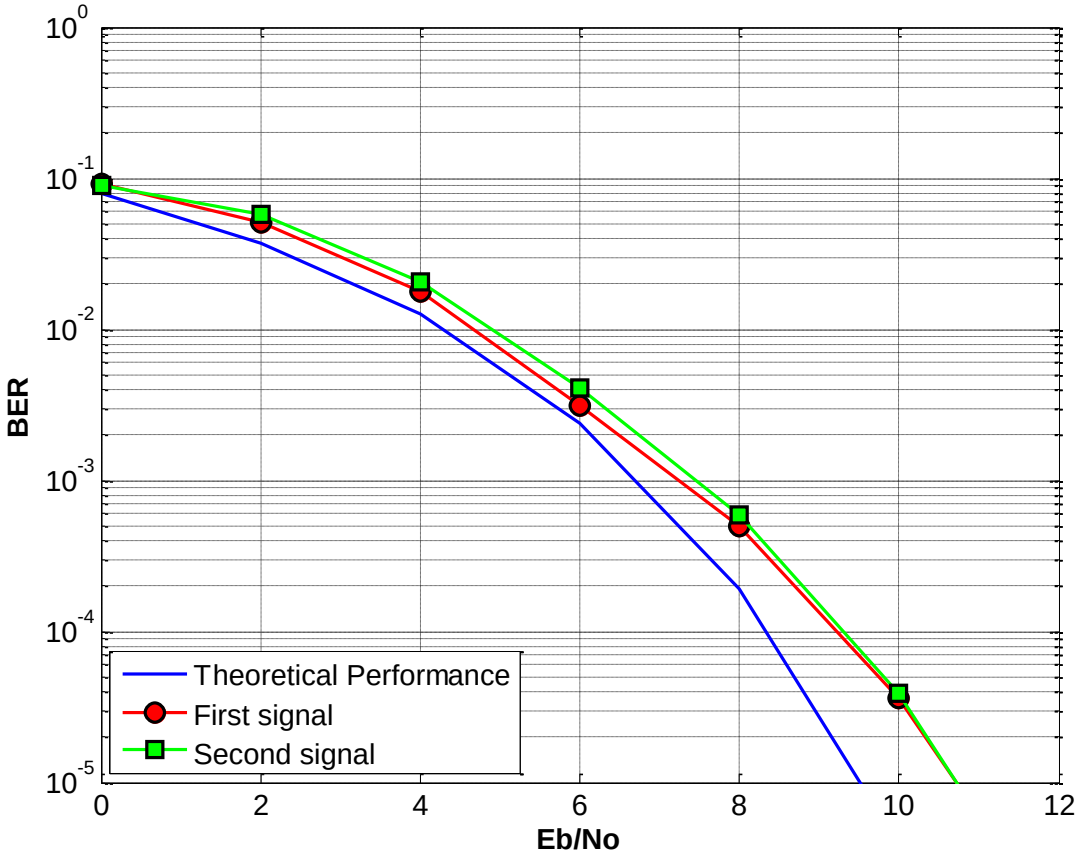

Figure 3-10 BER vs Eb/No in frequency-selective channel based in two PLLs (theoretical AWGN)

Table 3-4 EVM Values of Demodulated Signals based on two PLLs

	EVM_{RMS}	EVM max peak at
1st Signal	**2.02 %**	**9.36 %**
2nd Signal	**2.11 %**	**9.62 %**

Table 3-4 shows further indication of recovering the I and the Q data of the signals so that they are perfectly isolated between the signals in the digital domain without suffering from overlapping and the IQ mismatch.

2. Results of the second approach: Single CQPLL

Figure 3-11 displays the BER curves of demodulated signals in the frequency-selective channel. The curves of LMS and RLS have an acceptable increase compared with theoretical curve. Besides, these curves are approximately identical to each other, while the curve of demodulated signal without utilizing the equalizer algorithms is far from the acceptable values. These results are expected as the received signals have different Doppler frequency so the CQPLL cannot track them correctly, without employing the equalizer filter. It is more importantly to know that, the CQPLL is tracking the Doppler frequency change of the first signal and solving the Doppler frequency of the second signal based on the system in (3-10). Note that, the system in (3-10) becomes unsolvable when $\alpha\, cos(\varepsilon) = 0$, more specifically when ε value is equal to 90-degree, the adaptive filters will skip this value and perform the previous values. This will not affect the demodulation/tracking the signals because it will occur in one sample of data so we can recover the actual bit from the other samples.

The simulated measurement value of EVM in Figure 3-12 shows both the equaliser algorithms have the same performance. The EVM is increasing perfectly with the increasing SNR. This proves that the phase and the amplitude of the both signals are re-orthogonalising well based on the chosen algorithms, which also demonstrates that the front-end is perfectly orthogonalising the signals in the folding-

frequency.

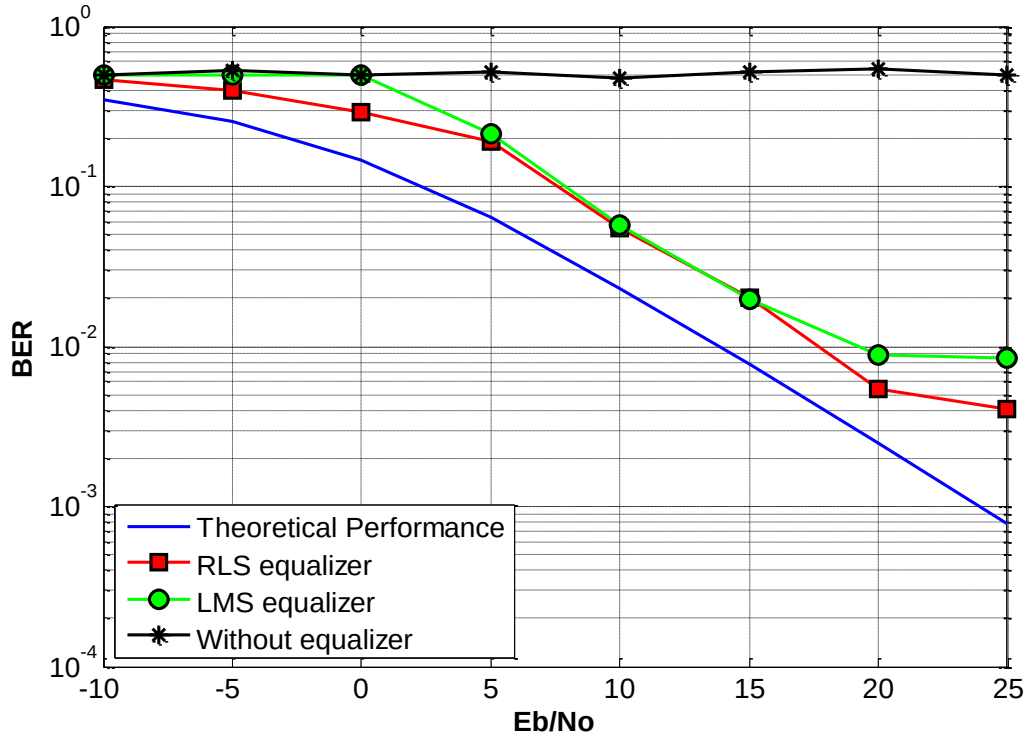

Figure 3-11 BER vs Eb/No in frequency-selective channel, OCBPSR

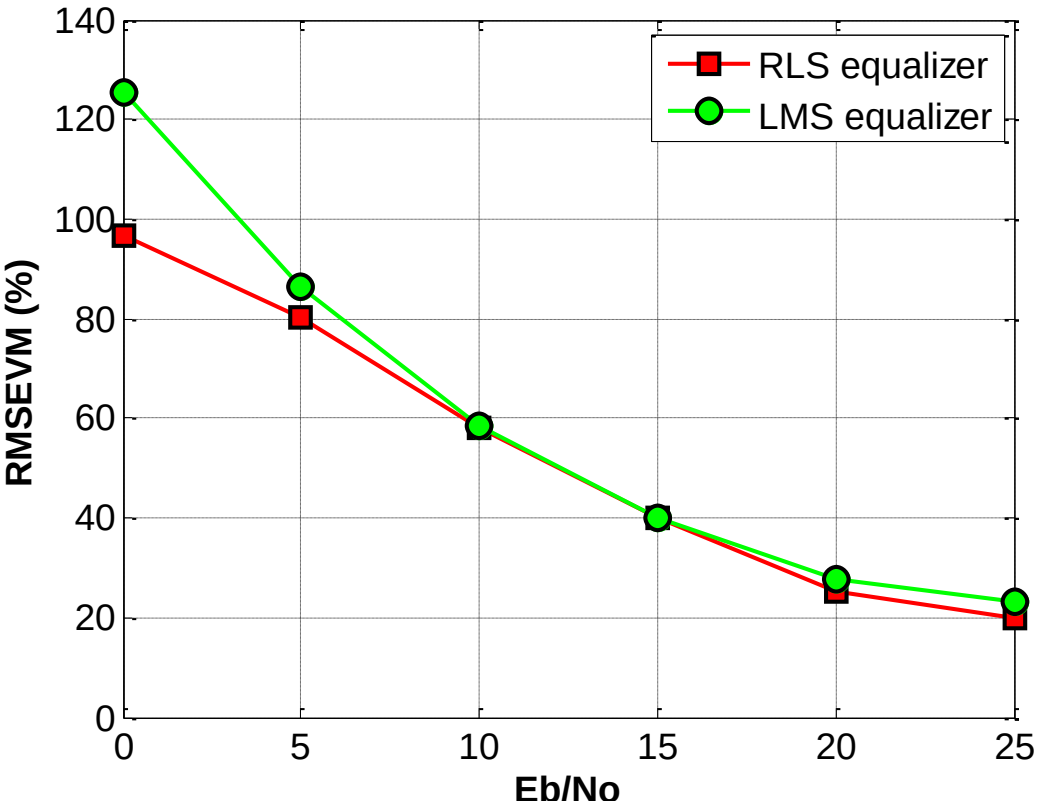

Figure 3-12 EVM vs Eb/No in frequency-selective channel, OCBPSR

Figure 3-13 shows the scattering plot of the two simulated signals. It is clear that the analytic demodulated signal without using the equaliser algorithms (with Doppler shifts), has wrong value of phase with respect to the value of the actual reference signal. Besides, the figure shows the two algorithms perfectly recover the correct phase and amplitude of the demodulated signal.

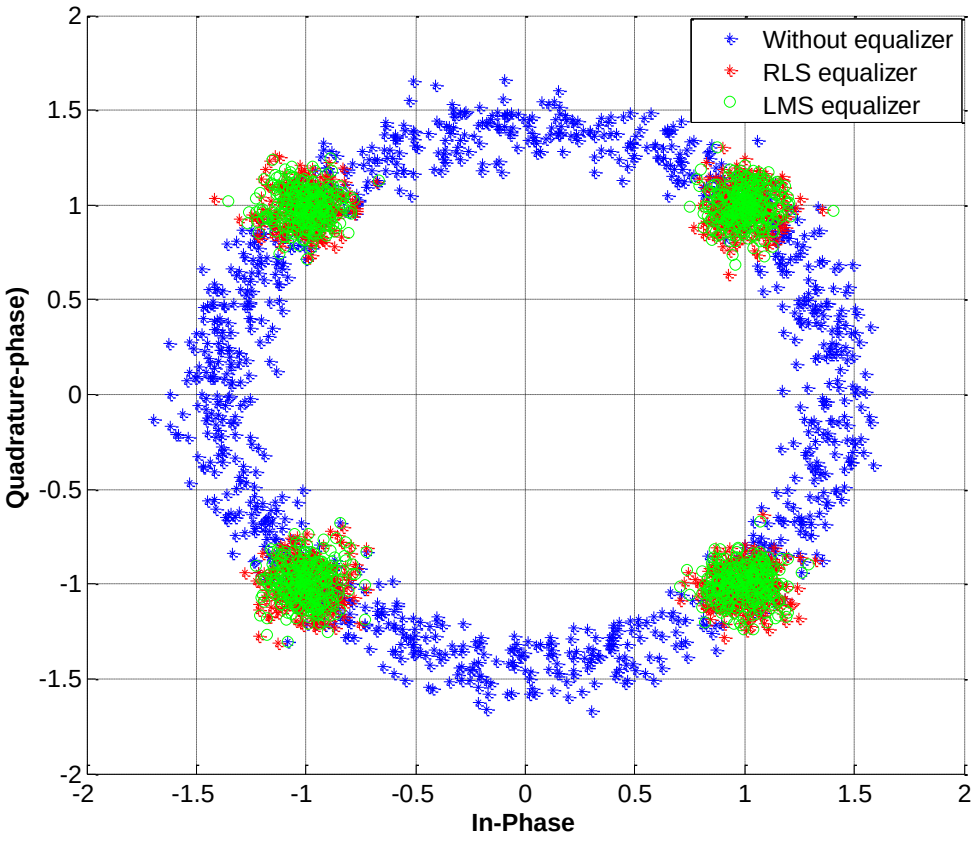

Figure 3-13 Scattering plot of signals demodulated in CQPLL@ SNR = 25 dB

3.3 Prove of Concept of the OIF in Real Environment

As shown in the previous sections, we have evaluated our orthogonal receiver by using MATLAB and Simulink software tool. This tool is highly advanced and has fairly accurate models for various wireless channels. However, these models have limitations for detailed simulations of all aspects of the effect of such communication channels; such effects include the propagation characteristics (fading, shadowing, scattering, etc.) for example. The Signalion-Halo-430 platform [39] does provide us with the ability to evaluate our receiver behaviour in real wireless communication channel.

Figure 3-14 shows the transmitter and the receiver parts of the Signalion-HaLo-430 platform. This platform is controlled entirely via the MATLAB software and allows the user to configure the transmission parameters such as carrier frequency, sampling frequency, bandwidth and power. We then upload the sampled baseband signal from MATLAB into the HaLo-430 transmitter, to transmit our scenario signal in the air periodically until the transmission is stopped. The receiver part of the HaLo-430 platform captures and records the received signals that can be triggered within any defined interval. Synchronization between the transmitted and received signal is based on using the defined interval. The surrounding environment will affect the received signal, specifically when we change the position of the transmitting antennae, i.e. the received signal is either an LOS signal or multipath signal and sometimes it can be a summation of LOS and multipath signal.

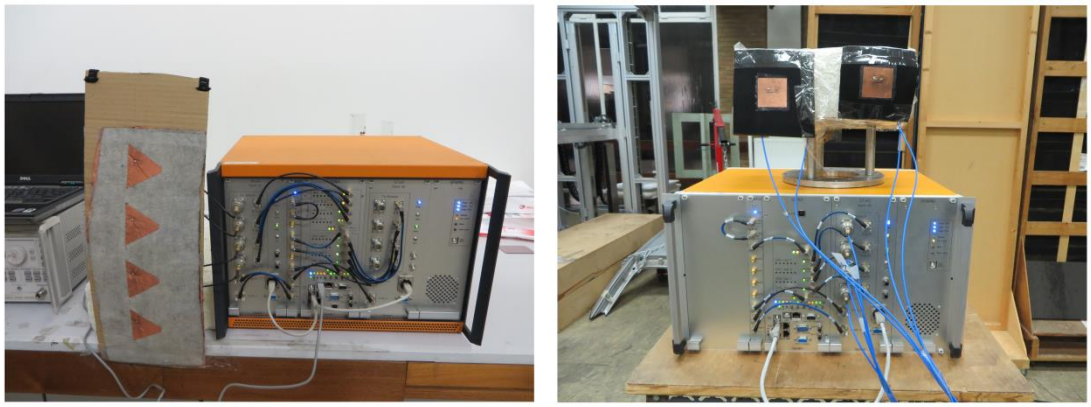

(a) *(b)*

Figure 3-14 HaLo-430 platforms (a) Receiver (b) Transmitter

The purpose of this experiment (using the Signalion-HaLo-430 platform) is to evaluate our orthogonal receiver in a more realistic environment. The design of our orthogonal receiver is based on using a Bandpass sampling front-end, but the front-end of the Signalion-HaLo-430 platform receiver can be used as Direct-conversion or Low-IF receiver. Therefore, instead of receiving two signals at the same time with same folding-frequency "in our original receiver design", the two signals will be received at different times with the same IF frequency based on the HaLo-430 front-end setup. Therefore, the digitised-output signals of the direct-conversion/Low-IF conversion can be orthogonalised and then can be fed to a single tracking channel. This means that the concept of the orthogonality (OIF) in the orthogonal receiver is

still plausible enough to be evaluated. Two scenarios have been designed to evaluate our OIF design, using fixed and unfixed antennae, when the signals are received by the two receivers (Direct-conversion & Low-IF). The receiver architecture of both Direct-conversion and Low-IF conversion are detailed in Chapter two, Sections 2.1.2 and 2.1.3 respectively.

3.3.1 Test Scenarios Setup

Two tests scenarios are carried out to evaluate our proposed concept of orthogonality (OIF) in the both receiver architecture (Direct-Conversion & Low-IF), which are fixed antennae and unfixed antennae.

1. Fixed antennae

The general setup of the first scenario, both antennae of the transmitting and receiving parts of the HaLo-430 platform are fixed during the transmission. However, the position of the antennae is changed for different tests as well as placing some obstacles in the path of the signals to prevent completely LOS signal, and so to get different SNR values. Note that these changes in the antennae positions are set before the actual transmission test is started. In the HaLo-430 platform setting, for both the receiver types (Direct-conversion and Low-IF), the carrier frequencies of the first signal and the second signal are set to 2.3 and 2.45 GHz respectively. The sampling frequency used is 10 MHz (I also used 20 MHz to evaluate the same scenario and I have obtained almost the same result as that of the 10 MHz scenario) and the transmission power is 0 dBm. In the MATLAB platform setting, the two transmit signals are modulated as BPSK signals with 1 MHz bit rate, and they are passed through a "root raised cosine filter" with a roll-off factor of 0.2.

2. Unfixed antennae

The HaLo-430 platform and the MATLAB setting of this test scenario is the same as the fixed antennae scenario, except that the transmission antennae will be moved (back & forth or sideways) during the signal transmission. The movement in the transmission antennae will generate more Doppler effect on the received signals, as shown in Figure 3-15 (b). The transmission antennae are moved manually in different patterns, like forward, backward and circular movements with respect to the

receiver position.

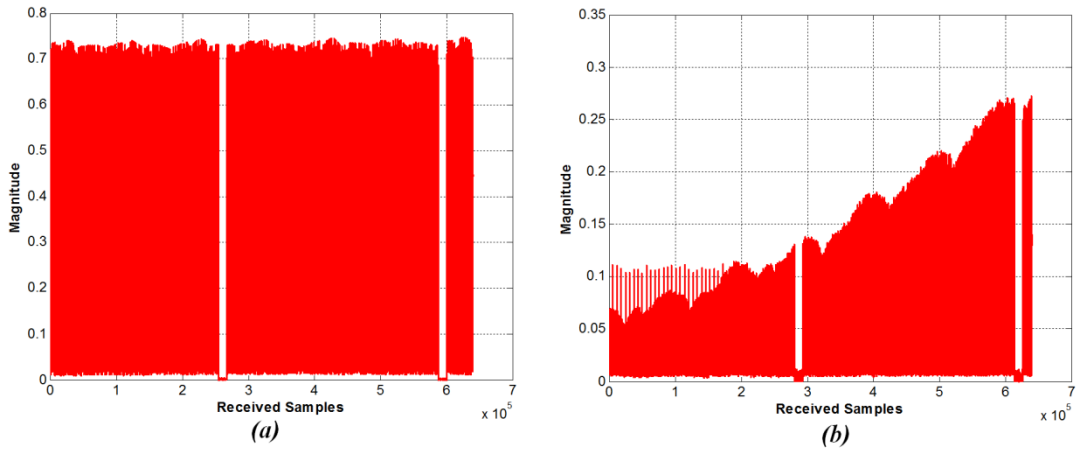

Figure 3-15 Received samples (a) Fixed antennae (b) Unfixed antennae

3.3.2 Results and Discussing

1. Direct-Conversion Receiver

The baseband signals samples are upload from MATLAB (installed on a PC) to the HaLo-430 platform, where the samples frame length of each baseband signal is 320,000 samples. At the same time, we specify a number of samples to pause after transmitting the frame (12800 samples), which is named “defined interval”. The HaLo-430 platform transmits the frame with a pause sample periodically in the air. In the receiver part, we will specify the length of the received/recorded signal; I set this length to be double that of the frame length with a defined interval to ensure we receive a full frame. Then, through a USB cable, the recorded sample data is downloaded as “2baseband signals” to the MATLAB (PC). These baseband signals are then orthogonalised to become a single complex baseband signal with I and Q components. The complex signal is then fed to an equalizer filter, to harmonise the signals correctly, and the output of which is then processed by the CQPLL.

A. Fixed Antennae Results:

Figure 3-16 shows that the measurement results of the BER versus SNR, which illustrates a slight degradation in BER of our receiver in comparison with the theoretical value. Figure 3-17 shows the EVM values are decreasing with increase the SNR values, which means that the estimated phase and amplitude of the

demodulated signals are approximately matching to the actual transmitted data.

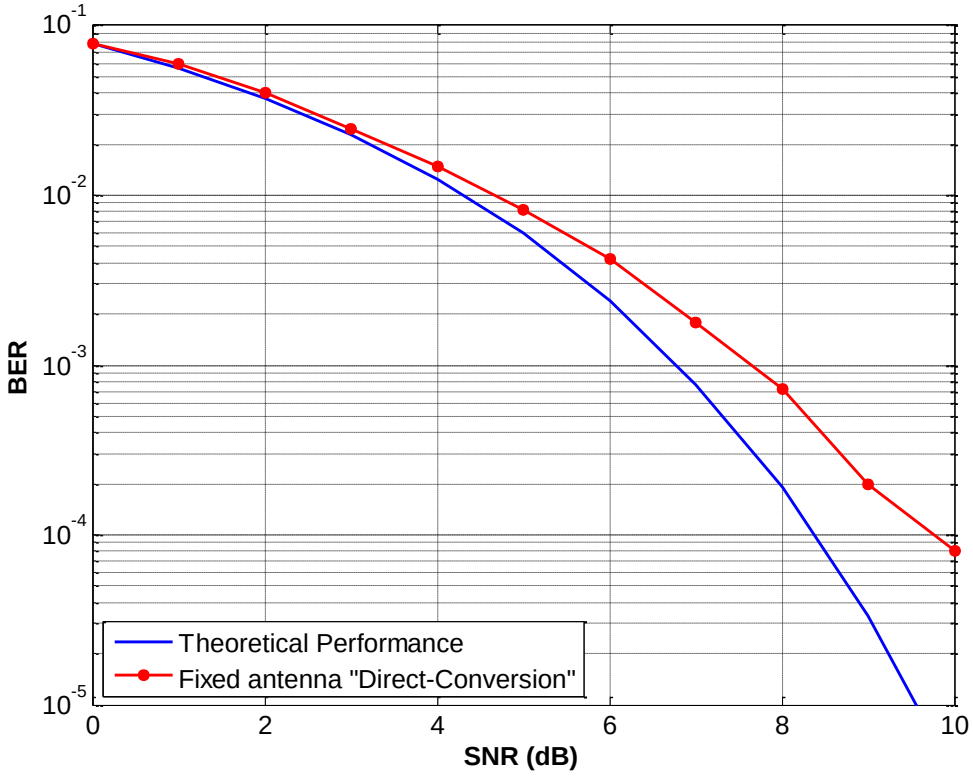

Figure 3-16 Scenario Fixed antennae "Direct-Conversion": Measurements data of BER vs. SNR based on HaLo-430 platform

B. Unfixed Antennae Results:

Figure 3-18 shows that the BER of this scenario, and it is less than 2% when compared with the theoretical values and around 1% when compared with fixed antennae values when SNR above 4 dB. Similarly, the values of the EVM are slightly less than the fixed antenna values, as shown in Figure 3-19. In addition, these values of the EVM do fluctuate with respect to the SNR because of the varying of the amplitude values due to the movement of the antennae when signals are being received. Obviously, our orthogonal receiver shows a good performance in tracking and demodulating the signals in both test scenarios. However, it is more favourable in the fixed antennae scenario rather than the unfixed antennae scenario. This is because the unfixed antennae scenario has more Doppler frequency that makes the power of the received signal fluctuating, as shown in Figure 3-15 (b).

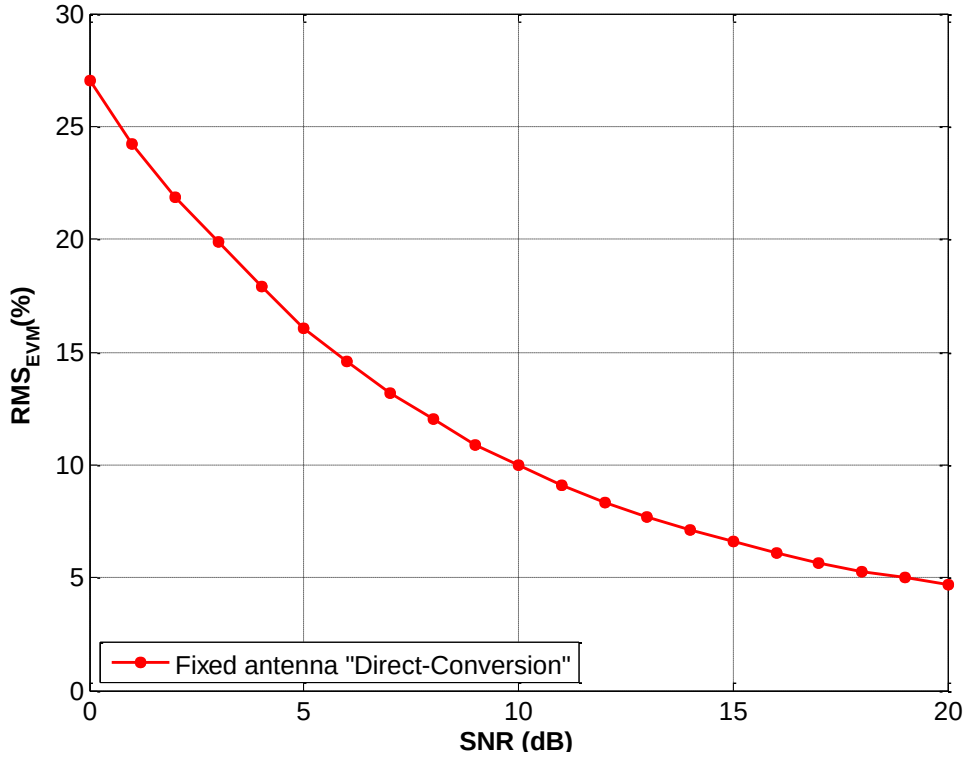

Figure 3-17 Scenario Fixed antennae "Direct-Conversion": Measurements data of EVM vs. SNR based on HaLo-430 platform

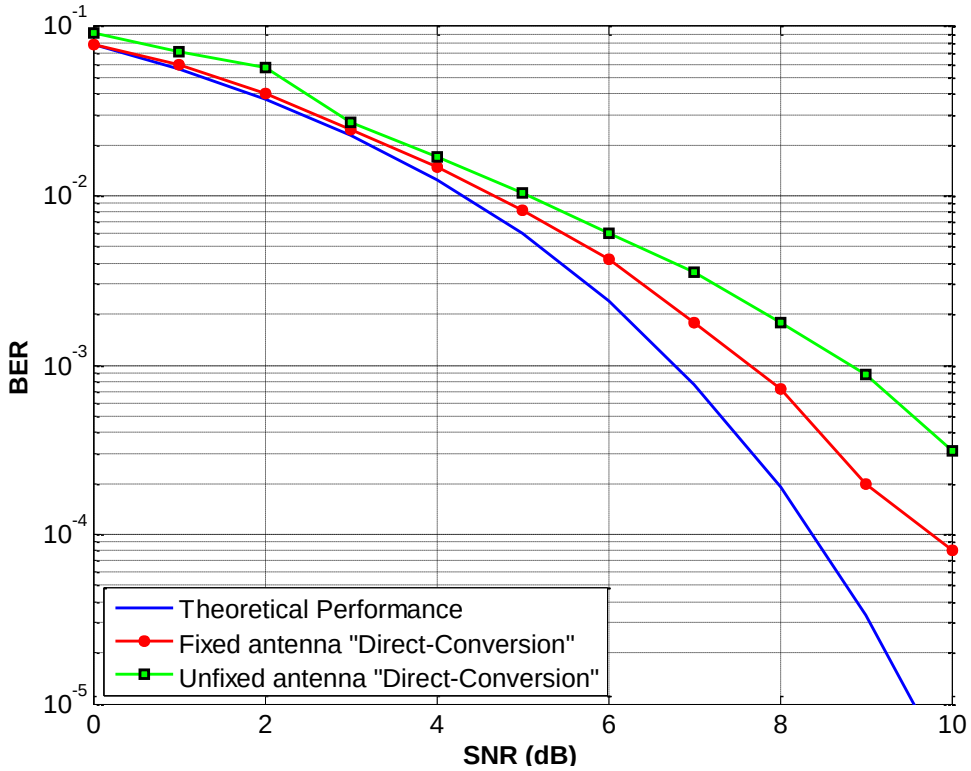

Figure 3-18 Scenario Unfixed antennae "Direct-Conversion": Measurements data of BER vs. SNR based on HaLo-430 platform

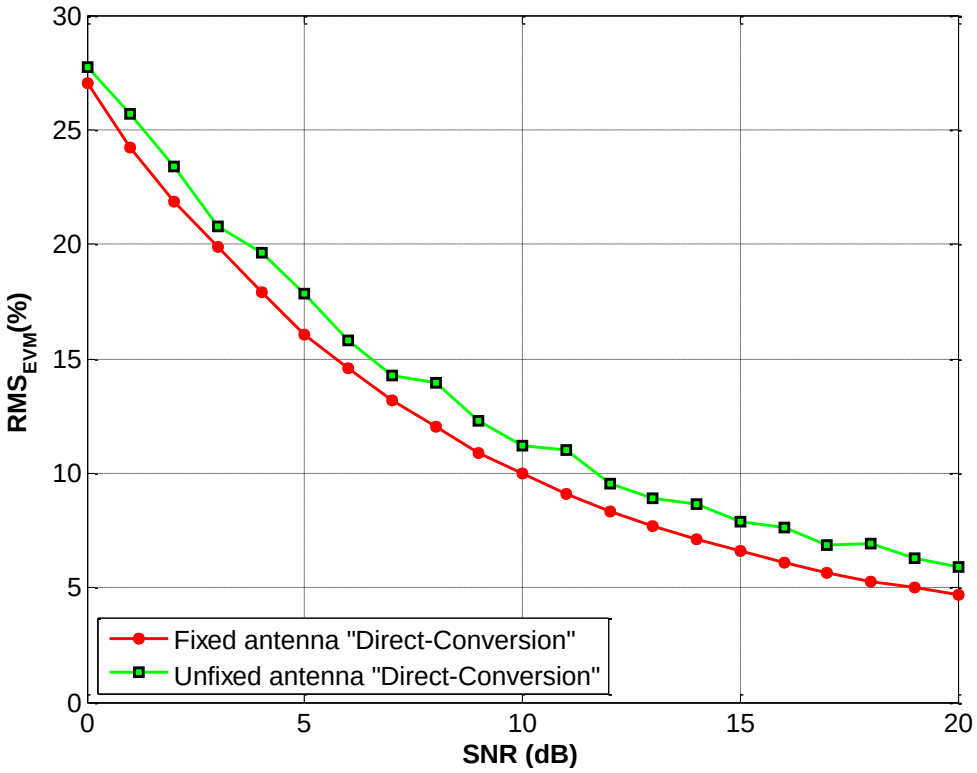

Figure 3-19 Scenario Unfixed antennae "Direct-Conversion": Measurements data of EVM vs. SNR based on HaLo-430 platform

2. Low-IF Receiver

The general settings of this test scenario are the same as the one that is used in the previous scenario (Direct-Conversion) except that the received signals are centred at 2 MHz. In this scenario, an equalizer filter is placed after the phase detector in the I-branch and also in the Q-branch of the CQPLL. Where, the phase detector is a mixer followed by an LPF that will help the equalizer to estimate the parameters channel of each signal, because these equalizers work only with baseband signal (0 Hz).

A. Fixed Antennae Test Scenario:

Figure 3-20 shows that the BER values of this test scenario are almost identical to the theoretical values. Further, these BER values are also similar to the fixed antennae scenario of the Direct-Conversion results. Figure 3-21 shows that the difference between the demodulated symbols and the ideal transmitted symbols are decreasing to reach 5% at SNR= 20 dB, which is almost the same as the trend of the EVM of the test scenario "fixed antennae scenario of Direct-Conversion".

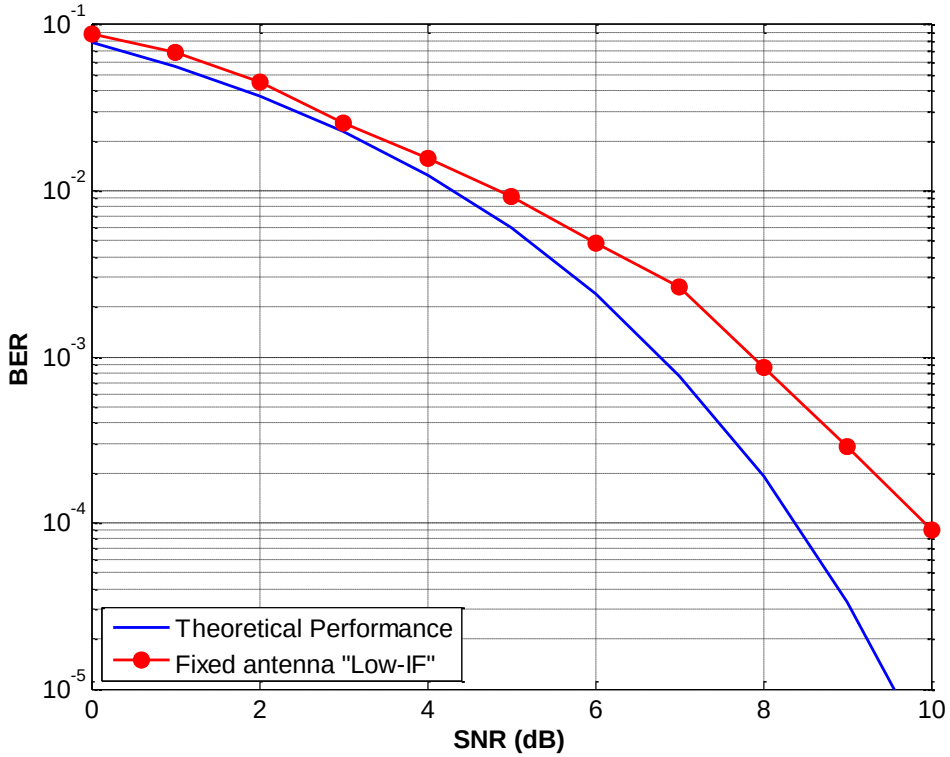

Figure 3-20 Scenario Fixed antennae "Low-IF": Measurements data of BER vs. SNR based on HaLo-430 platform

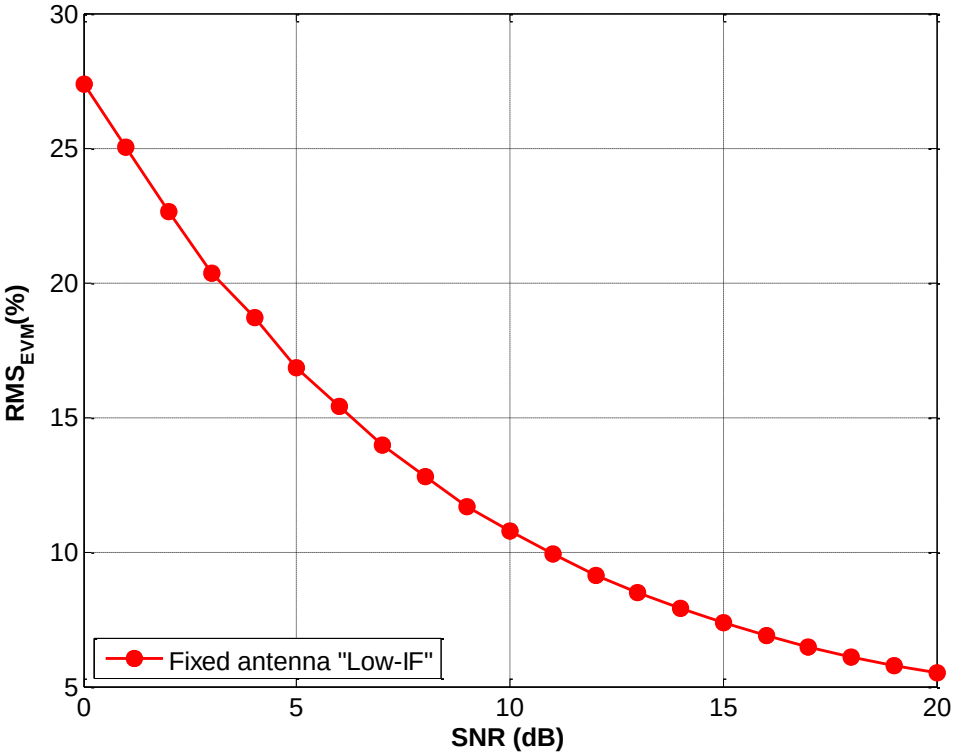

Figure 3-21 Scenario Fixed antennae "Low-IF": Measurements data of EVM vs. SNR based on HaLo-430 platform

B. Unfixed Antennae Test Scenario:

The trend of the BER and the EVM in the unfixed antennae test scenario are slightly less than in the fixed antennae, as shown in

Figure 3-22 and Figure 3-23 respectively. Furthermore, the BER and the EVM values are approximately similar in the Low-IF and Direct-Conversion receivers when the signals are received by unfixed antennae.

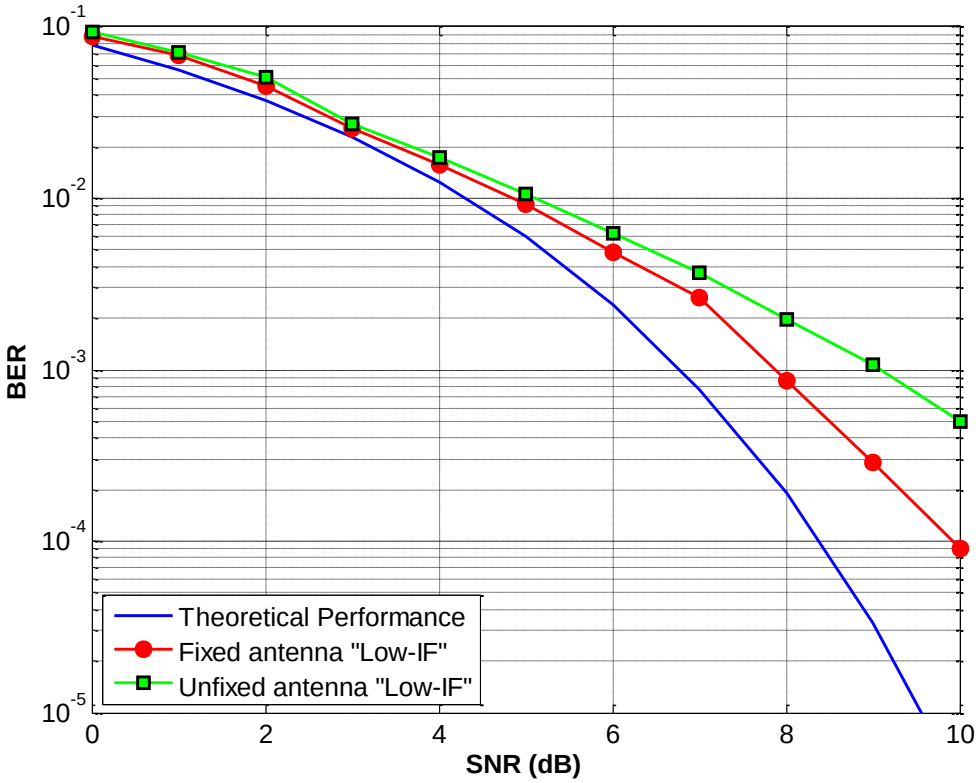

Figure 3-22 Scenario Unfixed antennae "Low-IF": Measurements data of BER vs. SNR based on HaLo-430 platform

Overall, the tracking and demodulation performance of both receivers, Direct-Conversion and Low-IF receiver, based on OIF, in the fixed antenna scenario perform slightly better than the unfixed antennae scenario. Even though, the Doppler Effect in the unfixed antennae test scenario is not significantly high because in the setup of the test scenario there is a small distance between the Halo-430 receiver and the transmitter, and also due to the movement of the antennae to induce the Doppler is not fast (moved by hand).

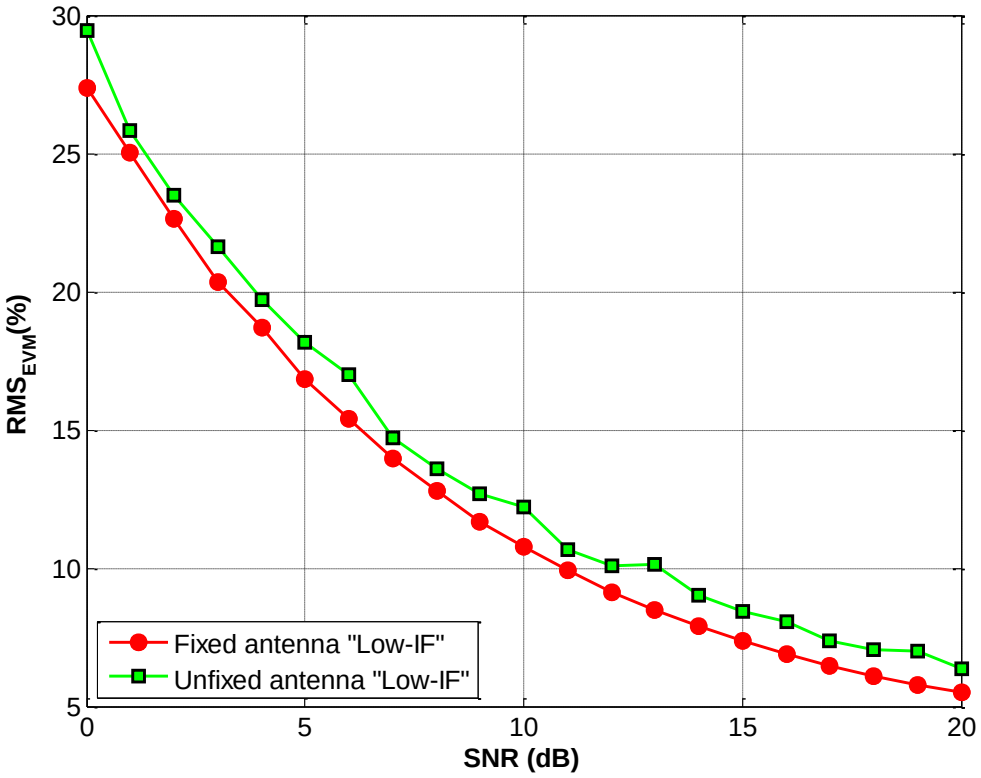

Figure 3-23 Scenario Unfixed antennae "Direct-Conversion": Measurements data of EVM vs. SNR based on HaLo-430 platform

3.4 Summary and Conclusions

In this chapter, two orthogonal receivers were designed based on BPSR, and their ability to capture and track multiple signals simultaneously was been verified (our implemented scenario was for 2-signals receiver) in sample rate less than Nyquist rate (The Nyquist rate is twice of the signal bandwidth that is sampled and guarantee that the signal is perfectly reconstructed). The concept of orthogonality "OIF" between two distinct received signals has been proved; it is applicable not only for BPSR architecture but also for two other receiver architectures, Direct-Conversion and Low-IF receiver. The OIF perfectly harmonises any two received signals and adapts them to form a single orthogonal signal allowing the "tracking and decoding" to be carried out a single CQPLL in the digital domain. Thus, save valuable attributes such as device and manufacturing costs, circuitry-power-dissipation, and processing-time, when compared with conventional side-by-side receivers.

Chapter 4 **Orthogonally Combined L1CA and L2C GPS Signal Acquisition**

We have concluded form Chapter 3 that our orthogonal receiver designs can capture and digitise any two signals simultaneously, at rate less than Nyquist rate, and pass them to the digital domain with the same folding-frequency. Therefore, in this chapter we intend to use our OCBPSR as front-end, to benefit from its property of folding the two signals to the same frequency in order to acquire L1CA and L2C GPS signals concurrently, based on employing our novel *"single orthogonal acquisition channel"*. The main gains of our channel, especially in commercial GNSS receivers, is to have more than one of these signals acquired by the same receiver so as to assure better signal acquisition and improved reliability at wider operating areas.

The L1CA GPS signal power reaches the receiver at around -158 dBW outdoors, while in challenging areas this signal power attenuates by at least another 25 dB, which makes it difficult to acquire the signal [40]. This is why GPS has provided other civilian signals, such as the L2C to improve availability and acquisition of the L1CA signal [41], both of which are transmitted from the same SV, as detailed in Section 4.1.4. That is to say, when L2C signal is combined with L1CA signal in a single receiver implementation, a faster GPS signal acquisition at low sensitivity can be achieved because the cross-correlation protection of the new combined signals has been improved.

Considering our literature review in Section 4.2, all published implementations of combined L1CA and L2C GPS front-end receivers are based on placing the two-acquisition channels side-by-side for each of the two signals, i.e. only their correlated results are combined. This kind of implementation consumes the same amount of power/resource to acquire each signal alone. Therefore, we believe, besides our main

gains, it is much desired, especially for battery powered devices such as Smartphones, to integrate the acquisition channels of these two signals into a single channel.

In this chapter, two orthogonal acquisition channels are proposed and each channel has three different "L1CA and L2C" combining methods. The first acquisition channel is Orthogonal Single acquisition Channel (OSC) that is devoted to enhancing the power consumption and the implementation complexity in the existing combination methods. The second acquisition channel is Orthogonal Parallel acquisition Channel (OPC) that is dedicated to enhancing the acquisition sensitivity. Full details about the OSC and the OPC regarding their structure, evaluating the performance and discussing/analysing the simulation results are documented in Section 4.4 and Section 4.5 respectively.

4.1 L1CA and L2C GPS Signals Structure

This section presents an overview of the characteristics of the L1CA and L2C GPS signals (see Sections 4.1.1 and 4.1.2). In addition, the current GPS acquisition methods are explained in Section 4.1.3, since the existing combined L1CA and L2C acquisition methods depend on these acquisition methods. Finally, the correlation between the characteristics of the two GPS signals is shown in Section 4.1.4.

4.1.1 L1CA GPS Signal Structure and Correlation Properties

The L1CA GPS signal uses the Code Division Multiple Access (CDMA) techniques as an access channel. The division code is a 1,023-bit deterministic pseudorandom binary sequence (PRN) and it is named Coarse Acquisition code (CA). The code firstly is added to the navigation message based modulo-2, where the bit rate of the navigation message is 50 Hz. The result is modulated as BPSK with the signal carrier at frequency 1575.42 MHz [42]. Figure 4-1 shows an MATLAB simulation of the generated GPS signal.

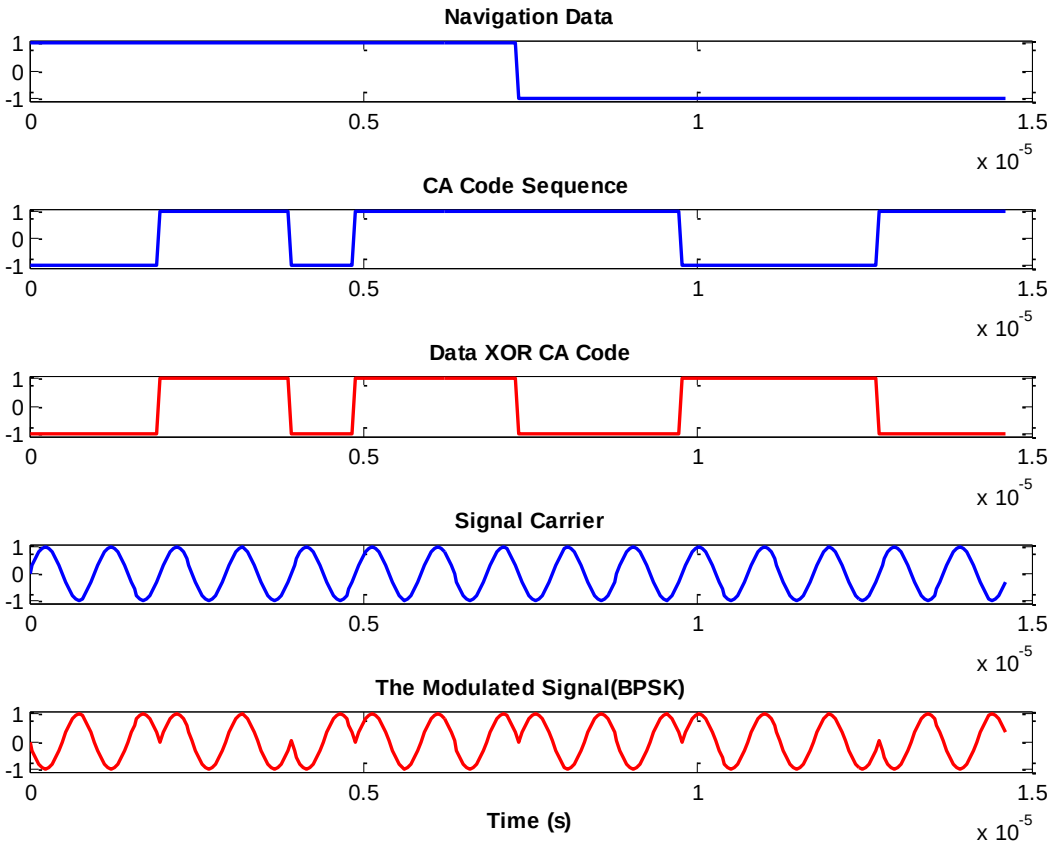

Figure 4-1 Simulated GPS signal

The mathematical expression of the transmitting L1CA signal from satellite *k* is:

$$S_{T,L1}^{k} = \sqrt{2P}CA^{k}(t)\oplus D^{k}(t)cos(2\pi f_{L1}t)$$

where P is the signal power, CA^k is the CA code sequence appointed to satellite number k, D^k is the navigation data; the sign $\oplus$ means an added modulo-2 and f_{L1} is carrier frequency of L1 signal frequency band.

It is clear from the above equation that the transmitted signal comprises three essential parameters (see the blue lines in Figure 4-1).

The first parameter is the navigation data that contains the information about the satellite such as its orbit, signal transmitted time and ionosphere parameters. All this information is crucial for localisation.

The second parameter is the CA code, and each satellite has a unique CA code or spreading sequence. The purposes of these codes are first, to spread the navigation

data on the ranging code so that the spread signal offers more resistance to intentional or unintentional interference/noise such as spoofing, jamming, multipath and reflection. The other purpose is to distinguish between the GPS signals that transmitted from different\same satellites at the same frequency band, which will help to acquire them. The properties of these codes can be listed in three important points:

1. The CA codes are uncorrelated with each other, as shown in Figure 4-2 (a). They are designed to be almost orthogonal. So, different codes CA^i and CA^k come from different satellites *i* and *k*. The cross-correlation function (*R*) can be expressed as:

$$R_{ik} = \sum_{n=0}^{1022} CA^i(n)CA^k(n+m) \approx 0 \ \ for\ all\ m$$

2. No correlation is expected by matching the codes with themselves if they are unaligned (more than one chip off), seen in blue as auto-correlation function across the graph in Figure 4-2 (b). The auto-correlation function of the same code CA^i that comes from the same satellite *i* can be written as:

$$R_{ii} = \sum_{n=0}^{1022} CA^i(n)CA^i(n+m) \approx 0 \ \ for\ all\ |m| \geq 1$$

3. High correlation peak value can be found when the codes are perfectly aligned with themselves. This property helps to distinguish the DSSS signals or GPS signal from surrounding high noise and multipath signals, specifically for GPS signal this property can protect the signal by 24 dB [43], as depicted in red colour in Figure 4-2 (b). In addition, this property can make it easy to find the beginning of the chip code and the code itself/SV identity. The auto-correlation function can be written as:

$$R_{ii,peak} = \sum_{n=0}^{1022} CA^i(n)CA^i(n+m) \approx 1023 \ \ for\ all\ |m| \leq 1$$

Figure 4-2 shows the "*auto-correlation*" and "*cross-correlation*" properties of the CA code (example; PRN=12&14). The right plot of Figure 4-2 shows low correlation when correlating two different codes (PRN=12&14) while high correlation peak can be found at lag 0 when the codes are the same and perfectly aligned.

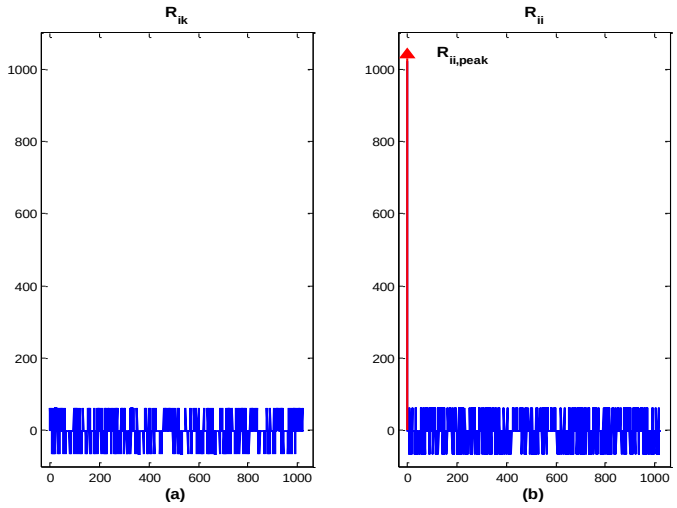

Figure 4-2 Correlation property of CA code; (a) uncorrelated, (b) correlated

The third parameter of the GPS L1CA transmitted signal is the carrier signal, which is 1575.42 MHz (L1 band). The main effect of do not have an accurate acquisition or a stable tracking state is the change of the carrier-signal-frequency value because of Doppler Effect. The motion of the transmitter/satellite, with respect to the receiver, produces shifts in the received carrier frequency as compared to the transmitted one, which is called Doppler-frequency-shifts. The maximum Doppler-frequency-shifts in GPS L1 frequency is ± 4 KHz for a stationary receiver while ± 10 KHz for moving at high-speed receiver. Also, there is a small effect on the CA code, which is around "3.2 Hz" and "6.4 Hz" for stationary and the non-stationary receiver, respectively [44].

After reviewing the main parameters of the transmitted GPS signal, the received GPS L1CA signal can be expressed as:

$$S_{R,L1}^{k} = \sqrt{2P}D^{k}(t-\tau) \oplus CA^{k}(t-\tau)\, cos\left(2\pi(f_{L1} + f_{d}^{k})\, t + \theta^{k}\right) + w_{RF}(t)$$

where, τ is the delay time, f_d^k is the Doppler frequency, θ^k is the received phase and w_{RF} is the additive white Gaussian noise.

The acquisition engine needs to determine the values of the code-phase-delay (time delay in the CA code) and Doppler-frequency-shifts accurately from the received L1CA GPS signal.

4.1.2 L2C GPS Signal Structure

The structure and the properties of the L2C GPS signal are the same as the L1CA GPS signal. The only difference is that the L2C signal comprises two PRN codes, named L2 Moderate length code (CM) and L2 Long length code (CL). The length of the CM code is 10,230-chips, repeating each 20 *msec* while the length of CL code is 767,250-chips, repeating each 1.5 *sec* and each code is clocked at 511.5 KHz. The CM code is added to the navigation message (bit rate 25 Hz) based modulo-2 and then the added code is mixed with CL code, as a chip-by-chip time multiplexing, so the result is a multiplexing code clocked at 1.023 MHz, which is similar to the chipping rate of the CA code. The multiplexing code is then modulated as BPSK with the signal carrier at frequency 1227.60 MHz, as represented Figure 4-3. Further details about the L2C signal such as the codes structures, their generated polynomial and navigation message are found in [45].

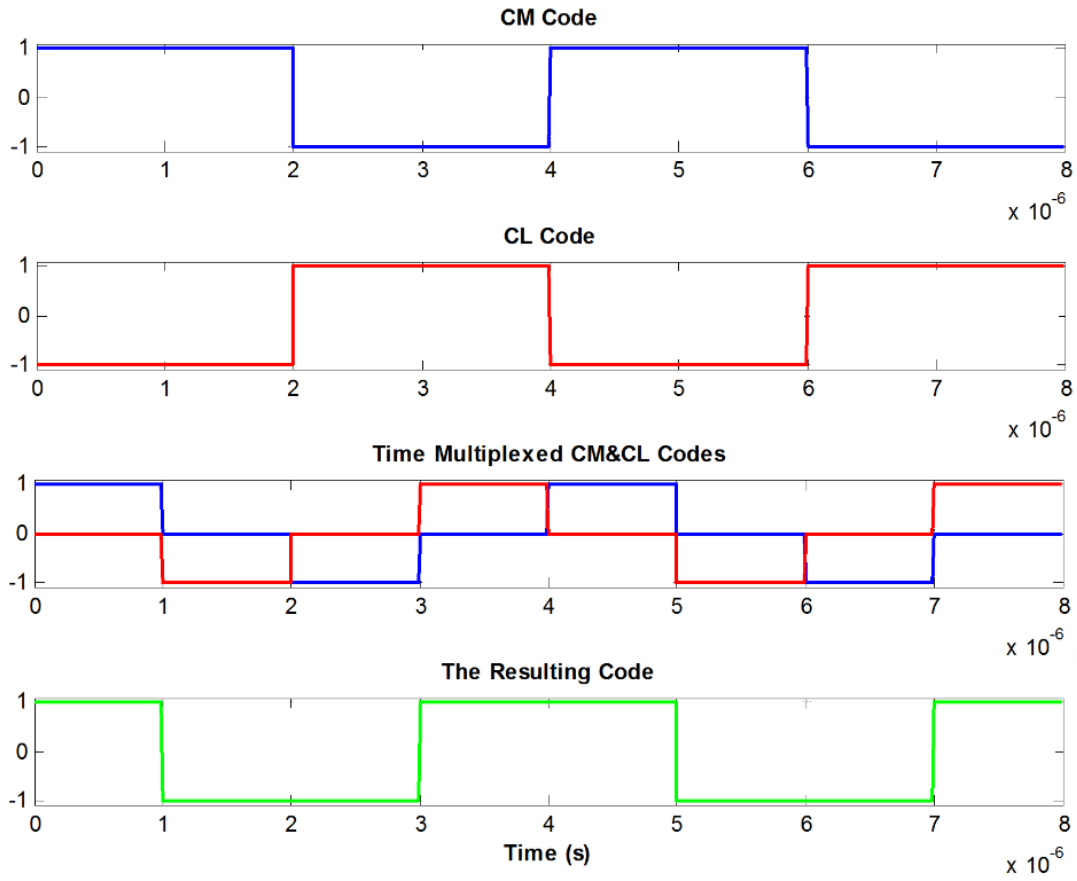

Figure 4-3 Time-multiplexed representation between CM and CL codes

L2C signal broadcasts at a higher efficient power than the L1CA signal and achieves 42 dB cross-correlations that are easier to receive in challenging environments such as urban-canyons and indoors [46]. Furthermore, when it is combined with L1CA signal, it will allow a faster signal acquisition as well as improving the receiver sensitivity, also in a dual-frequency receiver; L2C enables ionospheric correction that boosts accuracy. Commercially, this signal is estimated to yield *"$5.8 billion*" in economic productivity benefits by the year 2030 by the Commerce Department [47].

The received L2C GPS signal can express as:

$$S_{R,L2}^{k} = \sqrt{2P}D^{k}(t-\tau) \oplus (CM^{k}(t-\tau) \otimes CL^{k}(t-\tau))\, cos\left(2\pi(f_{L2} + f_{d}^{k})\, t + \theta^{k}\right) + w_{RF}(t)$$

where the sign $\oplus$ *and* $\otimes$ *indicate add based modulo-2 and time signal multiplexing chip-by-chip respectively.* CM^{k} *and* CL^{k} *are the CM and CL code sequences assigned to satellite number k.*

Finally, the minimum received power the of the L2C GPS signal is less than L1CA signal by 1.5 dB, i.e., in outdoor environments it is -160 dBW [48]; and also in the acquisition engine, the values of the code-phase-delay and Doppler-frequency-shifts needs to be determined.

4.1.3 GPS Acquisition Methods

The main aim of the acquisition process is to determine three unknown parameters of the received GNSS signal. These parameters are code-phase-delay, coarse values of the Doppler-frequency-shifts (carrier frequency), and the satellite's PRN identity (SV's ID). For the sake of simplicity, we will assume the receiver already knows the SV's ID and, therefore, the acquisition will be turned to a two-dimensional search for code-phase-delay and Doppler-frequency-shifts parameters. The estimated values of two parameters will be sent directly to tracking stage to keep followed the change in these two parameters. In the next sections, three common methods [49] of acquiring the GPS signal will be reviewed, which are serial search, parallel frequency space search, and parallel code phase search.

1. Serial search

The serial search engine examines the received signal successively at each possible code-delay and Doppler-shifts in the time domain. Given that there is no complexity involved in acquiring the signal and only addition and multiplication operations are needed, the serial search engine is easy to implement in the time domain. However, the high number of combinations involved makes the searching process very slow, and in weak signal scenarios it makes acquiring signals even more difficult since it requires long integration time.

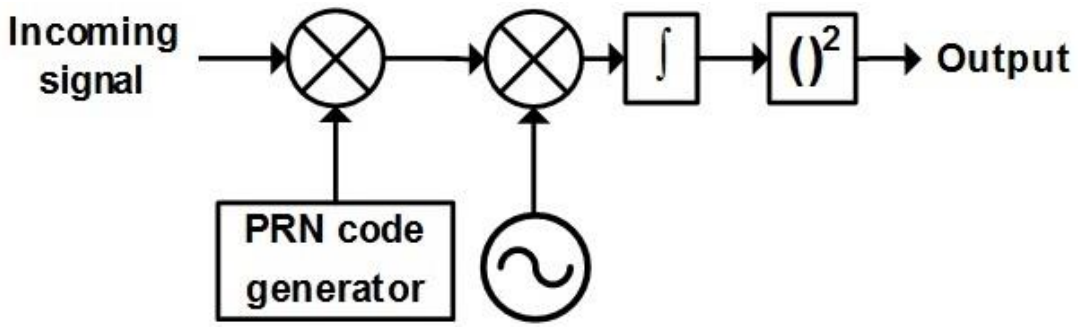

Figure 4-4 Block diagram of the serial search engine

As seen in Figure 4-4, the acquisition engine is based on multiplying locally generated PRN code and locally generated carrier signals. In the locally generated function, the PRN code corresponds to a specific satellite, with a code phase from 0 to 1022 chips. The incoming signal is firstly multiplied by a locally generated PRN code and then the resulting signal is multiplied by a locally generated carrier signal. The output signal is integrated over 1 *msec* (in case the signal is L1CA GPS) which corresponds to the length of one PRN code and is finally squared.

2. Parallel Frequency Space Search

The serial search acquisition is a very time-consuming acquisition process, so, to improve the acquisition one of the search parameters need be implemented in parallel. Therefore, Fourier Transform is used to parallelise the frequency search after removing the PRN code. As shown in Figure 4-5, the first step of wiping the PRN code is exactly the same as it is in the serial acquisition method. The resulting signal is transformed into the frequency domain “parallelise search” by a Discrete Fourier Transform (DFT) or a Fast Fourier Transform (FFT) and is finally squared.

The resolution of this search relies on signal length; the resolution becomes finer when the signal is longer. This method is also time consuming since for each code shift it needs to apply FFT. The minimum shift code is 2*1023 times.

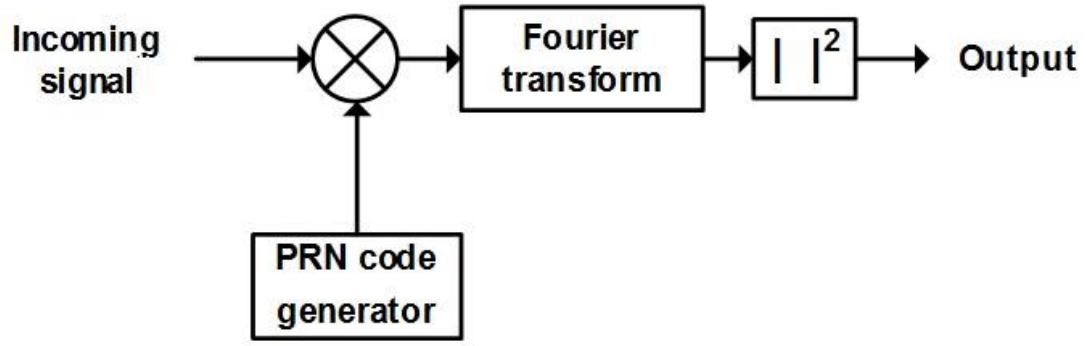

Figure 4-5 Block diagram of the parallel frequency search engine

3. Parallel Code Phase Search

The new method will also parallelise one of the search parameters, which being the code phase, to reduce time consumption; because the shifting search in the frequency is typically 500 Hz that means if the Doppler shift ±10 KHz so the total number of frequency shifts is 41.

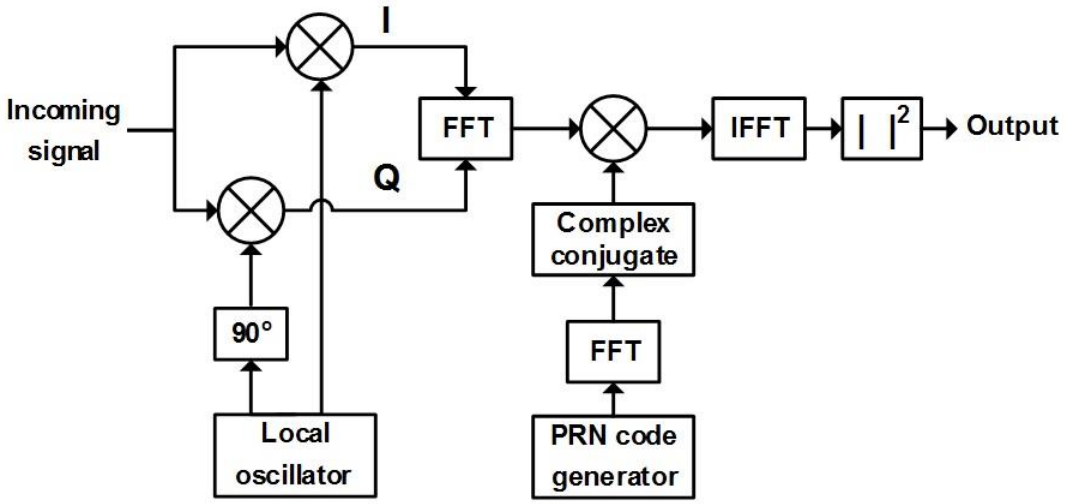

Figure 4-6 Block diagram of the parallel code phase search engine

As shown in Figure 4-6, the locally generated carrier signal is multiplied with the incoming signal. This result in generating two signals, in-phase (I) and quadrature (Q). The I and Q signals are then combined in complex format (I + j*Q) and the

resulting signal is finally fed to the FFT function. On the other hand, the generated PRN code is transformed into the frequency domain and the result is complex conjugated. The complex conjugate of the PRN code is multiplied with the Fourier Transform values of the complex signal. The multiplication result is then transformed back to the time domain by using an IFFT and then the result is squared. The maximum value of the squared result represents the correlation between the incoming signal and the locally-generated signal. If there is a peak present in the correlation result, it represents the index of the beginning of the PRN code and the value of the carrier frequency of the incoming signal.

This search method is used in our orthogonal channel, since it is less time consuming and also its input, after removing the carrier, is complex/orthogonal values which is consistent with our proposal.

4.1.4 Characteristics of the L1CA and L2C GPS Signals

The fact that both L1CA and L2C signals are transmitted from the same SV's means that all of the received signal error parameters (e.g., Doppler & delays) are related [45]. To achieve synchronization between our two signals of interest, we have studied three important parameters (navigation message bit, code-phase-delay and Doppler-frequency-offset). The actual navigation message bit format is different on L1CA and L2C, but the transition of navigation message does occur at the same time. Also, having the same transmission at the same time means that there is a correlation between the Doppler frequency on L1 and L2 by the ratio L2/L1, and also that both codes, L1CA and L2C, have the same code-phase-delay with respect to their code time length. This relationship gives us an opportunity to combine the two signals in the acquisition stage using a single channel. Note that, "relative group delay" errors caused by, for example, satellite transmitter hardware, ionosphere, and atmosphere are neglected in this implementation due to their total value is in nanoseconds, which will not affect the acquisition process, but must be taken into account in the tracking process [50].

4.2 Literature Survey: Combined Multi-GNSS Signal Acquisition

From correlation view, the acquisition of L2C signal is favoured over L1CA signal because L2C has long code length, which presents a possible 28 dB gain to help acquire weaker signals [51]. However, the time required for estimating the code-phase-delay and Doppler-frequency-offset of L2CM is at least 4000 times longer than L1CA (L2CL codes length is 1.5 *sec* and that of L2CM is 20 *msec*), requiring a stable oscillator, which is impractical. Aiding the acquisition of L2C signal with an estimated code-phase-delay and Doppler-frequency-offset of the L1CA signal was proposed to reduce the long time required for acquiring L2C signal alone [52]. This technique capitalises on the property that both received L1CA and L2C signal-errors (data, code, and the carrier) are coherently associated. Actually, this aiding reduces the number of the frequency bin searches in the L2CM acquisition by 95% as well as limiting the search range of finding the beginning of the L2CM code. However, this aiding technique loses 3 dB in signal power because it acquires the L2CM signal alone (i.e. L1CA is used only to aid the L2CM acquisition without combining their powers).

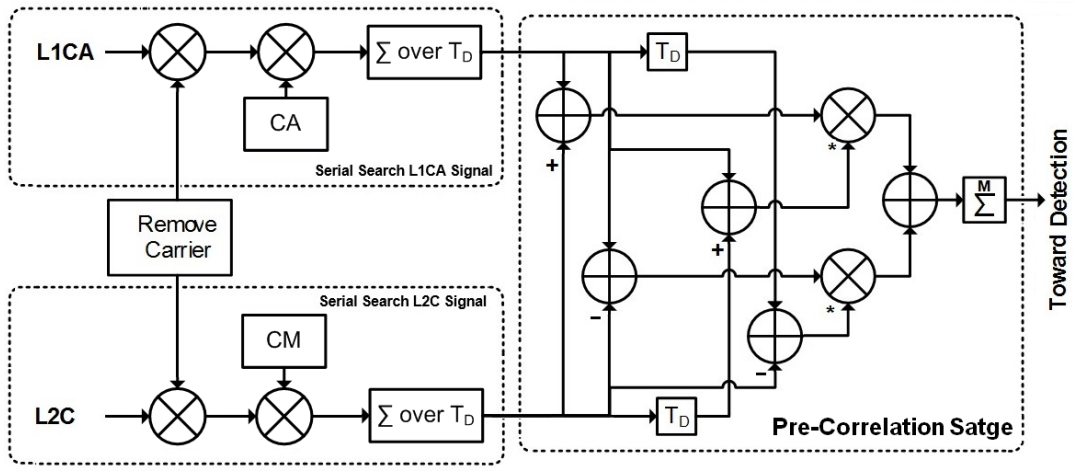

Figure 4-7 L1CA and L2C Combined Detection Scheme

One of the first to publish such combined receiver has claimed a 20 dB processor gain and improved the acquisition sensitivity be 2 dB [53]. As shown in Figure 4-7, this receiver utilized two side-by-side serial search channels, one for each signal, to

remove the carrier and the code of the received signals and then integrate their result over 1ms time individually. The output of these two channels is then fed to a post-correlation stage that performs a summation and mixing functions necessary to achieve a combined non-coherent acquisition as well as a differential acquisition over 1ms concurrently. The output of the post-correlation stage is then sent the detection stage after it has accumulated for M *msec* (*where M can be 1 for a clear outdoors reception and it will increase as the receiver environment get noisy up to a value of 20 for bad reception area/indoors*). This scheme avoids the noise of the received signal while combining the powers of the two signals because of the resultant noise being uncorrelated between the non-coherent and differential acquisition it uses.

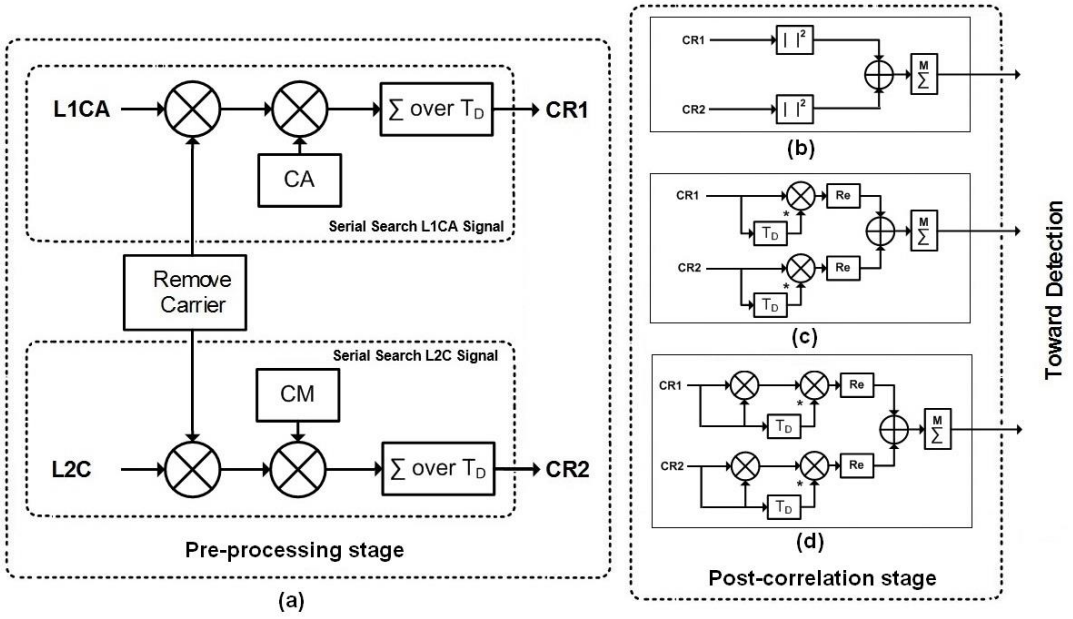

Figure 4-8 Structure of post-correlation technique based serial search engine (a) Pre-processing correlation stage (b) Non-coherent (c) Differential (d) Non-coherent and differential acquisitions

To gain more acquisition sensitivity, the authors of the aforementioned scheme went on to modify it by replacing the structure of the post-correlation stage. As exhibited in Figure 4-8, they proposed to use any one of the three structures: 1) non-coherent, 2) differential, and 3) combining the non-coherent with the differential acquisition [54]. The trade-off between these three structures is in their

implementation complexity and improved acquisition sensitivity as follows:

The first method (non-coherent acquisition) can be chosen due to the simplicity of its implementation, with low computation load. It performs the summation of the non-coherent output of the two acquisition channels prior to the detection stage, as shown in Figure 4-8 (b). This means the method performs the summation of the squared correlation values of the two signals and then accumulates the result for M *msec* and then forwards the result to the detection stage to denote the acquisition decision. The correlation power in this method is increased but the sensitivity improves only slightly because the noise has also been amplified/squared.

The second method (differential acquisition [55]) can be chosen to avoid the noise augmentation in the previous method. Here, the noise is not correlated since it comes from multiplying a successive correlated signal. The outputs of the serial search channels, which are CR1 and CR2 "values of Correlated signals" (see Figure 4-8 (a)), are multiplied with conjugate delay version of the same outputs separately, as depicted in Figure 4-8 (c). Then, the real parts of the previous multiplication are gathered and accumulated for M *msec*, after that this correlated signal is forwarded to the detection stage to announce the acquisition result. This method achieves better acquisition sensitively over the non-coherent method by 0.5 dB; meanwhile, its implementation remains low in terms of computational requirements.

The third method (combines the non-coherent and the differential acquisitions, named $NCDiff_{L1L2}$) is shown in Figure 4-8 (d). This method can be chosen to exploit all the correlator power outputs, based on the non-coherent and the differential techniques, so to improve the processing gain, which directly reflects on enhancing the acquisition sensitivity. Note that, $NCDiff_{L1L2}$ implementation is different from their earlier paper [53] reviewed earlier, in that it has 4 mixers, 2 unit delays and 1 adder. This is achieved by having the output of each serial search channels (CR1 or CR2) multiplied with a conjugate version of itself to get the non-coherent result, which is then multiplied with the differential result. The differential result comes from multiplying the serial search channels output (CR1/CR2) with the conjugate of one millisecond delayed samples of the same output (CR1/CR2). The multiplication of non-coherent and the differential outputs are then grouped and the real part is

accumulated for M *msec*, which is then sent to the detection stage to declare the acquisition decision.

$NCDiff_{L1L2}$ method is an efficient solution to combine the L1CA and L2C signals as it balances implementation complexity and improves sensitivity. Accordingly, it will be used to compare with the best performance one of our proposed methods.

Similarly, FFT technique has been used as a pre-processing stage to combine the two GPS signals (L1CA&L2C) [56], as shown in Figure 4-9. Obviously, the structure of the FFT-based acquisition method is the same as the previously discussed approach (see Figure 4-8), but by changing the serial search engine search with a FFT search engine. Therefore, the FFT-based acquisition method also requires two FFT search channels, which are placed side-by-side, as an initial process for estimating the code-phase-delay and the Doppler-frequency-offset of L1CA and L2C signals independently. Note that the process of the GPS signals inside the FFT search box in Figure 4-9 (a) has been explained earlier in Section 4.1.3, point two.

As presented in Figure 4-9, the FFT-based method proposes using any one of the three structures: 1) non-coherent, 2) differential, and 3) coherent summation. Also, the trade-off between these three structures is in their implementation complexity and enhanced acquisition sensitivity as follows:

The first combination method performs the summation of the non-coherent output of the two FFT acquisition engine prior to the detection stage, as shown in Figure 4-9 (b). While, in the second method prior to adding the values of the FFT outputs, firstly it differentiates them. The combination stage structure and the performance of the first method and the second method in FFT-based is the same as the first and the third methods in the previous approach (see Figure 4-8 (b) and (d)) respectively.

The third method of FFT-based approach performs coherent addition and subtraction for the correlated signals (CR1 and CR2) to produce two outputs, as shown in Figure 4-9 (d). Each one of these outputs will be squared and accumulated for M *msec* and then the maximum value will be selected to resultants. The reason for using addition and subtraction to the signals correlator outputs in this method is

to avoid relative signs between the L1CA and L2CM signals. The performance of this method is the same as the $NCDiff_{L1L2}$ method.

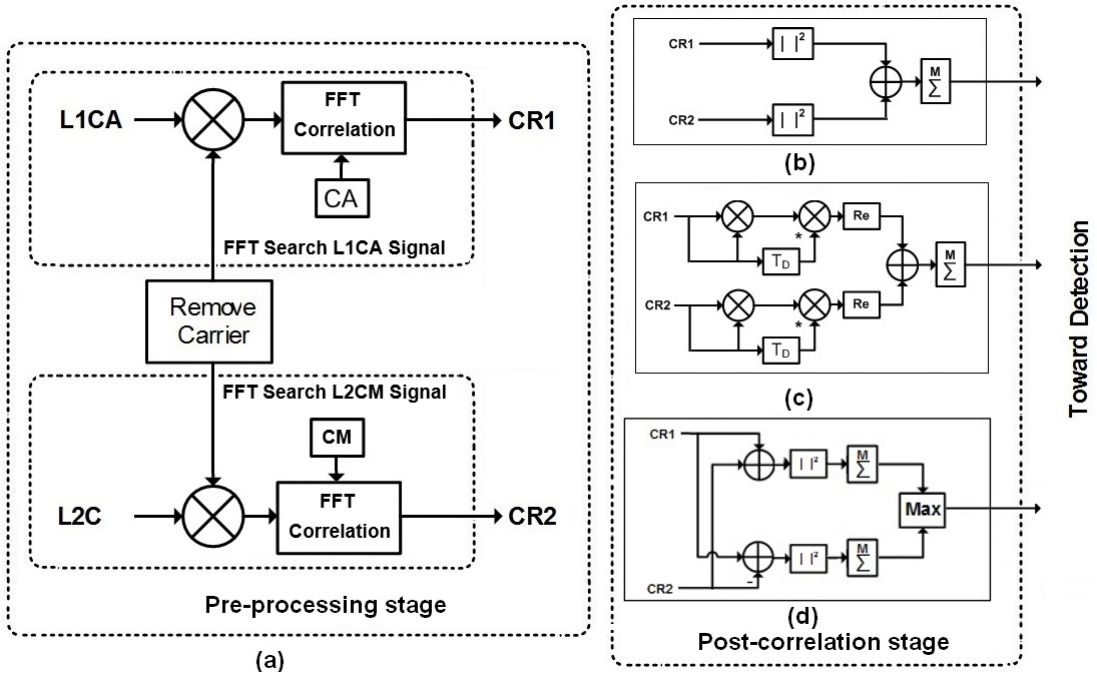

Figure 4-9 Structure of post-correlation technique based parallel code phase search engine (a) Pre-processing correlation stage (b) Non-coherent (c) Non-coherent and differential (d) Coherent acquisitions

The advantage of using FFT search technique over serial search is the reduced processing time, but the results in terms of enhancing the acquisition sensitivity of FFT search technique are identical to the serial technique. Since we are using FFT technique in our proposed acquisition channels, we will compare our simulation result of each one of our six methods with NC FFT-based method.

In the same vein, the MGDC (Modified Generalized Differential Combination) method is used for combining the L1CA and the L2C signals in the acquisition stage, as depicted in Figure 4-10. Equivalent dual channels of MGDC are employed to correlate the received L1CA and L2C signals separately [57].

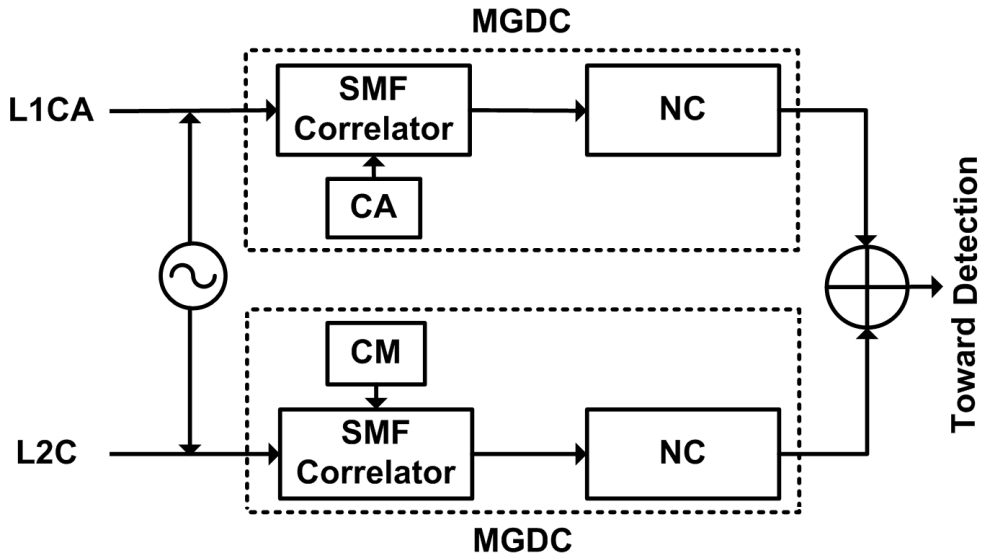

Figure 4-10 Combined L1CA and L2C GPS signal acquisition based on dual-MGDC

The received signals (L1CA&L2C) correlate with the local replicas of their codes at the pre-processing stage called Segmented Matched Filter (SMF). SMF firstly segments both received signals and then multiplied with the locally generated CM+CA codes in order to produce complex correlated values. The number of correlators is based on the time length of the L-segmentations and the correlated values at different time intervals are then differentially combined in different spans. The chosen length of the L segmentation is 1ms, which will be favourable with the length of the CA code, this leads to using 20 correlators in each channel. The correlator outputs of SMF stage are then fed to the 2 NC blocks.

An NC block is a non-coherent acquisition method. The output results of MGDC blocks are accumulated together prior to the detection stage. This technique has enhanced the acquisition sensitivity over the $NCDiff_{L1L2}$ method by 1.5 dB. However, the complexity of the MGDC is too high since it uses 20 correlators for each signal, which consumes lots of power. Since the results of the MGDC acquisition exhibit better signals detection over $NCDiff_{L1L2}$, our simulation results will also be compared with the MGDC implementation.

The mechanism of our proposed implementation is inspired by the implementation of an L1CA, and L1C GPS signals acquisition channel proposed to

capture the L1C signal at low Carrier to Noise density ratio (C/No) when the acquisition of the L1C signal alone fails [58]. This method is based on a conventional parallel code-phase search algorithm, as shown in Figure 4-11. This method, instead of generating a single code, it generates a combination of L1CA, L1CD (Channel of Data) and L1CP (Channel of Pilot) codes. The processing of the two signals in this acquisition method is the same as the processing of single GPS signal in the conventional acquisition channel. The A, B and C coefficients in Figure 4-11 are used to re-weigh the signal power since their relative powers are different, more details on how to calculate these coefficients in [59]. Additionally, since the relative sign between the two signals differs, the acquisition is performed in parallel four times by changing the sign of locally generated codes (A, B and C).

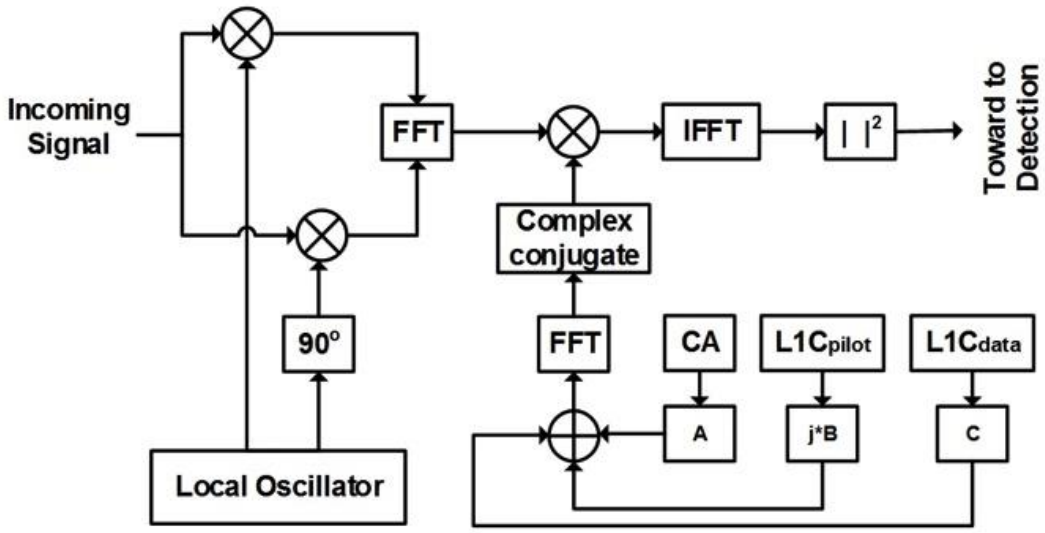

Figure 4-11 Structure of combined L1CA and L1C GPS signal acquisition scheme

The idea in this implementation is simple, but it is very effective since the two signals are transmitted from the same satellite at the same frequency and they are orthogonal in terms of their codes. Also, the two signal errors are related, so it is easy to process them together in a single acquisition stage without worrying about the overlap. In fact, this idea is the essence of our orthogonal acquisition channel in combining the L1CA and L2C signals in a single acquisition channel. Though, the L1CA and L2C signals transmit from the same SV with orthogonal codes they have different carrier frequencies. That will be an obstacle to using a single acquisition channel. So, to make the two signals run at the same frequency in the receiver part, a

pre-processing stage based on using our OCBPSR that is utilized to fold the two signals at the same frequency [60] in the digital domain prior to the acquisition channel.

Our conclusion from this short review is that side-by-side implementation for acquiring the L1CA and L2C signals consumes more power. However, we believe that improving the processing/overhead of such acquisition is a worthy task. Therefore, this chapter proposes two orthogonal acquisition channels to acquire these two signals and to improve the detection sensitivity.

4.3 Combining L1CA and L2C GPS Signals Acquisition

This section describes the methodology employed in our orthogonal acquisition channels. In addition, it explains the implementation procedure of the two channels and is then followed by the test methodology.

4.3.1 Acquisition Methodology

The methodology behind our proposed channels is cantered on orthogonalising the two GPS signals (L1CA and L2CM) prior to correlating them as a single signal to reduce the computational load of the acquisition process without impeding the acquisition sensitivity. As shown in Figure 4-12, the four acquisition stages in our orthogonal channels are; 1) the Frontend stage 2) the orthogonalising stage 3) the correlation stage and 4) the combination stage. The greyed blocks in Figure 4-12 demonstrate the processes that we have introduced for efficient implementation of the two signals in our channel.

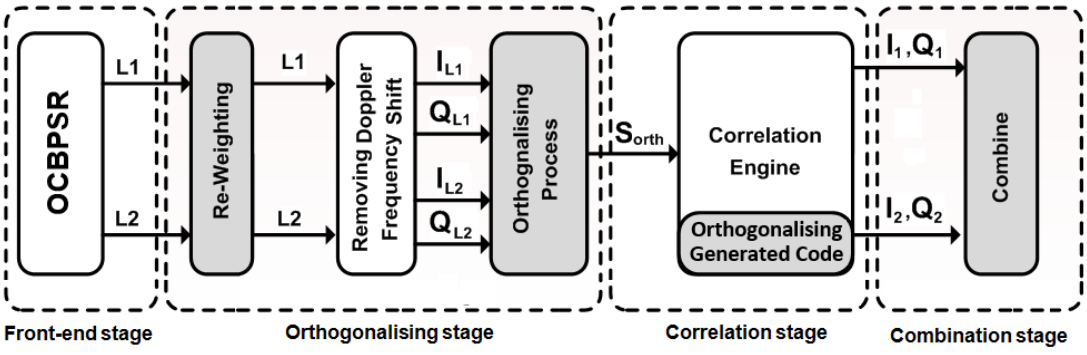

Figure 4-12 Our methodology of combined L1 and L2 signal acquisition channel

Stage 1: In the Front-end stage, the OCBPSR front-end is used to down-convert the two signals (L1CA&L2C) to baseband signals, so that both the baseband signals have the same folding-frequency. The mathematical equation of the two signals after ADC can be expressed as:

$$L1(nT_s) = A\, D_{L1}(nT_s - \tau) \oplus CA\,(nT_s - \tau)\, cos(2\pi(f_{fold} + f_d)nT_s + \theta_1) + w_{IF,L1}(nT_s) \quad (4\text{-}1)$$

$$L2(nT_s) = A\, D_{L2}(nT_s - \tau) \oplus CM(nT_s - \tau)\, sin(2\pi(f_{fold} + \beta f_d)nT_s + \theta_2) + w_{IF,L2}(nT_s) \quad (4\text{-}2)$$

where $(D_{L1}, \theta_1, w_{IF,L1})$ *and* $(D_{L2}, \theta_2, w_{IF,L2})$ *are the navigation data, the initial phase and additive noise of L1CA and L2C GPS signals respectively.* T_s, n *and* β *are the sampling time, integer number and the ratio between the signals frequencies (L2/L1=* $\alpha = 0.799$*) respectively.*

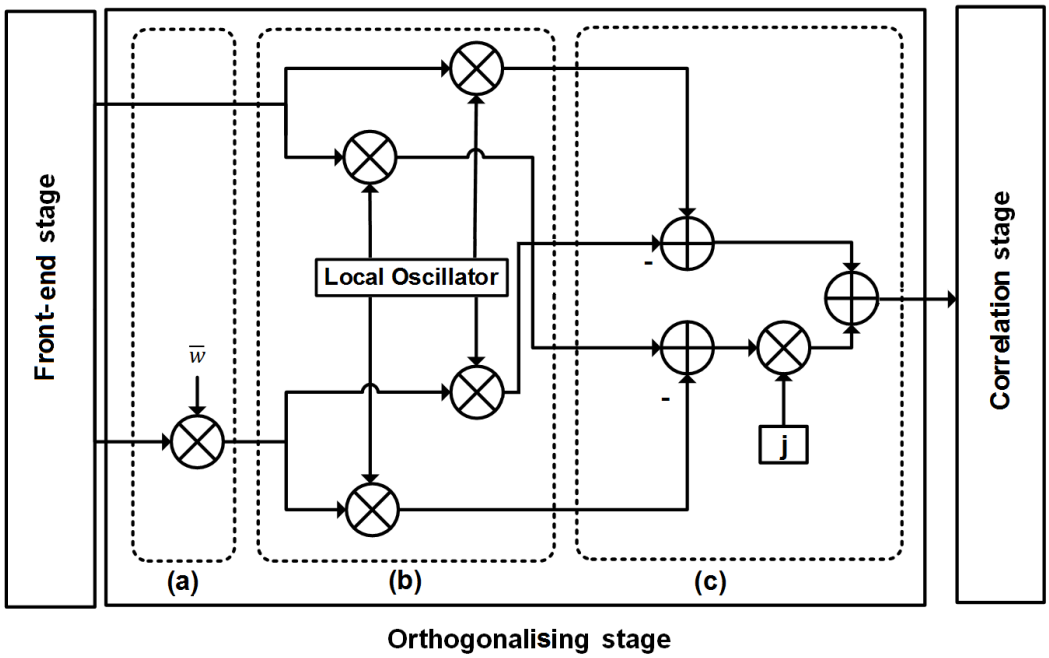

Figure 4-13 Orthogonalising stage of the combined methodology. (a) Re-weighting the signals (b) Removing the carrier and the Doppler-frequency-shifts (c) Orthogonalising the signals

Stage 2: The orthogonalising stage is divided into three processing steps; reweighting the signal power, removing the folding-frequency plus Doppler shifts,

and orthogonalising the signals into a single orthogonal signal, as shown in Figure 4-13.

In the first step of the orthogonalising stage, the required weight ($\bar{w}$) to equalising the relative signal power levels is calculated in advance, before the acquisition is started. That means each signal needs to be scaled individually in order to combine them optimally.

The received power of L2C signal is 1.5 dB lower than the L1CA, so, the received strength of L1CA is 1.4125 times higher than that of L2C on a linear scale.

$$1.4125\,\bar{w} + \bar{w} = 1 \Longrightarrow \bar{w} = 0.414 \qquad (4\text{-}3)$$

Based on (4-3), the L1CA and L2C signals have a portion $\bar{w}$ and $1 - \bar{w}$ of the total power in the combined signal respectively. Since only CM code is considered in this implementation, where the CL code is zeroed, an attenuation in the signal of 3 dB results because half of the signal power is neglected. Overall, the L2CM signal will decrease by 4.5 dB from L1CA signal. Therefore, this will require re-weighting the received power levels of the signals based on the new attenuation value. The newly calculated $\bar{w}$ is 0.2619, which is used to represent the power split for the L2CM component. Note that, our acquisition channels can also work with CL code, but because the code length is 1.5 *msec* and it results in a very large computational load and undesirable complexity so the CM code is preferable.

The second step of the orthogonalising stage is similar to the conventional acquisition method of removing the Doppler-frequency-shifts and the folding-frequency from the received signals in order to convert the signal into a baseband signal, as illustrated in Figure 4-13 (b). So (4-1) and (4-2) after applying the second step become:

$$I_{L1}(nT_s) = A_1 D_{L1}(nT_s - \tau) \oplus CA\,(nT_s - \tau)\,cos(2\pi\,\Delta f_{L1} nT_s + \theta_1) \qquad (4\text{-}4)$$

$$Q_{L1}(nT_s) = A_1 D_{L1}(nT_s - \tau) \oplus CA\,(nT_s - \tau)\,sin(2\pi\,\Delta f_{L1} nT_s + \theta_1) \qquad (4\text{-}5)$$

$$I_{L2}(nT_s) = A_2 D_{L1}(nT_s - \tau) \oplus C\,(nT_s - \tau)\,cos(2\pi\,\Delta f_{L2} nT_s + \theta_2) \qquad (4\text{-}6)$$

$$Q_{L2}(nT_s) = A_2 D_{L1}(nT_s - \tau) \oplus C\,(nT_s - \tau)\,sin(2\pi\,\Delta f_{L2} nT_s + \theta_2) \qquad (4\text{-}7)$$

where ($\Delta f_{L1} = f_d - \widehat{f_d}$) and ($\Delta f_{L2} = \beta f_d - \beta\widehat{f_d}$) are the residual carrier frequency of the L1CA and L2C GPS signals respectively and $\widehat{f_d}$ is estimated Doppler-frequency-shifts.

For the sake of simplicity, the notations in the above/following equations for the AWGN have been neglected, but it is still considered in our simulation. Theoretically the residual frequency values of the two signals (Δf_{L1} and Δf_{L2}) should be the same and in an ideal scenario ("*when the frequency of the locally generated signal matches the frequency of the received signal*") should be equal to zero, but practically it depends on how accurate the down-conversion components such as the local oscillator, mixer performance and the filters are. Therefore, we will consider the value of residual frequency further in the channels' evaluation.

The last step in the orthogonalising stage is combining the I's and Q's of the two signals into a signal orthogonal signal as depicted in Figure 4-13 (c). Since these two processed signals are baseband signals, meaning they have only code and data where the signal codes are almost orthogonal, we can add and orthogonalise them without any overlap between the two signals or being concerned whether one will dominate the other. So, the best combination of the baseband signals to create orthogonal signal is to subtract (4-6) from (4-4) to produce the I-branch of the new orthogonal combined signal, as expressed in (4-8) and also subtract (4-7) from (4-5) to produce the Q-branch of the orthogonal combined signal, as shown in (4-9).

$$I_{Comb}(nT_s) = I_{L1} - I_{L2} \tag{4-8}$$

$$Q_{Comb}(nT_s) = Q_{L1} - Q_{L2} \tag{4-9}$$

At the end of this stage, we will have a particular orthogonal signal by adding the I_{comb} and Q_{comb} components together as expressed in (4-10) that contains the information of the two signals.

$$S_{Orth}(nT_s) = I_{Comb} + j * Q_{Comb} \tag{4-10}$$

Stage 3: Note that, the correlation stage of each one of the proposed channels (OSC&OPC), it has owned structure, the following explanation of the correlation stage is for the OSC while the explanation of the OPC will be detailed in Section 4.5

(see Figure 4-36).

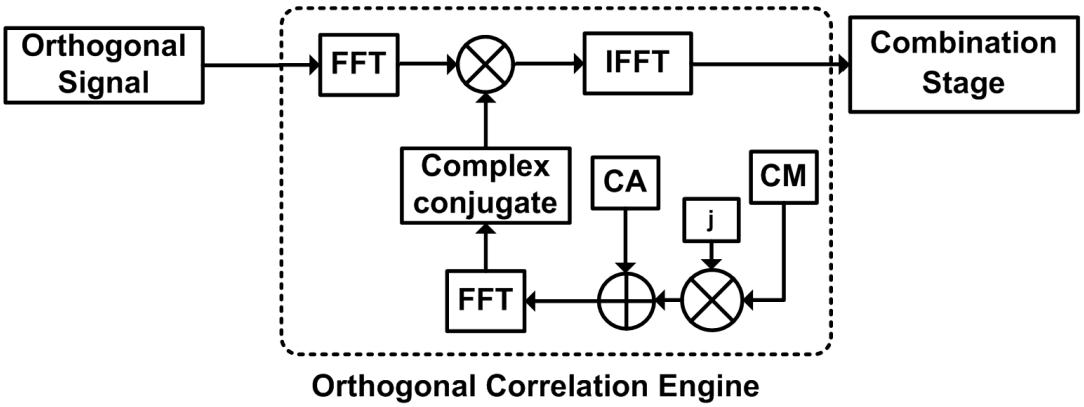

Figure 4-14 Developed correlation engine for combined L1CA and L2C GPS signals (orthogonal correlation engine)

In the correlation stage of OSC, the newly generated/resultant orthogonal signal in (4-10) will be fed to the orthogonal correlation engine, as illustrated in Figure 4-14. This engine is a parallel code-phase search engine, which has two codes added in the local generator code block. This advanced local generator code generates a 1 *msec* of the CA code and also 1 *msec* of the CM code and then combines them in orthogonal representation (*CA+j*CM*). After performing the code correlation, the output of the IFFT function is fed to the combination stage. The output represents a Complex Correlated Signal (CCS) that includes in its real part a correlated signal of I_1 and Q_2 signals and in its imaginary part a correlated signal of I_2 and Q_1 signals. The correlated signal components of the two signals can be written mathematically as:

$$I_1 = \frac{1}{Ns}\sum_{n=0}^{Ns-1} I_{L1}(n)\, CA\,(n-\hat{\tau})$$

$$\&Q_1 = \frac{1}{Ns}\sum_{n=0}^{Ns-1} Q_{L1}(n)\, CA\,(n-\hat{\tau}) \qquad (4\text{-}11)$$

$$I_2 = \frac{1}{Ns}\sum_{n=0}^{Ns-1} I_{L2}(n)\, C\,(n-\hat{\tau})$$

$$\&Q_2 = \frac{1}{Ns}\sum_{n=0}^{Ns-1} Q_{L2}(n)\, C\,(n-\hat{\tau}) \qquad (4\text{-}12)$$

where Ns is the number of signal samples in coherent integration time, which is 1 msec.

Stage 4: In the final stage the correlation component output ($I_{1,2}$ and $Q_{1,2}$) is combined again to obtain the final correlation value or the decision vector, as mentioned earlier there are three different combination methods for each channel, i.e., six methods will be explained/discussed in this chapter.

4.3.2 Acquisition Procedure

The following steps achieved the procedure that we have followed in our "OSC" implementation for acquiring the L1CA and L2CM GPS signals in the digital domain:

1. Re-weigh the signals power prior to down-converting them to the baseband signals.
2. Remove the Doppler frequency from the incoming L1CA/L2CM signals by multiplying them with the locally generated carrier wave at fixed Doppler frequency $fd/\alpha*fd$ that will generate in-phase component (I_{L1}/I_{L2}) and a quadrature component (Q_{L1}/Q_{L2}).
3. Orthogonalise, the signal components to the output combination, is (I_{L1}-I_{L2})+j*(Q_{L1}-Q_{L2}).
4. Calculate the FFT of the output combination.
5. Generate local replica of CA and CM codes and then gather in orthogonal form as CA +j*CM.
6. Compute the complex conjugate of the FFT of the composite code.
7. Multiply the output of step 4 and step 6 and then the IFFT is applied to the output.
8. Forward the real part and the imaginary part of the IFFT to three different combination methods; the output result of these methods is called a decision vector.
9. Calculate the maximum peak of the decision vector.

10. Exclude a number of samples of the main lobe width, which are around the maximum peak in the decision vector.

11. Calculate the second maximum peak from the remaining part of the decision vector.

12. If the ratio of the first and the second maximum peaks is greater than a predefined threshold (β), then the signal is acquired; else the whole procedure is repeated for all Doppler frequency range (from -10 KHz to +10 KHz).

In the implementation of the OPC, steps from 4 to 7 need to be performed twice or in parallel with changing the code combinations in each run, full detail documented in Section 4.5.

4.3.3 Testing Methodology

The following five performance factors are used to evaluate the two orthogonal acquisition channels in comparison with the conventional methods for acquiring L1CA and L2CM and other combining acquisition methods, which are the $NCDiff_{L1L2}$, FFT-based methods, and the MGDC methods that have been explained in the literature survey section (see Section 4.2). These are:

i. the probability of detection
ii. the receiver operating characteristics curve
iii. the ratio of the maximum correlation peak value
iv. the residual frequency effect
v. the initial phase effect.

MATLAB is used to simulate the two GPS signals L1CA and L2C, which they are sampled at the same rate 17.391 MHz (both signals have the same folding-frequency = 7.161 MHz) based on using OCBPSR. Also, we evaluate our orthogonal channels with the conventional L1CA & L2CM, the $NCDiff_{L1L2}$ method, FFT-based methods and the MDGC method.

In our test methodology, Monte Carlo simulation technique is dedicated to evaluating all the acquisition methods mentioned above.

1. Probability of detection and Receiver Operating Characteristics Curve (ROC) factors

ROC is a function of the Probability of Detection (P_D) and the Probability of false alarm (P_{fa}). The probability of detection (acquisition sensitivity) refers to the correct decision of detecting the signals, and that occurs when the ratio of the maximum peak value of correlation vector crosses the chosen threshold (β) and its frequency bin and code-phase-delay in the acquisition search are both correct. A false alarm is declared when the ratio of the maximum peak value of correlation vector result satisfies the β with wrong frequency bin, or wrong code-phase-delay. i.e. the acquisition is considered a false detection. However, if the ratio of the maximum peak value of the correlation vector does not satisfy β, it means that no signal could be detected and the acquisition is considered not detected. More details about the detection theory can be found in [61]. The simulation parameter settings in Table 4-1 and Table 4-2 will be used to assess our orthogonal acquisition channels in terms of the probability of detection and the ROC respectively. We will use two different test scenarios based on those tables to evaluate the performance of the orthogonal acquisition channels.

Table 4-1 Parameters used to evaluate signals detection probability

Parameters name	**L1CA**	**L2C**
C/No	**From 12 to 40 dB-Hz**	**C/No, L1CA – 1.5**
ΔF	**0**	
Initial Phase θ	**0**	
Nav. Data	**{-1, 1}**	
Threshold *β*	**2.5**	
Integration time	**1 *msec***	
Simulation length	**10,000 times**	

2. The ratio of maximum correlation peak factor

This factor is used to analyse the effect of the combined noise that comes from combining the L1CA and L2CM signals prior to acquisition channel as well as the noise that comes from the cross-correlation inside the correlation engine in our acquisition channels. The ratio (γ) can be written as:

$$\gamma = \frac{The\ maximum\ peak}{The\ second\ maximum\ peak}\ \text{dB}.$$

Furthermore, the γ ratio plays a significant role in deriving the false alarm probability [62]. Therefore, to make sure that the accumulated noise (inside and outside the correlation) will not affect the acquisition decision, a test scenario has been setup based on using the simulation parameters in Table 4-1.

Table 4-2 Parameters used to calculate the ROC

Parameters name	L1CA	L2C
C/No	26 dB-Hz	24.5 dB-Hz
ΔF	50 Hz	α ΔF (L1CA)
Initial Phase θ	0	
Nav. Data	1	
Threshold β	From 1 to 3	
Integration time	1 *msec*	
Simulation length	1,000,000 times	

3. The residual carrier frequency (ΔF which results after Doppler removal process) factor

This factor has a direct effect on the amplitude of the correlator outputs [63]. That means increasing the residual carrier frequency value will decrease the detection probability, so it is important to measure the effect of the residual carrier frequency on our acquisition channels and compare it with other methods. The simulation parameters in Table 4-3 are used for this purpose.

4. The initial phase effect factor

Since our orthogonal acquisition channels coherently apply the summation of the baseband signals (L1CA and L2C) prior to the correlation engine, the sign of the bits

transmitted (navigation message) and initial phase value can strongly affect the performance of the acquisition method. For example, if these signals have the same initial phase but the sign of the transmitted bit on L1CA signal was an opposite sign to the transmitted bit on L2C signal, then combining the two signals coherently will degrade the combined signal power. Likewise, if both L1CA and L2C signals have the transmitted bit sign but they are out of phase, adding them coherently will also degrade the combined signal power. The simulation parameters in Table 4-4 are used to assess our acquisition method.

Table 4-3 Parameters used to evaluate effects of residual frequency

Parameters name	L1CA	L2C
C/No	29 dB-Hz	27.5 dB-Hz
ΔF	[0: 500]	$\beta\ \Delta F_{L1}$
Initial Phase θ	0	
Nav. Data	1	
Threshold β	2.5	
Integration time	1 *msec*	
Simulation length	10,000 times	

Table 4-4 Parameters used to evaluate effects of Initial Phase

Parameters name	L1CA	L2C
C/No	26 dB-Hz	24.5 dB-Hz
ΔF	0	
Initial Phase θ	[0: 2π]	
Nav. Data	{-1, 1}	
Threshold β	2.5	
Integration time	1 *msec*	
Simulation length	10,000 times	

4.4 Orthogonal Single Acquisition Channel (OSC)

OSC is a new acquisition design that is used to acquire L1CA and L2C GPS

signals simultaneously in orthogonal combination format. The novelty of this channel is centred on orthogonalising the two received signals (L1CA&LC2) into a single orthogonal signal allowing the acquisition to jointly estimate the code-phase-delay and Doppler-frequency-offset of both signals in a single channel.

As illustrated in the block diagram in Figure 4-15, the acquisition channels will first orthogonalise the received signals, L1CA and L2C GPS signals. The orthogonal signal is then processed by an orthogonal correlation engine that produces a complex representation of the correlated signal, as detailed in Section 4.3.1. To obtain the maximum correlation peak, we have a choice of three combination methods/post-correlation methods to process the complex correlated signal. The first combining L1CA&L2CM method uses "Direct Sum/Non-coherent Summation", which is named OSC-DS_{L1L2}, it detailed in Section 4.4.1. The second method implies a differential technique, which is called OSC-$DiffL_{1L2}$ that documented in Section 4.4.2. The third method uses a combination of the previous two methods "Direct Sum and Differential", which is called OSC-$DSDiff_{L1L2}$, full details in Section 4.4.3.

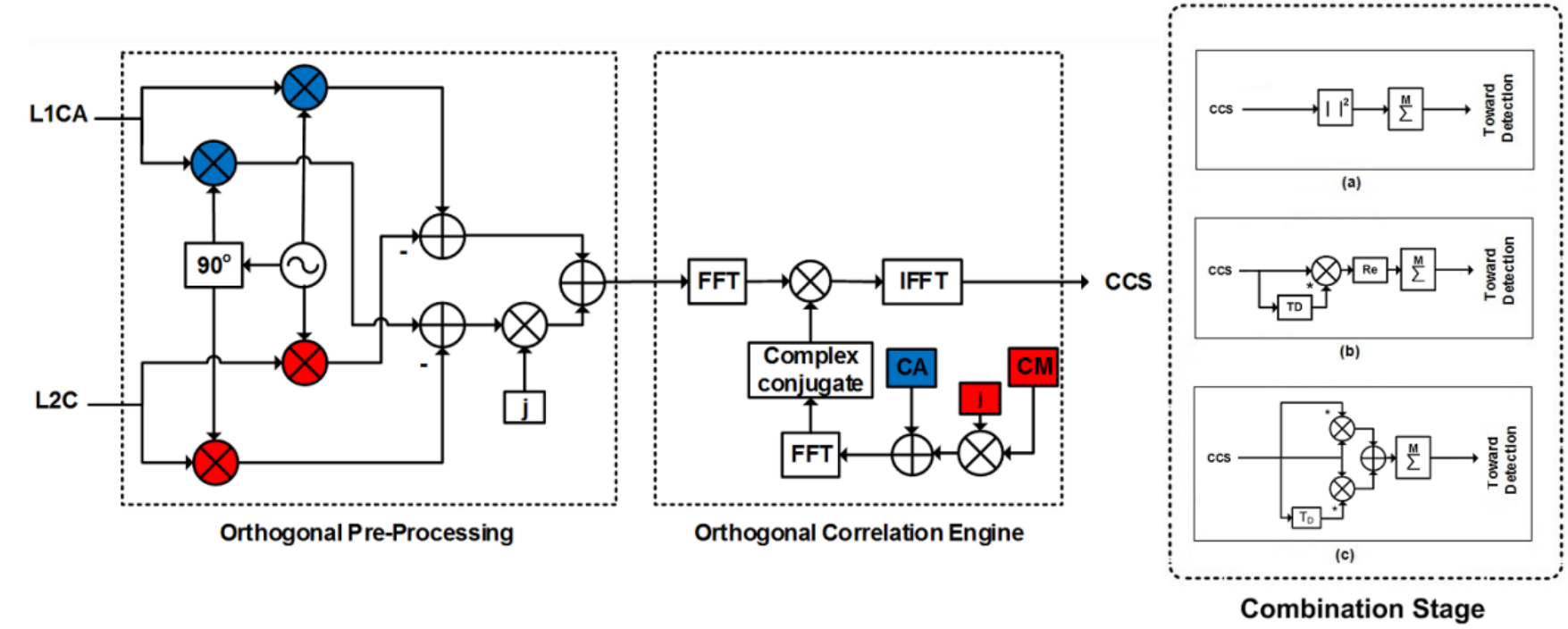

Figure 4-15 Structure of Orthogonal Single acquisition Channel (OSC) to acquire L1CA and L2C GPS signals

4.4.1 Direct Sum Acquisition: OSC-DS$_{L1L2}$

This method represents the direct sum of the complex correlated signal (CCS) that was obtained from correlating the L1CA and L2C GPS signals with the locally generated signal in the orthogonal correlation engine, as shown in Figure 4-16. The process of obtaining the CCS has explained in Section 4.3.1.

In order to obtain the final acquisition result two steps are required in this combination stage, as shown in Figure 4-16, which are:

1. The CCS feeds to the "Absolute Function" that is squared its inputs values, which are the real and imaginary parts of the complex signal, and then added together.
2. The "Absolute Function" output result is accumulated for M *msec*, and then the decision vector is processed by the detection stage to select the maximum value and compared with a preselected threshold in order to declare the acquisition result, as clarified in Section 4.3.2. Note that, in our implementation for both channels (OSC&OPC), M equals to 1.

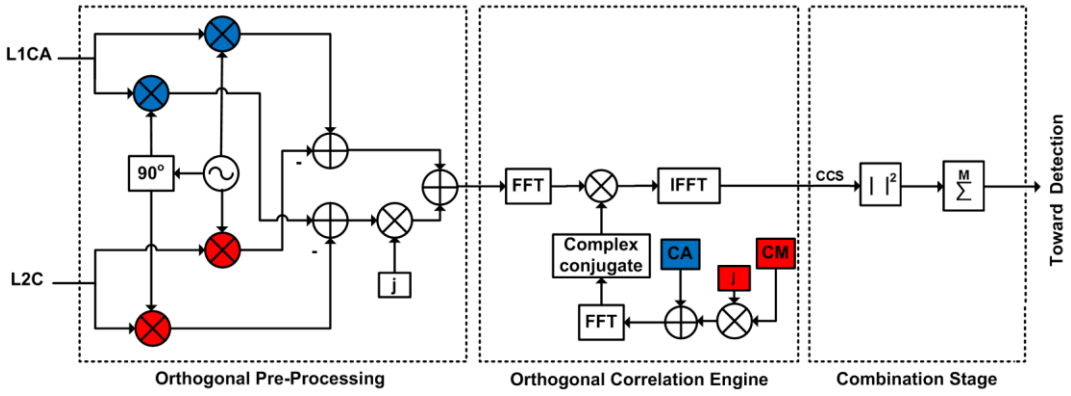

Figure 4-16 Structure of OSC with Direct Sum combination method

This method was chosen since the computation load in the combination stage is low. The decision vector of this method can be expressed mathematically as:

$$OSC - DS_{L1L2} = \sum_{k=1}^{M} \underbrace{(I_{1,k}^2 + Q_{1,k}^2)}_{L1\ term} + \sum_{k=1}^{M} \underbrace{(I_{2,k}^2 + Q_{2,k}^2)}_{L2\ term} + 2\sum_{K=1}^{M} \underbrace{(I_{1,k}\, Q_{2,k} - I_{2,k}\, Q_{1,k})}_{extra\ term} \quad (4\text{-}13)$$

From (4-13), there are three mathematical terms; the first two terms are exactly the same as those in the side-by-side non-coherent combined methods [50]. The third mathematical term/extra-term is produced in our method due to the orthogonal processes in pre-processing stage and the combination stage. The effects of this term will be analysed mathematically in this section.

1. Performance validation of OSC-DS_{L1L2}

In this section, the OSC-DS_{L1L2} method will be evaluated in four different scenarios, further, we will analyse and discuss the simulation results as well as comparing them with the other acquisition methods. The simulation parameters of generating the L1CA and the L2C GPS signals and the test simulation parameters that were used in those scenarios have been explained in the Section 4.3.3.

Probability of detection: Figure 4-17 illustrates the comparison of signal detection of the OSC-DS_{L1L2} method, L1CA and L2CM conventional method and side-by-side NC FFT-based combination method. The comparison shows that the probability of detection of the conventional acquisition method of L2CM signal alone is significantly lower than other acquisition methods. The reasons for having lower detection are; the first being that the L2CM signal has lower power than the L1CA signal/combined signals by at least 4.5 dB, secondly only one millisecond of signal length has been considered (it is length 20 *msec*). Figure 4-17 also shows that there is an improvement of around 1 dB signal reception in our method over the NC FFT-based method and around 1.5 dB over the L1CA acquisition method. Note that, mathematically and based the parameter settings in Table 4-1, our expression in (4-13) is exactly the same as the one in the NC FFT-based. However, the OSC-DS_{L1L2} method has 1 dB better reception and that is because the signal power in our method is combined the signals' power twice; one at pre-processing stage (orthogonalise the signals) and the second at the combination stage.

The ratio of maximum correlation peak: All the power ratio curves in Figure 4-17 have the same trend and the best performance of the four comparing methods is the ratio of our OSC-DS_{L1L2} method. This proves that the noise that accumulated in the inside/outside the acquisition engine (see Section 4.3.3) have no noticeable effect on the performance of our acquisition method either in low or high C/No values.

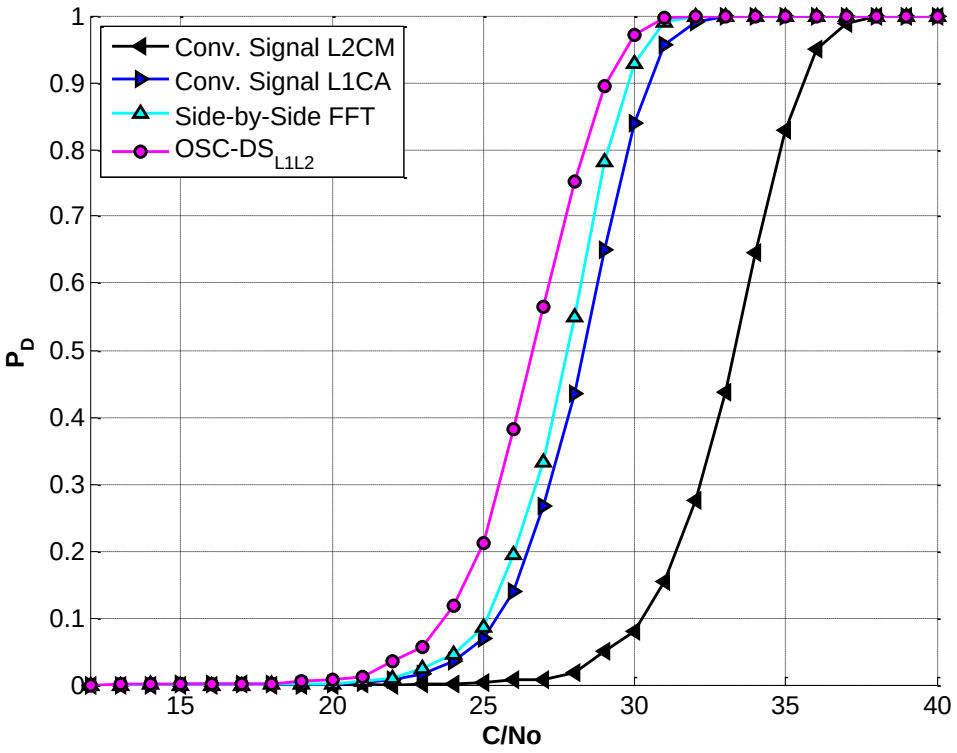

Figure 4-17 OSC-DS$_{L1L2}$: Probability of detection versus C/No

Residual frequency effect: Figure 4-19 shows the behaviour of all the combined and conventional methods when the residual carrier frequency is non-zero. The simulation results show that there is degradation in the probability of received signals for all compared methods when there is an increase in the residual frequency; however, our OSC-DS$_{L1L2}$ method shows better performance than the others do. Actually, the better performance was expected because the extra mathematical term in (4-13) adds more correlation power to the final acquisition result and that slightly increases the processing-gain of our method and reflects affirmatively on the probability of detection. However, this extra-term can perform poorly if the initial phase of the two signals varies or the sign of the navigation message of both signals is different, as we will see in the next test scenario.

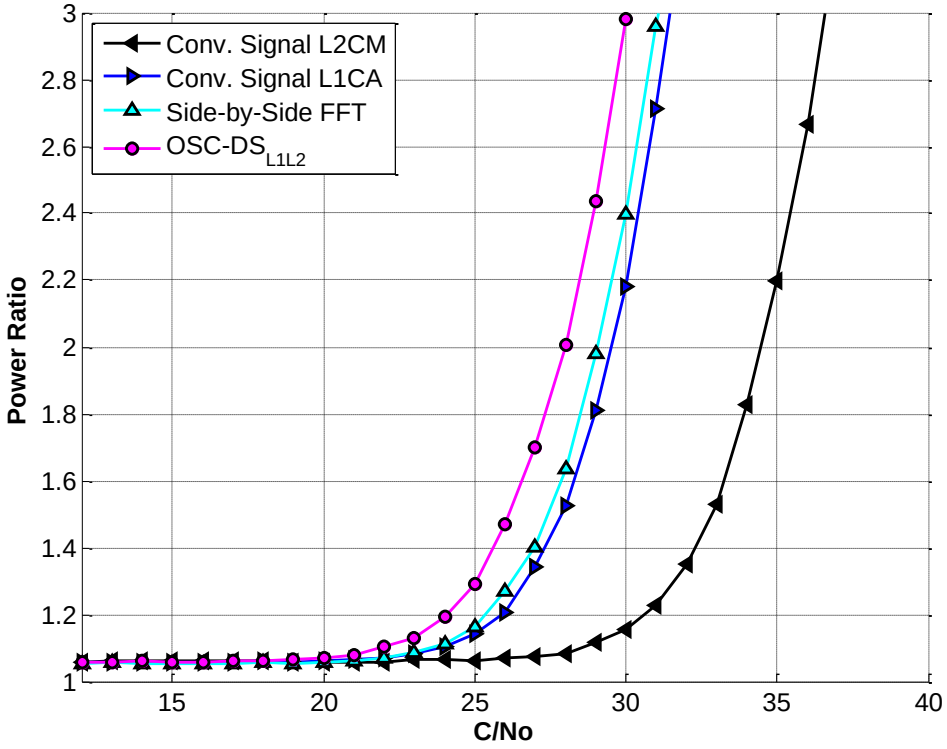

Figure 4-18 OSC-DS$_{L1L2}$: Power ratio of the maximum correlation peaks

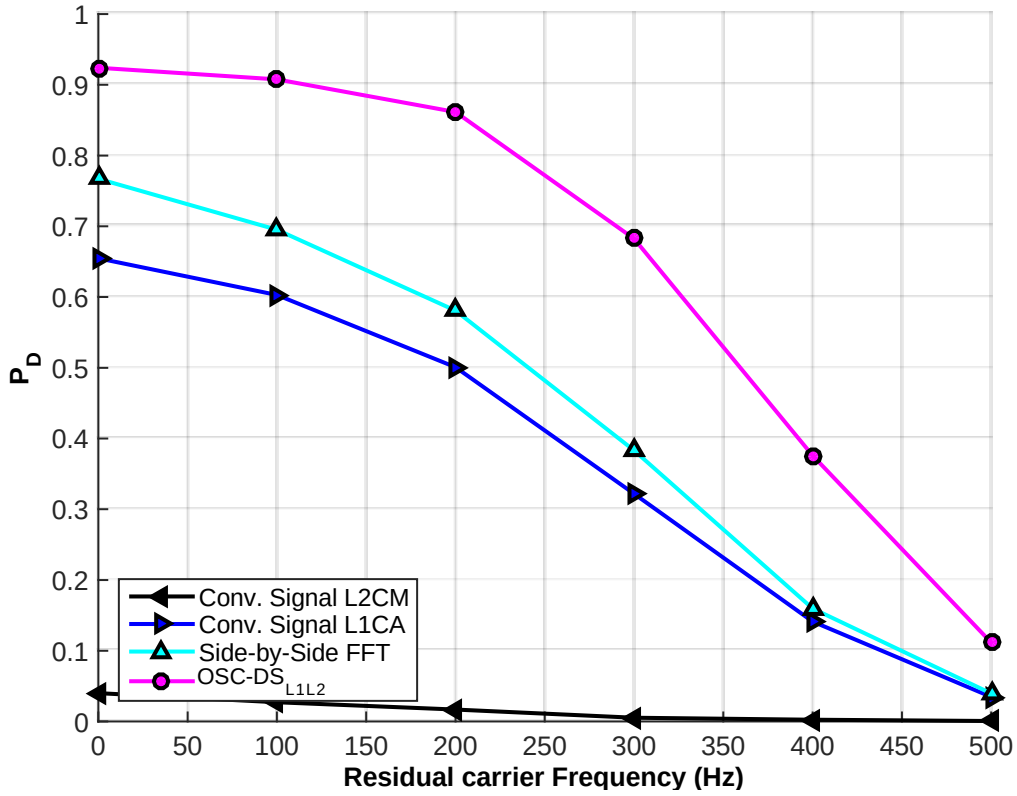

Figure 4-19 OSC-DS$_{L1L2}$: Probability of detection vs. residual carrier frequency

Initial phase effect: Figure 4-20 shows the PD simulation results of the traditional and the combined acquisition methods when the relative phase-offset between the two signals (L1CA&L2C) is defined.

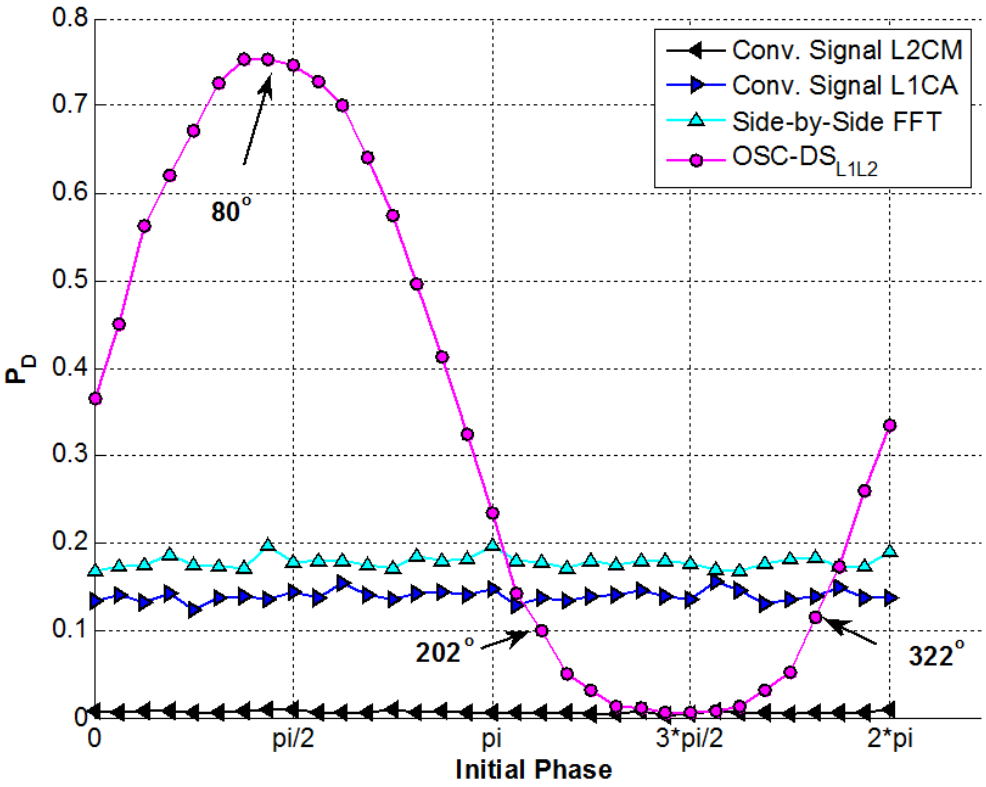

Figure 4-20 OSC-DS$_{L1L2}$: Probability of detection vs. phase offset

The results show that the OSC-DS$_{L1L2}$ method is strongly affected by the relative phase offset while the other methods show no influence. The detection output of the OSC-DS$_{L1L2}$ method (***the navigation message is 1***) becomes beneficially constructive when the relative phase offset varies between 0 to π and it becomes destructive when the relative phase offset is greater than π and less than 2π. On the contrary, ***when the navigation message is -1*** the effect is reversed. This unfavourable effect is clearly reflecting the result of the extra mathematical term in (4-13). To analyse this extra-term mathematically, the I-components and Q-components of the two signals can be expressed as:

$$I(k) = \frac{A}{\sqrt{2}} d(k)\, R(dt)\, sinc(\pi\, \Delta F\, T) cos(\pi\, \Delta F\, T\, (2k-1) + \varphi) \qquad (4\text{-}14)$$

$$Q(k) = \frac{A}{\sqrt{2}} d(k)\, R(dt)\, sinc(\pi\, \Delta F\, T) sin(\pi\, \Delta F\, T\, (2k-1) + \varphi) \qquad (4\text{-}15)$$

Based on the simulation parameters that were used to assess the relative phase offset effect, the residual carrier frequency will be removed from the above two equations. For the sake of simplicity, the values of A and *d(k)* are assumed to be 1. Equations (4-14) and (4-15) become as follows:

$$I(k) = \frac{1}{\sqrt{2}} R(dt)\, cos(\varphi) \quad (4\text{-}16)$$

$$Q(k) = \frac{1}{\sqrt{2}} R(dt)\, sin(\varphi) \quad (4\text{-}17)$$

By substituting (4-16) and (4-17) in the extra-term in (4-13) and simplifying the result by using the trigonometric properties, the extra-term becomes:

$$extra - term = \quad R_{L1}(dt)\, R_{L2}(dt)\, sin(\varphi_2 - \varphi_1) \quad (4\text{-}18)$$

From (4-18), it is clear that the multiplications of the correlation value of the two signals will be either added or subtracted from the other correlation value in (4-13) based on the following points: 1) the multiplication sign of the navigation message sign and, 2) the output sign of the "Sine Function" in the extra-term in (4-18). Obviously, the output sign of the multiplication result behaves as a sine wave, i.e. the extra-term based on that sign will be gathered or subtracted from the correlation of L1 and L2 signals. That means the extra-term has a direct effect on decreasing and increasing the probability of detection in the OSC-DS_{L1L2} method, as shown clearly in Figure 4-19.

Overall, the OSC-DS_{L1L2} acquisition method preforms better than the other compared methods when the sign of the extra-term in (4-13) is zero or positive, and still performs equally well as the conventional L2CM acquisition and worse than others if the sign of the extra-term is negative. However, that drawback of the phase-offset/the extra-term and the navigation message sign in the OSC-DS_{L1L2} method can be overcome completely by using the repetition acquisition technique. This technique is repeating the acquisition process of the OSC-DS_{L1L2} method three times to the same received signals (L1CA and L2C) by only shifting one of the received signal phase by 120-degree in each acquisition run and then choosing the maximum peak value of the three acquisition results, as shown in Figure 4-21. This means there is no extra cost or adding components to the OSC apart from the phase shifter, i.e., it

is the same channel will be used but the process will be repeated. The shifting process is achieved by employing a fixed time-delay to one of the received signals, the time-delay can be given mathematically as $\Delta T = 1/3*f$ for a fixed 120-degree shift, where the f is the frequency of the received signal in the digital domain.

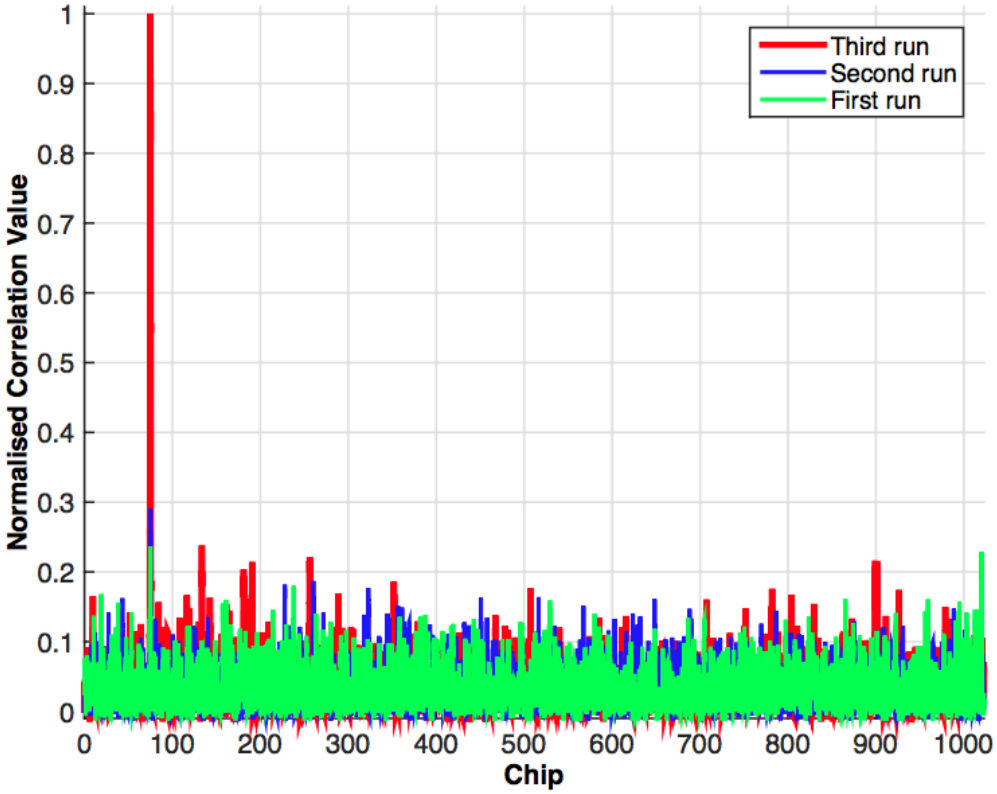

Figure 4-21 Correlation results of the OSC-DS$_{L1L2}$ method @ C/No = 26 dB-Hz

Figure 4-21 demonstrates how the repetition technique can overcome the above-mentioned problems. Next example will clarify why three times are required to repeat the acquisition. Suppose that the two signals are received with phase-offset equal to 202-degree (see Figure 4-20), so the OSC-DS$_{L1L2}$ method will be not able to detect the signals and this is assumed to be the first run, see the green line in Figure 4-21. Based on the repetition technique, the received phase-offset will shift by 120-degree so the new phase-offset becomes 322-degree in the second run also the method has not able to detect the signals, see Figure 4-20 and the blue line in Figure 4-21. While in the third run the phase-offset become 80-degree (see Figure 4-20) and it is clear that there is a high correlation value and the signals can be easily detected, as shown in the red line in Figure 4-21. Note that the correlation value in Figure 4-21

has been normalised based on the maximum value of the three runs.

4.4.2 Differential Acquisition: OSC-Diff$_{L1L2}$

This method applies a differential technique for acquiring the L1CA and L2C GPS signals concurrently. The three following steps are required to obtain the final acquisition result, as shown in Figure 4-22, which are:

1. Firstly, the CCS output values are delayed by 1 *msec*, where TD is block time delay.
2. Secondly, the current CCS values are multiplied by the conjugate of the delayed version of the CCS values, which was produced in the previous step.
3. The real part of the multiplication output is then accumulated for M *msec*, and then the decision vector output is fed to the detection stage to select the maximum value and compare with the preselected threshold to declare the acquisition results.

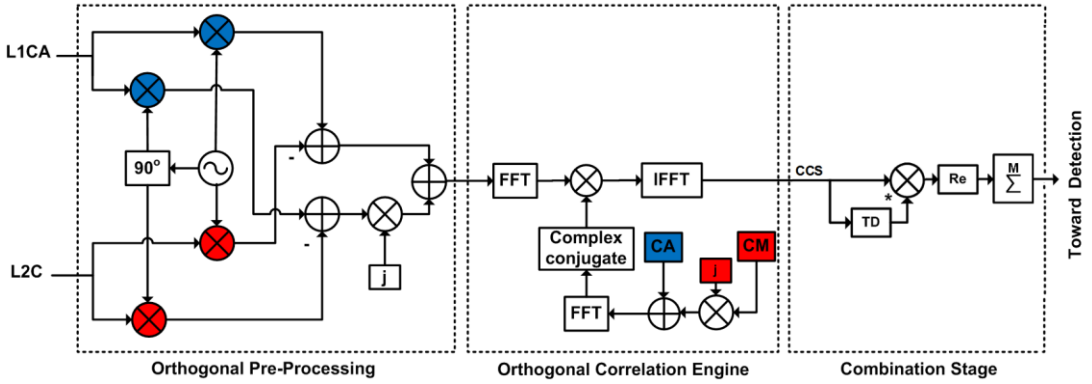

Figure 4-22 Structure of OS acquisition channel with Differential combination method

The combination stage of the OSC-Diff$_{L1L2}$ method is favourable to be chosen over the OSC-DS$_{L1L2}$ method since the first mentioned method avoids the noise squaring while keeping the computation load low. The decision vector of the OSC-Diff$_{L1L2}$ method can be expressed mathematically as:

$$OSC - Diff_{L1L2}$$

$$= \sum_{k=1}^{M} \underbrace{\left(I_{1,2k}\, I_{1,2k-1} + Q_{1,2k}\, Q_{1,2k-1}\right)}_{L1\ term}$$

$$+ \sum_{k=1}^{M} \underbrace{\left(I_{2,2k}\, I_{2,2k-1} + Q_{2,2k}\, Q_{2,2k-1}\right)}_{L2\ term}$$

$$+ \sum_{k=1}^{M} \underbrace{\left(\frac{R_{L2}R_{L1}^{'}}{2}\ sin\left(\varphi_2 - \varphi_1^{'}\right) + \frac{R_{L2}^{'}\, R_{L1}}{2}\ sin\left(\varphi_2^{'} - \varphi_1\right)\right)}_{extra\ term}$$

(4-19)

1. Performance validation of OSC-Diff$_{L1L2}$

The acquisition sensitivity is expected to improve significantly due to the reduction of the noise level in the final acquisition result. This reduction is achieved because the configuration of the OSC-Diff$_{L1L2}$ method, where the output noise will be not squared. Note that the correlation output of the two signals is highly correlated with consecutive correlation intervals while the noise turns to be de-correlated, i.e. there is a huge difference in the correlation results between squaring the noise samples or multiplying two of the consecutive noise samples, as shown in Figure 4-23. Where the correlation noise in Figure 4-23 has been normalised by the sampling frequency; that is the noise value is divided by the sampling frequency value.

Probability of detection: Figure 4-24 shows that overall the P_D of the OSC-Diff$_{L1L2}$ method is far better than the conventional acquisition methods, the NC FFT-based method and also our OSC-DS$_{L1L2}$ method by around 5.5 dB, 4 dB and 3 dB respectively. The noticeable point in Figure 4-24 is that the OSC-Diff$_{L1L2}$ method enhances the acquisition sensitivity to detect a weak signal, for example, the P_D of the OSC-Diff$_{L1L2}$ method is 0.1 while for the other methods it is almost zero at C/No = 21 dB-Hz.

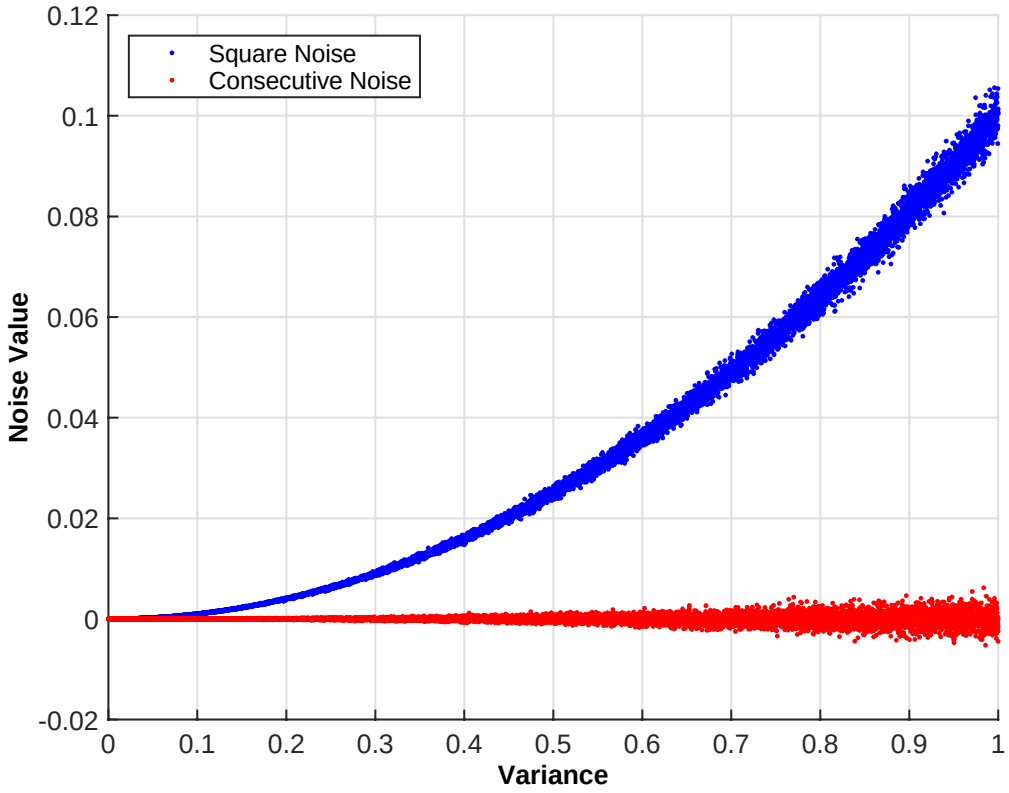

Figure 4-23 OSC-Diff$_{L1L2}$: Correlation result of additive white Gaussian noise

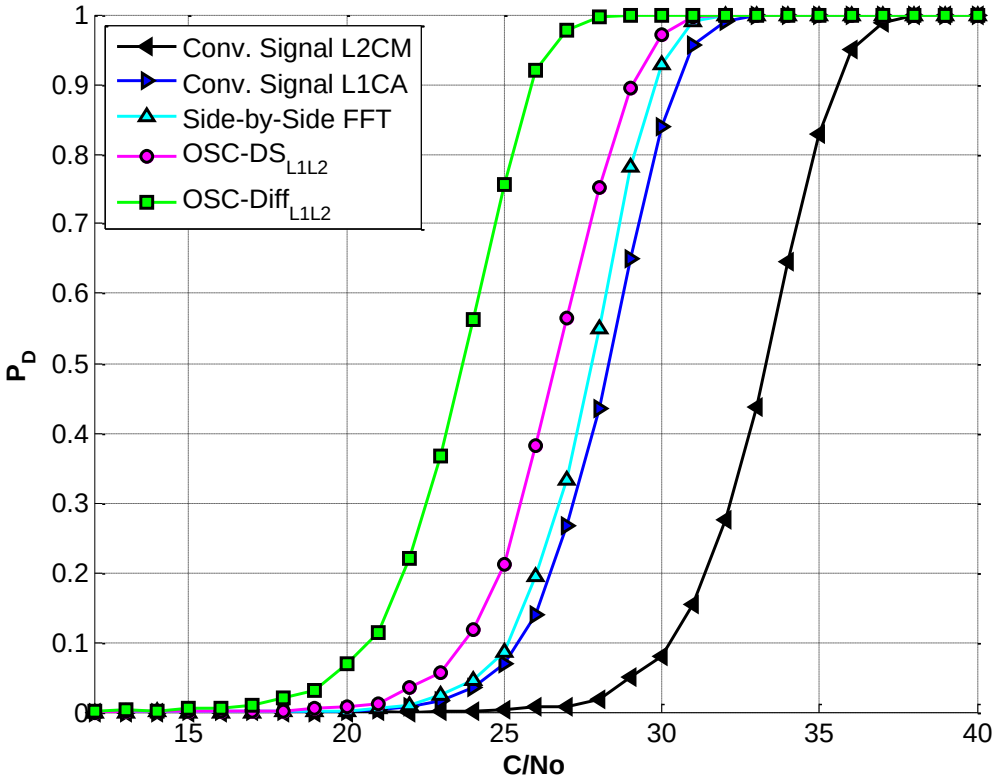

Figure 4-24 OSC-Diff$_{L1L2}$: The probability of detection versus C/No

Ratio of maximum correlation peak: Figure 4-25 shows there is also a significant improvement in the power ratio of the OSC-Diff$_{L1L2}$ compared with others methods. This improvement achieved since the output acquisition noise level has reduced, as shown in Figure 4-23. This test scenario also proves that the extra noise, which is coming from the cross-correlation between the two signals, has a slight effect on the correlation power.

Residual frequency effect: Figure 4-26 shows that the signal detection probability of the OSC-Diff$_{L1L2}$ method has no effect when the residual frequency is less the 300 Hz, after that the detection values decrease to reach around 0.5 at F = 500. This is because the extra-term in (4-19) adds more accumulated power to the acquisition results. Nevertheless, we are expecting the extra-term can slightly affect the acquisition performance of the OSC-Diff$_{L1L2}$ when the phase-offset between the signals defined.

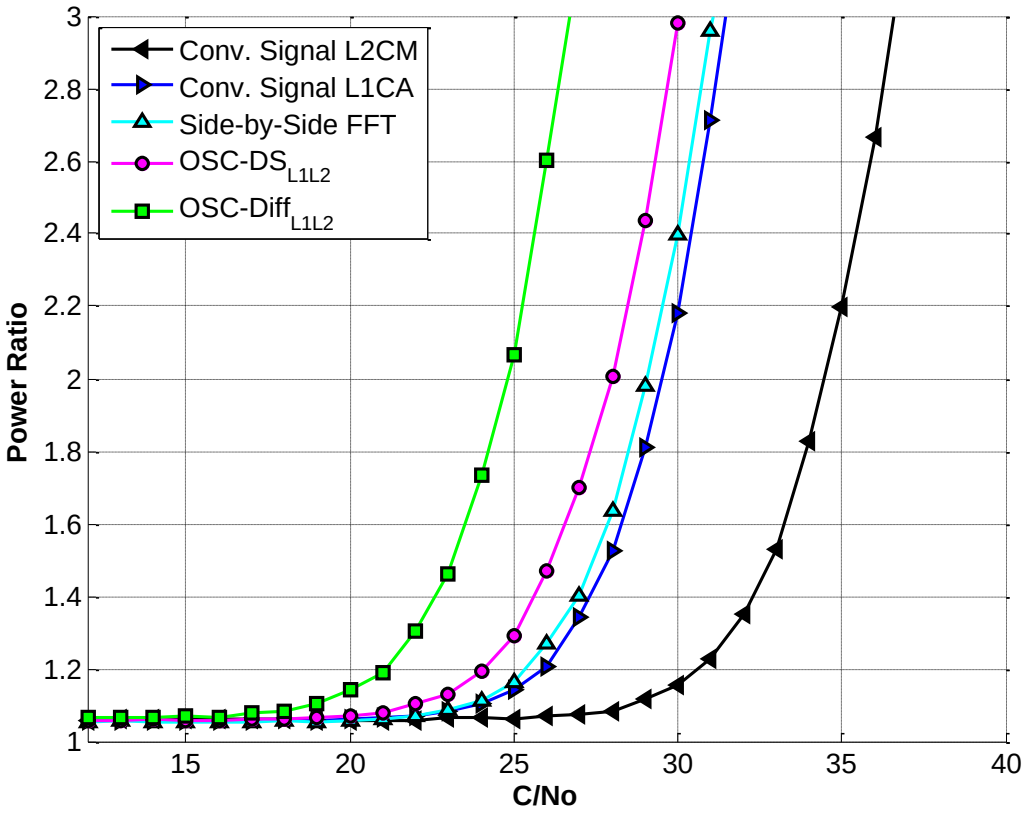

Figure 4-25 OSC-Diff$_{L1L2}$: Power ratio of the maximum correlation peaks

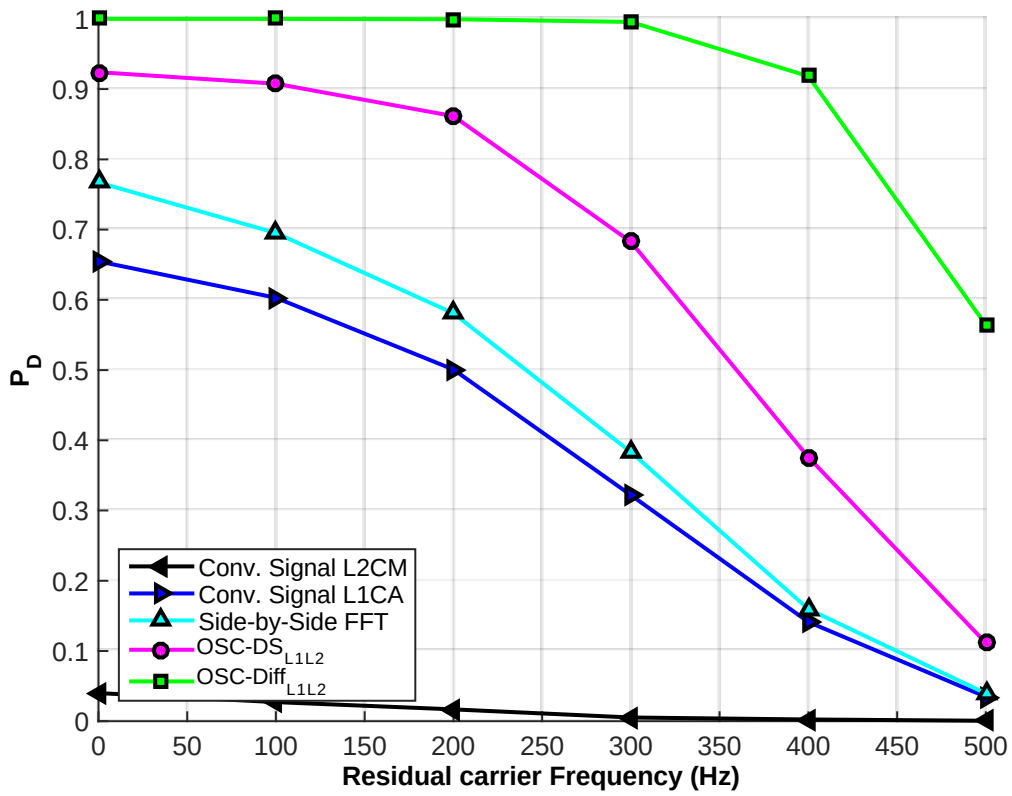

Figure 4-26 OSC-Diff$_{L1L2}$: Probability of detection vs. residual carrier frequency

Initial phase effect: Figure 4-27 exhibits the simulation results of the phase-offset effect on the signal detection performance of the OSC-Diff$_{L1L2}$ method along with other acquisition methods. Apparently the P_D of the OSC-Diff$_{L1L2}$ method is not stable along with changing the value of the phase-offset, and it reaches the maximum value of detection (P_D=1 when C/No = 26) when the phase-offset is around 90 degrees, and it reaches the minimum value of about 0.05 when the phase-offset is around 270-degrees. However, it is better than the L2CM and the OSC-DS$_{L1L2}$ acquisition methods.

Moreover, the percentage of the phase-offset values that makes the extra-term in (4-19) behave harmfully to the acquisition performance of the OSC-Diff$_{L1L2}$ method is only 18%, i.e., there is 82% of the phase-offset values in the period [0,2π] that make the OSC-Diff$_{L1L2}$ perform preferably as compared with all other methods. Observe that, the sign variation of the navigation message of the two signals has the same percentage effect on the acquisition performance of the OSC-Diff$_{L1L2}$ method too.

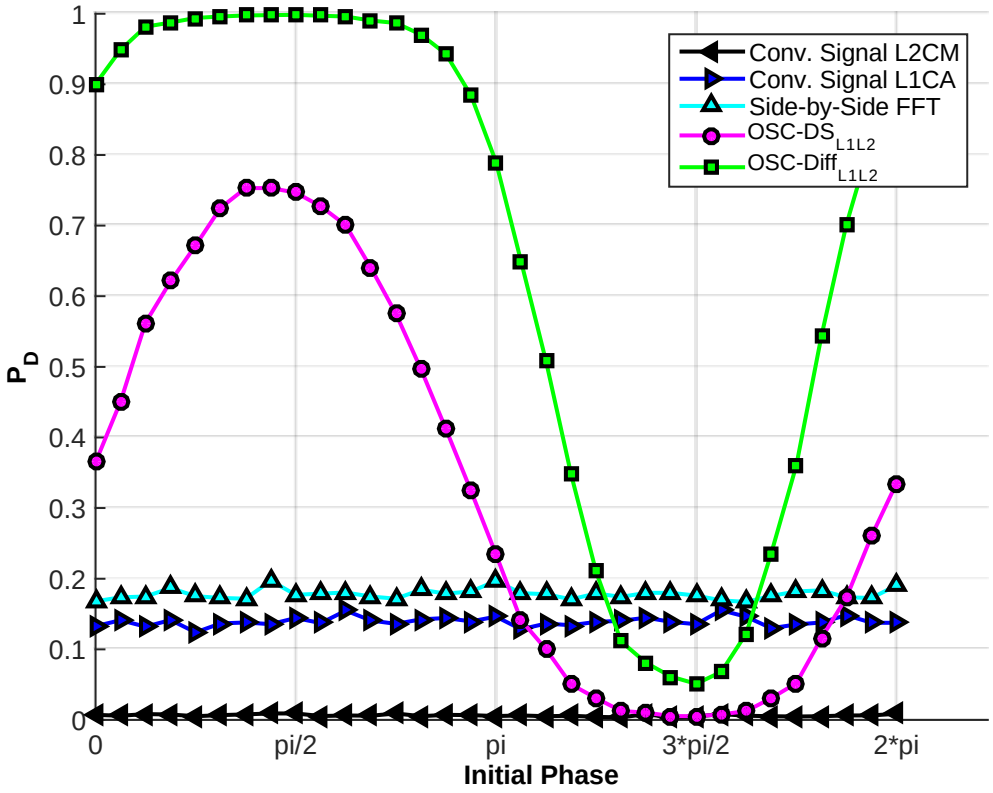

Figure 4-27 OSC-Diff$_{L1L2}$: Probability of detection vs. phase-offset

To sum up, the acquisition performance of the OSC-Diff$_{L1L2}$ method demonstrates a better ability to capture strong/weak L1CA and L2C signals when the effect of the extra-term is disregarded. Whilst, to consider the effect of the extra-term on the OSC-Diff$_{L1L2}$ method a repetition acquisition technique will be required. This technique has the same process that was used in our previous OSC-DS$_{L1L2}$ method in the previous section, but this time, the acquisition process will be repeated only twice and the maximum peak will be chosen, as shown in Figure 4-28.

Figure 4-28 proves that the repetition technique can detect the signals with only two acquisition runs. For instance, in the first acquisition run the phase-offset between the two signals was 270-degree and obviously the OSC-Diff$_{L1L2}$ method cannot be detected the signals while in the second run the phase-offset became 30-degree and signals are detected. Note that the correlation value in Figure 4-28 has been normalised based on the maximum value of the two run.

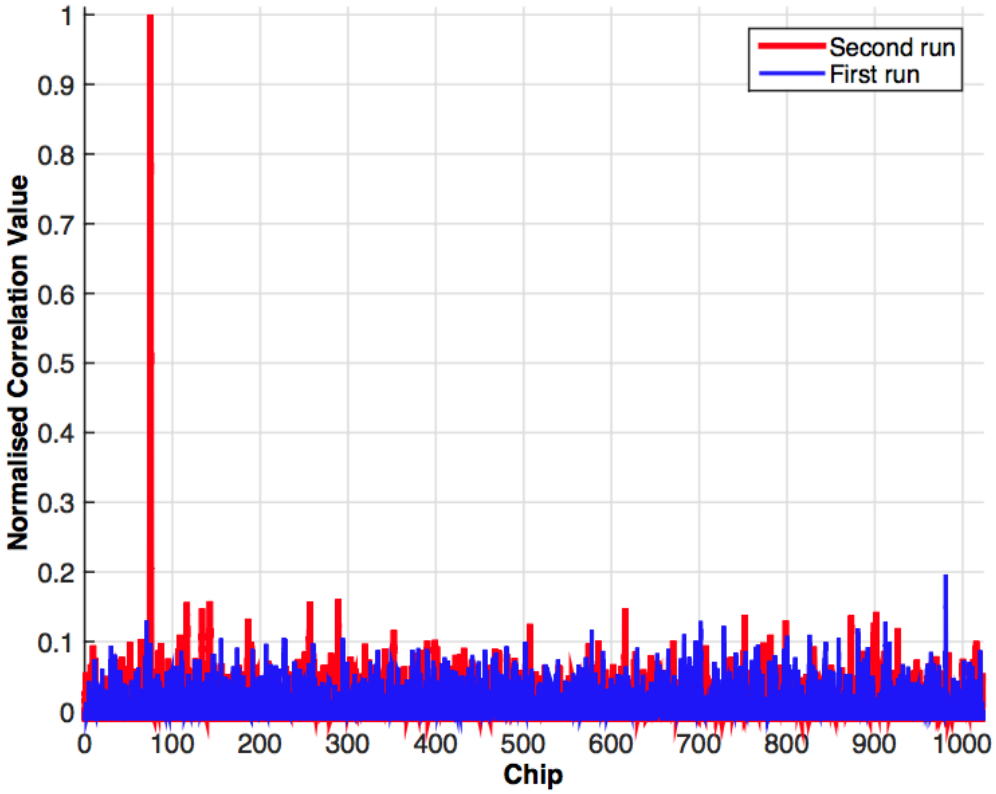

Figure 4-28 Correlation results of the OSC-Diff$_{L1L2}$ method at C/No @ 26 dB-Hz

4.4.3 Direct Sum and Differential Acquisition: OSC-DSDiff$_{L1L2}$

This method is characterised as a grouping of our two previous methods, the direct sum and differential acquisition methods, as shown in Figure 4-29. In this method, we try to exploit all correlator power outputs to improve the correlation processing gain, which directly reflects on enhancing the acquisition sensitivity.

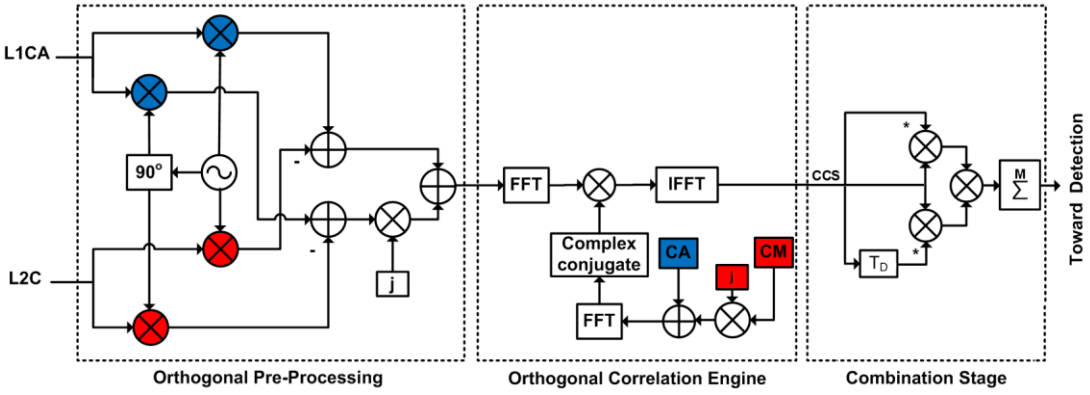

Figure 4-29 Structure of OSC with (Direct Sum+ Differential) combination method

The signal processing inside the combination stage is as follows:

1. Firstly, the CCS values are multiplied with the conjugate version of the same CCS values.
2. Then, the result is again multiplied by the conjugate of the 1 *msec* delayed version of the CCS values.
3. After that, the real part of the multiplication output is then accumulated for M *msec*, and then the decision vector is passed forward to the detection stage to choice the maximum value and compare with the predefined threshold to declare the acquisition decision.

The combination stage in this method is slightly sophisticated compared with two pervious proposed methods, but it combines the advantage of the two previous methods. The decision vector of the OSC-DSDiff$_{L1L2}$ method can be written mathematically as:

$$OSC - Diff_{L1L2} = \sum_{k=1}^{M} \underbrace{(I_{1,k}^2 + Q_{1,k}^2).\left(I_{1,2k}\, I_{1,2k-1} + Q_{1,2k}\, Q_{1,2k-1}\right)}_{L1\ term} + \sum_{k=1}^{M} \underbrace{(I_{2,k}^2 + Q_{2,k}^2).\left(I_{2,2k}\, I_{2,2k-1} + Q_{2,2k}\, Q_{2,2k-1}\right)}_{L2\ term} + extra\ term \quad (4\text{-}20)$$

The extra-term in (4-20) comes from a multiplication of the extra-terms in (4-19) and (4-13). The effect of this extra-term on the probability of detection is expected to be less than the previous two methods (OSC-DS$_{L1L2}$&OSC-Diff$_{L1L2}$), since the cross-correlation values in the both extra-terms in (4-19) and (4-13) plus the generated noise are a fraction of the collected power in the first two terms in (4-20).

1. Performance Validation of OSC-DSDiff$_{L1L2}$

The performance of the OSC-DSDiff$_{L1L2}$ method is expected to be better than the previous two proposed methods since the amount of its noise is very small. In fact, based on our design for this OSC-DSDiff$_{L1L2}$ method the final output noise in the acquisition result is uncorrelated noise. This is achieved from a multiplication of the square noise that comes from the direct sum method, which is represented the first multiplication in Figure 4-29 (combination stage) and the de-correlated noise that

produces from the differential method, which is the second multiplication in the same figure. Figure 4-30 shows the output noise that derives from multiplication of the two noises, square and de-correlated noises, which is very small compared with accumulated power in the first two terms in (4-20).

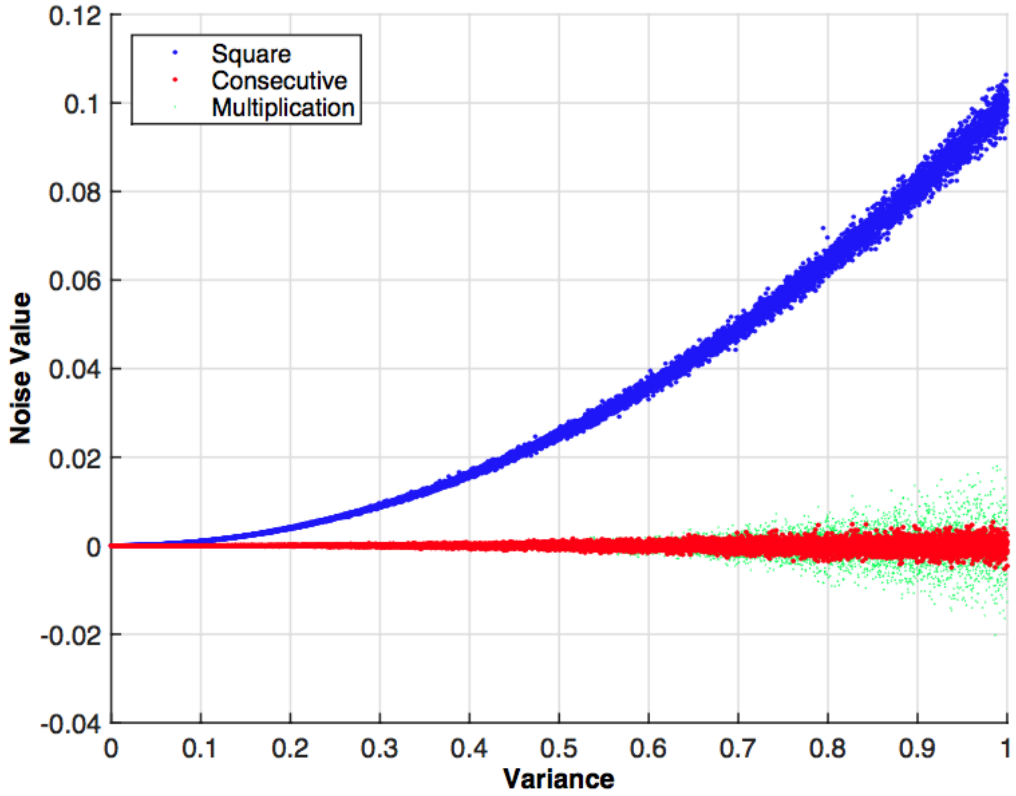

Figure 4-30 OSC-DSDiff$_{L1L2}$: Correlation result of additive white Gaussian noise

Probability of detection: Figure 4-31 displays the signal reception of six different acquisition methods, the OSC-DSDiff$_{L1L2}$ method shows better performance amongst all methods, and the P_D is improved by 10 dB, 5 dB and 5.5 dB compared with the conventional acquisition methods of the L2C, the L1CA signal, and NC FFT-based method respectively. Furthermore, the OSC-DSDiff$_{L1L2}$ method enhances the acquisition sensitivity by 0.5 dB over the OSC-Diff$_{L1L2}$ method. The most interested point in this method is that it starts detection the signal at low C/No, which equals to 16 dB-Hz.

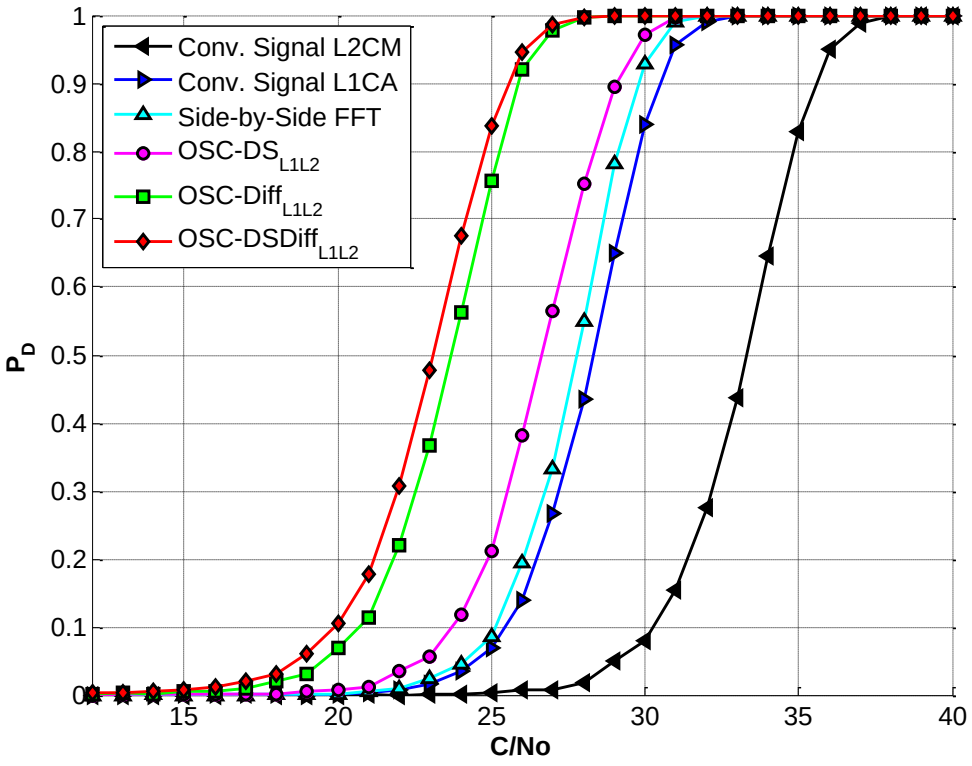

Figure 4-31 OSC-DSDiff$_{L1L2}$: The probability of detection versus C/No

Ratio of maximum correlation peak: Figure 4-32 shows that the OSC-DSDiff$_{L1L2}$ method has a better power ratio compared with others methods. This is because its processing-gain has been increased and the noise stays low, as we explained earlier, the noise in this method is a multiplication of the two noises in the OSC-DS$_{L1L2}$ and OSC-Diff$_{L1L2}$ methods and resulting an uncorrelated noise, as shown in Figure 4-30 the green dots.

Residual frequency effect: The influence of the residual carrier frequency on detection performance of the OSC-DSDiff$_{L1L2}$ method is obviously less than the other acquisition methods and almost identical to the OSC-Diff$_{L1L2}$ method, as shown in Figure 4-33. This because of both methods are using differential technique and the main difference between them is the level of the noise.

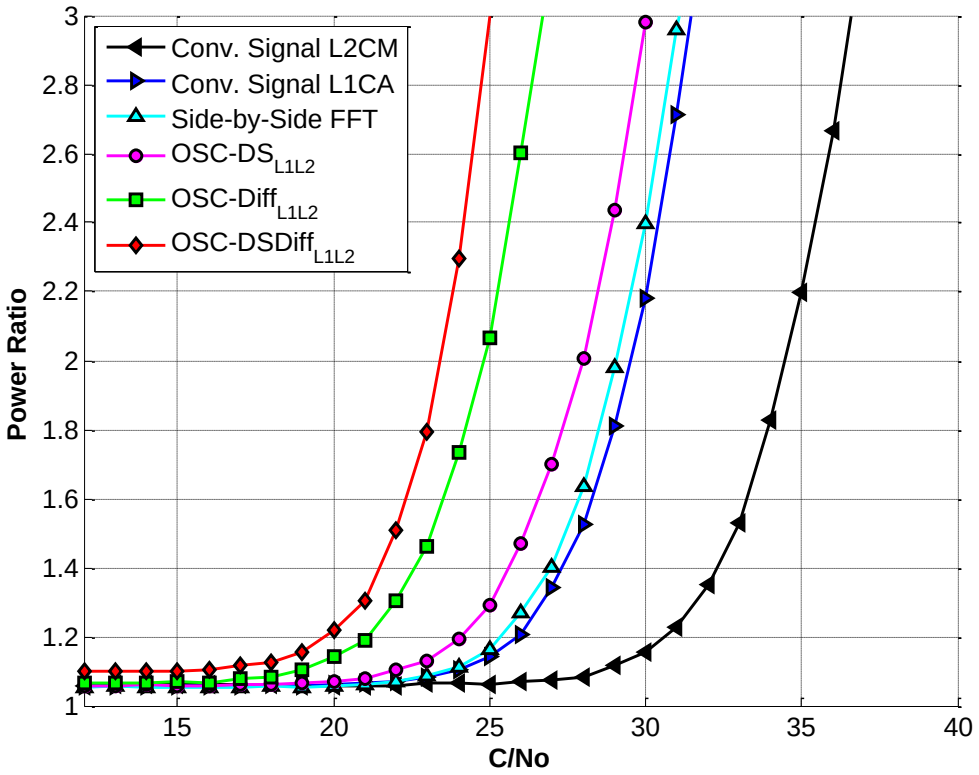

Figure 4-32 OSC-DSDiff$_{L1L2}$: Power ratio of the maximum correlation peaks

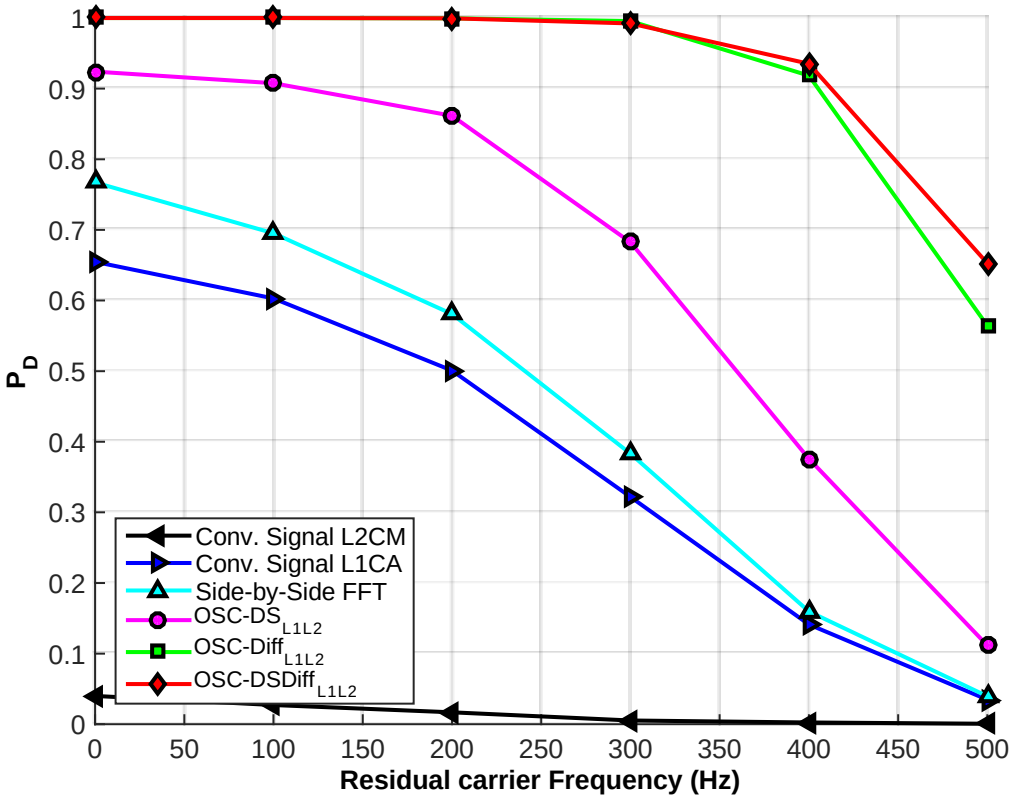

Figure 4-33 OSC-DSDiff$_{L1L2}$: Probability of detection vs. residual carrier frequency

Initial phase effect: the extra-term in (4-20) can perform badly on the OSC-DSDiff$_{L1L2}$ reception when the phase-offset between the L1CA and L2C signals is considered or the sign of the L1CA navigation message is unlike the sign of the L2C navigation message. However, the extra-term effect is marginal on the OSC-DSDiff$_{L1L2}$ performance since the design increases the correlation power in the first two terms and reduces the noise in the third term in (4-20). Indeed, the phase-offset impact on the OSC-DSDiff$_{L1L2}$ method is less than the OSC-Diff$_{L1L2}$ method by 6%. That means 88% of the phase-offset values in the period [0,2π] can produce a better acquisition performance in the OSC-DSDiff$_{L1L2}$ method as compared with the other methods. The navigation message sign of the two signals will not change the phase-offset impact percentage on acquisition performance of the OSC-DSDiff$_{L1L2}$ method due to the final sign of the extra-term being either plus or minus. The simulation results show that when the phase-offset is around 270-degree, the PD of the OSC-DSDiff$_{L1L2}$ method reaches a minimum (PD=0.1 @ C/No = 26), as shown in Figure 4-34.

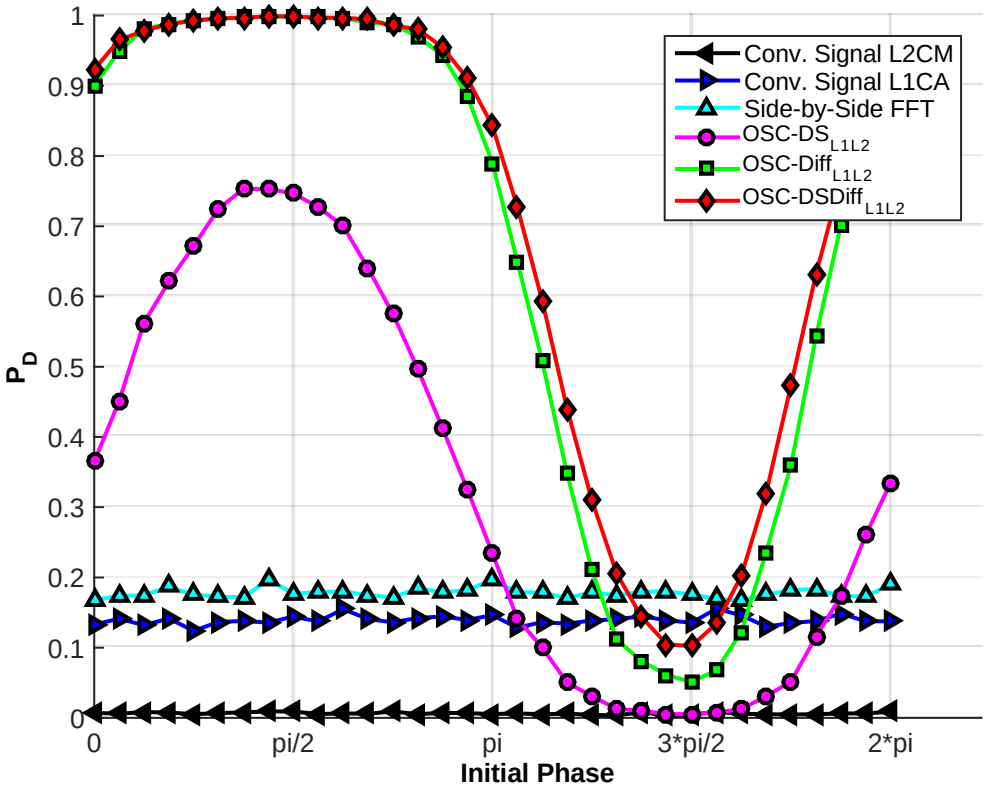

Figure 4-34 OSC-DSDiff$_{L1L2}$: Probability of detection vs. phase offset

Briefly, in spite of the OSC-DSDiff$_{L1L2}$ method being a half implantation

compared with side-by-side combination methods, it achieved a significant improvement in the acquisition sensitivity to capture the L1CA and L2C GPS signals at the same time. In addition, it showed a good resistance to the influence of the residual carrier frequency on the reception. Moreover, the OSC-Diff$_{L1L2}$ method showed that it is very useful in acquiring weak signals, which gave precedence to use it in harsh environments such as urban canyons and indoor environments. However, there is an effect on the OSC-DSDiff$_{L1L2}$ performance from the phase-offset. This effect can be eliminated by using the same repetition technique that is used in the OSC-Diff$_{L1L2}$ method. The result of the OSC-DSDiff$_{L1L2}$ method after applying the repetition technique is shown in Figure 4-35.

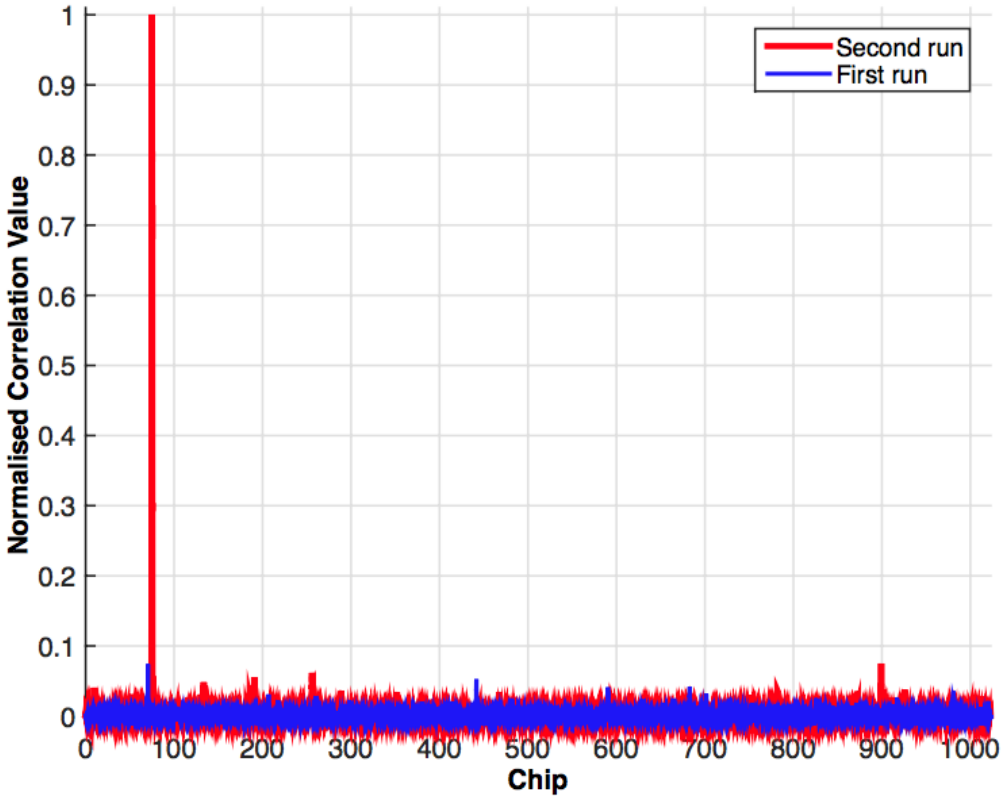

Figure 4-35 Correlation results of the OSC-DSDiff$_{L1L2}$ method at C/No @ 26 dB-Hz

4.5 Orthogonal Parallel Acquisition Channel (OPC)

OPC is designed to combine the acquisition of L1CA and L2CM GPS signal in single channel and it anticipated to improve the sensitivity of acquiring these signals specifically in harsh environments situation. The novelty of this channel, besides orthogonalising the two GPS signals (L1CA and L2C) into a single orthogonal

signal, is also utilising an orthogonal correlation engine, that included parallel correlation search to acquire these signals as shown in Figure 4-36, and each one of the correlation engines has different combination code. The new channel will duplicate the correlation power; meanwhile also eliminating the cross-correlation noise that is generated in each of orthogonal correlation engines.

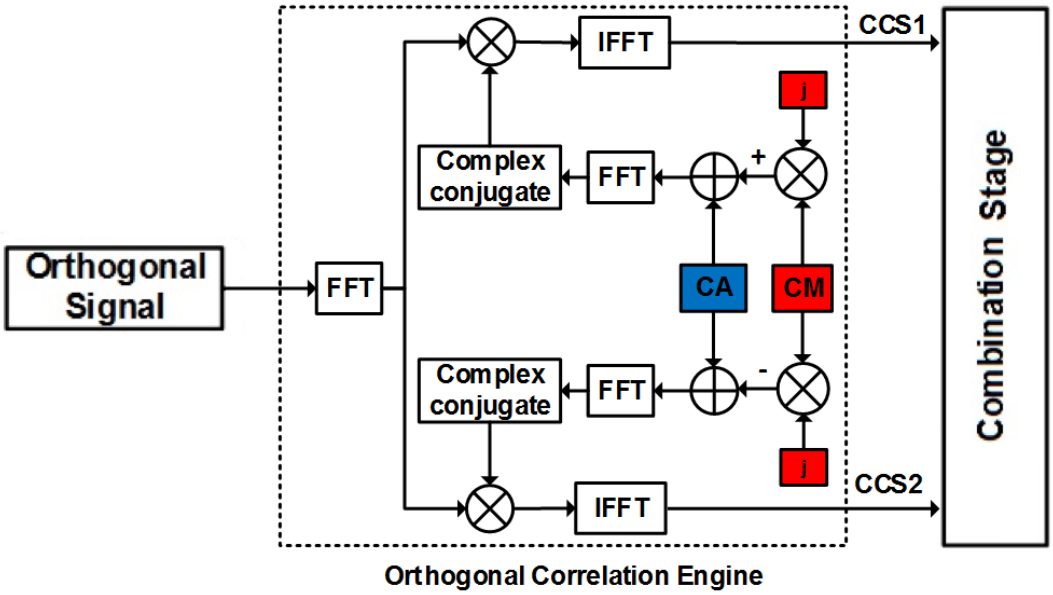

Figure 4-36 Developed correlation engine for combined L1CA and L2CM GPS signals in single channel (OPC)

Figure 4-36 show the structure of the orthogonal correlation engine that used in the OPC, which includes two parallel search engines. The orthogonal signal (see Section 4.3.1, Stage 2) will be processed by a single FFT function, and the output complex signal will feed to the two parallel engines, each one of these engines has owned/different combination codes. The process of the complex signal inside these engine has been explained in Section 4.3.1, stage 3. The outputs of the orthogonal correlation engine are two different complex correlated signals (CCS1&CCS2).

Note that, to clarify, the difference between our OPC and the side-by-side acquisition channels is that each channel in the side-by-side acquisition methods is specified for a specific signal. This means the first channel is indicated for L1CA signal and the second channel is used for L2C signal. While in our OPC, the "orthogonal correlation engine" is practically used for correlating a combination of

both signals. However, it can also acquire the L1CA signal alone, or L2C signal alone.

The next example will show how the OPC is favourable for acquiring GPS signals over the side-by-side acquisition. Let us assume that one of the received two GPS signals (L1CA& L2C) is not present in the receiver area for some reason, in the side-by-side acquisition implementation is one of the dual channels, which will not acquire any signal. This causes the receiver to thrash all its available resources to find the signal that not exist. This means there is no gain in the final acquisition correlation power in terms of an L1+L2 combination strategy. While, in our OPC both the parallel search engines, in the orthogonal correlation engine, will acquire the same signal and the correlation power will be doubled; consequently, improving the acquisition sensitivity.

Figure 4-37 illustrates the block diagram of the OPC structure. The first step in this channel is orthogonalising the received L1CA and L2C GPS signals. Then, the orthogonal signal is fed to orthogonal correlation engine that will produce two complex correlated signals. To find the maximum correlation peak we propose to use one of the three structures that are:

1. Non-coherent/direct-sum method that preforms a non-coherent summation into the CCS's and it named OPC-DS_{L1L2} (more details about the method in Section 4.5.1)

2. Differential method that applies a differential technique to the CCS's and it named OPC-$Diff_{L1L2}$ (more details about the method in Section 4.5.2)

3. The third method is a grouped of direct-sum and differential methods, that is called OPC-$DSDiff_{L1L2}$, full details in Section 4.5.3.

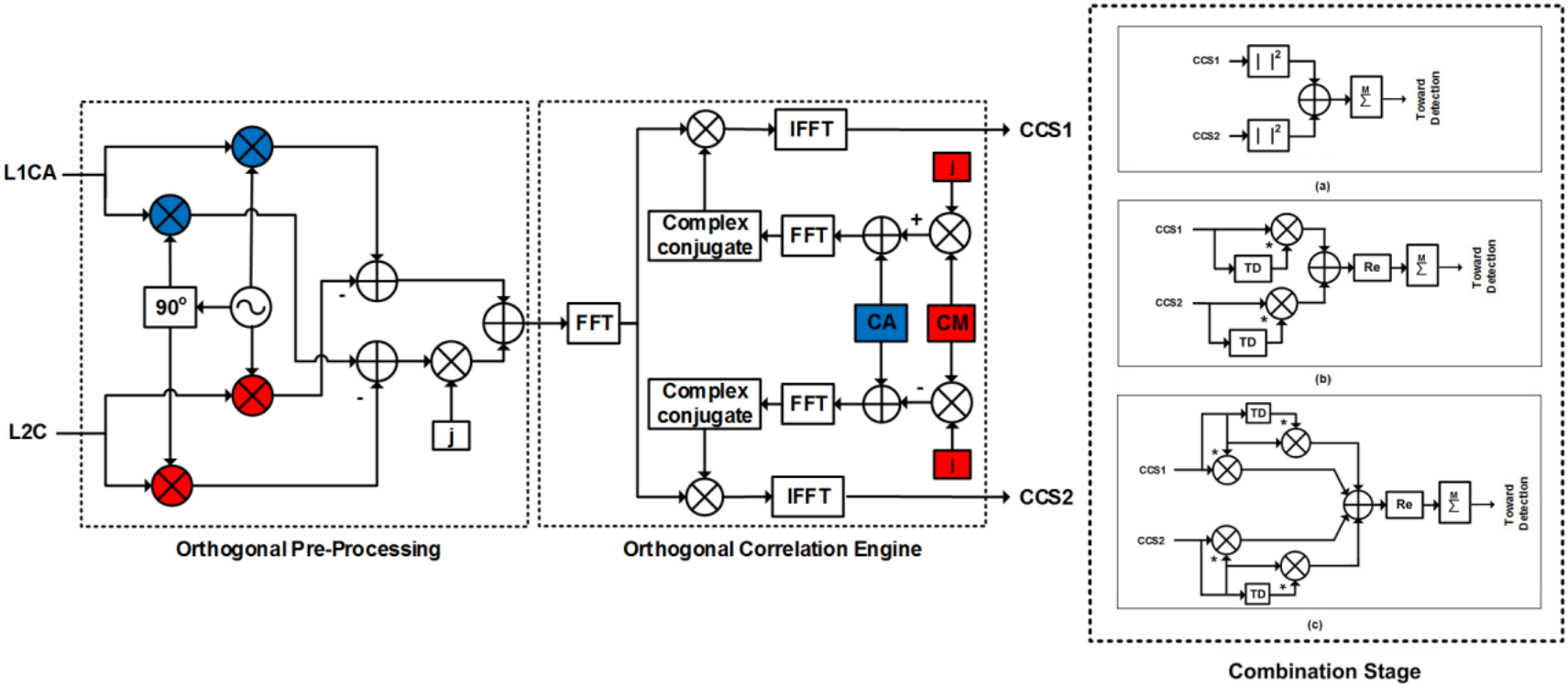

Figure 4-37 Structure of Orthogonal Parallel acquisition Channel (OPC) to acquire L1CA and L2C GPS signals

4.5.1 Direct Sum Acquisition: OPC-DS_{L1L2}

This method apples direct sum to the correlated signals (CCS1&CCS2), as shown in Figure 4-38. The final acquisition results will be obtained based on the as following steps:

1. The correlator output of each correlation engine is squared and then their results are gathered.
2. The output is then accumulated for M *msec*, and then the decision vector is moved to the detection stage to select the maximum value and match with a particular threshold value to state the acquisition result.

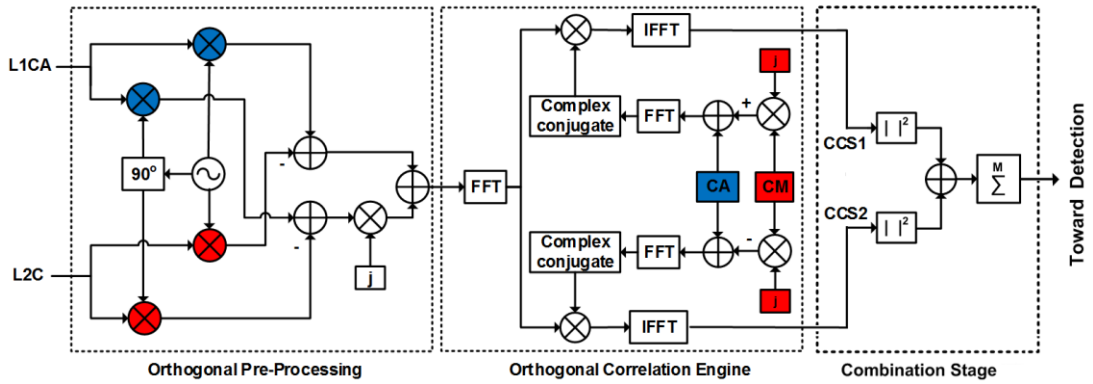

Figure 4-38 Block diagram of the OPC-DS_{L1L2} method

The combination stage structure of the OPC-DS_{L1L2} method is easy to implement and no computational load is required. The decision vector of the OPC-DS_{L1L2} method can be expressed mathematically as:

$$\mathrm{OPC}-\mathrm{DS}_{\mathrm{L1L2}} = 2\sum_{k=1}^{M}\underbrace{(I_{1,k}^2+Q_{1,k}^2)}_{\text{L1 term}} + 2\sum_{k=1}^{M}\underbrace{(I_{2,k}^2+Q_{2,k}^2)}_{\text{L2 term}} \qquad (4\text{-}21)$$

Obviously, there is no extra-term in (4-21) as in all-previous methods in the OSC; this is because of the orthogonal correlation engine design that subtracts the same value of the extra-term from both parallel output branches. The other noticeable advantage in (4-21) is that this method doubles the final correlation value as compared with side-by-side methods or the OSC-DS_{L1L2} method. This means that theoretically the OPC-DS_{L1L2} method has enhanced the acquisition sensitivity by 3 dB at least.

1. Performance validation of OPC-DS$_{L1L2}$

Probability of detection: the simulation results of P_D show that the OPC-DS$_{L1L2}$ method has a better signal reception than the other methods, as exhibited in Figure 4-39. This method improves its acquisition sensitivity by around 7.5 dB, 2.5 dB and 2 dB compared with L2CM, L1CA and NC FFT-based acquisition methods respectively.

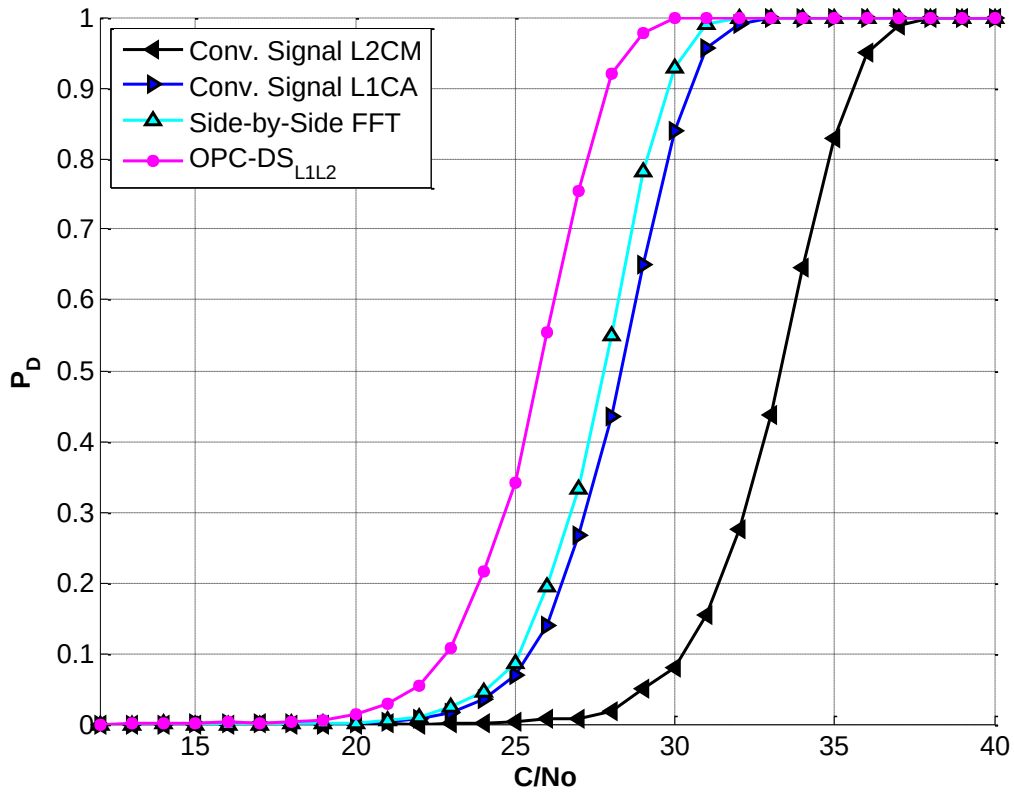

Figure 4-39 OPC-DS$_{L1L2}$: The probability of detection versus C/No

We are expecting a 3 dB enhancement in the acquisition sensitivity of our method over the NC FFT-based method because both methods have the same mathematical expression but in our method it multiply by 2. However, practically the method has achieved only 2 dB. This 1 dB loss could come from an increase in the number of the cross-correlation in the acquisition channel (L1 with itself, L2 with itself and L1 with L2); nonetheless, the 2 dB gain is a valuable achievement.

Ratio of maximum correlation peak: simulation results in this test scenario prove that the power ratio of the OPC-DS$_{L1L2}$ method is enhanced by approximately 2 dB compared with NC FFT-based method, as shown in Figure 4-40. The power ratio

values confirm that the 1 dB loss in previous test scenario comes from the number of cross-correlation in our method because the accumulated power in the acquisition branches has been enhanced but also, the noise has been increased. Therefore, the loss has occurred. However, there are no concerns about the noise that produces from the cross-correlation between the L2C signal and the CA code (or between the L1CA signal with the CM code). Since, the noise is relatively small compared with correlation value that will be realised in this method.

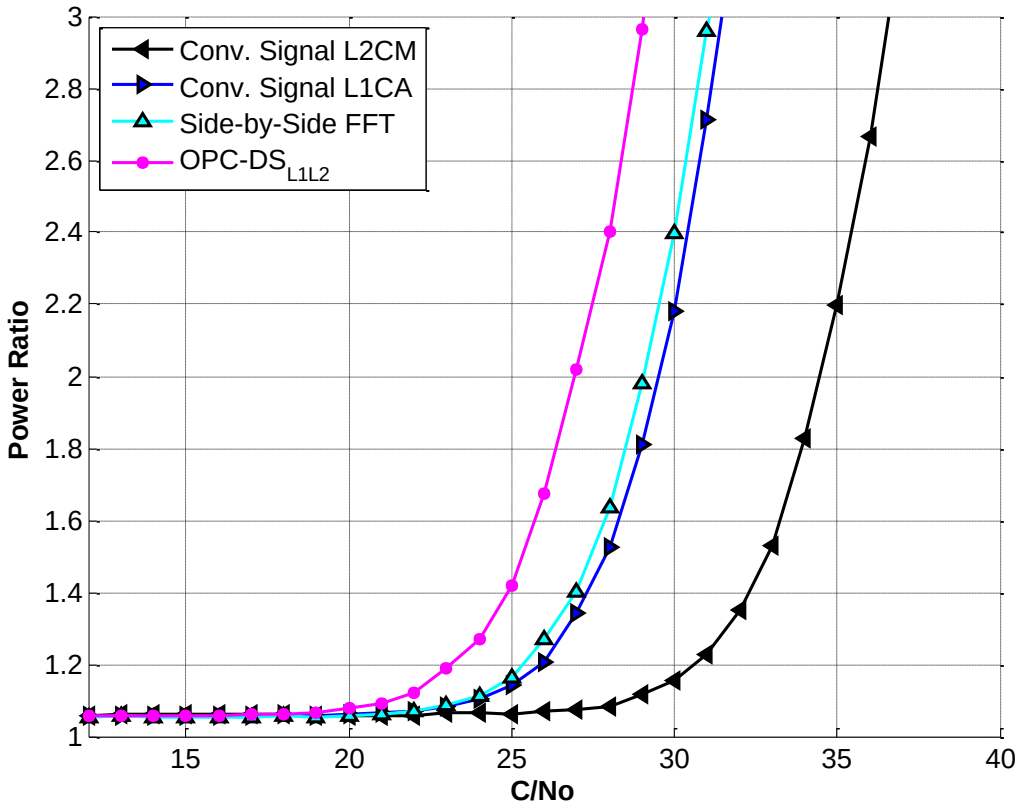

Figure 4-40 OPC-DS$_{L1L2}$: Power ratio of the maximum correlation peaks

Residual frequency effect: Figure 4-41 shows the detection performance of all the methods decreases when increasing the residual frequency, however, the performance of the OPC-DS$_{L1L2}$ method is much better than the compared methods. This result achieved because of our OPC-DS$_{L1L2}$ method has a considerable accumulated power that can influence on the degradation that occurred to the acquisition correlation value.

Initial phase effect: Figure 4-42 shows that the P_D values of the OPC-DS$_{L1L2}$ method are stable with around 5.5 detection probability at C/No = 26 dB-Hz. The

results are not unanticipated, since there is no extra-term in (4-21) that can destruct or construct the P_D of this method and also there is no degradation expected to appear from (4-14) and (4-15) due to the "*Sinc Function*" in both previously mentioned equations, the value of the *Sinc function* equal to 1 when the $\Delta F = 0$.

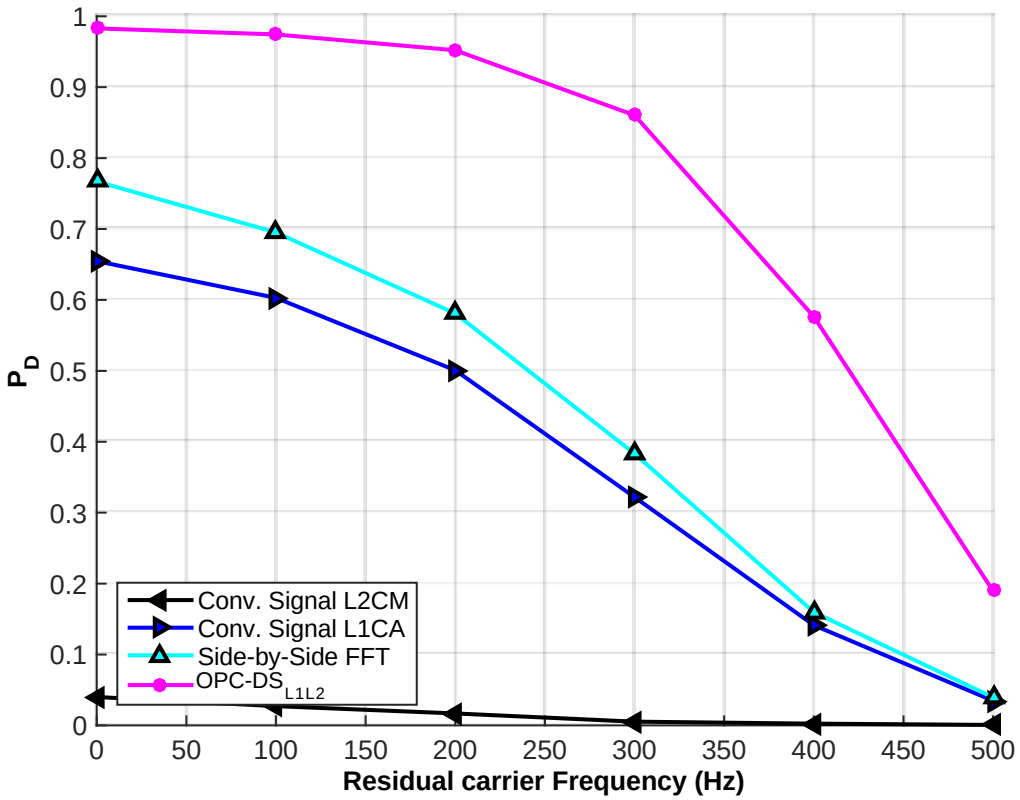

Figure 4-41 OPC-DS$_{L1L2}$: Probability of detection vs. residual carrier frequency

Essentially, the OPC-DS$_{L1L2}$ method enhances the acquisition sensitivity by at least 2 dB as compared with NC side-by-side FFT-based method, and also shows that its behaviour acquisition is more robust in the presence of residual carrier frequency or phase-offset.

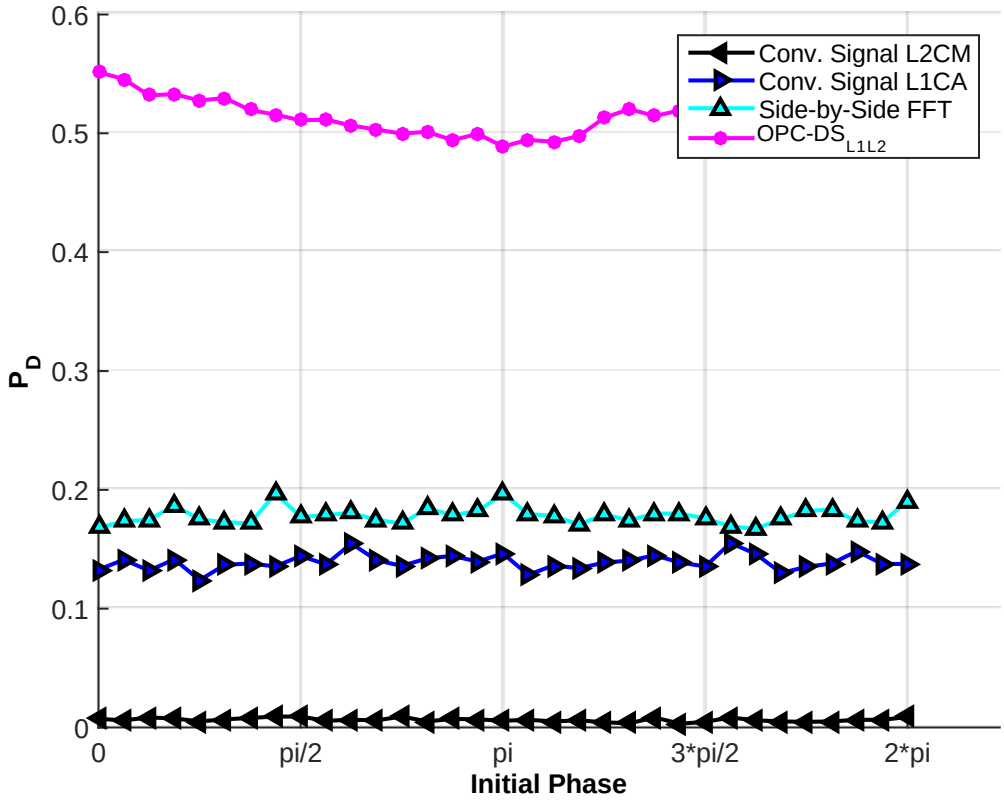

Figure 4-42 OPC-DS$_{L1L2}$: Probability of detection vs. phase-offset

4.5.2 Differential Acquisition: OPC-Diff$_{L1L2}$

This method applies a differential technique for the complex correlated signals (CCS1 and CCS2) that produce from the correlation engine (see Figure 4-36). As illustrated in Figure 4-43, the two following steps are essential to obtain the final acquisition result:

1. The correlator outputs of the correlation engine are multiplied with a conjugate delay of the same correlator outputs separately, and the results are then gathered.
2. The real part of the gathered signal is then accumulated for M *msec*, and then the decision vector is fed to detection stage to pick the maximum value out and compare with the predetermined threshold to affirm the acquisition decision.

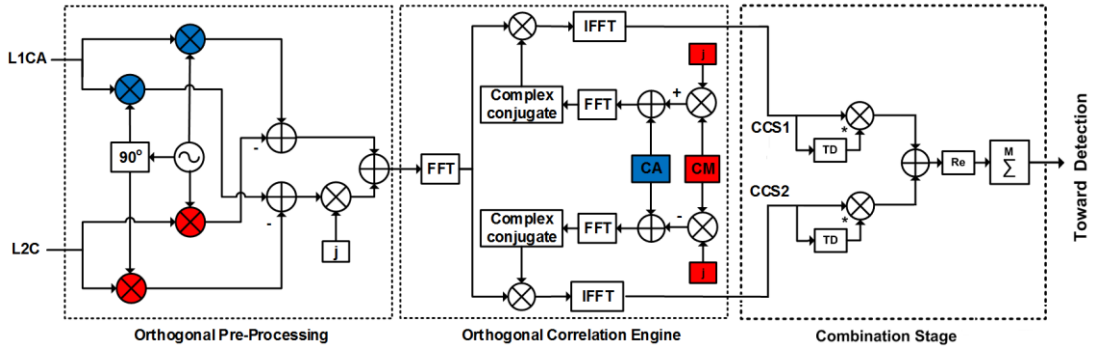

Figure 4-43 Block diagram of the OPC-Diff$_{L1L2}$ method

The decision vector of the OPC-Diff$_{L1L2}$ method can be expressed mathematically as:

$$\begin{aligned}\mathrm{OPC}-\mathrm{Diff}_{\mathrm{L1L2}} &= 2\sum_{k=1}^{M}\underbrace{\left(I_{1,2k}\,I_{1,2k-1}+Q_{1,2k}\,Q_{1,2k-1}\right)}_{\text{L1 term}} \\ &+2\sum_{k=1}^{M}\underbrace{\left(I_{2,2k}\,I_{2,2k-1}+Q_{2,2k}\,Q_{2,2k-1}\right)}_{\text{L2 term}}\end{aligned} \tag{4-22}$$

The advantage of this method is that the level of the noise is meant to be small and limited since the correlation output noise will be not squared, as shown in Figure 4-30. This is considered an essential factor in improving the acquisition sensitivity while keeping the computational load low. In addition, the correlation value of the OPC-Diff$_{L1L2}$ method is twice as much as it is for the differential side-by-side method, and no extra-term as the one that exists in the OSC-Diff$_{L1L2}$ method.

1. Performance validation of OPC-Diff$_{L1L2}$

Probability of detection: there is a substantial increase in the P_D values in the OPC-Diff$_{L1L2}$ and they reach to 10.5 dB and 5.5 dB, as they compared with conventional L1CA and L2CM methods respectively, as displayed in Figure 4-44. In the same figure, the P_D of the OPC-Diff$_{L1L2}$ method is improved by 3 dB and 5 dB favourably in comparison with the OPC-DS$_{L1L2}$ method and NC FFT-Based method respectively. The significant factor in this method is that the P_D has been enhanced

considerably in the low C/No. For instance, at C/No=20 dB-Hz, the P_D for all the compared methods is around zero apart from the OPC-Diff$_{L1L2}$ method, which equals 0.1, as shown in Figure 4-44.

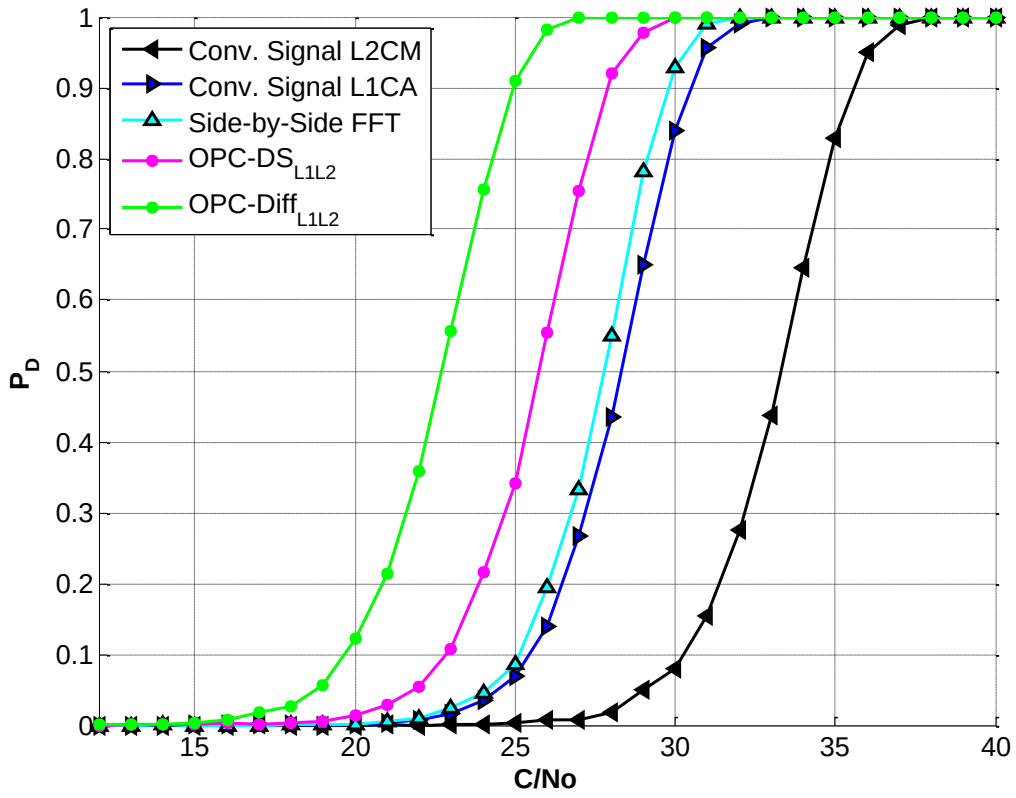

Figure 4-44 OPC-Diff$_{L1L2}$: The probability of detection versus C/No

Ratio of maximum correlation peak: Figure 4-45 shows that the power ratio of the OPC-Diff$_{L1L2}$ method is also improved by around 4 dB and 3 dB as compared with NC FFT-based method and the OSC-DS$_{L1L2}$ method respectively.

Residual frequency effect: The method shows a significant resistance to the residual carrier frequency effects and it has only slight degradation when ΔF >400, as shown in Figure 4-46. In this test scenario, the C/No value is equal to 29 dB-Hz so that the first maximum peak power in the OPC-Diff$_{L1L2}$ method is larger than the second maximum peak power by at least four times. This means by increasing the residual carrier frequency the power in the first maximum peak power is degraded but still exceeds the threshold until the power degradation reaches a maximum value at ΔF = 500.

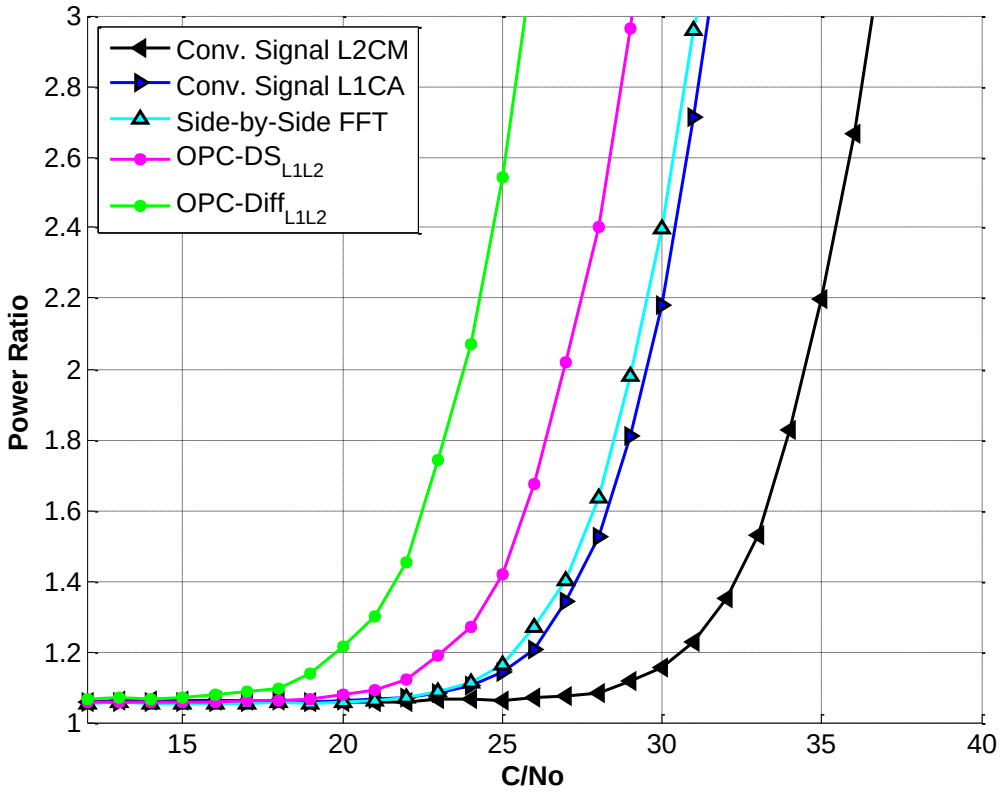

Figure 4-45 OPC-Diff$_{L1L2}$: Power ratio of the maximum correlation peaks

Initial phase effect: Figure 4-47 shows that the signal detection behaviour of the OPC-Diff$_{L1L2}$ method is stable as the other methods, but our method has showed a high P_D values due to the chosen C/No. The C/No is 26 dB-Hz and the corresponding P_D value in the OPC-Diff$_{L1L2}$ method is approximately 1.

In general, the simulation results of all test scenarios prove that the acquisition performance of the OPC-Diff$_{L1L2}$ method is much better amongst all the compared methods. In addition, the results demonstrate that the adopted method proves to be a good candidate in acquiring a weak signal in bad reception areas.

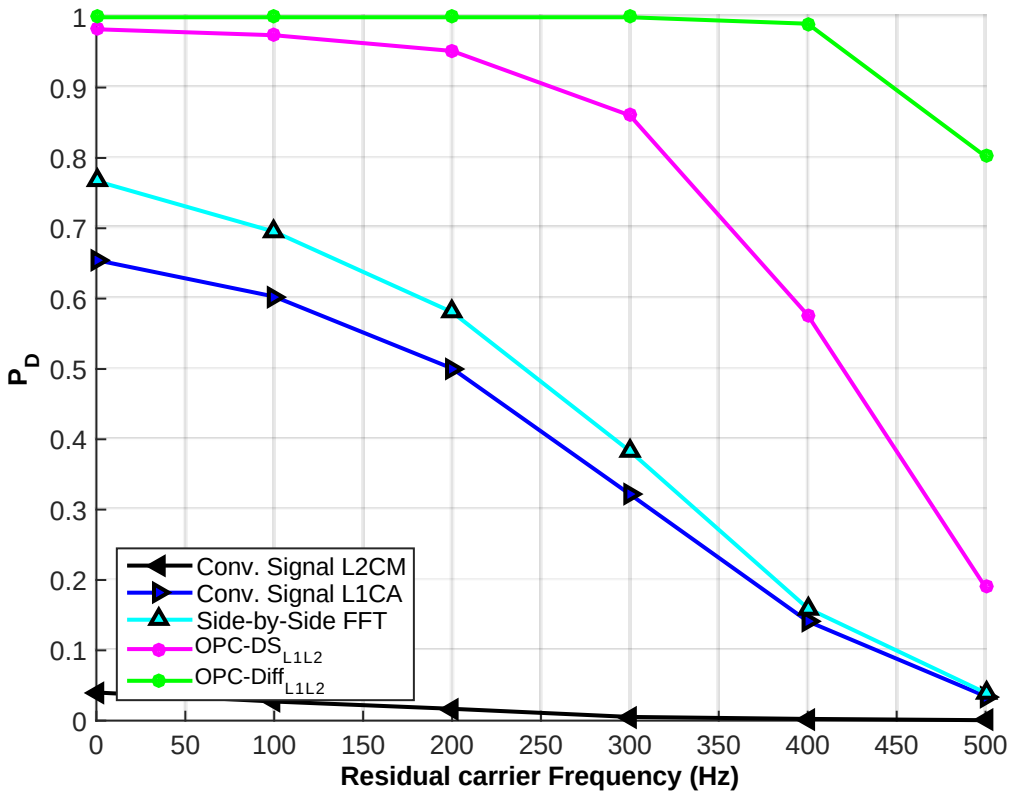

Figure 4-46 OPC-Diff$_{L1L2}$: Probability of detection vs. residual carrier frequency

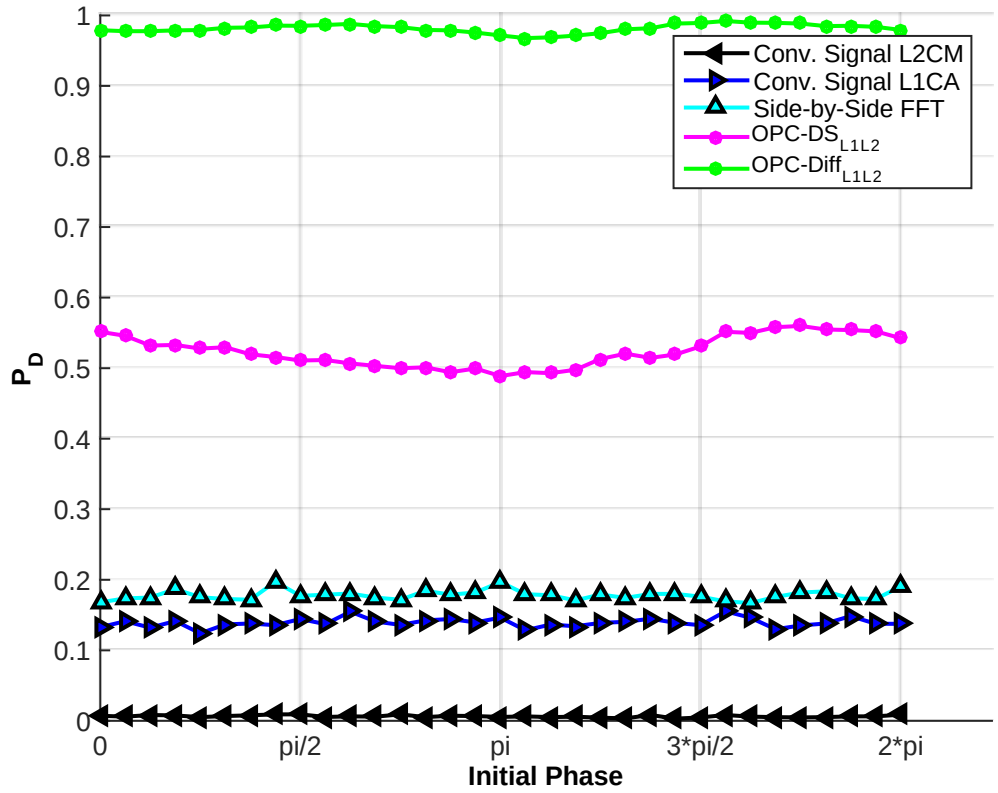

Figure 4-47 OPC-Diff$_{L1L2}$: Probability of detection vs. phase-offset

4.5.3 Direct Sum and Differential Acquisition: OPC-DSDiff$_{L1L2}$

This method couples the differential and non-coherent technique to acquire the L1CA and the L2C signals at the same time. The structure of the combination stage in this method as depicted in the block diagram (see Figure 4-48) is more complicated than the ones in the previous two proposed methods since it has four multipliers, two untie delay and one adder. However, it balances by the computational load and the improved acquisition gain.

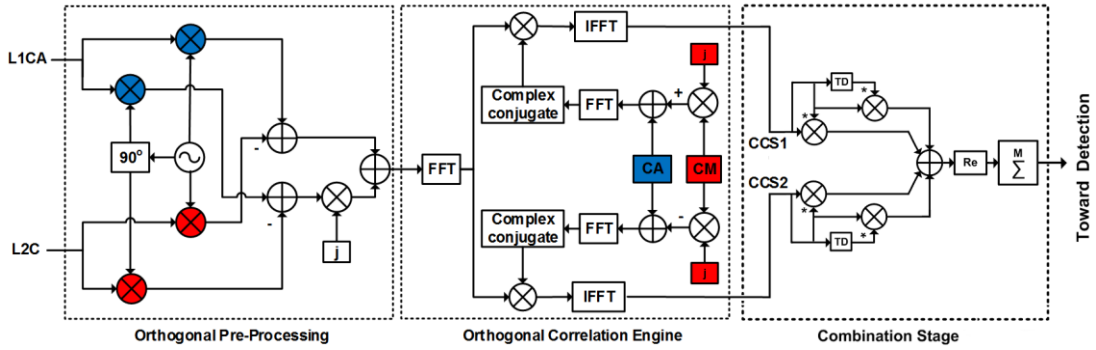

Figure 4-48 Block diagram of the OPC-DSDiff$_{L1L2}$ method

The signal correlation process in the combination stage is as follows:

1. The CCS1 value is multiplied with Conjugate value of itself to get the non-coherent correlation result. The same process is done for the CCS2 value.
2. Again, the CCS1 is multiplied with Conjugate value of 1 *msec* delay of the same CCS1 to get the differential correlation result. Also, the same process is performed to the CCS2 value
3. After that, the non-coherent correlation and the differential correlation results of the first and second steps are gathered.
4. The real part of the above summation values is calculated and then accumulated for M *msec*, and then the decision vector is sent forward to the detection stage to choose the maximum value and match with the predefined threshold to declare the acquisition decision.

The combination stage of the OPC-DSDiff$_{L1L2}$ method is slight complicated compared with all pervious methods in the OPC and the OSC since it has four

mixers and two unit delays. However, this method has kept the poise between computational costs and the improvement in the acquisition sensitivity.

The decision vector of the OPC-DSDiff$_{L1L2}$ method can be written mathematically as:

$$OPC - DSDiff_{L1L2} = 2\sum_{k=1}^{M} \underbrace{(I_{1,k}^2 + Q_{1,k}^2) + \left(I_{1,2k}\, I_{1,k-1} + Q_{1,2k}\, Q_{1,k-1}\right)}_{L1\ term} + 2\sum_{k=1}^{M} \underbrace{(I_{2,k}^2 + Q_{2,k}^2) + \left(I_{2,k}\, I_{2,k-1} + Q_{2,2k}\, Q_{2,k-1}\right)}_{L2\ term} \quad (4\text{-}23)$$

1. Performance validation of OPC-DSDiff$_{L1L2}$

Probability of detection: Figure 4-49 shows that the performance of the OPC-Diff$_{L1L2}$ method is the best amongst all the comparison methods. The same figure demonstrates that acquisition sensitivity is hugely improved compared with conventional acquisition methods L1CA and L2CM and reaches 11 dB and 6 dB for respectively. In a weak signal scenario, the OPC-DSDiff$_{L1L2}$ method starts detecting the signals at C/No equal to 15 dB-Hz.

Ratio of maximum correlation peak: Figure 4-50 shows that the power ratio of the OPC-DSDiff$_{L1L2}$ method is the best over all the compared methods, and improved by 5 dB and 10 dB as compared with traditional acquisition methods L1CA and L2C respectively. In addition, it improved by 1 dB and 3 dB compared with OPC-Diff$_{L1L2}$ and OPC-DS$_{L1L2}$ methods respectively. This considerable difference between the noise level and the max value of the processing-gain in the OPC-DSDiff$_{L1L2}$ method facilitates to choose a threshold that will reduce the false alarm probability.

Residual frequency effect: Figure 4-51 displays the behaviour of all OPC proposed methods along with the conventional and NC FFT-based methods when the nonzero residual carrier frequency exists. Once again, the combining strategy of the OPC-DSDiff$_{L1L2}$ method is perfectly robust for acquiring the L1CA and L2C signal, and it has a small degradation only when $\Delta F > 400$. For the same reason that mention in the previous test scenario in the OPC-DSDiff$_{L1L2}$ method.

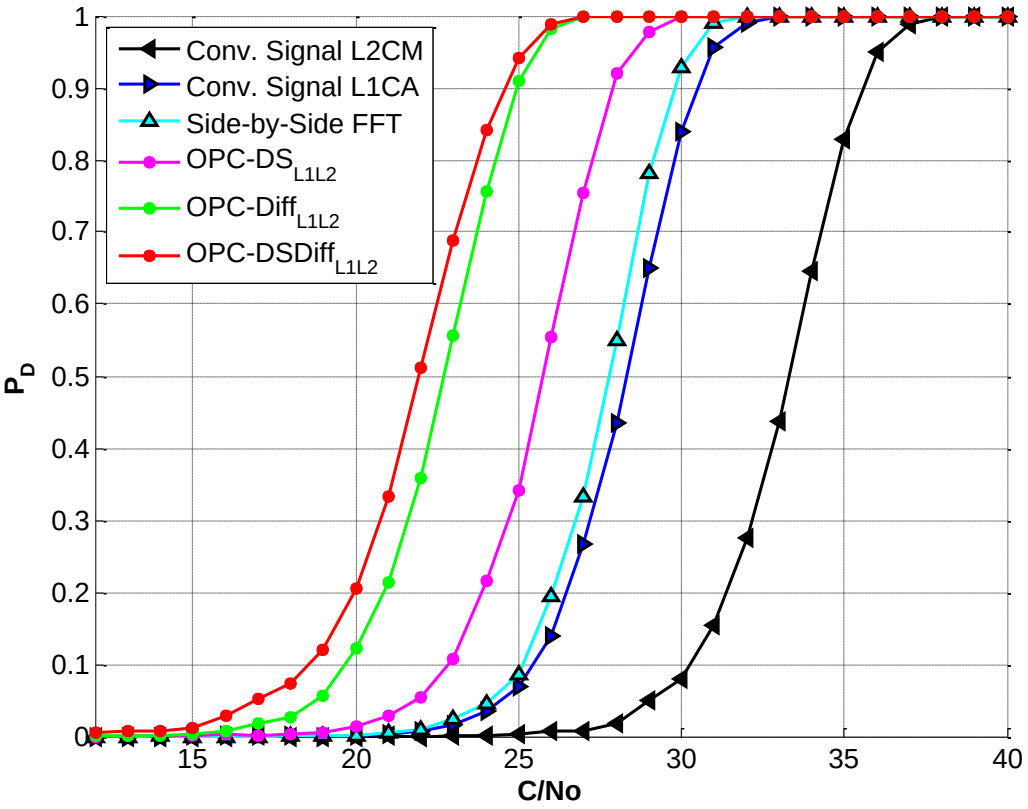

Figure 4-49 OPC-DSDiff$_{L1L2}$: The probability of detection versus C/No

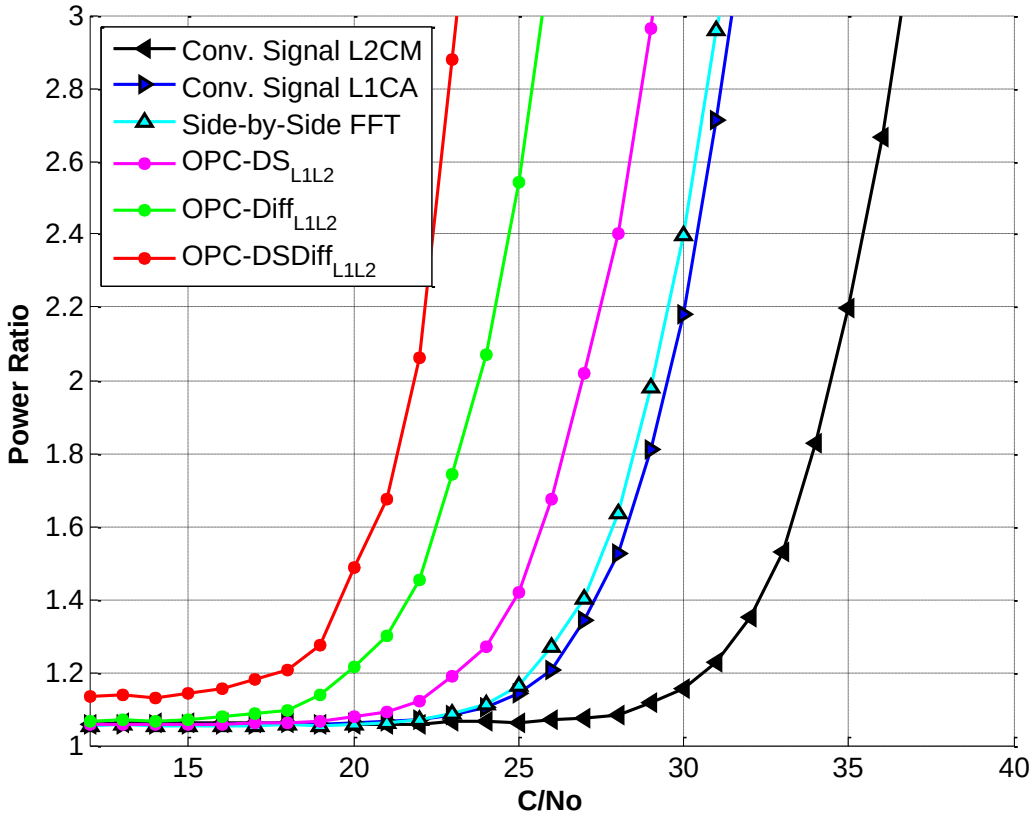

Figure 4-50 OPC-DSDiff$_{L1L2}$: Power ratio of the maximum correlation peaks

Initial phase effect: The simulation results in Figure 4-52 shows that the P_D of the OPC-DSDiff$_{L1L2}$ method is all most constant around 1, this results are expected since the C/No of the received signals is 26 dB-Hz and the PD at the value is a round 1 (see Figure 4-49). Also, in the decision vector of the OPC-DSDiff$_{L1L2}$ there is no mathematical extra-term (see equation in 4-23) that operates as a function of phase-offset to degrade the signal detection, so it is reasonable to see that the simulation result is stable around one value.

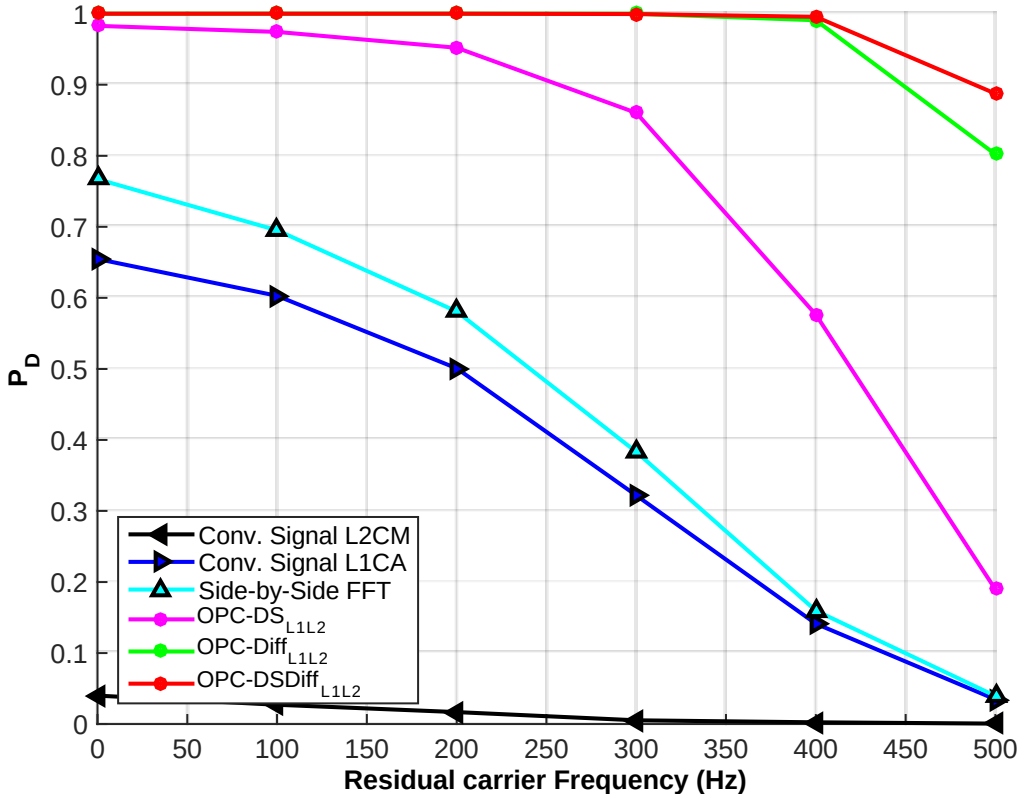

Figure 4-51 OPC-DSDiff$_{L1L2}$: Probability of detection vs. residual carrier frequency

Ultimately, the acquisition performance of the OPC-DSDiff$_{L1L2}$ method is the best amongst all the OPC proposed methods as well as the conventional L1CA and L2CM and side-by-side NC FFT-based methods. The simulation result proves that the OPC-DSDiff$_{L1L2}$ method starts detecting the signal at C/No equal to 15 dB-Hz with only 1 *msec* integrating time. This success is very helpful in acquiring a weak GPS signal with the low computational load.

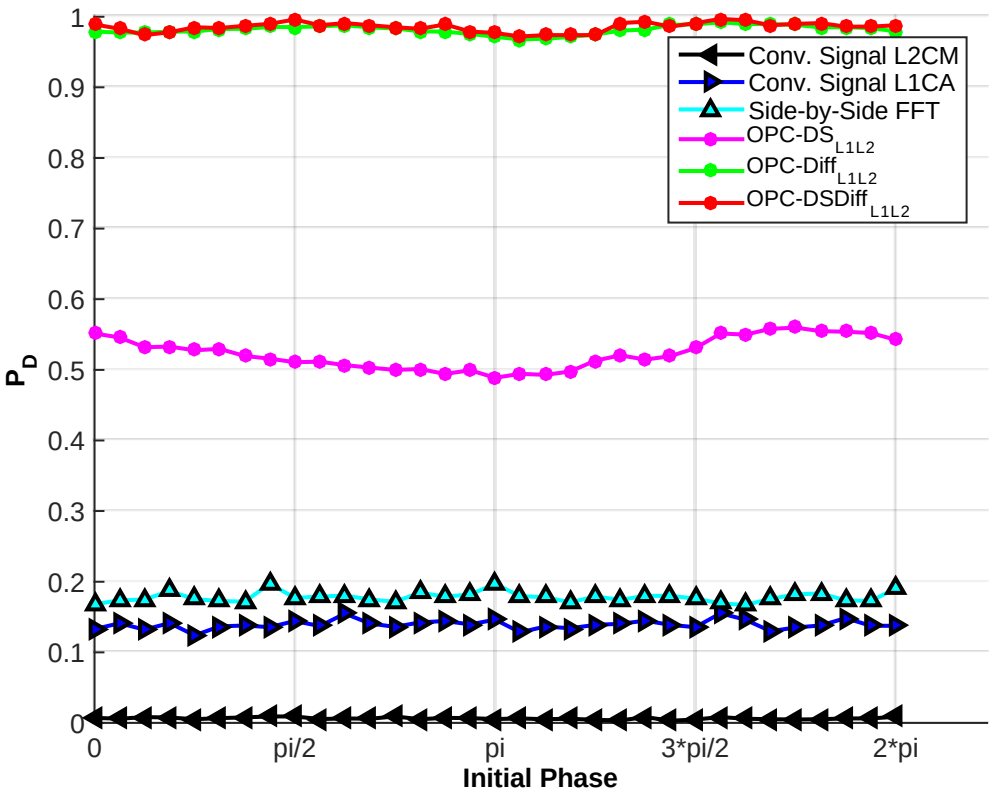

Figure 4-52 OPC-DSDiff$_{L1L2}$: Probability of detection vs. phase-offset

4.6 Compare Results and Conclusion

In this section, we will compare the performance of the best obtained methods in our two orthogonal channels (OSC-DSDiff$_{L1L2}$ and OPC-DSDiff$_{L1L2}$) with side-by-side acquisition methods (NCDiff$_{L1L2}$ and MGD, in terms of; 1) probability of detection, and 2) ROC curve.

The simulation parameters in Table 4-1 are used to evaluate the detection probability of all the above-mentioned methods. Furthermore, the simulation parameters in Table 4-2 are used to measure and compare all the acquisition methods mentioned in this section, in terms of on ROC curve.

Probability of detection: Figure 4-53 shows that all combined acquisition methods have better signal detection over the conventional methods. Similarly, our acquisition channels (OSC-DSDiff$_{L1L2}$&OPC-DSDiff$_{L1L2}$) also display a significant enhancement in the detection L1CA and L2C GPS signals as compared with other combined acquisition methods. The signal detection of the OSC-DSDiff$_{L1L2}$

acquisition method is improved by 2 dB and 1 dB over the NCDiff$_{L1L2}$ and MGDC methods respectively while the signal detection in the OPC-DSDiff$_{L1L2}$ acquisition method is increased by 1dB over the OSC-DSDiff$_{L1L2}$, which means the detection of the OPC-DSDiff$_{L1L2}$ method outperforms all the other combined methods.

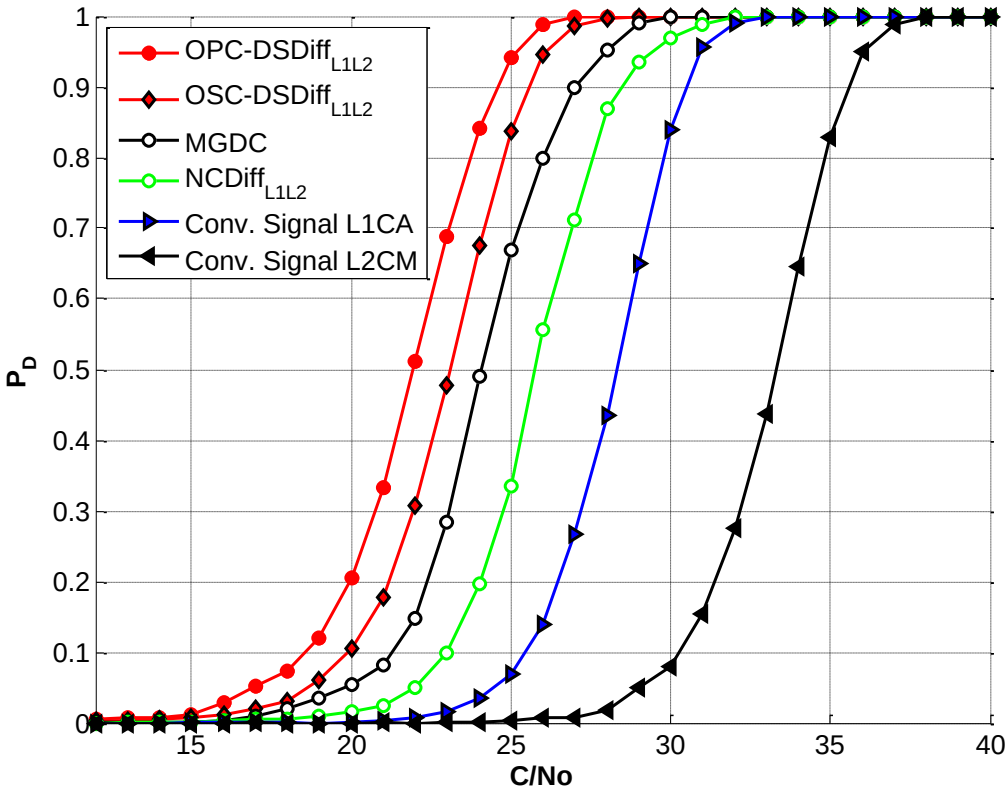

Figure 4-53 Detection probability of L1CA and L2CM conventional single acquisition channel, side-by-side combined acquisition channel and orthogonal combined acquisition channel at different C/No

ROC curve: It is clear in Figure 4-54, the advantage of combining L1CA and L2CM acquisition signal over the conventional acquisition methods. Certainly, all the L1CA and L2CM combined acquisition methods have a good separation line between the probability of detection and the false alarm probability when compared with the conventional methods. Figure 4-55 shows the simulation result of ROC curve of the L1CA+L2CM combined acquisition methods only. The trend of the ROC curves of these methods is almost identical; however, the OPC-DSDiff$_{L1L2}$ method exhibits the lowest overlapping between the probability of detection and the false alarm probability amongst the other methods. That means the OPC-DSDiff$_{L1L2}$ method has a better signal detection to the GPS signals and also a better rejection to

undesired signals.

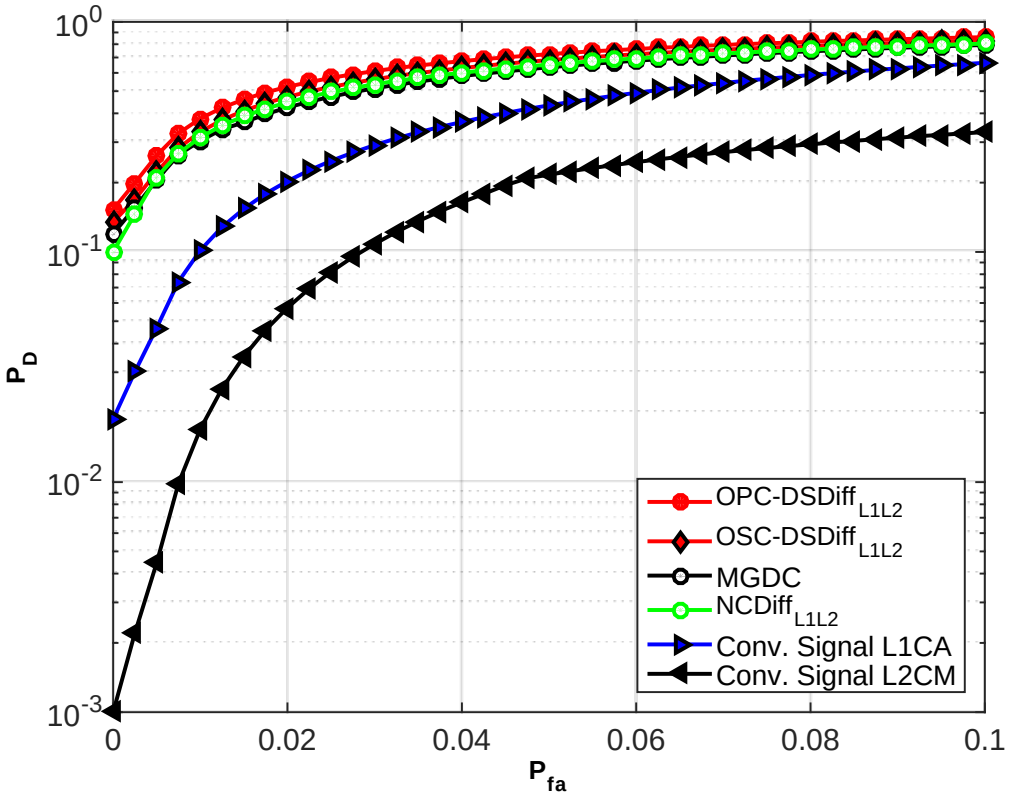

Figure 4-54 ROC curves of L1CA&L2CM conventional acquisition and combined acquisition methods when C/No = 26 dB-Hz

Implementation complexity and computation load: The MGDC characterises the most complex structure and has a substantial computation load since it needs at least 40 differential correlators to acquire the signals. However, the MGDC represents the fastest methods for acquiring the signals since it multiplies the incoming signals with 20 *msec* of locally generated signals at once, as detailed in Section 4.2. The OSC-DSDiff$_{L1L2}$ method has proven it has the less implementation complexity since it uses a signal channel. Nevertheless, this method needs to repeat the process two times for each 1 *msec* to get the maximum correlation peak. The implementation complexity of the OPC-DSDiff$_{L1L2}$ method is almost half of the NCDiff$_{L1L2}$ method; none the less our method has better signal detection by 3 dB as shown in Figure 4-53. The OPC-DSDiff$_{L1L2}$ methods showed the best signals detection and the less implementation complexity, which is the ultimate choose for the harsh environment/weak signals scenarios.

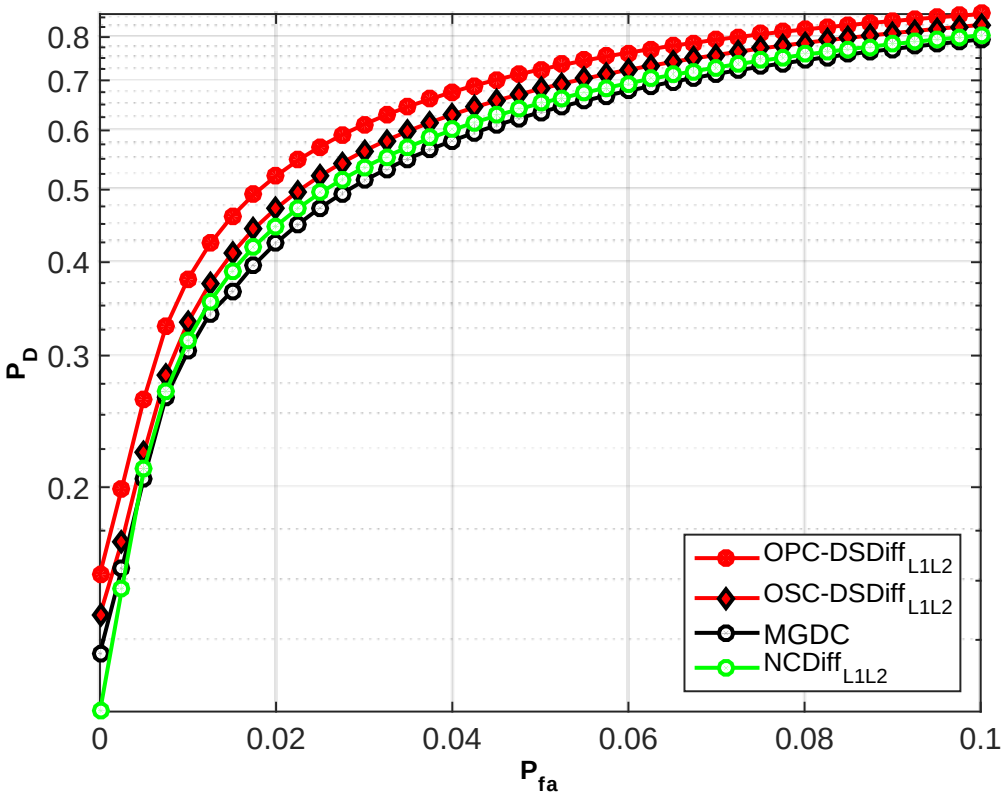

Figure 4-55 ROC curves of L1CA and L2CM combined acquisition methods when C/No = 26 dB-Hz

In conclusion, six combination methods have been designed to acquire L1CA and L2C signals simultaneously. The novelty of these methods is cantered on orthogonalising the two received signals (L1&L2) to a single orthogonal signal allowing the acquisition to jointly estimate the code-phase-delay and Doppler-frequency-offset of both the signals. Hence, there are valuable attributes such as circuitry power dissipation and processing time as compared to conventional side-by-side receivers. The simulation result of various signal power scenarios proves that the receiver design has a better acquisition performance compared with other combined methods. Besides, the implementations are almost half of other similar combined methods.

Chapter 5 Our Solution for Processing GPS and BT Signals in a Single Tracking Channel

As detailed in Section 2.1.4, our research has concluded that the BPSR architecture is a good candidate since it has the ability to process multi-signals to be digitised at the same time. In this chapter, we propose to use the BPSR to pass on the digitised data for tracking and demodulating processing in a single processing chain (thus achieving less complexity, power and cost overhead). Other solutions will use the BPSR receiver front-end to pass on the digitised data to then be processed side-by-side, in separate channels for each folded-signal, as depicted in Figure 5-1.

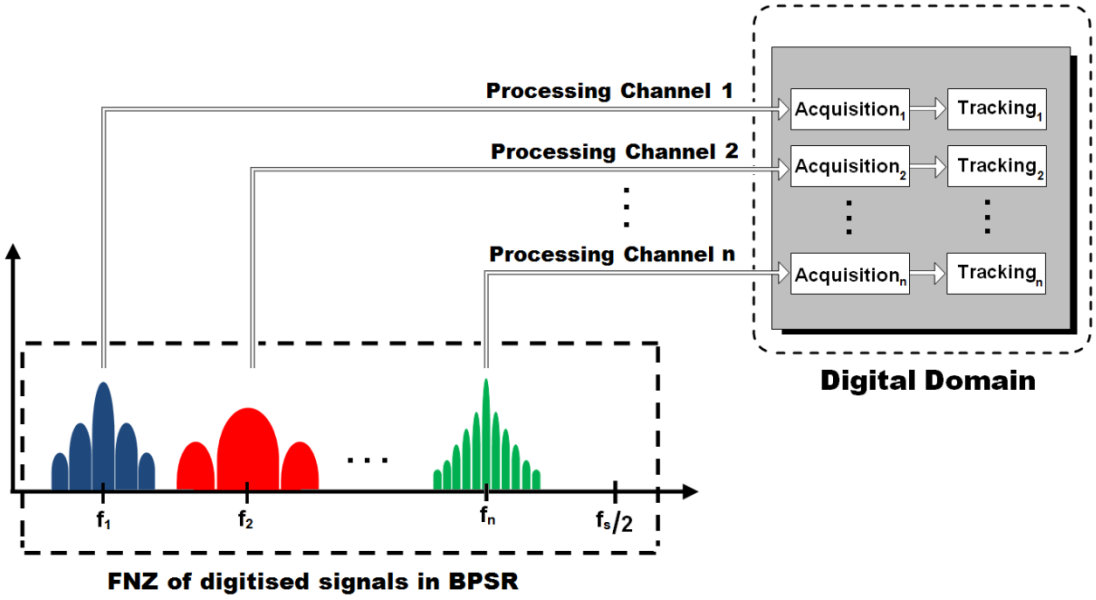

Figure 5-1 Typical BPSR multi-signals implementation scenario

We have focused on the "tracking and demodulation" function in this chapter because we believe that this is more active than the "acquisition" function that will normally go to sleep when a signal is acquired. Thus processing this in a single chain will achieve important saving, in terms of cost, size, processing time and power consumption.

As is well known, the most common function used in the tracking process is the PLL, and so, our efforts are focused on the challenge of designing "a single tracking channel PLL-based approach". Our research focus is therefore to design a new multi-signal-PLL that can track the BT and GPS-L1 signals without losing lock to any of them, irrespective of the frequency step/gap between the input signals frequencies.

We have chosen the Bluetooth (BT) and the GPS-L1 signals as being truly diverse type of signals as an application for our multi-signal PLL, and also, these two signals are used in every Smartphone and so integrating their solutions will have a big commercial benefit. We have found that combining these two signals (BT+GPS) in a single tracking channel is logically possible to process at the same time, because a typical BT transceiver is active intermittently with large standby/inactive windows (see Figure 5-2). i.e. we worked out that there is enough time to track GPS signal while BT is active, even in most demanding BT profiles when, for example, BT is used to stream data between a headset and media devise (Smartphone playing music). We have conducted an experiment to monitor the actual BT receiver activity relative to the time it is paired, to help understanding of these "standby time windows" available in between activities. The results show that there is an inactive gap-time of 2150 *µsec* in between active slots of 1250 *µsec*, as shown in Figure 5-2. This gap is, as described later, sufficient enough to track the GPS signal without losing the bit information, since the GPS signal has very low bit rate "50 Hz", if we can figure out a method to lock/relock the signal from BT to GPS, and vice versa, within a short time at the beginning and end of this 2150 *µsec* gap.

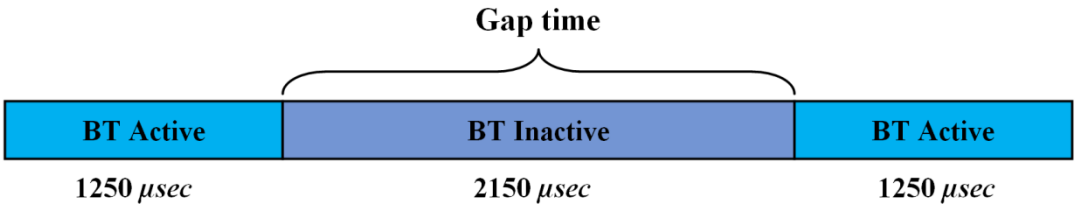

Figure 5-2 Time-multiplexing of BT and GPS signals

When studying the active-inactive timing of BT, we can see that, irrespective of the chosen folding-frequency of the BPSR front-end issue, the VCO/NCO of PLL needs to track the BT signal in "the active 1250 *µsec* window" at a frequency equal

to the frequency of the BT signal at the current hop. That is, in the next 2150 *µsec* (available gap time), the PLL has to switch its mode to track the GPS signal. This means that the PLL needs to adjust its locally generated frequency to GPS signal frequency, which requires making the PLL jump at least 10 *KHz* (owing to the Doppler Effect) to catch up with the GPS signal frequency. This is impossible since the PLL has fixed narrow Loop Filter (LF) bandwidth (GPS PLL is too small (25-100 *Hz*)) [28]. However, increasing the LF bandwidth will help the PLL to achieve fast lock on the GPS frequency, but this will allow more noise to enter the PLL, which makes the generated frequency too noisy that will cause the system/PLL to be unstable. (Not that this frequency-jump needs to be repeated the other way before exiting the 2150 *µsec* inactive gap). However, using an adaptive LF bandwidth can make the PLL cover the *10 KHz* frequency step [64], but in this case the adaptive LF requires a line-of-sight GPS signal, i.e. it has a very high C/No of 55 *dB-Hz*. More importantly, the filter update time will become too small "3 *nsec*", which means the time required to get PLL synchronised with GPS signal is more than the available gap-time.

On the other hand, considering the current multi-mode/multi-band PLLs (see, e.g., [65], [66], and [67]) as a solution to our case (tracking and demodulation BT&GPS in a single channel) is not feasible, since these PLLs have been designed to switch from one mode to another without maintaining the phase-lock. This has led us to think about feeding both the received (BT+GPS) signals simultaneously, combine them and feed them to a single PLL, and then study/analyse its behavioural response.

Other literature has studied the behaviour of the PLL when its input is two signals. It has been concluded that there are three parameters that can affect the stability of the PLL, which are:

1- Amplitude-Ratio (AR) is the ratio between the amplitudes of the two signals.
2- Frequency-Difference (FD) is the difference between the frequencies of the two signals.
3- ω is the frequency difference between the free-running frequency of VCO/NCO and the desired signal.

In other words, based on the values of those parameters (AR, FD & ω), the PLL will change its response automatically to be synchronized either with one of the two signals or with neither, as we will discuss them in the literature review section (see Section 5.1).

Therefore, in this chapter and as shown in Figure 5-11, we have designed a new PLL named "Adaptive Multi-Mode Phase Locked Loop (AMM-PLL)", which is based on integrating an adaptive Frequency Estimator (FE) into a standard version of Costas PLL. The FE provides an estimated frequency of the received signal to modify the free-running frequency of the NCO that will enhance extensively the performance of PLL by increasing largely its lock-in range in spite of using the narrow LF bandwidth. The new AMM-PLL will be tracked and demodulated both signals "BT and GPS-L1" simultaneously.

Note 1: Full details of the BT technology is available in [68] published spec [69]. In short, the BT signal is designed and intended to operate at the 2.4 *GHz* ISM band. In most European countries, the available bandwidth of the BT signal is 83.5 *MHz*. This operating band of the BT signal is divided into 1 *MHz* spaced channels, with throughput expected at 1 *Mb/s* or more in the recent BT versions. For higher bandwidth efficiency, the Gaussian Frequency Shift Keying (GFSK) modulation scheme is used, with bandwidth time "BT=0.5" and modulation index 0.3, and to enhance the data rate, different type of modulation technique can be used such as QPSK or 8PSK. A Frequency Hopping Spread Spectrum (FHSS) is used as a Multiple Access method to combat fading and interference in short distance connectivity. The transmitted signal carrier switches rapidly amongst many frequency channels based on a pseudorandom sequence over 79 RF channels in this band. The nominal hop rate is 1600 *hops/s* and therefore the slot length is 625 *μsec*. The mathematical representation of BT signal is expressed as:

$$S_{BT}(t) = A(t)\cos(2\pi f_c t + 2\pi h \int_{-\infty}^{t} m(\tau)d\tau) \qquad (5\text{-}1)$$

where f_c is the carrier frequency; fc = (2402 + k) MHz and k = 0:78; m is the message after it passed Gaussian filter and h is the modulation index.

Note 2: Full details of the GPS technology is available from [28]. The basic

characteristic of the GPS signal has been explained in detail in Chapter 4, Section 4.1.1, and can be expressed mathematically as:

$$S_{GPS}(t) = A(t)\, m\,(t) CA(t) cos(2\pi(f_c + f_d)t) \qquad (5\text{-}2)$$

where f_c is the carrier frequency (f_c =1575.42 MHz) and f_d is the Doppler frequency ($f_c = \mp 10$ KHz) and CA is the PRN code.

Therefore, the mathematical equation of the BT+GPS signals that are generated from a BPSR front-end where the signals are folded to FNZ will be input into our AMM-PLL, explained in Section 5.4. Note that the GPS signal at the PLL input is now BPSK signal with data and amplitude, such that the CA code has been removed from the signal before it is fed to the PLL. BT signal is also considered as BPSK signal since the PLL extracts only the phase of the BT signal and then the output is passed on to a differentiation block [70]. Therefore, the digitised signal of the BPSR of both signals (BT and GPS) in (5-1) and (5-2), is expressed mathematically as:

$$S_{BPS}[n] = A_{BT}[n]\cos[2\pi n(f_{BT} + f_{offset}) + \Phi] + A_{GPS}[n]\,\mathrm{m_{GPS}}[\mathrm{n}]\cos[2\pi\, n(f_{GPS} + f_d)].$$

where f_{BT} and f_{GPS} are the folding-frequency of the BT and GPS signals respectively, and n is simplified to nTs (T_s and n are the sampling time and the time index respectively) and $\Phi = 2\pi h \int_{-\infty}^{t} m(\tau)d\tau$. Also, f_{offset} is the offset frequency between the actual frequency value of the BT signal and the locally generated frequency that is used to remove the hopping frequency from the BT signal.

5.1 Literature Review and Analysis of Multi-Signal-PLLs

A Phase Locked Loop is a feedback system used for maintaining a continuous stable relationship between the phase of received signal and a locally generated one. PLLs are commonly used in wireless transceivers for clock synchronisation, frequency synthesis, modulation, demodulation and so on. There are many types of PLL designs [71], this review focuses on the Costas PLL, which is an improved version of the basic-PLL, and it is typically used for tracking and instantaneously demodulating a received signal. As shown in Figure 5-3, the phase detector of the

Costas loop consists of two multipliers and then it follows by two LPFs to wipe off the carrier signal, thus producing the in-phase ($\varphi_I(t)$) and the quadrature ($\varphi_Q(t)$) components. These components are then multiplied together in a discriminator block (Discr.) to produce the phase error, and the loop filter is used to filter this phase error to yield a smooth phase error (*g(t)*), which is fed back to the VCO to fine-tune the frequency of the local signal.

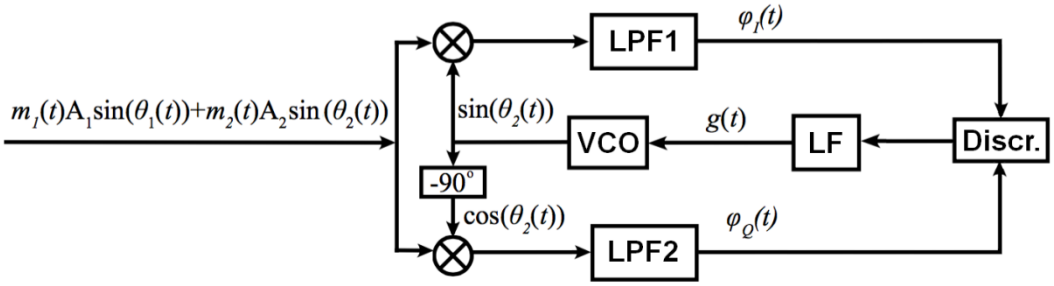

Figure 5-3 Costas PLL Model

In the tracking mode, the behaviour response of the Costas loop is very sensitive to any in-band signal-noise. However, because of our decision to use BPSR to fold the received two signals (BT and GPS) to a same folding/IF-frequency in the FNZ, and then process this resultant signal in a single receive chain, using a single PLL. This means that the two signals will be sharing the same band and will be fed directly to the PLL at the same time. Therefore, this necessitated a thorough analysis of the behaviour response of the PLL to help us design an appropriate solution if this idea will work.

From the PLL point of view, the PLL views its input as two signals, and so considers one of them as being the desired signal and the other as an interfering signal. In our case, both signals are actually desired signals as we have orthogonalised two received signals to be synchronised by the two phases of the PLL, but appear at different specific times as illustrated in Figure 5-2. Analysis of the PLL behaviour response is currently limited to studying the frequency and the amplitude change of the received signals only, which means that the literature does not include studying the effects of the phase-change of the received signals that we need to take into consideration. This PLL phase-change analysis has led us to a new mathematical model that we proposed/published and detailed in Section 5.3.

Analysing the PLL behaviour by choosing a stochastic analysis has been proposed in [72] to evaluate the degradation of the PLL performance when its input is actually two desired signals multiplexed in time. This analysis uses the measurement of probability density function (pdf) and the joint-pdf [73] of the loop phase error and the cycle-slipping rate to prove that the PLL response is dependent on the AR and the FD of the two signals. However, this analysis did not show explicit details about the relationship between the AR and the FD with respect to the PLL synchronisation and stability.

Another analysis has evaluated the behaviour of the PLL when it uses to track and demodulate FHSS signals when there is a collision between two signals at the same frequency band (both signals hopped to the same frequency band) [74]. This analysis has determined the effect of the AR and the FD on the stability of the PLL. Based on the values of those parameters (AR&FD), the PLL synchronises either with the one of the two signals or with neither. However, the analysis was limited to evaluate only the lock range of the PLL, i.e., it excludes cases of the pull-in and the pull-out PLL ranges.

In the same vein, another approach (of analysing the PLL behavioural response and its nature at saddle-node bifurcation points-breaks phase lock) has been proposed to cover all the PLL synchronisation ranges by using Poincare map [75]. The purpose of this map is to study and solve the autonomous nonlinear differential equation that expresses the PLL behaviour when it tracks two signals at the same time. This means analysing the PLL system stability at bifurcations points focusing only on the PLL synchronisation range response by taking just the effect of the AR and the FD and ignoring the phase-change variation of the two signals.

On the other hand, a scheme based on controlling the AR value, has been proposed to manipulate the PLL synchronisation area [76]. This is achieved by utilising a band-pass limiter prior to the PLL. Mathematically, this manipulating of the AR value means that the AR will become a bifurcation parameter, so that, based on its value, the PLL could have two, one, or none of the equilibrium points. So, having two equilibrium points means the performance of the PLL will be stable at one equilibrium point and unstable at another point, i.e., the PLL will be

synchronised with one of the two signals and ignoring the other signals even if they are sharing the same frequency, and it is the same if there is one equilibrium point. In the case of no equilibrium point, the PLL will not synchronise with any one of the two signals, which means that the PLL has lost lock and needs to reacquire the signal. Similarly, the FD and ω will also become bifurcation parameters when the AR is assumed a state variable. Therefore, the response of the PLL system can be assumed as a function of three parameters, which are AR, FD, and ω. So that, controlling these parameters will change the PLL behaviour and it can switch between the two signals and become stable.

Since our aim is to demodulate the two GPS and BT signals besides tracking them, the phase of the two signals needs to be included in our analysis, i.e. the phase-change (based on the transmitted information data) of the two signals needs to be analysed. Therefore, we have introduced a new mathematical/numerical model that considers the effect of this phase-change. This model is based on the phase space model of the Costas loop [77]. Also, this study has allowed us to obtain more information about the characteristics of PLL nature, such as lock time and lock range as well as see the effect of the phase-change of the received signal on the synchronisation process in both ω <1 and ω >1 cases. This model is used, basically, to analyse the nature of the nonlinear non-autonomous differential equation for Costas loop in the presence of two signals.

5.2 Our Mathematical Model for Studying the Effect of Phase-Change in Costas-PLLs

The FPE/PLL-system that describes the probability density function of the phase errors, $\phi(t)$, for only one signal input is [2],

$$\frac{\partial f(\phi,t)}{\partial t} = \frac{\partial}{\partial \phi}\big(C_1(\phi,t)\ f(\phi,t)\big) + \frac{\partial^2}{\partial \phi^2}(C_2(\phi,t)\ f(\phi,t))$$

where C_1 and C_2 are the moments of the PLL-system.

The above PDE becomes very difficult to analyse, when the PLL-system is fed by two signals. Therefore, our mathematical model of the PLL in this section is developed to measure the phase-change effect on the system stability when its input is two signals. We will consider Costas loop before synchronization (see Figure 5-3).

The input signal is the sum of two BPSK signals (S1+S2)

$s_{in} = A_1 m_1(t)\, sin\big(\theta_1(t)\big) + A_2 m_2(t) sin(\theta_2(t))$.

where

$\theta_{1,2}(t) = w_{1,2}(t) + \theta_{1,2}(0)$

and $w_{1,2}$ *are the frequencies of input carriers and* $\theta_{1,2}(0)$ *are the initial phases. Two orthogonal outputs of VCO are given by:*

$s_{vco} = sin\big(\theta_{vco}(t)\big)$,

$s_{vco} = sin\big(\theta_{vco}(t)\big), s_{vco}^{90} = cos\big(\theta_{vco}(t)\big)$

where

$\theta_{vco}(t) = w_{vco}(t) + \theta_{vco}(0)$

and w_{vco} *is the frequency of locally generated carrier and* $\theta_{vco}(0)$ *is the initial phase of VCO.*

After multiplying the VCO signal by the input signal and applying LPF's, two branches of the signal are produced. The upper branch named the "in-phase" signal/component and can be expressed as:

$$\varphi_I(t) = \frac{1}{2}\big[A_1 m_1(t)\, cos\big(\theta_1(t) - \theta_{vco}(t)\big) + A_2 m_2(t)\, cos\big(\theta_2(t) - \theta_{vco}(t)\big)\big].$$

While, the lower branch is named the "quadrature" signal/component and can be given as:

$$\varphi_Q(t) = \frac{1}{2}\big[A_1 m_1(t)\, sin\big(\theta_1(t) - \theta_{vco}(t)\big) + A_2 m_2(t)\, sin\big(\theta_2(t) - \theta_{vco}(t)\big)\big].$$

The relation between the inputs $\varphi_{I,Q}(t)$ and the outputs $g_{I,Q}(t)$ of the linear low-pass filters (LF) are as follows [78]

$$\frac{dx_{I,Q}}{dt} = A_{I,Q} x_{I,Q} + b_{I,Q}\varphi_{I,Q}(t) \text{ and, } g_{I,Q}(t) = c_{I,Q}^{*}(t) x_{I,Q} \qquad (5\text{-}3)$$

where, $A_{I,Q}$ *are constant matrices, the vectors* $x_{I,Q} \in \mathbb{R}^m$ *are filter states,* $b_{I,Q}$*,*

$c^*_{I,Q}(t)$ *are constant vectors, and the vectors* $x_{I,Q}(0)$ *are initial states of filters.*

The control signal $g(t)$ is used to adjust the VCO frequency to the frequency of input carrier signal its phase representation is expressed as follows:

$$\dot{\theta}_{vco}(t) = \ w_{vco}(t) = \ w_{vco}^{free} + Lg(t) \qquad (5\text{-}4)$$

where, w_{vco}^{free} *is the free-running frequency of the VCO and L is the VCO gain.*

Taking into account (5-3) and (5-4), we obtain the mathematical model in the "signal space" describing the real model of the Costas loop:

$$\begin{aligned}
\dot{x}_I &= \ A_I x_I + b_I \varphi_I(t) \\
\dot{x}_Q &= \ A_Q x_{QI} + b_Q \varphi_Q(t) \qquad (5\text{-}5) \\
\dot{x} &= \ Ax + b(c_I^* x_I)\ (c_Q^* x_Q) \\
\dot{\theta}_{vco} &= \ w_{vco}^{free} + L(c^* x) + L(c_I^* x_I)\ (c_Q^* x_Q)
\end{aligned}$$

Example: Consider first-order proportionally-integrating filter as a loop filter with Transfer Function (TF)

$$H(s) = \ K_f \frac{1 + s\tau_2}{s\tau_1}$$

Then (5-5) changes to

$$\begin{aligned}
\dot{x}_I &= \ A_I x_I + b_I \varphi_I(t) \\
\dot{x}_Q &= \ A_Q x_{QI} + b_Q \varphi_Q(t) \\
\dot{x} &= \ \tau_1 x_I x_Q \\
\dot{\theta}_{vco} &= \ w_{vco}^{free} + LK_f x + LK_f \tau_2 x_I x_Q.
\end{aligned}$$

The mathematical model in the signal space (5-5) is a "*nonlinear non-autonomous differential system*", so generally its analytical study is a difficult task even for the continuous case when *m(t)* ≡ const. Besides, since it is a "*slow-fast system*", its numerical study is rather complicated for the high-frequency signals. The problem is

that, it is necessary to consider simultaneously both very fast time scale of the signals $sin(\theta_{1,2}(t))$ and slow time scale of phase difference between the signals $\theta_{\Delta}(t)$, therefore a very small simulation time-step must be taken over a very long total simulation period [79] [80]. Applying the TF of the first-order filter on (5-5), then it can be reduced to become:

$$\dot{x} = Ax + b\varphi(t)$$

$$\dot{\theta}_{vco} = w_{vco}^{free} + L(c^{*}x) + Lh(c^{*}x)$$

Where,

$$\varphi(t) = \frac{1}{8}\left[A_1^2 m_1^2(t)\, sin\big(2\,\theta_1(t) - 2\,\theta_{vco}(t)\big) + A_2^2 m_2^2(t)\, sin\big(2\,\theta_2(t) - 2\,\theta_{vco}(t)\big) + 2\,A_1 m_1(t) A_2 m_2(t)\; sin(\theta_1(t) + \theta_2(t) - 2\,\theta_{vco}(t))\right]. \quad (5\text{-}6)$$

Since the data signal $m_{1,2} = \mp 1$ and $m_{1,2}^2 \equiv 1$, then only the last component of (5-6) that is

$$A_1 m_1(t) A_2 m_2(t)\; sin(\theta_1(t) + \theta_2(t) - 2\,\theta_{vco}(t)) \quad (5\text{-}7)$$

Depending on the input signal, reducing the impact of the (5-7) on the synchronisation process is possible to make amplitudes $A_{1,2}$ small enough to be filtered (5-7) by a loop filter.

Next section shall provide numerical examples that will demonstrate the effects of false-lock due to phase-changes (data signals $m_{1,2}(t)$ of the input/received signal.

5.2.1 Simulation/Analysis of Phase-Change Effect for Time-multiplexed Multi-Signal PLL

A MATLAB/Simulink implementation is used for our Costas PLL model as shown in Figure 5-4; where Figure 5-5 shows the input signal block, which represents the upper and lower branches indicating the first signal (S1) and the second signal (S2) respectively. In Figure 5-5, (freq1, amplitude1, m1) and (freq2, amplitude2, m2) are the carrier frequency; the amplitude and the information

message of the S1 and S2 signals respectively.

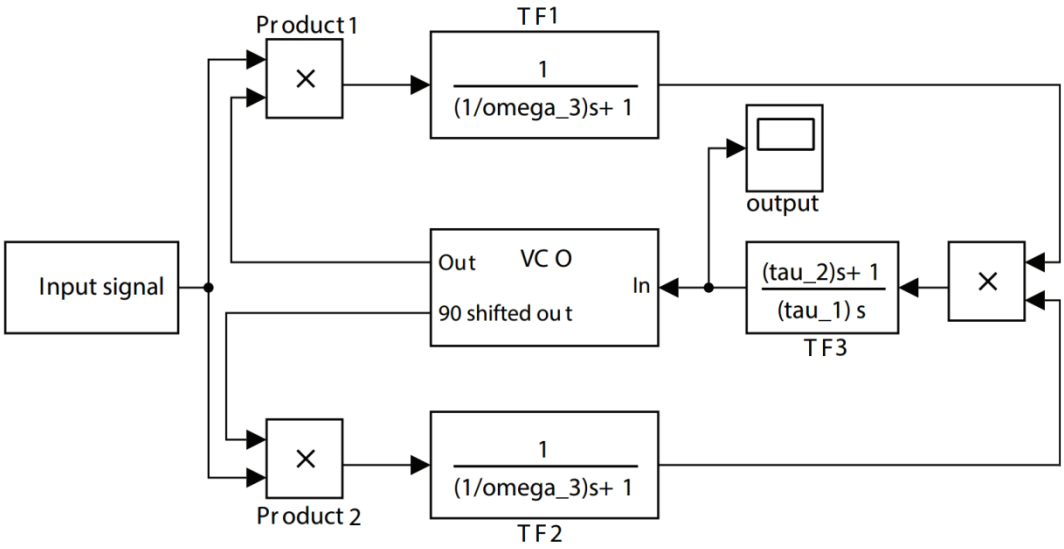

Figure 5-4 Costas PLL model in MATLAB/Simulink

Note that, the amplitude of the S1 signal is 1 *RMS*, while that of the S2 signal is 0.1 *RMS*. Also, the bits of the information messages of the BT and GPS signals are generated randomly based on a bit rate of 100 *KHz* for the S1 signal and 130 *KHz* for the S2 signal. Finally, the loop filter parameters are omega_3 = 1.25 *MHz*, tau_2 = 3.9789 *µsec*, tau_1 = 20 *µsec*.

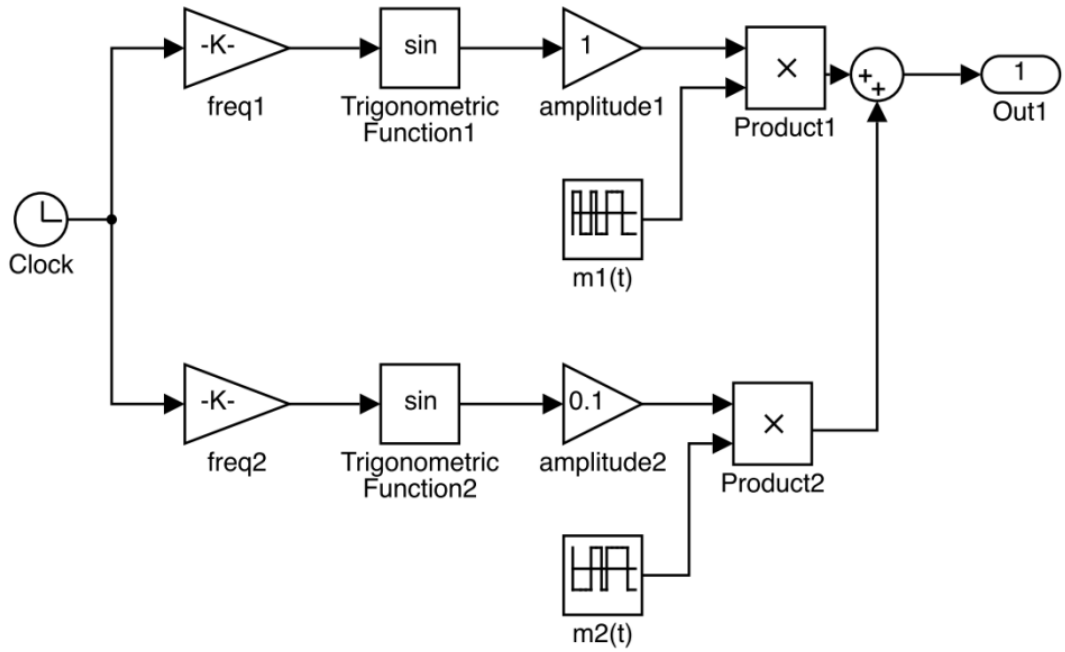

Figure 5-5 Model of input signal in MATLAB/Simulink

Implementation of the VCO block is shown in Figure 5-6. It has the following set of parameters: feedback gain K_0 is 1.2633e+06 *rad/sec. V* and the initial phase shift is 0 *rad*. The normalised frequency difference between the S1 and S2 signals is 0.1 *Hz*.

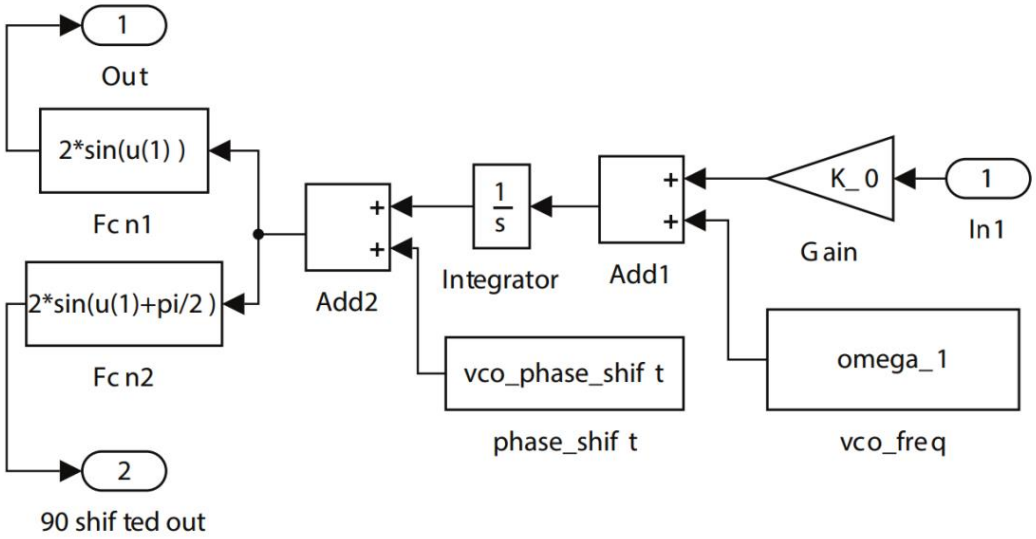

Figure 5-6 Model of VCO in MATAB/Simulink

Our simulations consider two scenarios of $\omega<1$ and $\omega\geq1$ to evaluate the phase-changes effect on the PLL synchronization process in the presence of S2, as follows:

1. The first scenario (ω<1)

***Case*1**, in this scenario, the phase-changes are not taken into account ($m2(t)$=1); the simulation results show that the Costas PLL of the typical model is synchronised with the S1 signal within the lock time of 100 μsec and the VCO input oscillates around −0.2 *V/rad*, as shown in Figure 5-7 (a).

***Case* 2**, is designed to simulate when the phase-changes of the S2 signal are taken into consideration, i.e., *m2 (t)* alternates between 1 and −1. The results show that, the PLL behaviour response becomes different, and the Costas PLL needs a period of about 2.2 *msec* to be synchronised with the S1 signal, as shown in Figure 5-7 (b).

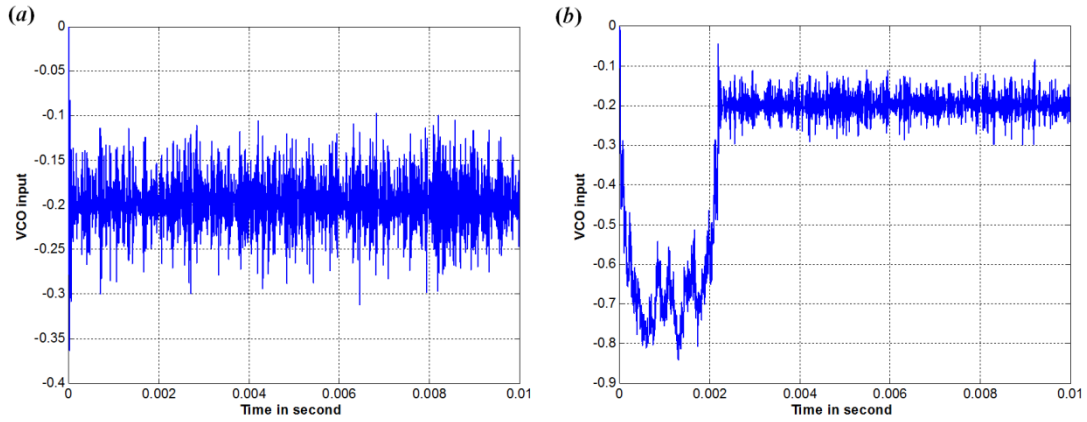

Figure 5-7 First scenario (ω<1), (a) typical model, (b) our model

Note that the width of unstable period is subject to change, depending on the PLL parameters settings as well as the bit rate and the amplitude-ratio of the S1 and S2 signals. Figure 5-8 shows that this period becomes a (200 *µsec*) when the amplitude-ratio is changed (amplitude of S2 = 0.01 RMS).

2. The second scenario (ω≥1)

***Case* 1**, illustrates when the phase-changes are not taken into account (*m2(t)*=1); the simulation results show that the Costas PLL of the typical model will be synchronised after 3.2 *msec*, the phase lock to the S1 signal has occurred, and the VCO input oscillates is around −0.9 *V/rad*, as shown in Figure 5-9 (a).

***Case*2**, while, in our model, which the phase-change is considered, the PLL becomes unstable and will not synchronise with S1 or S2, as can be seen in Figure 5-9 (b).

Theoretically, therefore, when $\omega \geq 1$, the PLL is impossible to lock with the S1 signal phase. But, as shown in the second test scenario (***Case 1***), the phase lock has been occurred. The reason is that adding S2 signal to S1 signal will pull the PLL system to produce an equilibrium point that is responsible to make the PLL synchronise with S1 signal [76]. i.e. in the typical model, the S2 signal is added to the S1 signal as a constant value, while in our model, the resulting signal from mixing S1 to S2 will either be constructive or destructive based on the instantaneous phase of the two signals. Thus, our model demonstrates a more realistic PLL behaviour.

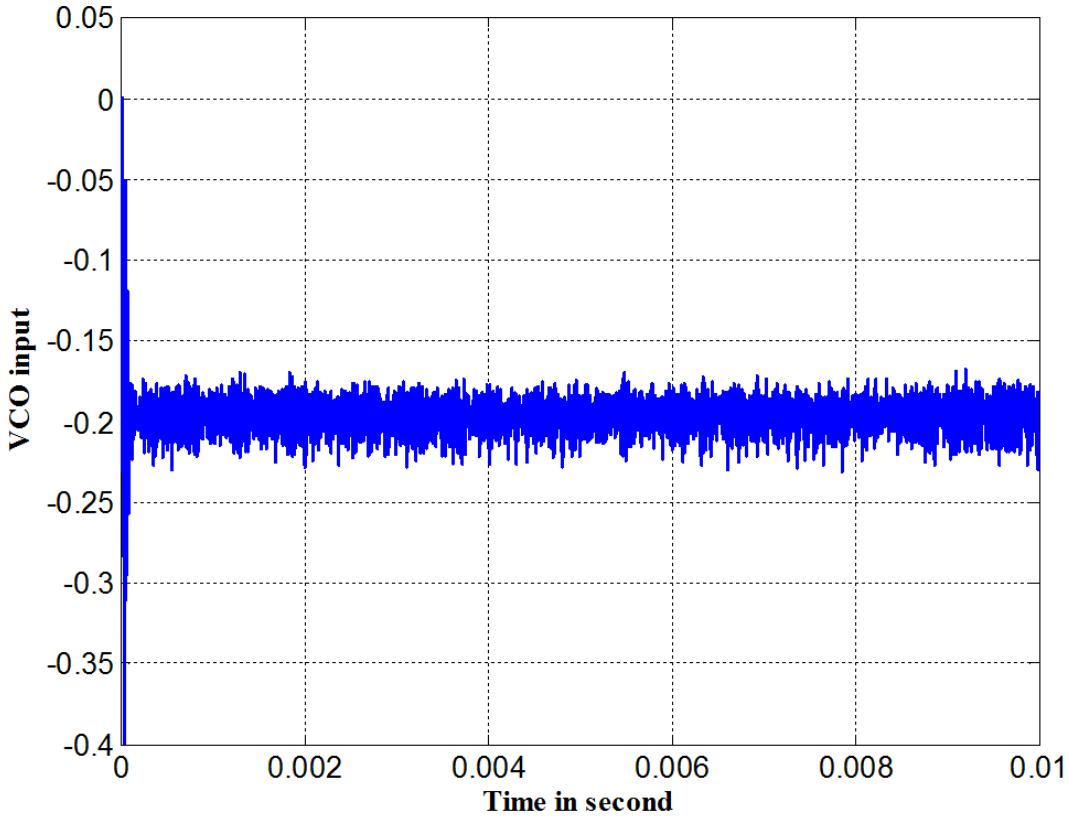

Figure 5-8 First scenario (ω<1), Case 2; result of changing AR in our model

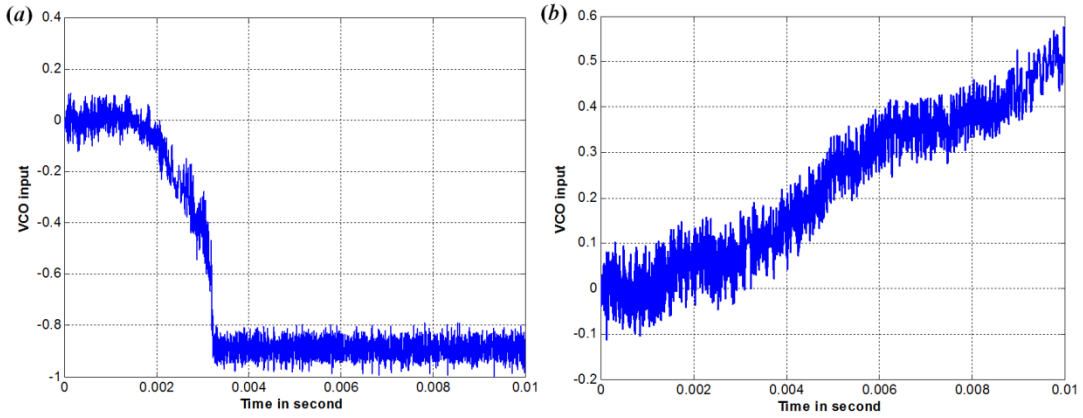

Figure 5-9 Second scenario (ω>1), (a) typical model, (b) our model

Reaching a conclusion from the previous two sections (Section 5.2 and 5.3) we can deduce that there are four parameters that can affect the PLL behaviour when it has two input signals, these parameters are the (AR), (FD), ω), and the phase-change. Manipulating the value of these parameters can change the behaviour and the performance of the PLL; i.e. it can synchronise with one of the two signals or

desynchronise with any one of them. Therefore, in our new design the value of these parameters needs to be considered.

5.3 Design Considerations for Multi-Signal Tracking and Demodulation

In order to design a single tracking and demodulation channel that has the ability to handle the BT and the GPS signals concurrently, the value of the four parameters (AR, FD, ω, phase-change), that were concluded from the PLL study, need to be considered. Two of these parameters, the FD and the phase-change, are uncontrollable when combining BT+GPS; however, the other two parameters can be used to eliminate the effect of them on the PLL synchronisation and stability, as we will explain later in this section. i.e. Before we start to discuss our consideration about the four parameters, we will first explain our plan to utilise the gap-time to track the GPS signal and then represent the digitised signals mathematically as a piecewise function based on the BT active time.

Figure 5-10 shows the first 4.65 *msec* of BT tracking activity, where the gap-time is 2.15 *msec*. Our plan is to divide the gap-time into two windows, the first window (t_{Switch}) is used to synchronise the frequency and phase of the locally generated signal with the frequency and phase of the GPS signal, while the second window is used to track and demodulate the GPS signal. t_{Switch} is therefore set to be 150 μsec of maximum time, which means around 7% of the available gap-time will be lost. So increasing this window can have an adverse effect on acquiring the full information of the GPS signal.

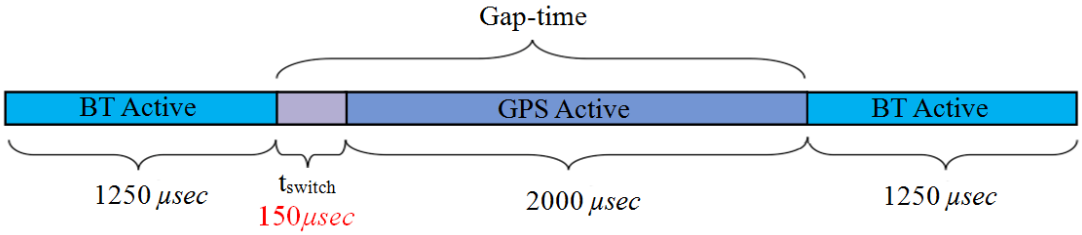

Figure 5-10 A scheme of exploiting the gap-time

When the BT signal is present, the frequency of the PLL needs to be adjusted to

match the BT signal frequency and phase; i.e. at any frequency hop of the BT signal the PLL needs to leave the GPS signal frequency and match the BT signal frequency in a short time. Fortunately, BT technology provides a time window of 260 *µsec* for the synchronisation and stabilisation purpose only at the beginning of each hop.

Based on our BPS front-end design both signals, BT and GPS, will be fed to the PLL as a combined signal (S_{in}) and the input of the combined signals is scheduled based on the time-multiplexing (see Figure 5-10) and can be expressed mathematically as:

$$S_{in} = \begin{cases} S_{BT}(t) + S_{GPS}(t) & if \quad 0 \le t \le 1250 \\ S_{GPS}(t)\ switching\ window & if \quad 1250 < t < 1400 \\ S_{GPS}(t) & if \quad 1400 \le t \le 2400 \\ S_{BT}(t) + S_{GPS}(t) & if \quad 2400 < t \le 4650 \end{cases} \tag{5-8}$$

where the S_{BT} and the S_{GPS} are the BT and GPS signals respectively. Note that the t is the time in µsec.

Equation (5-8) shows the time cut off of multiplexing BT and GPS signals, where the GPS signal are available all the time at the tracking channel (with amplitude value less than the BT by 4 times), while the BT signal will be idle at specific time, for example between 1250 to 2400 *µsec in our test case measurement.*

Now, considering our design, based on time-multiplexing let us observe the values of the control parameters that are required to let the PLL track both signals simultaneously.

1. The first period ($0 \le t \le 1250$ *µsec*):

In this period, the PLL is designed to track and demodulate the S_{BT} signal, while the input signal is a summation of the two signals (S_{BT}+S_{GPS}). Therefore, the control parameters value need to be set as follows:

Phase-change: This parameter will not affect the PLL performance when tracking the S_{BT}, because the bit rate of the S_{GPS} is too low as compared with the S_{BT}. This

means that during the first period there is only one phase-change possible in the GPS signal.

Frequency-difference (FD): This parameter is not controllable, since both signals have different frequency trends. The S_{GPS} signal has changeable Doppler frequency and the S_{BT} has different ω at each hop, so the frequency difference between the two signals is unknown at any new active BT period, but is nevertheless bounded. However, the effect of this parameter can be reduced by controlling the value of the AR and ω, and can be eliminated completely by setting AR = 12 *dB* and $\omega = 0$.

Amplitude-ratio (AR): the amplitude of the S_{BT} needs to be at least four times greater than the amplitude of the S_{GPS}. This means that the value of this parameter needs to be set in advance for the entire duration of the multiplexing-time line. However, the value of AR alone is not enough to let the PLL track the S_{BT} signal but it is subjective to the ω value, which should be equal/close to zero. The AR is expressed in dimensionless form, we can express a logarithmic scale in decibels (dB) as follows; AR (dB) = 20 log10 AR (dimensionless), so the AR = 12 *dB* in this case.

ω: Obviously, the value of this parameter is crucial to the success of our signal-tracking channel, since both the pervious parameters depend on their values. The ω value needs to be pulled in to zero rapidly. As discussed in the literature survey, pulling the ω to zero in the traditional PLL is not an easy task since it is mainly depending on the LF bandwidth, i.e., the wider LF bandwidth, the faster synchronisation between the frequency of NCO and the received signal. However, this will not be applicable in our case and furthermore, the LF bandwidth value needs to satisfy both signal (BT and GPS) requirements.

2. The second period ($1250 < t < 1400$ µsec):

In this window, the PLL has to adjust its NCO frequency to match with the S_{GPS} frequency, while its current frequency synchronises with the S_{BT} frequency. The input signal to the PLL in this window is the S_{GPS} only since the S_{BT} is inactive at this time, which means that the first three parameters (phase-change, AR and FD) are not present. Thus, the only parameter left in this case is *w*.

ω: The value of this parameter needs to be zero as in the previous case, but this

time the synchronisation has to be between the frequency of the S_{GPS} and the frequency of the NCO. The challenging issue here is that the PLL needs to be synchronising with the frequency of the S_{GPS} within 150 μsec, while its current frequency is the S_{BT} frequency. The frequency step between the S_{GPS} and the current locally generated frequencies could be greater than the lock-in range of the PLL. Consequently, the S_{GPS} needs to be acquired again and the time required to acquire the signal is more than the available gap-time. In other words, the whole idea of combining the BT and the GPS signals will be broken. Therefore, a fast mechanism to pull the ω to the zero within the time window "150 μsec" is required.

3. The third period ($1400 \leq t \leq 2400$ µsec):

The input signal of the PLL is S_{GPS} signal only and ω must be equal/close to zero from the previous time window, and the other control parameters will hold the same value. Thus, the PLL will smoothly track and demodulate the S_{GPS}.

4. The fourth period ($2400 < t \leq 4650$ µsec):

The control parameter values at this time are the same as they were in the first period. There is only one difference here, that is, the frequency of the NCO in first period was the free-running frequency of the PLL, while in this period it is the last value of the S_{GPS} frequency. Therefore, it is necessary to have a fast mechanism to bring the current NCO frequency to the free-running frequency or to the frequency closest to the S_{BT} frequency.

To sum up, AR needs to be equal to12 dB in advance for all PLL intervals, ω needs to be pulled to zero rapidly (within 150 μsec) at the beginning of each hop and the gap-time interval requires a fast mechanism. Consequently, in our AMM-PLL design, we use FE as fast mechanism to switch between the signals, as will be described in the next section.

5.4 Our Two Designs Based on (AMM-PLL)

The new design of our AMM-PLL is based on integrating an adaptive (FE) into a standard version of Costas PLL, as shown in Figure 5-11. The FE provides an estimate frequency of the received signal to modify the free-running frequency of the

NCO that will extensively enhance the performance of the PLL by increasing largely its lock range. Consequently, AMM-PLL can be utilised to track and demodulate multi-signal, even the gap among their frequencies up to10 *KHz*.

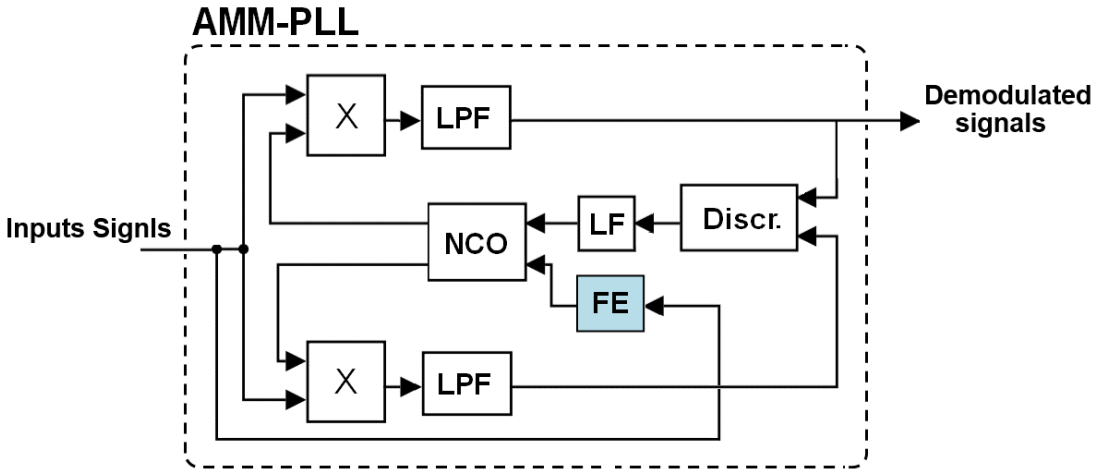

Figure 5-11 Adaptive Multi-Mode Phase Locked Loop (AMM-PLL)

Practically, the purpose of the FE part is to control the value of ω by updating the free-frequency of the NCO with respect to the frequency of the received signal, so that the FE will pull the ω value to the zero in a short time. Estimating unknown frequency of a noisy signal is not an easy task, however, there are many methods that can be adopted to achieve that such as the Zero crossing method [81], Least squares method [82], Fourier transform [83], Kalman filter [84], numerical differentiation method [85], and IIR notch filter [86]. We have studied all these possibilities and all of these methods have a trade-off between the accuracy, complexity, and frequency estimating range. In this work, two methods of FE are chosen based on having less complexity, good accuracy and cover a wide frequency range. These are 1) Infinite Impulse Response (IIR) notch filter (see Section 5.4.1), and 2) numerical differentiation method (see Section 5.4.2).

Figure 5-12 depicts our single tracking and demodulating channel based on applying the AMM-PLL function to handle BT and GPS signals simultaneously. The *control-unit* in this figure is used to switch the FE ON for a period of 150 μsec at any frequency hop or gap-time, as well as to enable and disable the differentiation block [70]. The functionality/knowledge of the control unit is dedicated for the BT protocol time, i.e. this unit is able to recognise the next coming hop frequency or

gap-time. The *differentiate block* is used to differentiate the output of the AMM-PLL function when the BT is active because the BT signal is a frequency modulated; and the AMM-PLL output represents the phase demodulation of the signal.

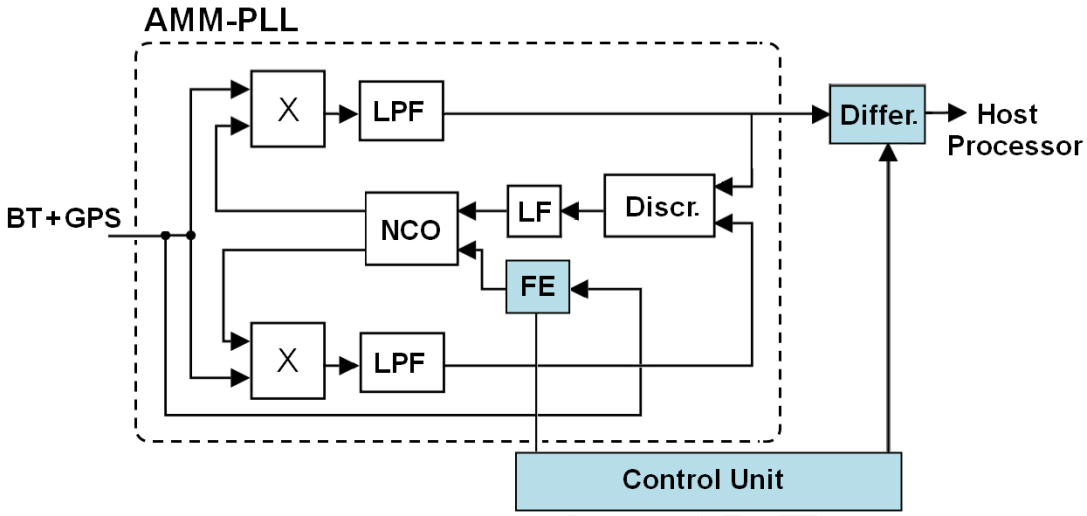

Figure 5-12 AMM-PLL used for tracking and demodulation BT and GPS signals simultaneously

The AMM-PLL operates in two modes; mode one is for when the BT signal is active and mode two is for when the BT signal is inactive (gap-time).

1. **BT Mode**, the AMM-PLL input is a combined BT and GPS signals. The control unit will permit the FE to estimate the input signal frequency, the time window for FE is 150 *µsec*, since the amplitude-ratio is 12 *dB* so the FE will estimate the BT frequency and then feed the estimated frequency to the NCO to update the free-running frequency. That will make the AMM-PLL operate at a lock range of tracking the BT signal, and the phase synchronization will then occur within a single cycle loop, even though the bandwidth of the LF is narrow. At the same time of allowing the FE to perform, the control unit will also enable the "differentiation" function.
2. **GPS Mode;** in the allowed gap-time, the control unit permits the FE to start estimating the frequency of the received signal with time window equal to 150 *µsec*, since the received is only GPS signal, the FE returns an estimated GPS signal frequency. The estimated frequency will feed to the NCO as a free-running frequency and the phase synchronisation will be occurred. The

control unit in this mode will disable the differentiation function since the output is the GPS which is a BPSK signal.

Note that, MATLAB is used to simulate BT and GPS signals. Both signals have the same IF-frequency (IF=0 *Hz*), and also the same sampling frequency, which is equal to 5 *MHz* and 20 *MHz* when it used in the IIR-based method and the derivative-based method respectively. The ω value in the BT signal changes at each hop and it is limited to 500 *Hz*. The Doppler frequency in the GPS signal is set at a maximum value (10 *KHz*). The natural frequency and damping-ratio of the AMM-PLL are set to be 100 *Hz* and 0.7 receptively.

5.4.1 IIR-Based AMM-PLL Design

The adaptive IIR notch filter model is a second-order narrowband filter that has a single adaptive coefficient to estimate a frequency [86]. The transfer function of the IIR notch filter is given by:

$$H(z) = \frac{Y(z)}{X(z)} = \frac{1 - 2\,z^{-1}\cos(\theta) + z^{-2}}{1 - 2\,r\,z^{-1}\cos(\theta) + r^2\,z^{-2}}$$

where θ is the adaptive coefficient (filter notch frequency), and the parameter r is used to control the notch filter bandwidth.

The difference equation of the IIR filter used in our implementation is expressed as:

$y[n] = x[n] - 2\,cos(\theta)\,x[n-1] + x[n-2] + 2r\,cos(\theta)\,y[n-1] - r^2\,y[n-2]$, *where n indicates discrete time.*

For estimating a centre frequency θ_x of input signal $x[n]$, the filter output *y[n]* needs to be minimised as:

$$\hat{\theta}_x = \hat{\theta} = arg_\theta\, min \frac{1}{N}\sum_{n=0}^{N}|y[n]|^2 \qquad (5\text{-}9).$$

Solving the above minimisation problem that will yield a coarse frequency estimated $\widehat{\theta}_x$, and then the least square algorithm is applied for refining the estimated frequency [87] .

Three parameters are used to evaluate the performance of the IIR notch filter alone, when it is estimated that, a frequency has stepped up to 10 *KHz*; the three parameters are the transition time, the standard deviation (STD), and Δ-mean. The transition time is the time required to estimate/switch form frequency to a new frequency. The STD measures the frequency deviation from the required fundamental frequency. The Δ-mean calculates the difference between the mean of the estimated and the actual frequencies.

1. Test scenarios for evaluating IIR notch filter individually:

To assess the FE performance alone, a 150 *µsec* of sampled data are simulated at sampling frequency 5 *MHz* and frequency step 10 *KHz* between the two signals. The number of samples used for the GPS and the BT signals are 750 and 375 samples receptively. The carrier frequency of the GPS and the BT signals are 110 *KHz* and 100 *KHz* respectively. Two test scenarios are used for evaluation purpose of estimating the frequency of GPS and BT signals respectively. Figure 5-13 (a) depicted the setup of the first test, where BT samples are added to the first 375 samples of GPS signals and the length of the resulting signal is 750 samples.

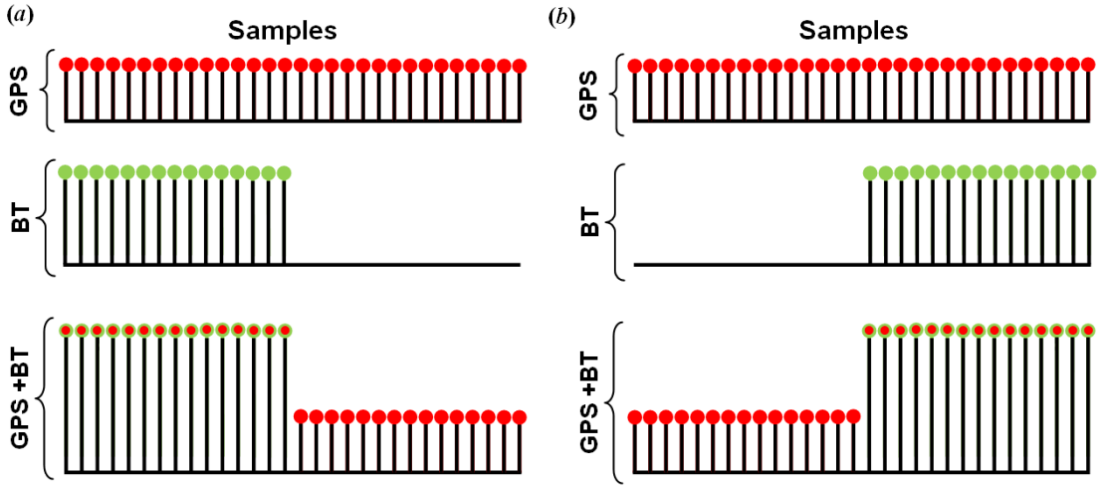

Figure 5-13 Samples multiplexing scheme to estimate (a) GPS frequency, (b) BT frequency

Figure 5-14 shows that FE is stable at BT frequency and then switched to the GPS frequency when the samples of the GPS signal become solitary (after 75 *µsec*). The required transition time is around 38 *µsec*, and after that the FE becomes stable

at the GPS frequency. The same transition time "38 μsec" is required, in the second test scenario, to estimate the BT frequency if the samples of the BT signals are added to the end of the GPS samples, as shown in Figure 5-13 (b). In addition, the same transition time is required to estimate BT/GPS frequency even if the test starts at any given samples of the resulting signal (GPS+BT), prior to the frequency step.

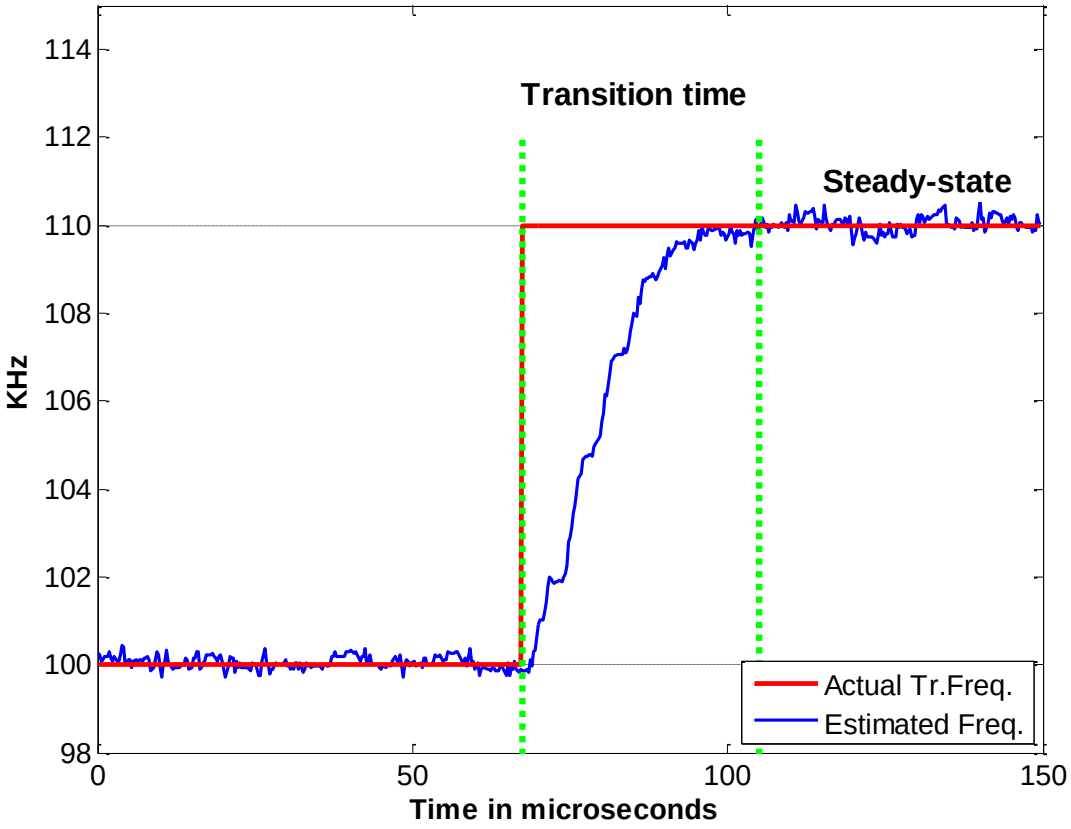

Figure 5-14 Transition time of FE based on IIR-notch filter @ SNR=25dB

Figure 5-15 (a) shows the accuracy of the estimated frequency in steady-state time at different SNRs. The STD of the last 100 estimated samples is calculated. As clearly shown, at high SNR value the estimated frequency will be closer to the actual frequency value and reach zero at 45 dB. While, at low SNR values, the estimated frequency shows a wide deviation from the actual fundamental frequency. However, in our AMP-PLL design, the mean of the estimated frequency value of the steady-state period is used to change the free-running frequency in the NCO.

Figure 5-15 (b) shows that the Δ-mean reaches the value zero when SNR equals 30 dB and that means if the FE is applied to the AMP-PLL it will need a single cycle

to lock to the phase. The signals have SNR less than 10 dB, the estimated frequency becomes larger than the LF bandwidth of the AMP-PLL, which means the signal will be ahead of the lock-in range.

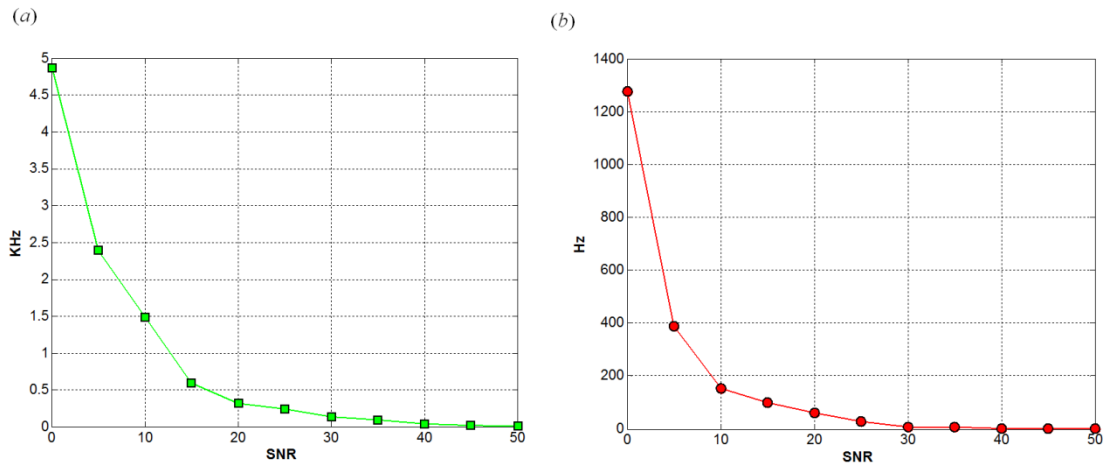

Figure 5-15 (a) STD and (b) Δ-mean of the estimated frequency versus SNR's

2. Test scenario for evaluating AMM-PLL based on using IIR notch filter:

Figure 5-16 shows the first 3.4 *msec* of the time multiplexing of the two signals. The simulation length of this test is 40.8 *msec*, so the first time needs to be repeated 12 times to cover the simulation length. Based on the simulation time, the AMM-PLL needs to switch between the frequencies of the two signals, at 10 *KHz* frequency step, 23 times.

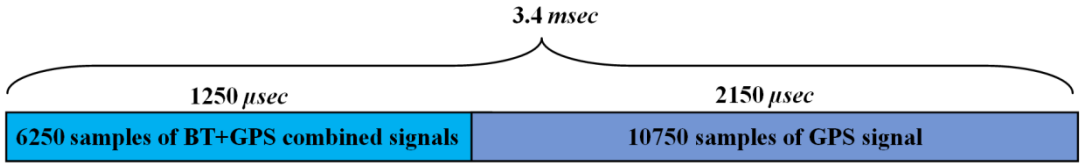

Figure 5-16 The first 3.4 msec time of the simulation time

The experiment results show that the AMM-PLL has a large lock-in range and after any perturbations in phase-error/discriminator output, it goes back to being a steady-state in a short time, as shown in Figure 5-17 (a). The phase-error perturbations actually occur when the AMM-PLL changes its mode, i.e. when it is switching between the two signal frequencies. The AMM-PLL shows a very stable

phase-error and it reaches 0.05 *rad*, as shown in Figure 5-17 (b). On the other hand, the BER of the demodulated data of the BT and the GPS signals is almost 1^{e-3} and zero at SNR greater than 10 *dB*.

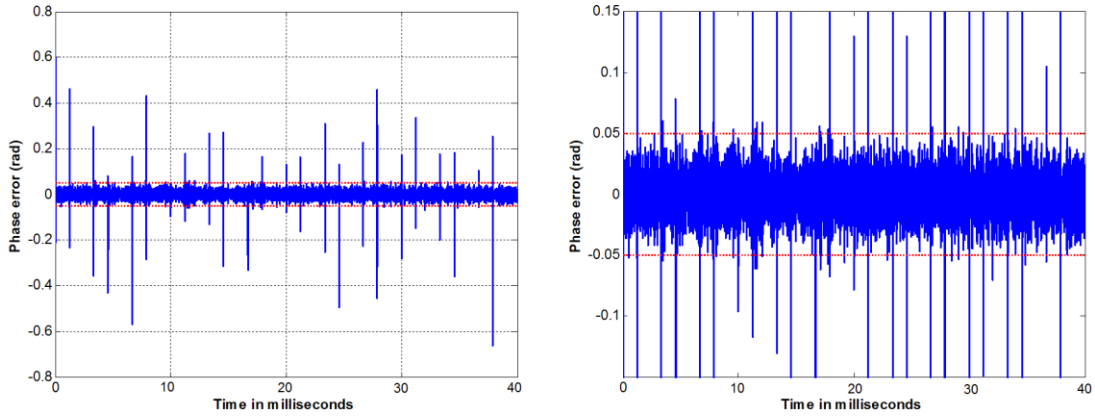

Figure 5-17 Phase-error of the AMM-PLL based IIR-notch FE design

5.4.2 Derivative-Based AMM-PLL Design

A numerical differentiation model is used to take the first and forth derivative of the received signal samples to calculate the fundamental frequency [85]. This model has been proposed to determine the frequency, amplitude and the phase of sinusoidal signals. However, in our work a simplified version of this model is used for estimating the frequency only, so that it fits with our purpose to control the ω parameter and also to reduce the cost of implementation complexity. The mathematical representation of the numerical differentiation model is given by:

$$\hat{\theta}_x = \sqrt[5]{\frac{x_I'[n]\, x_Q^{(4)}[n] - x_I^{(4)}[n]\, x_Q'[n]}{(x_I[n])^2 + (x_Q[n])^2}},$$

where $\hat{\theta}_x$ *is the angular estimated frequency of the input signal*$x[n]$. *The* $x_I'[n]$ *and* $x_I^{(4)}[n]$ *are the first and the forth derivative of* $x[n]$ *respectively. The* $x_Q'[n]$ *and* $x_Q^{(4)}[n]$ *are the first and the forth derivative of quadrature-phase of the* $x[n]$ *respectively.*

The same three parameters that are used in Section 5.4.1 to evaluate the

performance of the IIR notch filter are used here, which are transition time, standard deviation (STD), and Δ-mean.

1. Test scenario for evaluating numerical differentiation model alone:

The simulation length time is 150 *µsec*. The sampling frequency and the frequency step used are 20 *MHz* and 10 *KHz* receptively. The carrier frequency of the GPS and the BT signals are 110 *KHz* and 100 *KHz* respectively. The samples numbers of the GPS and the BT signals are 3000 and 1500 receptively. Figure 5-13 (a) and (b) depicted the setup of the first and the second test scenarios respectively. In the first test, the BT samples are added to the first 1500 samples of the GPS signals and the length of the resulting signal is 3000 samples. Figure 5-18 shows that a required transition time to estimate the new frequency (GPS frequency) at frequency step 10 *KHz* is 25 *µsec*. In the second test scenario, the same transition time is required to estimate the frequency of the BT signal. In addition, the same transition time is required to estimate BT/GPS frequency if the test starts with any samples of GPS (or BT) signal.

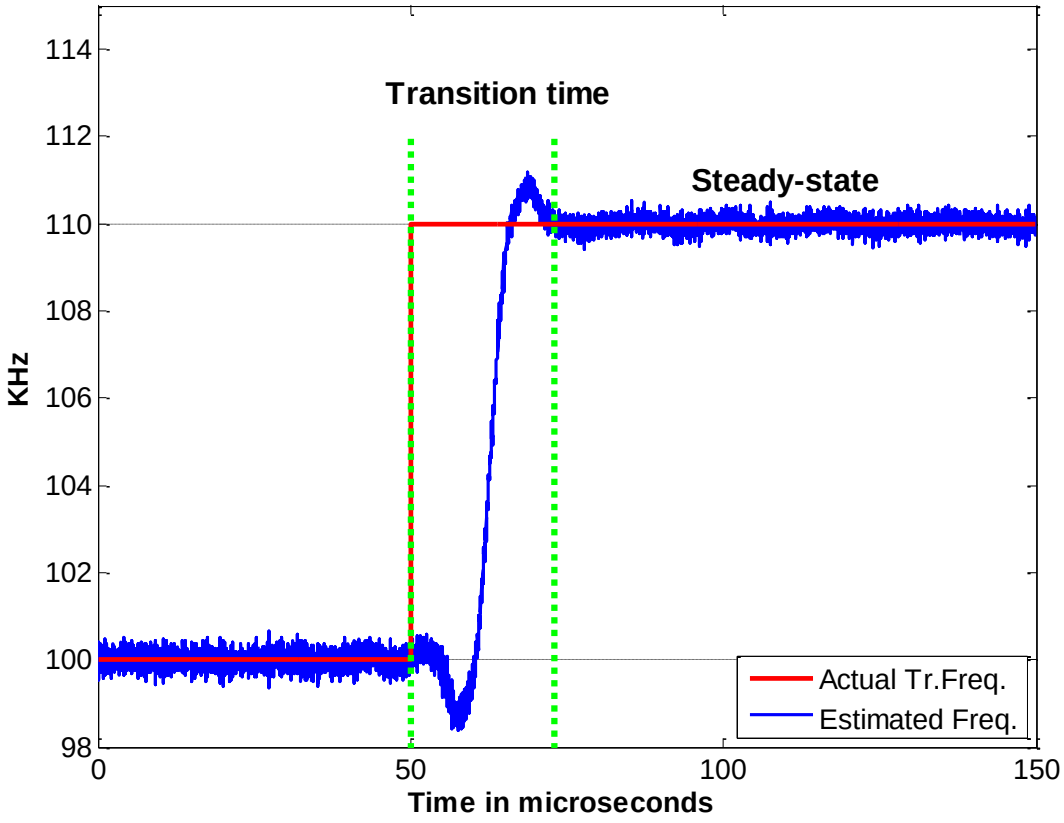

Figure 5-18 Transition time of FE based on derivative-based method @ SNR=35dB

Figure 5-19 (a) shows the STD values of the estimated frequency (STD of the last 200 value of estimated frequency) versus the SNR. This method is not able to estimate accurate frequency in SNR value less than 10 *dB* since the deviation frequencies from the required frequency are more than the allowable step frequency in the AMM-PLL. The accuracy of this method starts improving with increased the SNR value and reach the acceptable value at 15 *dB* (i.e. the corresponding mean value is less than the LF bandwidth of the MAB-PLL), as shown in Figure 5-19 (b).

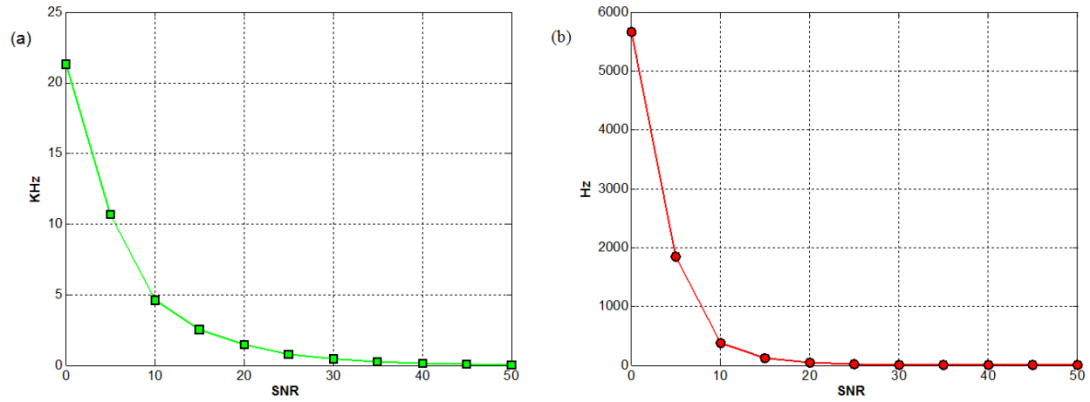

Figure 5-19 (a) STD and (b) Δ-mean of the estimated frequency versus SNR's

2. Test scenario for evaluating AMM-PLL based on using the derivative method:

The experiment results show that the AMM-PLL based differentiation model has minor disturbance when the AMM-PLL changes its mode, as shown in Figure 5-20 (a). However, after each disturbance the phase-error reverts to a stable value at around 0.22 *rad*, as illustrated in Figure 5-20 (b). This stability in the phase-error helps the modulated bits of the two signals (BT+GPS) to be less error prone, and the BER of the demodulated bits reaches almost 1^{e-3} and zero at SNR greater than 15 *dB*.

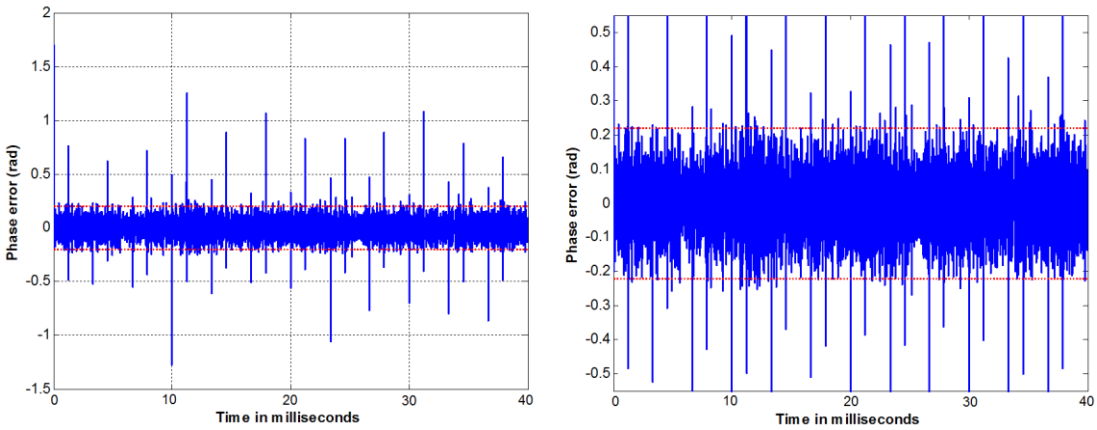

Figure 5-20 Phase-error of the AMM-PLL based on derivative FE design

5.5 Comparison of AMM-PLL Designs and Conclusion

Each Frequency Estimators design has pros and cons in terms of its requirements, performance and implementation; the results reflects on the overall performance of AMM-PLL. The derivative-based requires more signals samples than IIR-based method to estimate accurate frequency since it does not have a feedback mechanism and this means more power consumption. In addition, the same method involves more voltage "0.22 *V/rad*" to let the close loop in the AMM-PLL be a stable compared with IIR-based method required only "0.05 *V/rad*". Further, the derivate-based method operates at SNR equal or greater than 15 *dB* while, IIR-based methods operate at wider range of SNR start from 10 *dB*. However, the derivate-based method has less transition time "25 *μsec*" as compares with IIR-methods "38 *μsec* ", which the crucial part in our single tracking channel design, and also it has less implementation complexity.

Overall, the AMM-PLL implementation reduces by half the size and processing time of tracking and demodulating these two signals simultaneously. In this implementation, the solution permits the use of the GPS receive chain for window-slots of up to 1250 *μsec* for processing BT signal, without losing lock (or needing to re-acquire the GPS signal). The two Adaptive Frequency Estimators designed for this multi-mode PLL can also be used for other dual-signals with a lock range up to 10 *KHz* using narrow bandwidth loop filter. For example, the AMM-PLL can be used to track and demodulate BT signals with any one of the GNSS civilian signals

L1, L2, and L5, since these signals have very low bit rate so the AMM-PLL can switch on and off from these signals without losing the information bits.

Chapter 6 **Conclusion and Future Work**

From the outset, the brief of this research (now documented in this thesis) was to design a new receiver architecture to process multi-GNSS/wireless signals in a single received chain. The aims and motivation were to reduce the receiver's overhead in terms of size, processing time and power consumption to ensure it is ideal for implementation on-board Smartphones.

What we have achieved through our work regarding new innovative and novel techniques has the potential of contributing to the commercial world, especially when it comes to Smartphones. It will significantly help in managing savings in both silicon size and processing time, which will lead to reducing costs and more so more help in conserving the battery energy. We are truly happy to have made this significant contribution to the industry at large and we feel this will be a major step in taking forward the scientific research and development arena.

Our work over the past five years has resulted in several technical achievements that led to 9 publications detailing our novel contributions. These are:

1. In a typical multi-GNSS receiver, and specifically in the acquisition process, the receiver shall use all its resources to acquire the GNSS signals. In urban environments where the GNSS signals are blocked by obstacles, the receiver will continue thrashing on wasting valuable resources. This thrashing can be saved if the receiver knows that there are no signals available at that time at that vicinity. We have accomplished such solution by designing an early signal detection frontend which is achieves measurable savings to the receiver resources. This proposed solution is detailed in Section 2.3.
2. The sampling frequency in most multi-signal GNSS receiver implementations has to be based on the Nyquist rate, which is equal to

double the summation of information bands for all received multi-singles. We have proposed that this rate can be reduced if these signals are orthogonalised, where the new rate is proportional to the maximum information band of one of the received signals. Further details in Sections 3.1 and 3.2.

3. By combining the acquisition of L1CA and L2C GPS signals, the receiver can achieve better signal acquisition, boost the localisation accuracy, and improve reliability at wider operating areas. The current implementations have achieved these advantages but only by implementing two-acquisition channels side-by-side and then combining their correlated results. This will increase the overhead in such a receiver. Our proposed implementations have integrated the two-acquisition channels into a single channel by integrating the two signals into a single orthogonal signal. The complexity of our 6 proposed implementation have almost halved the complexity of other methods; besides, our implementations have not only succeeded in achieving all the advantages of combining these two signals but also has resulted in enhancing the acquisition sensitivity. See Sections 4.4 and 4.5.
4. Designing an adaptive-multi-mode PLL with a wide lock-in range for tracking certain types of wireless signals that can be multiplexed together will help the receiver to save power, and reduce cost and size. This is because the “tracking” engine is made to be active continually while the signal is processed; enabling the receiver to put the acquisition engine to sleep once the signal is acquired. Our proposed new PLL design has the ability to track and demodulate the “BT and GPS” signals simultaneously without losing the lock of their phase synchronization. This solution is robust against any interfering signals too, since our designed frequency estimator is used inside the loop. See Section 5.4.
5. the AMM-PLL implementation has been proven to reduces complexity and processing of tracked signals by half. Our implementation was focused on the GPS/L! and BT signals, however, our multi-mode PLL implementation can also be used for other dual-signals with a lock range up to 10 *KHz* using narrow bandwidth loop filter. For example, the AMM-PLL can be used to

track and demodulate BT signals with any one of the GNSS civilian signals L1, L2, and L5, since these signals have very low bit rate so the AMM-PLL can switch on and off from these signals without losing the information bits.

Looking at our technical achievements/solutions from a different angle, we have successfully implemented new and novel solutions at different stages of the receiver chain; the front-end stage, the acquisition stage, and the tracking stage, as explained in the following sections.

6.1 Front-End Stage Achievements

3. Early-Detection of L1-GNSS signals

Most of the multi-GNSS receiver challenges lie in finding the available signals (GPS-L1, Galileo-E1 and GLONASS-L1) at the acquisition stage, which will cost a lot of power and time, seeking signals that may not exist.

We have successfully developed two approaches, based on the BPSR technique, that are capable of detecting the availability of the GNSS signals before engaging the acquisition engine.

C. The First Approach: BPSR Non-Linear (BPSR-NL)

In this approach, the information bands of the three GNSS signals and their harmonics are folded back to the FNZ. To select an appropriate sampling frequency, there is a guard band between the fundamental frequency of the folded signals and their harmonics. This makes the power distribution of the signals in FNZ unique, which makes it easier to detect them quickly, as detailed in Chapter 2, Section 2.3.1.

D. The Second Approach: BPSR-Side Lobe Filtering (BPSR-SLF)

The right-side lobe and the left-side lobe of the GLONASS and the Galileo signals were filtered out respectively and then were combined with the third harmonic of the GPS signal. A single BPSR ADC was then used to sample the combined signal, and with choosing an appropriate sampling frequency, the BPSR folded the GNSS signals to three distinct frequency locations in the FNZ. This approach has been documented in Section 2.3.2.

The main benefits of these two approaches are:

1. Rapid detection of multi-GNSS signals in a single view by sensing the powers of the present signals.
2. Stop thrashing the receiver resources to find the signals that are not available.
3. Reducing the sampling frequency based on the available signals only, which saves more processing time.
4. Prepare the required acquisition and tracking channel in the digital domain.

4. Orthogonal Multi-Signal Receiver

Two multi-signal receivers were designed, named OBPSR and OCBPSR, to capture and track multi-signals simultaneously, as detailed in Chapter 3, Section 3.1 and 3.2 respectively. The novelty of this work is centred on the Orthogonal Integrate Function (OIF) that continuously harmonises the two received signals to form a single orthogonal signal allowing the "tracking and decoding" to be carried out by in single PLL in the digital domain. The OBPSR and OCBPSR receivers utilise a Hilbert Transform for shifting one of the signals by 90-degree in order to prevent overlapping before using a BPSR to fold the two signals to the same frequency in the FNZ. The resultant orthogonal signal was then passed into a single tracking and demodulation channel.

The benefits of the orthogonal multi-signal receiver's design are:

1. Reduce the sampling frequency to the rate proportional to the maximum information bandwidth of the received signals rather than the summation of their bandwidth.
2. The digitised signal can be processed in a single channel for acquisition, tracking and demodulation.
3. Over all, the receiver design saves valuable attributes such as device and manufacturing costs, power dissipation and processing time when compared with conventional side-by-side receivers.

6.2 Our Achievements in the Acquisition Stage

Two new novel receivers' design were proposed to acquire both the L1CA and

L2C GPS signals in a single acquisition channel simultaneously. The novelty of the work is centred on orthogonalising the two received GPS signals so to enable their acquisition in a single processing channel. That is, to jointly estimate the phase-code-delay and Doppler-frequency-offset of both signals in a signal acquisition engine. The first combined L1&L2 channel named Orthogonal Single acquisition Channel (OSC) is devoted to enhancing the power consumption issue in the existing combination methods. The other L1&L2 combined channel named Orthogonal Parallel acquisition Channel (OPC) is dedicated to enhancing the acquisition sensitivity.

Uniqueness and advantages of the two combined L1CA/L2C GPS acquisition channels:

1. The complexity of our implementation was almost half of other methods. This has been achieved by orthogonalising the received two GPS signals so as to process them in a single channel, while the other methods combine the acquisition result of the two signals, by having side-by-side acquisition channels.
2. Our proposals have resulted in enhancing the acquisition sensitivity by at least 5 dB. This has been achieved by estimating both L1CA and L2CM code delay and Doppler frequency at the same time, while keeping the frequency-bins size as small as possible by using only 1 *msec* coherent acquisition.

5. Orthogonal Single Acquisition Channel (OSC)

In this channel, the two received GPS signals (L1CA&L2C) were orthogonalised as follows; after removing the Doppler frequency, the quadrature components of two GPS signals were added together. This new signal was then shifted by 90-degree and then added to the remaining components of these two signals. Thus, an orthogonal form of these two signals was created. The orthogonal signal was then processed by an orthogonal correlation engine that produces a complex representation of the correlated signal. One of three different combination methods/post-correlation methods was then used to process the complex correlated signal in order to obtain the maximum correlation peak that declares the acquisition result. The trade-off

among these three combination methods was “the implementation complexity” and “detection accuracy”. The implementation of the OSC has been described in Chapter 4, Section 4.4.

6. Orthogonal Parallel Acquisition Channel (OPC)

The same process that was done in the OSC to orthogonalise the two signals has also been performed in this channel. Two orthogonal correlation engines are used in this channel to duplicate the correlation power and eliminate the cross-correlation noise, in order to improve the acquisition sensitivity. The implementation of this channel has been described fully in Chapter 4, Section 4.5.

6.3 Tracking Stage Achievements

Two approaches based on a new multi-signal PLL design were proposed to combine Bluetooth and L1CA-GPS signals in a single tracking channel. The 2 new approaches have permitted the use of the GPS receive chain in window-slots of up to 1250 μsec for processing the Bluetooth signal, without losing lock or needing to re-acquire the GPS signal. The implementations of these approaches were based on integrating an Adaptive Frequency Estimator (FE) into a standard-version of the Costas PLL. This FE provides an estimated frequency of the received signal to modify the free-running frequency of the NCO that will enhance the performance of the PLL by increasing its lock-in range. The first approach was based on an adaptive IIR notch filter (see Chapter 5, Section 5.4.1) and the second approach uses a numerical differentiation model (see Chapter 5, Section 5.4.1). These two approaches have been simulated against various test scenarios and proven to track multi-signal with up to 10 KHz frequency steps.

The advantages of this work are:

1. The implementation complexity has been reduced by half in size and in processing time of tracking and demodulating these two signals simultaneously.
2. The two Adaptive FE were designed for combining GPS and Bluetooth signals can also be used for other appropriate dual-signals with a lock range

up to 10 KHz using narrow bandwidth loop filter.

3. Faster lock time of 25 μsec is achieved by feeding free running frequency to the NCO.

6.4 Future Development

Combining wireless signals in a single chain is a wide research area with vast potential; however, our thesis research has focused mainly on particular aspects of combining GNSS/BT signals. Based on the results presented in the previous chapters and the subsequent conclusions made in this chapter, the following recommendations can be made to further develop this research:

1. Volterra-Series is used to represent the nonlinear behaviour of multi-signal BPSR front-end. Based on the mathematical model of Volterra-Series we can derive a new model for the Kalman Filter that may be able to track all the received signal parameters such as frequency, amplitude and phase in a single channel. This means that a single receiver can be used to acquire multi-signals concurrently (based on BPSR front-end) and to track and decode them (based on Kalman Filter).

2. Our orthogonal receivers, in Chapter 3, were designed to handle two signals simultaneously. Developing the orthogonal receivers to capture three signals at the same time is possible when the AWGN channel is used. The output of the receiver front-end will be an orthogonal signal, and each phase change of this orthogonal signal will be represented in the three information bits (each bit from a distinct signal). However, this type of receiver requires more investigation specifically when applying a fading channel.

3. In Chapter 3, our orthogonal receiver requires RLS/LSM algorithm inside the PLL to track and decode the orthogonal signal when the fading channel is used. As an alternative, Kalman Filter can be applied with lesser overhead. This requires designing a new Kalman model that analyse the mismatch between the folded-frequencies of the two signals in FNZ.

4. The same orthogonal approach that was applied to combine L1CA and L2C

GPS signal in a single acquisition channel can be developed to acquire the GPS civilian signal L5. L5 GPS signal is also transmitted from the same SV so it too has the same relevant error as with L1 and L2 signals. The challenge in this task is that the cross-correlation noise will increase dramatically, i.e., the cross-correlation between L1&L2, L1&L5 and L2&L5, which might diminish an effective signal detection.

References

[1] E. G. Agency, “GNSS Market Report: Issue 4,” 2015, avaliable at: http://www.gsa.europa.eu/system/files/reports/GNSS-Market-Report-2015-issue4_0.pdf (Accessed: 20 April 2016).

[2] W. M. O'Dowd, “A new finite difference solution to the Fokker-Planck equation with applications to phase-locked loops,” 1973.

[3] A. Simsky and J.-M. Sleewaegen, “Experimental and Professional Galileo Receivers,” in *GALILEO Positioning Technology,* Springer, 2015, pp. 273-288.

[4] M. Wildemeersch, C. Slump, T. Quek and A. Rabbachin, “GNSS signal acquisition in harsh urban environments,” in *Communications Workshops (ICC), 2013 IEEE International Conference on,* 2013.

[5] R. F. Cordeiro, A. Prata, A. S. R. Oliveira, N. B. Carvalho and J. N. Vieira, “FPGA-based all-digital software defined radio system demonstration,” in *2015 25th International Conference on Field Programmable Logic and Applications (FPL),* 2015.

[6] R. K. Loper, *Phase and gain error control system for use in an i/q direct conversion receiver,* Google Patents, 1993.

[7] R. Svitek and S. Raman, “DC offsets in direct-conversion receivers: characterization and implications,” *Microwave Magazine, IEEE,* vol. 6, no. 3, pp. 76-86, Sept 2005.

[8] D. M. Akos, “A software radio approach to global navigation satellite system receiver design,” 1997.

[9] R. G. Vaughan, N. L. Scott and D. White, “The theory of bandpass sampling,” *Signal Processing, IEEE Transactions on,* vol. 39, no. 9, pp. 1973-1984, 1991.

[10] D. S. G. Pollock, R. C. Green and T. Nguyen, Handbook of time series analysis, signal processing, and dynamics, Academic Press, 1999.

[11] J. Liu, X. Zhou and Y. Peng, “Spectral arrangement and other topics in first-order bandpass sampling theory,” *Signal Processing, IEEE Transactions on,* vol. 49, no. 6, pp. 1260-1263, 2001.

[12] A. G. Dempster, “Quadrature bandpass sampling rules for single-and multiband communications and satellite navigation receivers,” *IEEE Transactions on*

Aerospace and Electronic Systems, vol. 4, no. 47, pp. 2308-2316, 2011.

[13] C.-H. Cheng, L. L. Liou, D. M. Lin, J. B. Tsui and H.-M. Tai, "Wideband in-phase/quadrature imbalance compensation using finite impulse response filter," *Radar, Sonar \& Navigation, IET,* vol. 8, no. 7, pp. 797-804, 2014.

[14] P. M. Cruz, N. B. Carvalho and M. E. Valkama, "Evaluation of second-order bandpass sampling receivers for software defined radio," in *Microwave Integrated Circuits Conference (EuMIC), 2012 7th European*, 2012.

[15] A. Bourdoux, J. Craninckx, A. Dejonghe and L. V. d. Perre, "Receiver architectures for software-defined radios in mobile terminals: The path to cognitive radios," in *Radio and Wireless Symposium, 2007 IEEE*, 2007.

[16] A. Brown and B. Wolt, "Digital L-band receiver architecture with direct RF sampling," in *Position Location and Navigation Symposium, 1994., IEEE*, 1994.

[17] D. Akos, M. Stockmaster, J. Tsui and J. Caschera, "Direct bandpass sampling of multiple distinct RF signals," *Communications, IEEE Transactions on,* vol. 47, no. 7, pp. 983-988, Jul 1999.

[18] D. M. Akos, A. Ene and J. Thor, "A prototyping platform for multi-frequency GNSS receivers," in *Proceedings of the 16th International Technical Meeting of the Satellite Division of The Institute of Navigation (ION GPS/GNSS 2003)*, 2001.

[19] A. Alonso, J. Perre and I. Arizaga, "SDR direct-sampling device for multistandard GNSS signals," in *Communication Systems, Networks and Digital Signal Processing, 2008. CNSDSP 2008. 6th International Symposium on*, 2008.

[20] Y.-R. Sun and S. Signell, "A generalized quadrature bandpass sampling in radio receivers," in *Proceedings of the 2005 Asia and South Pacific Design Automation Conference*, 2005.

[21] Y.-R. Sun and S. Signell, "Implementation of generalized uniform Bandpass Sampling with complex FIR and IIR Filtering," in *Circuit Theory and Design, 2007. ECCTD 2007. 18th European Conference on*, 2007.

[22] Y.-R. Sun and S. Signell, "Generalized quadrature bandpass sampling with FIR filtering," in *Circuits and Systems, 2005. ISCAS 2005. IEEE International Symposium on,* 2005.

[23] P. Cruz and N. B. Carvalho, "Modeling band-pass sampling receivers nonlinear behavior in different Nyquist zones," in *Microwave Symposium Digest (MTT), 2010 IEEE MTT-S International*, 2010.

[24] P. Cruz and N. Carvalho, "Wideband Behavioral Model for Nonlinear Operation of Bandpass Sampling Receivers," *Microwave Theory and*

Techniques, IEEE Transactions on, vol. 59, no. 4, pp. 1006-1015, April 2011.

[25] P. M. Cruz and N. B. Carvalho, "Multi-carrier wideband nonlinear behavioral modeling for cognitive radio receivers," in *Microwave Integrated Circuits Conference (EuMIC), 2011 European*, 2011.

[26] J.-H. WON, D. Dotterbock and B. Eissfeller, "Performance Comparison of Different Forms of Kalman Filter Approaches for a Vector-Based GNSS Signal Tracking Loop," *Navigation,* vol. 57, no. 3, pp. 185-199, 2010.

[27] M. Al-Aboodi, A. Albu-Rghaif and I. Lami, "GPS, Galileo and Glonass L1 signal detection algorithms based on bandpass sampling techniques," in *Ultra Modern Telecommunications and Control Systems and Workshops (ICUMT), 2012 4th International Congress on*, 2012.

[28] B. Hofmann-Wellenhof, H. Lichtenegger and E. Wasle, GNSS--global navigation satellite systems: GPS, GLONASS, Galileo, and more, Springer Science \& Business Media, 2007.

[29] M. Muha, C. Clark, A. Moulthrop and C. Silva, "Validation of power amplifier nonlinear block models," in *Microwave Symposium Digest, 1999 IEEE MTT-S International*, 1999.

[30] M. K. Simon and W. K. Alem, "Tracking performance of unbalanced QPSK demodulators: Part I-biphase costas loop with passive arm filters," *Communications, IEEE Transactions on,* vol. 26, no. 8, pp. 1147-1156, 1978.

[31] W. R. Dieter, S. Datta and W. K. Kai, "Power reduction by varying sampling rate," in *Proceedings of the 2005 international symposium on Low power electronics and design*, 2005.

[32] K. Bowman, B. Austin, J. Eble, X. Tang and J. Meindl, "A physical alpha-power law MOSFET model," in *Low Power Electronics and Design, 1999. Proceedings. 1999 International Symposium on*, 1999.

[33] T. Sakurai and others, "Alpha-power law MOSFET model and its applications to CMOS inverter delay and other formulas," *Solid-State Circuits, IEEE Journal of,* vol. 25, no. 2, pp. 584-594, 1990.

[34] J. F. Sevic and J. Staudinger, "Simulation of adjacent-channel power for digital wireless communication systems," *Microwave Journal,* vol. 39, no. 10, pp. 66-74, 1996.

[35] H. Packard, "Using Error Vector Magnitude Measurements to Analyze and Troubleshoot Vector Modulated Signals," *Product Note HP*, pp. 89400-8, 2000.

[36] S. Taleie, Y. Han, T. Copani, B. Bakkaloglu and S. Kiaei, "A 0.18 μm CMOS fully integrated RFDAC and VGA for WCDMA transmitters, Radio Frequency Integrated Circuits Symposium, 2008. RFIC 2008," *IEEE, Page (s),*

pp. 157-160.

[37] L. Lolis, “Agile bandpass sampling RF receivers for low power applications,” 2011.

[38] M. Patzold, Mobile fading channels, John Wiley \& Sons, Inc., 2003.

[39] [Online].Available, “http://www.signalion.com/files/m011-v5-1_datasheet_halo430_2010.pdf,” Signalion, 2010. [Online].

[40] G. Seco-Granados, J. Lopez-Salcedo, D. Jimenez-Banos and G. Lopez-Risueno, “Challenges in Indoor Global Navigation Satellite Systems: Unveiling its core features in signal processing,” *Signal Processing Magazine, IEEE,* vol. 29, no. 2, pp. 108-131, March 2012.

[41] S. K. Shanmugam, “Improving GPS L1 C/A code correlation properties using a novel multi-correlator differential detection technique,” *ProcION GNSS2006. Fort Worth, TX: ION,* vol. 26, p. 29, 2006.

[42] J. Spilker, “GPS signal structure and theoretical performance,” *Global Positioning System: Theory and applications.*, vol. 1, pp. 57-119, 1996.

[43] S. U. Qaisar and A. G. Dempster, “An analysis of L1-C/A cross correlation \& acquisition effort in weak signal environments,” in *Proceedings of International Global Navigation Satellite Systems Society, IGNSS Symposium. Sydney, Australia*, 2007.

[44] J. B.-Y. Tsui, Fundamentals of global positioning system receivers, Wiley-Interscience, 2000.

[45] M. J. Dunn, *Global Positioning System Directorate Systems Engineering and Integration Interface Specification IS-GPS-200H*, Spet., 2013.

[46] S. Qaisar and A. Dempster, “Cross-correlation performance assessment of global positioning system (GPS) L1 and L2 civil codes for signal acquisition,” *IET radar, sonar \& navigation,* vol. 5, no. 3, pp. 195-203, 2011.

[47] A. Cameron, “To L2C or Not to L2C? That Is the Operational Question,” *GPSWORLD,* July 2015.

[48] C. Gernot, K. O'Keefe and G. Lachapelle, “Assessing three new GPS combined L1/L2C acquisition methods,” *Aerospace and Electronic Systems, IEEE Transactions on*, vol. 47, no. 3, pp. 2239-2247, 2011.

[49] F. S. T. Van Diggelen, A-GPS: Assisted GPS, GNSS, and SBAS, Artech House, 2009.

[50] C. Gernot, “Development of combined GPS L1/L2C acquisition and tracking methods for weak signals environments,” *Department of Geomatics*

Engineering, 2009.

[51] R. D. Fontana, W. Cheung, P. M. Novak and T. Stansell, "The new L2 civil signal," in *Proceedings of ION GPS*, 2001.

[52] D. Lim, S. Moon, C. Park and S. Lee, "L1/L2CS GPS receiver implementation with fast acquisition scheme," in *Proceedings of IEEE/ION PLANS 2006*, 2001.

[53] C. Gernot, S. K. Shanmugam, K. O'Keefe and G. Lachapelle, "A novel L1 and L2C combined detection scheme for enhanced GPS acquisition," in *Proceedings of the 20th International Technical Meeting of the Satellite Division of The Institute of Navigation (ION GNSS 2007),* 2007.

[54] C. Gernot, K. O'Keefe and G. Lachapelle, "Comparison of L1 C/A-L2C combined acquisition techniques," in *Proceedings of European Navigation Conference, Toulouse, France*, 2008.

[55] T. H. Ta, S. U. Qaisar, A. G. Dempster and F. Dovis, "Partial differential postcorrelation processing for GPS L2C signal acquisition," *Aerospace and Electronic Systems, IEEE Transactions on*, vol. 48, no. 2, pp. 1287-1305, 2012.

[56] S. Han, R.-f. Ma, W.-j. Wang, W.-x. Meng and Y. Zhang, "FFT-based L1 C/A and L2C combined acquisition techniques," in *International Conference on Space Information Technology 2009*, 2009.

[57] T. H. Ta, M. Pini and L. Presti, "Combined GPS L1C/A and L2C signal acquisition architectures leveraging differential combination," *Aerospace and Electronic Systems, IEEE Transactions on*, vol. 50, no. 4, pp. 3212-3229, 2014.

[58] F. Macchi-Gernot, M. G. Petovello and G. Lachapelle, "Combined acquisition and tracking methods for GPS L1 C/A and L1C signals," *International Journal of Navigation and Observation,* vol. 2010, 2010.

[59] F. Macchi, Development and testing of an L1 combined GPS-Galileo software receiver, Ph. D. thesis, Department of Geomatics Engineering, The University of Calgary, Calgary, Canada, 2010.

[60] M. Al-Aboodi and I. A. Lami, "OCBPSR: Orthogonal Complex BandPass Sampling Receiver," in *Computer Applications and Information Systems (WCCAIS), 2014 World Congress on*, 2014.

[61] H. V. Poor, An introduction to signal detection and estimation, Springer Science \& Business Media, 2013.

[62] B. Geiger, M. Soudan and C. Vogel, "On the detection probability of parallel code phase search algorithms in GPS receivers," in *Personal Indoor and Mobile Radio Communications (PIMRC), 2010 IEEE 21st International Symposium on*, 2010.

[63] T. H. Ta and S. H. Ngo, “A novel signal acquisition method for GPS dual-frequency L1 C/A and L2C receivers,” in *Advanced Technologies for Communications (ATC), 2011 International Conference on*, 2011.

[64] Y. Lou, C. Zhang, X. Jin and Z. Jin, “Method of adaptive PLL bandwidth adjustment without phase slipping,” *Systems Engineering and Electronics, Journal of,* vol. 25, no. 6, pp. 949-958, 2014.

[65] R. C. Van de Beek, D. M. Leenaerts and G. van der Weide, “A fast-hopping single-PLL 3-band MB-OFDM UWB synthesizer,” *Solid-State Circuits, IEEE Journal of,* vol. 41, no. 7, pp. 1522-1529, 2006.

[66] S. Traverso, M. Ariaudo, J.-L. Gautier, I. Fijalkow and C. Lereau, “A 14-band low-complexity and high-performance synthesizer architecture for MB-OFDM communication,” *Circuits and Systems II: Express Briefs, IEEE Transactions on*, vol. 54, no. 6, pp. 552-556, 2007.

[67] G. Hueber and R. B. Staszewski, Multi-mode/Multi-band RF transceivers for wireless communications: Advanced techniques, Architectures, and Trends, John Wiley \& Sons, 2011.

[68] C. Bisdikian and others, “An overview of the Bluetooth wireless technology,” *IEEE Commun Mag,* vol. 39, no. 12, pp. 86-94, 2001.

[69] S. Bluetooth, “Specification of the Bluetooth System, version 1.1,” *http://www. bluetooth. com,* 2001.

[70] R. Schiphorst, F. Hoeksema and K. Slump, “Bluetooth demodulation algorithms and their performance,” 2002.

[71] R. a. Kuznetsov, N. a. Leonov, G. a. Yuldashev, M. a. Yuldashev. R. Best, “A Survey on Dynamic Analysis of the Costas Loop,” *arXiv preprint arXiv:1511.04435,* 2015.

[72] C. Yoon and W. Lindsey, “Phase-locked loop performance in the presence of CW interference and additive noise,” *Communications, IEEE Transactions on,* vol. 30, no. 10, pp. 2305-2311, 1982.

[73] B. Sarkar, “Phase error dynamics of a first-order phase locked loop in the presence of cochannel tone interference and additive noise,” *Communications, IEEE Transactions on,* vol. 38, no. 7, pp. 962-965, Jul 1990.

[74] O. Takahiro, T. Iritani and H. Kawakami, “Response of PLL Demodulator by Two Sinusoidal Inputs,” *IEICE TRANSACTIONS on Fundamentals of Electronics, Communications and Computer Sciences,* vol. 77, no. 11, pp. 1771-1776, 1994.

[75] M. Tillman and J. Stensby, “Response of a first-order phase locked loop to two sinusoidal inputs,” in *System Theory, 2003. Proceedings of the 35th*

Southeastern Symposium on, 2003.

[76] J. Stensby and M. Tillman, "Input band-pass limiting in a PLL: its influence on interference-induced bifurcation," in *System Theory, 2004. Proceedings of the Thirty-Sixth Southeastern Symposium on*, 2004.

[77] M. AL-Aboodi, N. Kuznetsov, G. Leonov, M. Yuldashev and R. Yuldashev, "Response of Costas PLL in the Presence of In-band Interference," *IFAC-PapersOnLine*, vol. 48, no. 11, pp. 714-719, 2015.

[78] L. Thede, Practical analog and digital filter designa, Artech House, 2005.

[79] D. Abramovitch, "Efficient and flexible simulation of phase locked loops, part {I}: simulator design," in *American Control Conference*, Seattle, WA, 2008.

[80] D. Abramovitch, "Efficient and flexible simulation of phase locked loops, part {II}: post processing and a design example," in *American Control Conference*, Seattle, WA, 2008.

[81] M. M. Begovic, P. M. Djuric, S. Dunlap and A. G. Phadke, "Frequency tracking in power networks in the presence of harmonics," *Power Delivery, IEEE Transactions on*, vol. 8, no. 2, pp. 480-486, 1993.

[82] I. Kamwa and R. Grondin, "Fast adaptive schemes for tracking voltage phasor and local frequency in power transmission and distribution systems," in *Transmission and Distribution Conference, 1991., Proceedings of the 1991 IEEE Power Engineering Society*, 1991.

[83] H. Lin and C. Lee, "Enhanced FFT-based parametric algorithm for simultaneous multiple harmonics analysis," in *Generation, Transmission and Distribution, IEE Proceedings-*, 2001.

[84] H. Hajimolahoseini, M. R. Taban and H. Soltanian-Zadeh, "Extended Kalman filter frequency tracker for nonstationary harmonic signals," *Measurement*, vol. 45, no. 1, pp. 126-132, 2012.

[85] J. Wu, J. Long and Y. Liang, "Estimation of frequency, amplitude and phase of sinusoidal signals," in *Industrial Electronics, 2004 IEEE International Symposium on*, 2004.

[86] L. Tan and J. Jiang, "Novel adaptive IIR filter for frequency estimation and tracking [DSP Tips Tricks]," *Signal Processing Magazine, IEEE*, vol. 26, no. 6, pp. 186-189, November 2009.

[87] L. Tan and J. Jiang, "Simplified Gradient Adaptive Harmonic IIR Notch Filter for Frequency Estimation and Tracking," *American Journal of Signal Processing*, vol. 5, no. 1, pp. 6-12, 2015.